

University of Strathclyde  
Biomedical Engineering Department

Improvements to Iontophoresis Devices for  
Transdermal Glucose Monitoring

Shiny Puthenkalam, BSc

A thesis presented in the fulfilment of the requirements for  
the degree of Doctor of Engineering

April 2021

## COPYRIGHT STATEMENT

'This thesis is the result of the author's original research. It has been composed by the author and has not been previously submitted for examination which has led to the award of a degree.'

'The copyright of this thesis belongs to the author under the terms of the United Kingdom copyright acts as qualified by University of Strathclyde regulation 3.50. Due acknowledgement must always be made of the use of any material contained in, or derived from, this thesis.'

Signed:

Date:



# ABSTRACT

Self-monitoring of blood glucose plays a crucial role in diabetes care. Current methods apply invasive means, which causes pain and discomfort to the people with diabetes. Therefore, non-invasive methods are in high demand. Reverse Iontophoresis (RI) is a technique for non-invasive transdermal glucose monitoring. Thereby, electric current is applied across the skin to extract glucose from the interstitial fluid into a gel-reservoir, where it is measured with an *in situ* glucose sensor. One of the key problems in RI based wearable sensors, is the glucose build-up in the gel-reservoir, which results in poor correlation between the extracted glucose and blood glucose level. Activated Carbon (AC) has excellent adsorption capabilities to organic molecules and could therefore act as a glucose binding agent in the RI devices leading to more accurate glucose readings and ultimately better correlation between the extracted and blood glucose levels.

The overall aim was to study and compare glucose fluxes in *in vitro* RI experiments using the developed AC-integrated electrodes to the standard electrodes without AC. The extracted glucose was quantified using glucose assay kits. Furthermore, this study involved embedding a biosensor in the electrode system to allow direct glucose measurements.

*In vitro* RI experiments using the newly developed AC-integrated electrodes showed increased glucose fluxes of 61% in the high glucose concentration level in the diffusion cell. Besides, the extracted glucose correlated well with increasing glucose concentrations in the diffusion cell ( $R^2=0.90$ ). Thus, confirming AC's suitability as a glucose binding agent in the RI environment.

*In vitro* RI experiments with an integrated mediated enzymatic glucose sensor in the electrode system showed limited success for electrochemical glucose quantification of the extracted glucose. However, a thorough electrochemical characterisation of the developed glucose sensor using cyclic voltammetry was performed, which may provide good basis to make improvements for future glucose sensors.

# ACKNOWLEDGEMENT

First of all, I want to express my gratitude to my supervisor Prof Patricia Connolly for giving me the opportunity to perform this study, her advice and her support. Her expertise in this field is inspiring and has broadened my knowledge.

I want to acknowledge the Engineering and Physical Sciences Research Council (EPSRC) for funding this project and allowing me to conduct this research.

I want to thank all the Biomedical Engineering Department staff for their support and cooperation. I sincerely want to thank Chris, Carol, David, Louise, Brian, Stephen and Katie for their help and advice and introducing me to the laboratory techniques.

Thank you to all my friends in Glasgow, Olivia, Yu-Lin, Ian, Sarah, Caroline and everyone in the Glasgow Geeky Maniac Group. They all made my time in Glasgow very memorable and I will always cherish the great times we had together. I want to thank Shailesh for proof-reading my thesis and his encouragement during my studies.

To all my friends from Austria, Misha, Manu, Carina and Chrissi I value our long-lasting friendships and thank you for visiting me in Glasgow and your support throughout my studies. I also want to thank Miha and Aaron for their motivation.

I sincerely want to thank Paula, my supervisor during my internship at the IAEA for challenging me and giving me the confidence to achieve greater heights.

I want to express my deepest gratitude to my Daddy and Mummy, Joseph and Jancy for their constant support and their love. Thank you for your endless prayers and your patience especially during the writing-up phase. I want to thank my Chechymare, Sherin and Roshan and their husbands Leo and Justin for their advice and support. Also thank you Roshan for proof-reading my thesis. Special thanks to my nephew, Sean and my nieces, Shivonne, Rubaix and Leora for always making me smile. I also want to thank the most loving and caring person I know, my Ammachy. Thank you for being you and for all the care and love you shower upon each and every one in our family. I also want to thank all my aunts, uncles and cousins for their prayers and support. Without my family I could not have completed my studies. I am indebted to all of you.

Above all, I want to thank God for his guidance and blessings throughout my life and making me the person I am today.

## PUBLICATION DETAILS

Training Activity on the Establishment of an SSDL and a QMS. Toroi, Paula and **Puthenkalam, Shiny**, SSDL Newsletter Issue No.69, IAEA 2019

Current calibration capabilities and future needs in the Latin-American and the Caribbean SSDLs. Toroi, Paula, **Puthenkalam, Shiny**, Cruz Suárez, Rodolfo, Abstract from the XI Congreso Regional de Seguridad Radiológica y Nuclear Congreso Regional IRPA, La Habana, Cuba 2018 (*conference paper*)

Establishment of a Secondary Standard Dosimetry Laboratory – A Practical Guide for SSDLs, International Atomic Energy Agency (*in preparation*)

Best poster price at University of Strathclyde’s Research day 2015, “Improvements to Iontophoresis Devices for Transdermal Glucose Monitoring”

# CONTENTS

ABSTRACT .....	iii
ACKNOWLEDGEMENT .....	iv
PUBLICATION DETAILS .....	v
CONTENTS .....	vi
LIST OF FIGURES.....	xii
LIST OF TABLES .....	xxii
LIST OF SYMBOLS AND ABBREVIATIONS.....	xxiv
1 Introduction .....	1
1.1 Field of research.....	1
1.2 Research problem.....	2
1.3 Structure of the thesis.....	3
2 Literature review .....	5
2.1 Anatomy and physiology of the pancreas .....	5
2.2 Blood glucose regulation.....	6
2.2.1 Glucagon .....	7
2.2.2 Insulin.....	8
2.3 Diabetes mellitus.....	10
2.3.1 Type 1 diabetes .....	11
2.3.2 Type 2 diabetes .....	12
2.3.3 Diagnosis of Diabetes .....	13
2.3.4 Treatment options.....	16
2.4 History of glucose monitoring .....	22
2.5 Glucose biosensors for intermittent glucose monitoring .....	26
2.5.1 First generation glucose sensors.....	27

2.5.2	Second generation glucose sensors .....	29
2.5.3	Third generation glucose sensors .....	31
2.5.4	The Clarke Error Grid .....	31
2.5.5	Commercially available blood glucose meters for intermittent glucose measurements .....	32
2.6	Continuous blood glucose monitoring .....	36
2.6.1	Commercially available continuous glucose monitoring systems .....	40
2.7	Problems with self- monitoring of blood glucose .....	44
2.8	Towards non- invasive glucose monitoring .....	44
2.8.1	Currently/ Upcoming commercially available non-invasive glucose monitoring systems .....	45
2.8.2	Glucose monitoring using reverse iontophoresis .....	48
2.9	Factors, which have an impact on RI of human skin for molecular and ionic extraction.....	56
2.9.1	Biological factors .....	56
2.9.2	Operational factors .....	59
2.10	Means to control glucose flux .....	64
2.11	Adsorption.....	67
2.11.1	Adsorbent .....	69
2.11.2	Adsorbate .....	74
2.11.3	Solution chemistry .....	74
2.11.4	Temperature and pressure .....	75
2.12	Summary .....	76
3	Study design .....	78
3.1	Rationale of the study.....	78
3.2	Aim of the investigation.....	79
3.3	Research objectives .....	79
3.4	Research questions .....	80
4	Theory .....	81

4.1	Glucose detection techniques .....	82
4.1.1	Enzyme kinetics .....	82
4.2	Colourimetric assay and optical spectrophotometer .....	84
4.2.1	Limit of detection and Limit of Quantification.....	87
4.3	Electrochemical detection of glucose.....	88
4.3.1	Electrode - electrolyte interface .....	88
4.3.2	Operation of a mediated amperometric glucose sensor .....	94
4.3.3	Three- electrode system and potentiostat.....	95
4.3.4	Cyclic voltammetry .....	98
4.3.5	Reference electrodes .....	103
4.4	Reverse iontophoresis .....	104
4.4.1	Electromigration.....	107
4.4.2	Convection due to electroosmosis.....	108
4.4.3	Diffusion .....	112
4.5	Integrating a glucose binding agent in the sensor in the RI environment	113
4.6	Statistical analysis .....	115
5	Materials and Methods.....	116
5.1.1	Materials.....	117
5.1.2	Chemicals.....	117
5.1.3	Other materials.....	117
5.1.4	Other devices.....	118
5.2	Methods.....	118
5.2.1	Preparation of 0.1 M phosphate buffer solution.....	118
5.2.2	Preparation of 5 mM sodium hydroxide solution .....	118
5.2.3	Preparation of 3% w/v of methylcellulose hydrogel.....	118
5.2.4	Glucose sample preparation for calibration curve .....	119
5.2.5	Glucose sample preparation in gel format .....	120
5.2.6	Preparation of the buffer solution for the diffusion cell .....	120
5.3	Glucose quantification method using glucose assay kits.....	121
5.3.1	Randox Assay Kit .....	121

5.3.2	Sigma Aldrich Assay Kit .....	123
5.4	Investigation of glucose quantification method using the Genova Nano spectrophotometer (GNSPM).....	125
5.5	Fabrication of screen-printed electrodes .....	128
5.5.1	Electrode design .....	128
5.5.2	Preparation of well in electrode to contain skin contact gel .....	129
5.5.3	Procedure for screen printing electrodes:.....	130
5.6	<i>In vitro</i> transdermal extraction via RI .....	132
5.7	Comparison of two artificial membranes in terms of glucose flux .....	139
5.8	Activated carbon experiments.....	140
5.8.1	Preparation of AC for glucose adsorption experiments .....	141
5.8.2	Preliminary glucose adsorption experiments to AC Pellets.....	142
5.8.3	Glucose adsorption experiments to AC foam .....	145
5.8.4	Developing and testing AC foam integrated electrodes.....	148
5.9	Preparation of glucose sensor.....	149
5.9.1	Preliminary CV experiments.....	150
5.9.2	Testing the potential of the screen-printed reference electrodes.....	153
5.9.3	Glucose sensor fabrication .....	153
5.10	Experiments with the glucose sensor .....	155
5.10.1	Scan rate (SR) .....	155
5.10.2	Standard calibration curve for glucose sensors.....	155
5.10.3	RI experiments using glucose sensors with AC and glucose sensors without AC .....	157
6	Results .....	163
6.1	Comparison of two commercially available glucose assay kits.....	165
6.2	Glucose quantification using Genova Nano spectrophotometer .....	168
6.3	Results of the RI experiments .....	171
6.3.1	RI experiments with changing the concentration in the buffer solution in the diffusion cell.....	172

6.3.2	RI experiments with changing duration .....	173
6.3.3	RI experiments comparing glucose flux through two artificial membranes .....	175
6.4	Proof of concept of glucose adsorption to activated carbon (AC).....	177
6.4.1	Adsorption of glucose to AC pellets from solutions.....	177
6.4.2	Adsorption of glucose to AC foam from solutions .....	179
6.4.3	Glucose adsorption to AC foam from glucose gel samples.....	185
6.4.4	Glucose adsorption profile to AC foam over time.....	187
6.4.5	Impact of glucose adsorption to AC to sample volume .....	190
6.4.6	RI experiments with AC foam .....	191
6.5	Preliminary cyclic voltammetry (CV) results .....	193
6.5.1	Study of electrochemical behaviour of FMCA .....	194
6.5.2	Mediator – enzyme interaction in free solution .....	197
6.5.3	Testing screen printed Ag/AgCl reference electrode vs standard 3M Ag/AgCl electrode .....	199
6.6	Electrochemical characterisation of the DMFc - mediated enzymatic glucose sensor	200
6.6.1	Testing different scan rates with glucose sensor.....	200
6.6.2	Establishment of a standard calibration curve with the glucose sensor	203
6.7	<i>In vitro</i> RI experiments with the DMFc - mediated enzymatic glucose sensor with and without AC.....	206
6.7.1	Standard laboratory glucose detection using colorimetric assay and an optical spectrophotometer .....	207
6.7.2	Electrochemical detection of glucose: .....	210
7	Discussion .....	220
7.1	Evaluation of two commercially available glucose assay kits.....	221
7.2	Evaluation of the analysis method for glucose quantification with Genova Nano in comparison to the microplate reader .....	222
7.3	<i>In vitro</i> RI experiments for glucose monitoring.....	225



7.4	Control of glucose flux using AC .....	228
7.5	Electrochemical detection of glucose.....	236
7.5.1	Preliminary experiments .....	236
7.6	Glucose sensors .....	238
7.6.1	Electrochemical characterisation of the DMFc-GOD sensor in the gel environment.....	241
7.6.2	Sensor performance.....	244
7.7	Glucose sensors used <i>in vitro</i> RI experiments using the diffusion cell....	245
7.8	Research limitations .....	249
8	Summary and Conclusion .....	254
	REFERENCES.....	258
	APPENDIX.....	287

# LIST OF FIGURES

Figure 2.1 Anatomy of the pancreas (adapted from Betts et al. 2017) .....	5
Figure 2.2 Blood glucose regulation when homeostasis is disturbed. The green cycle illustrates how the body reacts in case of hyperglycaemia (elevated blood glucose) and the blue cycle is followed in case of hypoglycaemia (low blood glucose). (adapted from Betts et al. 2017) .....	7
Figure 2.3 Example of variation of insulin concentrations over 24 hours' period after a high-starch diet in comparison to a high-sucrose diet. It is observable that insulin level increases after a meal intake so that blood glucose levels decrease. Furthermore, it can be seen that the higher the sugar content in the meal, the more insulin has to be secreted to keep blood glucose levels in normoglycaemia. (adapted from Daly et al. 1998) .....	9
Figure 2.4 Estimated people with diabetes in an age group between 20 years and 79 years in 2019 and the expected number of people with diabetes by 2045 (adapted from International Diabetes Federation, 2019) .....	10
Figure 2.5 Examples of glucose profiles after an OGTT in a person with normoglycaemia (bold violet line), a person with IGT (green line) and a person with diabetes mellitus (bold green line) (adapted from Paulev & Zubieta-Calleja 2004) .....	15
Figure 2.6 Overview of glucose sensing technologies for continuous and intermittent glucose monitoring (adapted from Oliver, Toumazou, Cass, & Johnston, 2009)	21
Figure 2.7 Colour chart to quantify the glucose using Clinitest® Reagent Tablet (adapted from Clarke and Foster, 2012) .....	23
Figure 2.8 First electronic blood glucose reader based on reflectance photometry by Clemens Anton in 1970 (adapted from Mendosa, 2006) .....	24
Figure 2.9 The first glucose analyser Model 23A based on electrochemical glucose detection from YSI (adapted from Newman & Turner 2005).....	27
Figure 2.10 Pen-sized glucose meter and test strip (adapted from Matthews et al. 1987) .....	30
Figure 2.11 Example of Clarke Error grid with Zones A, B, C, D and E indicated (adapted from Oliver et al. 2009).....	32
Figure 2.12 Example of a blood glucose meter with a test strip and a lancing device from Accu-Chek® Aviva (adapted from Healthcare4All, 2014).....	33
Figure 2.13 Example of a glucose test strip Freestyle (adapted from Abbott 2013) .	34
Figure 2.14 Example of intermittent glucose readings of a type 1 diabetes patient over three days. In 14a, three to four glucose readings were taken per day. In comparison in 14b, four to five readings were taken a day. The two circled areas in the bottom pictures indicate states of hypoglycaemia, which were missed in the top scenario due to less frequency of glucose measurement. (adapted from Pickup et al. 2005).....	37

Figure 2.15 Continuous glucose monitoring system from Minimed a) with the sensor attached to body and glucose meter (adapted from Bode et al. 1999) b) Glucose meter on the com-station for data transfer (adapted from Mastrototaro 2000)..	39
Figure 2.16 Medtronic’s CGMS with a) Guardian 3 glucose sensor and Guardian 3 Link transmitter (Medtronic 2019a) b) Minimed 670G pump (Medtronic 2019b)	40
Figure 2.17 Dexcom G6 CGMS with a) the auto-applicator b) the Dexcom G6 glucose sensors with transmitter and c) the receiver in form of a smart phone	41
Figure 2.18 a) Glucose sensor for the Freestyle Libre (front view) (adapted from Abbott Laboratories Limited 2017b) b) Glucose sensor for the FreestyleLlibre (side view) (adapted from Abbott Laboratories Limited 2017b) c) FreeStyle Libre glucose reader (adapted from Abbott Laboratories Limited 2017a) d) Glucose sensor applicator (left) with a new sensor in a package(right) (adapted from Children With Type 1 Diabetes 2016)	42
Figure 2.19 Senseonics’ CGMS with a) the eversense transmitter and b) the implantable glucose sensor	43
Figure 2.20 GlucoWise device from MediWise (adapted from MediWise 2017)	45
Figure 2.21 GlucoTrack device by integrity applications (adapted from Integrity Applications 2017)). It consists of a main unit and a Personal Ear Clipper	46
Figure 2.22 a)Glucosewatch in use (adapted from Tierney et al. 2001) b)Autosensor unit (adapted from Tierney et al. 1999)	50
Figure 2.23 Example of glucose variation at night time measured with the GlucoWatch; The dashed lines indicate the thresholds for hyper- and hypoglycaemia. The arrows show alarms raised by the device because of hypoglycaemia.(adapted from Pickup et al. 2005)	52
Figure 2.24 SugarBeat® patch (red box) applied on an arm (modified from Nemaura 2016)	53
Figure 2.25 Tattoo sensor applied on forearm (adapted from Bandodkar et al. 2014)	54
Figure 2.26 Panda-shaped screen-printed three electrode system with iontophoresis electrodes (adapted from Kim et al., 2018)	55
Figure 2.27 a) Structure of skin with the three layers A) epidermis, B) dermis and C) subcutaneous tissue( (adapted from Kern et al. 2011) b) Layers of epidermis stratum basale (1), the stratum spinosum (2), the stratum granulosum (3), then the stratum lucidum (4) and the stratum corneum (5) (adapted from Betts et al. 2017)	57
Figure 2.28 Stratum corneum with corneocytes in a brick and mortar structure.(adapted from Dhote et al. 2012)	58
Figure 2.29 Routes of penetrations across the skin (adapted from Barry 2002) 1) via sweat pores, 2) through the skin and 3)via hair follicles.	58
Figure 2.30 Schematic view of wearable sensor with AC in the outer layer. There are three mechanisms (migration, diffusion and convection) for molecules and ions	

to be transported from the bulk solution across the membrane. Due the the adsorption capabilities of AC to organic compounds, glucose transport is further ensured across the gel layer towards the electrode vicinity, where the glucose detection takes place. ....	67
Figure 2.31 Types of adsorption isotherms (a) linear, b) Langmuir, c) Freundlich d) high- affinity and e) sigmoidal.....	69
Figure 2.32 Example of surface structure of AC with micropores and mesopores acquired using scanning electron microscopy (adapted from Belhamdi et al., 2016) .....	71
Figure 2.33 Atomic structure from AC (adapted from Harris, Liu and Suenaga, 2008) .....	72
Figure 2.34 Heteroatoms at the edges of the atomic structure of AC (Cárdenas-López et al. 2007).....	73
Figure 4.1 Molecular ring structure of glucose.....	82
Figure 4.2 Changes of the concentration of the enzyme (E), substrate (S), enzyme-substrate (ES) and product (P) over time during an enzymatic reaction (adapted from Bisswanger, 2008).....	83
Figure 4.3 Function of reaction velocity over substrate concentration (adapted from Berk, 2009).....	84
Figure 4.4 Schematic design of the spectrophotometer (adapted from Bibby Scientific 2012) .....	85
Figure 4.5 Example of a calibration curve obtained with LOQ, LOD, linear range, sensitivity indicated (left side) Linear range of the calibration curve starting from the LOQ (right side). (adapted from Eurachem 2014).....	88
Figure 4.6 Schematic representation of redox reaction at an electrode-solution interface. a) Oxidation of species A in a solution b) Reduction of species A in a solution. The molecular orbits (MO) shown in this figure are the lowest vacant molecular orbital and the highest occupied molecular orbital of species A (adapted from Bard and Faulkner, 2001) .....	90
Figure 4.7 Electrode double layer according to Helmholtz model. A metal electrode with a negative charge $q^M$ immersed in a solution with charge $q^S$ .(adapted by Bard and Faulkner, 2001).....	92
Figure 4.8 Redox reaction at electrode surface of a mediated glucose sensor (adapted from Hsueh et al., 2014).....	94
Figure 4.9 Circuit of an basic potentiostat with an electrochemical cell consisting of a three electrode system; opamp A works as a voltage follower and opamp B works as a current to voltage converter (adapted from Allen, Hill and Sanghera, 2011) .....	96
Figure 4.10 Diagram of an opamp .....	96
Figure 4.11 Circuit of a voltage follower.....	97
Figure 4.12 Circuit of a current to voltage follower .....	97
Figure 4.13 Typical excitation signal for cyclic voltammetry .....	99

Figure 4.14 Example of a cyclic voltammogram of a ferrocene derivative: 0.5 mM ferrocenemonocarboxylic acid (Fecp <sub>2</sub> R). Epa and Epc being the anodic peak potential and cathodic peak potential respectively and Ipa and Ipc being the anodic peak current and cathodic peak current respectively;.....	99
Figure 4.15 Schematic view of reverse iontophoresis with the transport mechanisms indicated with the arrows (1= electromigration, 2= electro-osmotic flow and 3= passive diffusion) at each electrode. Three transport mechanism are active on the cathodal side of electrodes, two are active on the anodal side and one is active on the control electrode.....	105
Figure 4.16 Schematic view of the electroosmotic flow in a glass capillary (adapted from Bard and Faulkner, 2001).....	109
Figure 4.17 Contribution of diffusion and electroosmosis to glucose flux across hairless mouse skin over time with an iontophoretic current of 0.32 mA/cm <sup>2</sup> . The glucose concentration in the donor cell was 0.05 M. (adapted from Pikal and Shah, 1990) .....	113
Figure 4.18 Transport mechanisms of molecules and ions from the bulk solution across the membrane to the mediated glucose sensor with AC as a glucose binding agent in the outer layer of the sensor. ....	113
Figure 5.1 Example of a well plate layout with glucose samples for establishing a calibration curve after the incubation of 90 minutes with the Randox reagent. Standard glucose samples with increasing concentrations were dispensed to columns 1 to 9 with five replicas for each concentration (rows A to E) Column 1 is filled with the Control .....	122
Figure 5.2 Potassium electrode design.....	128
Figure 5.3 Electrode with three electrode arrangement and iontophoresis electrode a) Front view b) Back view .....	129
Figure 5.4 a) Potassium electrode design with electrode well b) Three-electrode design with iontophoresis electrode with well .....	130
Figure 5.5 Electrode design for three electrode system with iontophoresis electrode. a) Ag/AgCl ink design for the first layer b) Carbon ink design for second layer c) The final electrode design.....	130
Figure 5.6 Screen mask for the a) Ag/AgCl ink printing and b) Carbon ink printing .....	131
Figure 5.7 Screen printing unit (adapted from Cooper & Cass 2004).....	132
Figure 5.8 Filled diffusion cell with electrodes attached .....	133
Figure 5.9 a) Portable electrochemical analyser and b) Cable which was used to connect the portable electrochemical analyser with electrodes (adapted from (Marco Specialities 2017) .....	134
Figure 5.10 a) Diffusion cell with syringe to fill the buffer solution b) diffusion cell with closed holes using PTFE caps.....	135
Figure 5.11 Experimental setup to perform in vitro transdermal extraction via RI using a diffusion cell and the portable electrochemical analyser .....	137

Figure 5.12 a) AC pellets b) Sheets of AC foam c) Disc-shaped AC foams .....	141
Figure 5.13 Experimental setup for preliminary glucose adsorption experiments to AC pellets .....	143
Figure 5.14 Well- plate arrangement to measure the glucose diffusion time profile .....	147
Figure 5.15 Potassium electrodes with 16 holes drilled a) 3D view of electrode b) Front view of electrode .....	149
Figure 5.16 Experimental setup for performing cyclic voltammetry experiments. a) Final electrode setup with a three-electrode system with a solution filled connected to the ribbon cable b) The other end of the ribbon cable connected to an alligator cable via wires c) the applied 3-terminal cell setup was used for the experiments and d) full experimental setup .....	151
Figure 5.17 Example voltammogram of the standard calibration curve experiments from a standard gel sample with a glucose concentration of 62 $\mu\text{M}$ . The graph in the black colour shows the result of the Side A of the electrode and the red coloured graph is the result of Side B of the electrode. ....	156
Figure 5.18 Measurement setup for RI experiments using glucose sensors with and without AC foam. EI 1 is connected to the computer and was used to perform CV to ensure sensor performance. EA 1 was responsible to apply the iontophoretic current between E1 and E2 electrodes and also to take "Pre RI" and "After RI" cyclic voltammograms of the E1 electrode. EA 2 was responsible to take "Pre-RI" and "After-RI" cyclic voltammograms of the E2 and C electrodes. ....	158
Figure 5.19 Electrode with well attached and holes drilled .....	159
Figure 5.20 Photographed AC integrated glucose sensor preparation for RI experiment: a) Electrode with 11 holes punched; b) Electrode with well attached (front); c) Electrode with well attached (back); d) Electrode with AC foam attached (front); e) Electrode with AC foam attached and secured with an acetate sheet (back) .....	159
Figure 5.21 Pre-testing of sensors before using them for the RI experiment. The graph in the black colour shows the result of the Side A of the electrode and the red coloured graph is the result of Side B of the electrode. ....	160
Figure 6.1a Calibration curve of glucose gel samples with increasing glucose concentrations using the Radox reagent with a colorimetric assay. The error bars represent the standard deviation (n=5).....	166
Figure 6.1b Magnification of the glucose calibration curve shown in Figure 6.1a of glucose gel samples in the concentration range of interest from 3.51 $\mu\text{M}$ to 56.25 $\mu\text{M}$ .....	166
Figure 6.2a Calibration curve of glucose samples in gel with increasing glucose concentrations using the Sigma Aldrich reagent with a colorimetric assay. The error bars represent the standard deviation (n=5) .....	167

Figure 6.2b Magnification of the glucose calibration curve shown in Figure 6.2a of glucose gel samples in the concentration range of interest from 0.22 $\mu\text{M}$ to 28.13 $\mu\text{M}$ .....	167
Figure 6.3a Calibration curve of glucose samples in gel format with increasing glucose concentrations using the Radox reagent with a colorimetric assay in a glucose solution to gel ratio of 1: 4. ....	169
Figure 6.3b Magnification of the glucose calibration curve shown in Figure 6.3a of glucose gel samples in the concentration range of interest from 2.93 $\mu\text{M}$ to 46.88 $\mu\text{M}$ .....	169
Figure 6.4a Calibration curve of glucose samples in gel format in a glucose solution to gel ratio of 1 to 4 with increasing glucose concentrations using the Radox reagent acquired using the Genova Nano.....	170
Figure 6.4b Magnification of the glucose calibration curve shown in Figure 6.4a of glucose gel samples in the concentration range of interest from 11.72 $\mu\text{M}$ to 46.88 $\mu\text{M}$ .....	170
Figure 6.5 Quantification of the glucose concentration of three samples with known glucose concentrations (204 $\mu\text{M}$ and 408 $\mu\text{M}$ ) using the calibration curve acquired (1) with the microplate reader (orange bars) and (2) with the Genova Nano (blue bars). The green dashed lines indicate the actual glucose concentration in Sample 1 and Sample 2. n=3 .....	171
Figure 6.6 Results of glucose extraction after in vitro RI experiments on the diffusion cell for a duration of 60 minutes with switching polarities every 15 minutes. The diffusion cell was prepared with a concentration of 5 mM (red bars) and 20 mM (yellow bars) glucose in the buffer solution. The glucose concentrations from the extracted gel were calculated using the equation from the calibration curve. C indicates the control electrode, E1 indicates the initial anodic iontophoretic electrode and E2 indicates the initial cathodic electrode.n=3 .....	172
Figure 6.7 In vitro RI experiments with a glucose concentration of 5 mM in the buffer solution at three different RI durations: a) with 15 minutes of direct current b) 30 minutes of direct current and c) 60 minutes with switching polarities every 15 minutes . n=3 .....	174
Figure 6.8 Glucose concentrations in each electrode (C, E1 and E2) from the extracted gel across the Vitro-Skin® (blue bars) with n=6 and the Spectrapore membrane (orange bars) with n=3. The diffusion cell was prepared with a 20 mM glucose HEPES buffer solution and the measurement cycle was 60 minutes long with switching polarities every 15 minutes. The glucose concentrations from the extracted gel were calculated using the equation from the calibration curve. .	176
Figure 6.9 Glucose measured in the remaining solution after an incubation time of 1 hour of the standard sample with a glucose concentration of 500 $\mu\text{M}$ with AC pellets (green bar) (n=38) in comparison to the standard concentration of 500 $\mu\text{M}$ (blue bar) ( n=9). The error bars represent the standard deviation.....	178

Figure 6.10 Examples of disc- shaped AC foam, which were used for the adsorption experiments .....	180
Figure 6.11 Glucose measured in the remaining solution after an incubation time of 1 hour of the standard sample with a glucose concentration of 500 $\mu$ M with one unit of AC foam (orange bar) (n=61) in comparison with the standard solutions (blue bar) (n=17) and the results shown in Figure 6.10, the remaining glucose concentration after an incubation time of 1 hour of the standard sample with a glucose concentration of 500 $\mu$ M with AC pellets. The error bars represent the standard deviation. ....	180
Figure 6.12 Average initial dry weight of used AC pellets (green bar) with n=78 and AC foam (orange bar) with n=130. The error bars represent the standard deviation. ....	181
Figure 6.13 Increase of weight of the AC pellet (green bar) with n=38 and AC foam (orange bar) with n=28 after incubation with the glucose sample with a concentration of 500 $\mu$ M . Th error bars represent the standard deviation. ....	182
Figure 6.14 Initial glucose concentration in the glucose sample versus the remaining glucose concentration after an incubation time of 60 minutes with one unit of AC foam (orange dots) and two units of AC foam (red triangles). The error bars represent the standard deviation.....	184
Figure 6.15 Remaining glucose concentration after the incubation of the sample with one unit of AC foam (orange dots) and two units of AC foam (red triangles) for 60 minutes in relationship with the amount of glucose adsorbed by one gram of AC foam.....	185
Figure 6.16 Initial glucose concentration in the glucose gel sample versus the remaining glucose concentration after an incubation time of 60 minutes with one unit of AC foam. The error bars represent the standard deviation.....	186
Figure 6.17 Remaining gel glucose concentration after the incubation of the sample with one unit of AC foam for 60 minutes in relationship with the amount of glucose adsorbed by one gram of AC foam. ....	187
Figure 6.18 Adsorption time profile of a 1000 $\mu$ M glucose sample on AC foam. .	188
Figure 6.19 Adsorption time profile of a 900 $\mu$ M glucose sample on AC foam. ....	189
Figure 6.20 Remaining sample volume of the glucose solution samples with n=3 (blue triangles) and of the glucose gel samples with n=3 (orange dots) after the incubation with AC foam over a time period of 80 minutes.....	191
Figure 6.21 Glucose concentrations in each electrode (C, E1 and E2) from the extracted gel across the Spectrapore membrane using electrodes without AC (blue bars) and with AC (yellow bars). The diffusion cell was prepared with a 20 mM glucose HEPES buffer solution and the measurement cycle was 60 minutes long with switching polarities every 15 minutes. The glucose concentrations from the extracted gel were calculated using the equation from the calibration curve. The error bars represent the standard error. n=7. ....	192



Figure 6.22 CV of 0.5 mM FMCA in PBS with ethanol and sodium perchlorate at different scan rates 10 mV/s (blue), 50 mV/s (red) and 100 mV/s (green).....	194
Figure 6.23 CV of 0.5 mM FMCA in PBS and sodium perchlorate with applied tangent indicating the extrapolation of the baseline current to identify capacitive current. ....	196
Figure 6.24 Relationship between scan rate and peak current of the 0.5 mM FMCA in PBS and sodium perchlorate .....	196
Figure 6.25 a) CV of FMCA in PBS buffer with 50 mM glucose (blue) and b) upon addition of 10.9 $\mu$ M of GOD (orange) at a scan rate of 1 mV/s with diffusion current of FMCA( $I_{pa}$ ) and the catalytic current ( $I_{cc}$ ) upon the addition of GOD .....	198
Figure 6.26 Screen printed electrodes (SPE) vs standard electrode (SE) in 0.1 M phosphate buffer solution and 3% w/v of methylcellulose gel .....	199
Figure 6.27 CV of Side A of the glucose sensor at a glucose concentration of 62 $\mu$ M at different scan rates .....	201
Figure 6.28 Peak current vs the square root of the scan rate. Peak current acquired using the glucose sensor tested in a glucose gel sample with a concentration of 62 $\mu$ M.....	202
Figure 6.29 CV obtained from Side A of the glucose sensor during establishment of the calibration curve.....	203
Figure 6.30 Voltammogram of a standard gel sample with a glucose concentration of 62 $\mu$ M obtained from side A of the glucose sensor, which has the immobilised enzyme on the working electrode (blue) in comparison to side B of the sensor, which has no enzyme on the working electrode (grey); both voltammograms were taken at a scan rate of 60 mV/s .....	204
Figure 6.31 Calibration curve established using electrochemical detection of glucose using biosensors. The ratio of the current value obtained at a voltage of 0.14 V at side A of the glucose sensor to the current value obtained at a voltage of 0.14 V at side B of the glucose sensor, Side A of the sensor is immobilised with the enzyme; Side B of the sensor has no enzyme coating and is responsible to detect any background current.n=3 .....	205
Figure 6.32 Measurement setup for RI experiments using glucose sensors with and without AC foam. EI 1 is connected to the computer and was used to perform CV to ensure sensor performance. EA 1 was responsible to apply the iontophoretic current between E1 and E2 electrodes and also to take CV from the E1 electrode. The EA2 took CV measurements from the E2 electrode and from the control electrode .....	206
Figure 6.33 Glucose concentrations quantified using the standard method using glucose assay kit and an optical spectrophotometer. The amount of glucose extracted in each electrode (C, E1 and E2) from the extracted gel across the Spectrapore membrane using without the AC- integrated glucose sensors). The diffusion cell was prepared with a 0 mM (blue bars), 5 mM (orange bars), 10 mM	

(grey bars), 15 mM (yellow bars) and 20 mM (green bars) glucose HEPES buffer solution and the measurement cycle was 60 minutes long with switching polarities every 15 minutes. The glucose concentrations from the extracted gel were calculated using the equation from the gel calibration curve. The error bars represent the standard error. n=3.....	207
Figure 6.34 Glucose concentrations quantified using the standard method using glucose assay kit and an optical spectrophotometer. The amount of glucose in each electrode (C, E1 and E2) from the extracted gel across the Spectrapore membrane using the AC- integrated glucose sensors. The diffusion cell was prepared with a 0 mM (blue bars), 5 mM (orange bars), 10 mM (grey bars), 15 mM (yellow bars) and 20 mM (green bars) )glucose HEPES buffer solution and the measurement cycle was 60 minutes long with switching polarities every 15 minutes. The glucose concentrations from the extracted gel were calculated using the equation from the gel calibration curve. The error bars represent the standard error. n=3.....	208
Figure 6.35 Relationship between extracted glucose at the E1 and E2 electrode and the glucose concentration in the diffusion cell.....	210
Figure 6.36 Examples of after RI voltammograms obtained from the glucose sensors without AC, which were applied on the in vitro cell prepared with a 5mM glucose concentration in the buffer solution a) left- E1 electrode-Side A, right - E1 electrode-Side B b) left- E2 electrode-Side A, right - E2 electrode-Side B and c) left- C electrode-Side A, right - C electrode-Side B.....	212
Figure 6.37 Cyclic voltammogram from side A of the E1 electrode of the AC-integrated glucose sensor after the application of RI. The sensors was applied on the in vitro cell prepared with a 20 mM glucose concentration in the diffusion cell. The applied tangent indicates the extrapolation of the baseline current to identify capacitive current.....	214
Figure 6.38 Cyclic voltammogram from side A of the E1 electrode of the AC-integrated glucose sensor after the application of RI. The sensor was applied on the in vitro cell prepared with a 15 mM glucose concentration in the diffusion cell. The applied tangent indicates the extrapolation of the baseline current to identify capacitive current.....	215
Figure 6.39 Electrochemical analysis of the extracted glucose via RI using the glucose sensors a) without AC and b) with AC. The ratio of current obtained at side A of the E1 electrode to side B of the E1 electrode of the glucose sensor without AC of each electrode (C, E1 and E2) at a potential of 0.082 V. The error bars represent the standard error. The diffusion cell was prepared with a 0 mM (blue bars), 5 mM (orange bars), 10 mM (grey bars), 15 mM (yellow bars) and 20 mM (green bars) glucose HEPES buffer solution and the measurement cycle was 60 minutes long with switching polarities every 15 minutes.....	216
Figure 6.40 Cyclic voltammogram from side A of the E1 electrode of the glucose sensor without AC after the application of RI. The sensor was applied on the in	

vitro cell prepared with a 5 mM glucose concentration in the diffusion cell. The applied tangent indicating the extrapolation of the baseline current to identify capacitive current. .... 217

Figure 6.41 Electrochemical analysis of the extracted glucose via RI using the glucose sensors a) without AC and b) with AC. The ratio of current obtained at side A of the E1 electrode to side B of the E1 electrode of the glucose sensor without AC of each electrode (C, E1 and E2) at a potential of 0.306 V. The error bars represent the standard error. The diffusion cell was prepared with a 0 mM (blue bars), 5 mM (orange bars), 10 mM (grey bars), 15 mM (yellow bars) and 20 mM (green bars) glucose HEPES buffer solution and the measurement cycle was 60 minutes long with switching polarities every 15 minutes..... 218

# LIST OF TABLES

Table 2.1 Criteria for the diagnosis of diabetes mellitus, impaired fasting glucose and impaired glucose tolerances in the venous blood plasma (American Diabetes Association, 2013).....	13
Table 2.2 Selected currently available glucose meters for intermittent glucose monitoring for self-testing.....	34
Table 2.3 Technical details of selected commercially available glucose sensors for continuous glucose monitoring .....	43
Table 4.1 Mediators with redox potentials from literature .....	103
Table 5.1 Preparation of the standard glucose solution samples .....	119
Table 5.2 Preparation of standard glucose gel samples .....	120
Table 5.3 Required quantities of solutes for making up 500 mL of the buffer solution .....	120
Table 5.4 Standard glucose concentration range for different gel to glucose solution ratios.....	126
Table 5.5 Electrode area of the final device exposed to the test solution .....	129
Table 5.6 Pin configuration of the male IDC ribbon cable connector of the portable electrochemical analyser .....	135
Table 5.7 Overview of testing conditions of 1) Variation of the glucose concentration in the buffer solution .....	138
Table 5.8 Overview of testing conditions of 2) Changing the duration of RI .....	138
Table 5.9 Overview of testing conditions of 5.7 Comparison of two artificial membranes in terms of glucose flux .....	140
Table 6.1 Summary of LOD, LOQ, upper limit of the linear calibration curve, equation of the linear relation using the Randox assay kit and the Sigma Aldrich Assay kit .....	168
Table 6.2 Transdermal flux of glucose to electrodes after RI of 60 minutes with switching polarities with a glucose concentration of a) 5 mM and b) 20 mM of glucose in the diffusion cell .....	173
Table 6.3 Calculated transdermal flux of glucose across each electrode after a) 15 minutes of RI, b) 30 minutes of RI and c) 60 minutes of RI with switching polarities with a glucose concentration of 5 mM of glucose in the diffusion cell .....	175
Table 6.4 Transdermal flux of glucose to electrodes across Spectrapore membrane and Vitro-Skin® after 60 minutes of RI with switching polarities with a glucose concentration of 20 mM of glucose in the diffusion cell .....	177
Table 6.5 Calculated glucose flux across glucose solution and glucose gel sample to AC foam.....	190
Table 6.6 Transdermal fluxes across the Spectrapore membrane using sensor without AC foam and with AC foam .....	193
Table 6.7 Parameters used to calculate the glucose diffusion coefficient of FMCA197	

Table 6.8 Transdermal fluxes across the Spectrapore membrane using sensor without AC foam and with AC foam and the 0 mM glucose diffusion cell.....	209
Table 7.1 Details of selected glucose sensors used for glucose quantification sampled by RI.....	239

# LIST OF SYMBOLS AND ABBREVIATIONS

## Symbols

$\epsilon_0$	Permittivity of free space
A	Absorbance
C	Coulombs
c	Molar concentration
D	Diffusion coefficient
Da	Dalton
$e^-$	Electron
$E^0$	Standard reduction potential
$E_{\text{lambda}}$	Switching potential
$E_{\text{pa}}$	Anodic peak potential
$E_{\text{pc}}$	Cathodic peak potential
F	Faraday's constant
I	Current
$I_{\text{pa}}$	Anodic peak current
$I_{\text{pc}}$	Cathodic peak current
$J_i$	Flux of species i
k	Boltzmann constant
$K_M$	Michaelis constant
$\lambda$	Wavelength
l	Path length
n	Number of electrons
Q	Charge
R	Gas constant
T	Temperature
$t_i$	Transport number of species i
V	Voltage
V	Reaction Velocity
$V_{\text{MAX}}$	Maximum Reaction Velocity
$z_i$	Charge number of species i
$\epsilon$	Molar adsorptions coefficient
$\epsilon$	Permittivity of the medium
$\eta$	Viscosity of the solution
$\mu_i$	Mobility of ion i
$\xi$	Zeta potential

## Abbreviations

AC	Activated Carbon
ACF	Activated Carbon Fibers
Ag/AgCl	Silver/ Silver Chloride
ANOVA	Analysis of Variance

ARM	Ames Reflectance Meter
ATP	Adenosintriphosphate
BET	Brunauer-Emmet-Teller
C- electrode	Control chamber in RI experiments
CDI	Carbodiimide
CE	Counter Electrode
CGMS	Continuous Glucose Monitoring Systems
Con A	Concanavalin A
CV	Cyclic Voltammetry
DMFc	Dimethylferrocene
DNA	Desoxyribonucleic acid
E	Enzyme
E. coli	Escherichia coli
E1-electrode	Initial anodal chamber in RI experiments
E2-electrode	Initial cathodal chamber in RI experiments
EDL	Electrical Double Layer
EOF	Electroosmotic Flow
ES	Enzyme-Substrate complex
FAD	Flavin Adenine Dinucleotide
Fecp <sub>2</sub> R	Ferrocene
FFC	Flexible Flat Cable
FMCA	Ferrocenemonocarboxylic acid
G6PDH	Glucose-6-phosphate dehydrogenase
GAC	Granular Activated Carbon
GDH	Glucose Dehydrogenase
GGBP	Glucose/Galactose Binding Protein
GNSPM	Genova Nano Spectrophotometer
GOD	Glucose Oxidase
HbA1c	Glycated Haemoglobin
HEPES	4-(2-hydroxyethyl)-1-piperazineethanesulfonic acid
HPLC	High- Performance Liquid Chromatography
IDC	Insulation- Displacement Contact
IDF	International Diabetes Federation
IFG	Impaired Fasting Glycaemia
IGT	Impaired Glucose Tolerances
IHP	Inner Helmholtz Plane
ISF	Interstitial Fluid
ISO	International Organisation for Standardisation
IUPAC	International Union of Pure and Applied Chemistry
KCl	Potassium Chloride
LOD	Limit of Detection
LOQ	Limit of Quantification
MARD	Mean Absolute Relative Difference
MO	Molecular Orbit
MSC	Mesenchymal Stem Cell
MW	Molecular Weight

NaCl	Sodium Chloride
NAD	Nicotinamide Adenine Dinucleotide
OGTT	Oral Glucose Tolerance Test
OHP	Outer Helmholtz Plane
P	Product
PMMA	Polymethylmethacrylate
PPQ	Pyrrloquinoline Quinone
PQ	Phenanthroline Quinone
PTFE	Polytetrafluoroethylene
REDOX	Reduction-Oxidation
REF	Reference Electrode
RI	Reverse Iontophoresis
RNA	Ribonucleic acid
S	Substrate
SCE	Standard Calomel Electrode
SEM	Standard Error of Mean
SHE	Standard Hydrogen Electrode
SMBG	Self-Monitoring of Blood Glucose
SPF	Sun Protection Factor
SR	Scan rate
TANCN	Triazacylcononane chelate
TCNQ	Tetracyanoquinodimethane
TTF	Tetrathiafulvalene
UVA	Ultraviolet A
WE	Working Electrode
WHO	World Health Organisation
YSI	Young Spring Instrument



# 1 Introduction

## 1.1 Field of research

In 2019, estimated 463 million people worldwide were suffering from diabetes mellitus, commonly referred to as diabetes (International Diabetes Federation, 2019b). 1 in 11 persons is affected by the disease. It is a chronic and serious disease where the blood glucose regulation in the body is impaired. The disease is increasing at an unprecedented pace and it is expected to rise to 700 million globally by 2045 (International Diabetes Federation, 2019b).

There are mainly two types of diabetes, type 1 diabetes and type 2 diabetes. Type 1 diabetes, which was previously also referred to as insulin-dependent diabetes, occurs because of the destruction of the insulin producing islet cells of Langerhans in the pancreas due to an autoimmune disorder. Type 2 diabetes is developed by inadequate insulin production; either the body does not produce enough insulin, or the produced insulin is impaired and cannot enter the cell, which is also called insulin resistance. Untreated diabetes can cause macrovascular and microvascular complications, kidney disease, eye disease, amputation, depression, neuropathy, sexual dysfunction and dementia (Diabetes UK, 2016).

It was shown that tight glycaemic control in the body can delay the onset and progression of some of such long term complications (The Diabetes Control and Complications Trial Research Group, 1993; UK Prospective Diabetes Study (UKPDS) Group, 1998).

Self- monitoring of blood glucose (SMBG) helps to monitor and control blood glucose levels and has become an essential part of diabetes management. There are intermittent and continuous glucose monitoring systems. For intermittent blood glucose measurements, people with diabetes need to prick their fingers several times a day. Blood will be collected with the lancing device and lancets and via a capillary action, it will be drawn to a test strip. Glucose is measured based on an enzymatic reaction and the glucose value will be shown on the blood glucose meter.

Continuous glucose monitoring systems (CGMS) offer tighter control of glycaemic levels as they acquire glucose measurements in a certain interval automatically. Most

of the continuous glucose monitoring systems nowadays consist of an implantable subcutaneous glucose sensor, which measures the glucose, and a transmitter which transfers the measured glucose values to a receiver such as a smartphone to monitor the activity.

## 1.2 Research problem

Self- monitoring of blood glucose plays a crucial role in diabetes care. There are intermittent and continuous glucose monitoring systems. Intermittent systems provide discrete glucose measurements where the user decides the timepoints of the test and performs the measurement, whereas continuous systems are able to automatically provide glucose measurements in a certain time interval without any participation from the user. Both systems apply invasive means to measure blood glucose levels. The problem is that this method causes pain and discomfort to the patients, which is one of the reasons for patients' non-compliance to treatment plans from the care giver. Non-invasive glucose monitoring techniques are an emerging field of study, which can overcome this problem and improve the quality of life of people with diabetes.

Reverse Iontophoresis (RI) has been proposed as means of non-invasive, transdermal diagnostics for the monitoring of small circulating molecules and ions in the blood. In this technique, electric current is applied across the skin to extract a substance of interest. Devices based on RI have the potential to be used for blood glucose level monitoring as part of diabetes care. However, RI has not yet gained long term acceptance amongst healthcare systems. One reason for this is the poorly controlled glucose once it leaves the skin. The Medical Diagnostics and Wearables Group at Strathclyde has a patent on methods to control glucose by the use of different binding agent such as activated carbon (AC) (Connolly, 2014).

The aim of this project was to test the concept of glucose adsorption to AC and evaluate the suitability of AC for better controlled and improved glucose flux in wearable sensors flux within iontophoresis devices due to its ability to bind organic compounds. In addition, this study involved integrating an electrochemical glucose sensor in the iontophoresis device to allow direct glucose measurement.

## 1.3 Structure of the thesis

This thesis is structured as following:

**Chapter 2 Literature review:** Chapter 2 starts with the anatomy and physiology of the pancreas, followed by the types of diabetes mellitus, diagnosis and treatment options. The focus lies in self- monitoring of blood glucose as means of diabetes management. It begins with the history of glucose monitoring for people with diabetes and reviews existing literature about the development of glucose sensors for intermittent and continuous glucose monitoring system with currently available devices in the market. It then discusses current studies on non- invasive methods for glucose monitoring focussing on RI. Biological and operational factors are described, which have an impact on RI on human skin for molecular and ionic extraction. In the final section of the chapter, fundamentals of adsorptions and parameters, which have an influence on the adsorption process are explained.

**Chapter 3 Study design:** Chapter 3 elucidates rationale of the study, followed by the research objectives and research questions.

**Chapter 4 Theory:** Chapter 4 introduces theory on glucose detection and quantification methods via standard laboratory techniques using colorimetric assay and optical spectrophotometers. In addition, electrochemical glucose detection methods are also explained. It covers fundamental electrochemical processes on the electrode - electrolyte interface and the operation of an electrochemical glucose sensor. Moreover, the principles of cyclic voltammetry, which is an electroanalytical technique applied for electrochemical glucose detection, is explained. The final section of this chapter describes the principles of RI and the transport mechanisms involved during RI.

**Chapter 5 Materials and Methodology** Chapter 5 begins with the chemicals and materials which were used for this project, followed by the standard procedures for the preparation of basic buffers and gel. The experimental procedure to perform *in vitro* RI experiments using a diffusion cell is explained, followed by the glucose quantification method of the extracted glucose using assay kits. Subsequently, the experimental procedure to test glucose adsorption to AC and to evaluate the suitability of AC to act as a glucose binding agent in the RI environment is depicted. The fabrication of the glucose sensor is described, followed by the experiments conducted

to electrochemically characterise the sensor and to test its suitability to electrochemically quantify the extracted glucose via RI.

**Chapter 6 Results:** Chapter 6 starts with the results of experiments conducted to optimise the *in vitro* RI experimental setup and glucose analysis method. Glucose fluxes during *in vitro* RI experiments and the findings of the glucose adsorption to AC studies are reported. Glucose fluxes during RI experiments with the newly designed AC- integrated electrodes are shown. The electrochemical characteristics of the developed mediated enzymatic glucose sensor is presented. Finally, the outcome of the electrochemical glucose quantification of the glucose extracted via RI using the glucose sensor is shown.

**Chapter 7 Discussion** Chapter 7 interprets the outcomes reported in the chapter 6. Furthermore, it discusses research limitations and gives recommendation for future work.

**Chapter 8 Summary and Conclusion** Chapter 8 provides a summary of the findings of this study in reference to the raised research questions in chapter 3 and an overall conclusion.

## 2 Literature review

### 2.1 Anatomy and physiology of the pancreas

The human pancreas is a slender and oblong organ and can be located transversely posterior to the stomach (Figure 2.1) (Betts et al., 2017a). The pancreas has exocrine as well as endocrine functions. As an exocrine organ, it has the responsibility to produce digestive enzymes and to secret them to the small intestine via the pancreatic duct. These digestive enzymes are produced by the acinar cells in the pancreas.

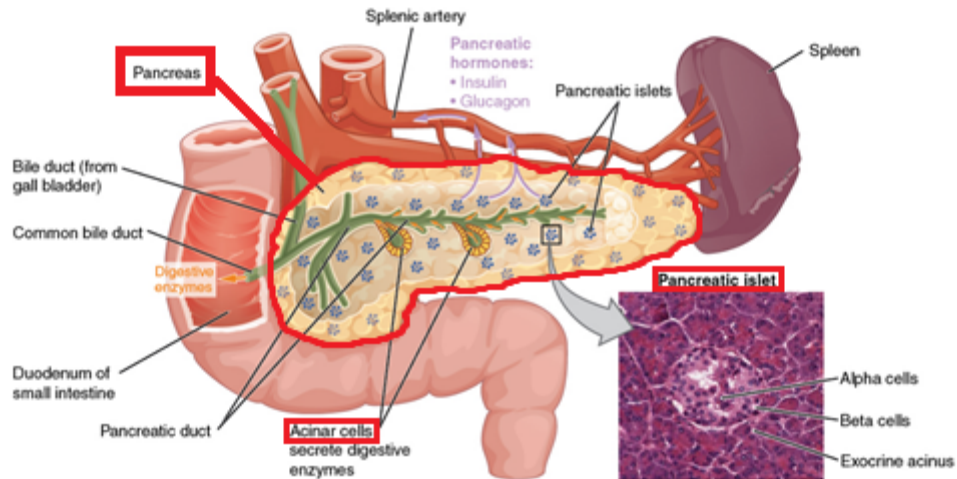


Figure 2.1 Anatomy of the pancreas (adapted from Betts et al., 2017a)

The endocrine function of the pancreas involves secreting the following hormones: insulin, glucagon, somatostatin and polypeptides directly to the blood stream. These hormones are produced by pancreatic islets (also called as islet of Langerhans).

There are four types of cells in the islets:

- **Alpha cells:** 20% of each islet consists of alpha cells. They have the responsibility to produce glucagon, the hormone which is required to increase blood glucose levels.
- **Beta cells:** 75% of each islet is comprised of beta cells. This type of the pancreatic islets forms the insulin hormone, which has the ability to decrease the blood glucose levels.
- **Delta cells:** 4% of each islet accounts for delta cells. They secrete the hormone somatostatin. This hormone is also produced by the hypothalamus, the stomach and the intestines and can inhibit secretion of glucagon and insulin.

- **Pancreatic polypeptide cells:** 1% of each islet includes polypeptide cells. They produce the pancreatic polypeptide hormone, which can regulate the endocrine and exocrine secretions of the pancreas. (Betts et al., 2017a)

## 2.2 Blood glucose regulation

Glucose is the main energy source for all the organs and cells in the body. The prime uptake of glucose is by the consumption of carbohydrates from food and drinks. Glucose can be derived by breaking down carbohydrates and can be stored by the liver and muscles (in the form of glycogen) or by adipose tissue once it is converted to triglycerides. The hormones insulin and glucagon play a major role in the glycaemic control in the body. The storage and utilisation of glucose are regulated by these hormones. The normal range of blood glucose levels in a healthy body is between 3.9 and 6.1 mmol/L (70 and 110 mg/dl respectively), this state is referred to as homeostasis or normoglycaemia. The unit of blood glucose is mmol/L in the United Kingdom; however the glucose is measured in mg/dL in the USA and continental Europe (Diabetes.co.uk, 2017a). The conversion factor between the units is 18; hence 1 mmol/L equals to 18 mg/dL.

Receptors on the pancreas can detect blood glucose levels and secrete the blood glucose regulating hormones (either insulin or glucagon) to maintain homeostasis. The production as well as the effects of insulin and glucagon are crucial for the regulation of blood glucose concentration. These hormones ensure that the blood glucose level in the body is in homeostasis. Hence, if the homeostasis is disturbed, they will act until it is restored (Martini et al., 2014a). Figure 2.2 illustrates how the body reacts in case of disturbance of the homeostasis.

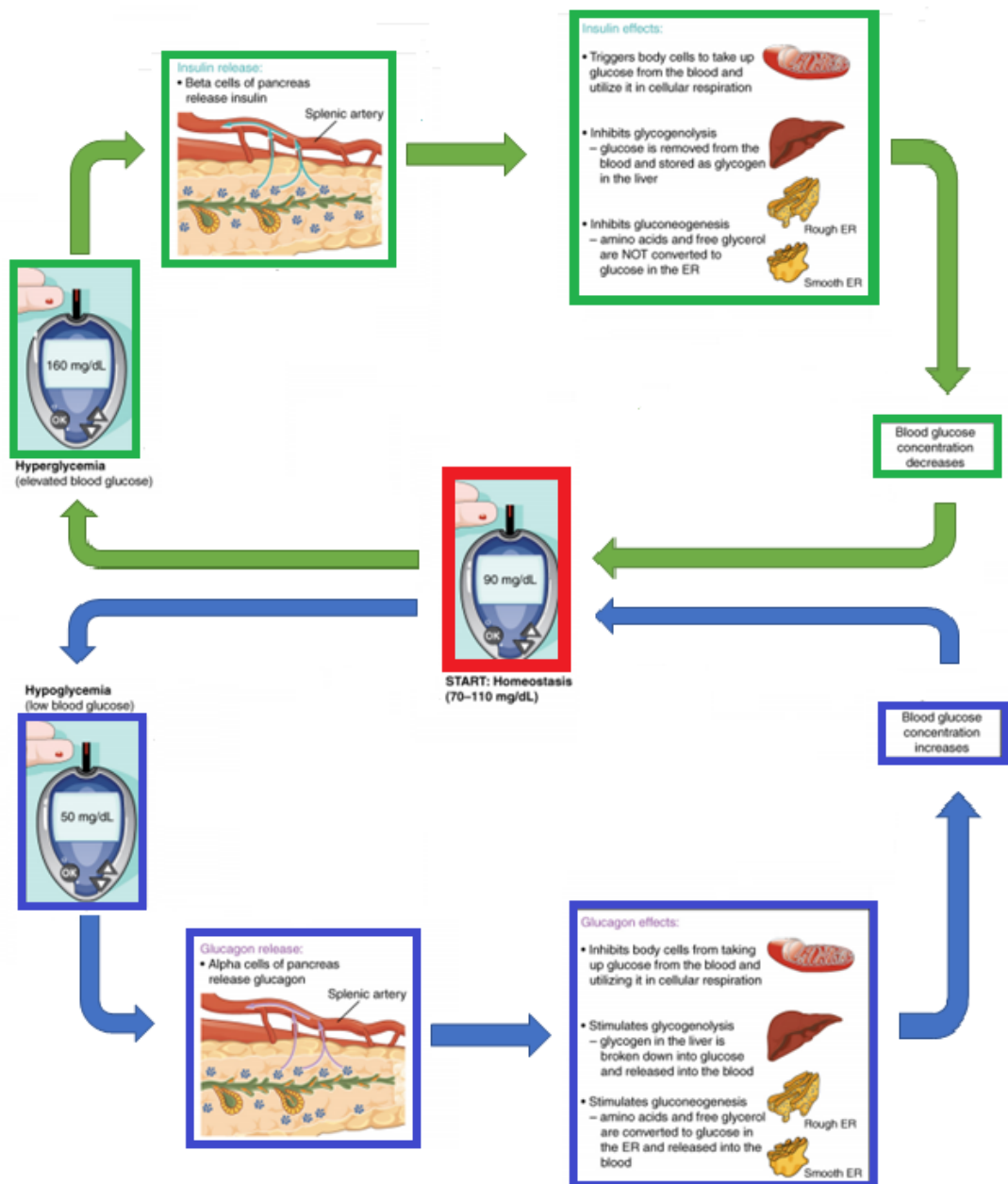


Figure 2.2 Blood glucose regulation when homeostasis is disturbed. The green cycle illustrates how the body reacts in case of hyperglycaemia (elevated blood glucose) and the blue cycle is followed in case of hypoglycaemia (low blood glucose). (adapted from Betts et al., 2017a)

## 2.2.1 Glucagon

If blood glucose concentrations are below normal levels (below 3.9 mmol/L or 70 mg/dl), the alpha cells of the pancreatic islets secrete glucagon. The secretion of glucagon triggers a variety of mechanisms, which in effect lead to an increase of blood glucose concentrations.

Glucagon initiates following mechanisms:

- Glucagon stimulates the breakdown of glycogen to glucose in skeletal muscle and liver cells. The glucose obtained is directly released to the blood stream.
- The glucose production in the liver is referred as gluconeogenesis. Thereby, the liver cells absorb amino acids and glycerol from the bloodstream and convert them into glucose. Glucagon stimulates gluconeogenesis to increase blood glucose levels.
- Cells need glucose for their cellular respiration and therefore take up glucose from the blood stream. In case of hypoglycaemia, glucagon inhibits this process.

A negative feedback mechanism regulates the release of glucagon: As blood glucose levels increase, the less glucagon is secreted and vice versa.

### 2.2.2 Insulin

If blood glucose concentrations exceed normal levels (above 6.1 mmol/L or 110 mg/dl), the beta cells of the pancreatic islets secrete insulin. When food reaches the intestine, the hormone called, glucose-dependent insulinotropic peptide, gets released, which is the initial trigger for producing and secreting insulin from the beta cells. More insulin is secreted, once nutrients from the food will be absorbed and consequently the blood glucose level increases.

Insulin prompts following mechanisms, which in effect result in decrease of blood glucose levels.

- Insulin induces an accelerating glucose uptake from all target cells by increasing the number of glucose transport proteins in the plasma membranes for insulin dependent cell.

Some type of cells require insulin to take up glucose from the blood stream. These cells are called insulin dependent and have insulin receptors in their plasma membranes, for example, skeletal muscle cells and adipose cells. Insulin-dependent cells need glucose transporter proteins to move glucose from the cell membrane into the cell inner. This movement is triggered by



insulin and carried out by a process called facilitated diffusion which is a carrier- mediated transport mechanism, that can passively transport glucose across the membrane down the concentration gradient without the need of adenosine triphosphate (ATP).

Cells, which lack of insulin receptors, are called insulin independent. These cells are able to absorb and utilise glucose without having insulin receptors. Red blood cells, cells in brain, kidney, liver and cells in the lining of the digestive tract are insulin independent.

- Insulin stimulates increased glycogen formation. If there is an excess glucose entering skeletal muscles and liver cells, an increased conversion of glucose to glycogen occurs in the liver.
- Insulin inhibits gluconeogenesis.

A negative feedback mechanism regulates the release of insulin: As glucose levels decrease in blood, the less insulin is secreted and vice a versa. Figure 2.3 shows an example of insulin variations due to meal intakes.

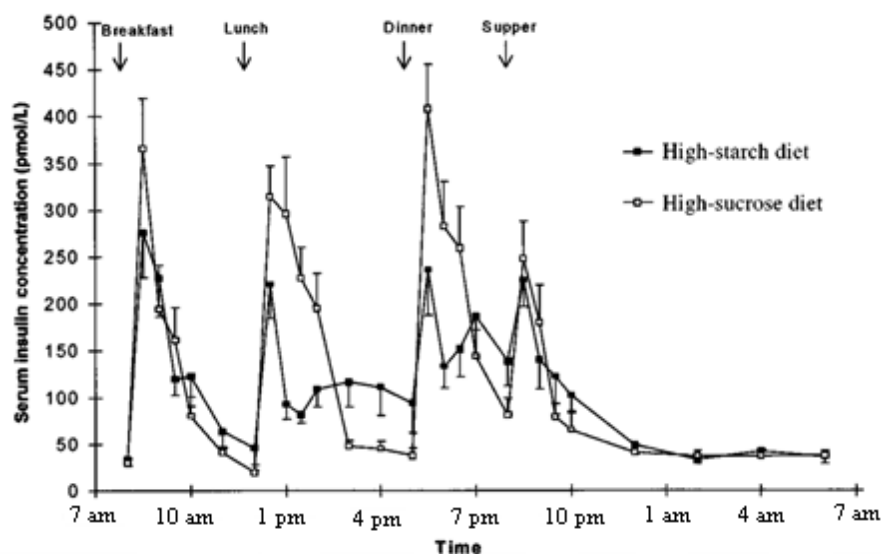


Figure 2.3 Example of variation of insulin concentrations over 24 hours' period after a high-starch diet in comparison to a high-sucrose diet. It is observable that insulin level increases after a meal intake so that blood glucose levels decrease. Furthermore, it can be seen that the higher the sugar content in the meal, the more insulin has to be secreted to keep blood glucose levels in normoglycaemia. (adapted from Daly et al. 1998)

## 2.3 Diabetes mellitus

Diabetes is typically characterised by an impaired blood glucose regulation in the body. It is caused by a deficiency of insulin or when produced insulin malfunctions or a combination of both (Holt & Kumar, 2010a).

The first time, diabetes was mentioned in history in 1500 BC by the Egyptians (Clarke & Foster, 2012). They had made note of a disease which caused rapid weight loss and frequent urination. It was later in 200 CE that the Greek physician Aretaeus named this disease as diabetes, which means ‘flowing through’. He identified that people with that condition were losing weight, urinated in excess and had a high thirst. It was in the early 1800 that glucose was associated with diabetes. George Rees confirmed this theory by identifying high glucose content in diabetes patients’ blood sample (Rees, 1838).

In 2019, estimated 463 million people, aged between 20 and 79 years, were living with diabetes, accounting for 9.3 % of the world population (International Diabetes Federation, 2019b). 4.2 million deaths were estimated by IDF in 2019 due to diabetes (aged between 20 and 79).

Figure 2.4 shows the regions with the prevalence of diabetes around the world. IDF estimates that 700 million people worldwide will be affected by diabetes by 2045.

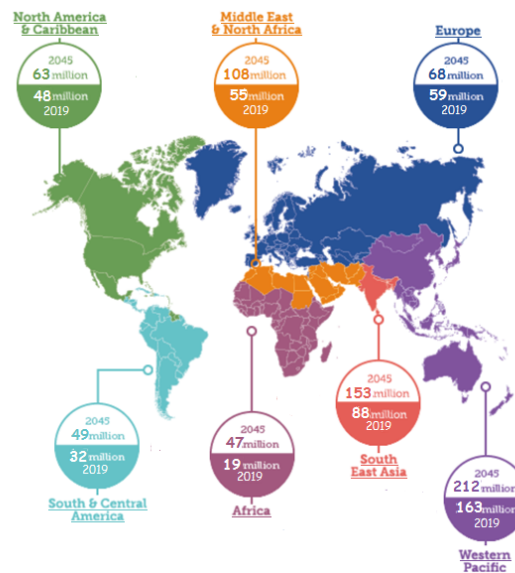


Figure 2.4 Estimated people with diabetes in an age group between 20 years and 79 years in 2019 and the expected number of people with diabetes by 2045 (adapted from International Diabetes Federation, 2017a)

It was reported that approximately 3.4 million people in the United Kingdom suffered from diabetes in 2015 which accounted for 5% of the whole population in the UK (Holman et al., 2015). 8.5 % of the diabetes patients in the UK suffered from type 1 diabetes, 90.4% were affected by type 2 diabetes and 1.2% had ‘other’ types of diabetes, such as gestational diabetes or monogenic diabetes (Holman et al., 2015).

Elevated glucose levels in blood is the direct result of diabetes. If blood glucose level exceeds normal glucose tolerances, it is classified as hyperglycaemia. There are different stages of hyperglycaemia: The pre- stages of diabetes are impaired fasting glycaemia (IFG) and impaired glucose tolerances (IGT). IGT is related to resistancy of insulin by liver and muscles; whereas IFG is more likely caused by deficiencies in insulin secretions. Patients diagnosed with these conditions are at high risk to develop type 2 diabetes. Estimated 374 million people aged between 20-79 have impaired glucose tolerances in 2019 (International Diabetes Federation, 2019b).

If glucose levels exceed the pre- stages, it is classified as diabetes. The most commonly forms of diabetes are type 1 diabetes and type 2 diabetes, which are explained here in further detail:

### 2.3.1 Type 1 diabetes

Type 1 diabetes can be caused by a destruction of insulin producing beta cells by an autoimmune destruction of the islet cells. Approximately 10 % of diabetes patients, have type 1 diabetes (Diabetes UK, 2016). People of all ages can be affected by type 1 diabetes, but the onset of this disease is commonly in childhood or youth. 1.1 million children, aged between 0 and 19 years, worldwide were estimated to suffer from type 1 diabetes (International Diabetes Federation, 2019b). The rate of how fast the beta cells are destroyed varies from person to person. It is said that the process is slower in adults and faster in children (Magliano et al., 2015). It is caused by genetic factors as well as poorly understood environmental triggers. It is said that family history of the patient or autoimmune diseases, such as hypothyroidism, pernicious anaemia, Addison’s disease, vitiligo in the patient or any of its family members, increases the risk of developing type 1 diabetes enormously. Sudden weight loss, polyuria, polydipsia, blurring of vision, very high plasma glucose concentrations, lethargy and

ketonuria are some common symptoms for this type of diabetes. The presences of ICA, islet antigen 2 (IA2), anti-GAD or insulin autoantibodies are indicators of type 1 diabetes (Atkinson & Maclaren, 1994).

There is also idiopathic type 1 diabetes, where the insulin producing cells are also destroyed. Idiopathic diabetes is commonly found in people with African or Asian origin (Magliano et al., 2015).

### 2.3.2 Type 2 diabetes

90% of diabetes patients suffer from type 2 diabetes (Diabetes UK, 2016). It is predominantly caused by insulin resistance and due to a relative insulin deficiency with beta cell failure.

Mostly, middle aged to older adults are diagnosed with type 2 diabetes. However, nowadays more and more children and adolescents are affected by this disease because of the increase of childhood obesity (Health and Social Care Information Centre, 2016; Ogden et al., 2015), which is one of the risk factors of type 2 diabetes.

People, who are often affected by type 2 diabetes, also suffer from obesity, dyslipidaemia and hypertension at the same time. The metabolic syndrome is defined as the clustering of all latter mentioned conditions (Grundy et al., 2004). Hence, patients with hypertension, dyslipidaemia and obesity have a high tendency of having undiagnosed diabetes or impaired glucose tolerances. The concept of the metabolic syndrome is used by clinicians for diagnosing diabetes. Symptoms for type 2 diabetes are lack of energy, slow wound healing, blurred vision, excessive thirst and frequent urination (International Diabetes Federation, 2019c).

There is a genetic susceptibility of having type 2 diabetes (Jafar-Mohammadi & McCarthy, 2008). However, the causes for type 2 diabetes are more complex. Age, obesity and lack of exercise and poor nutrition could increase the risk of getting diabetes. Besides, ethnicity and history of gestational diabetes are also risk factors of getting type 2 diabetes. Gestational diabetes is another type of diabetes, which is found in pregnant women but usually the condition reverts after giving birth. However, the risk of getting diabetes is still there for the mother and the child (Fetita et al., 2006).

People with type 2 diabetes can be undiagnosed for years as noticeable symptoms only show when the disease is progressed enough. And there is the possibility that by the

time it is diagnosed, complications might have already emerged. It was shown that people with south Asian or African background have two to four times higher tendency to develop type 2 diabetes compared to Caucasians (Diabetes UK, 2016). People with diabetes are twice more likely to die of a cardiovascular disease.

### 2.3.3 Diagnosis of Diabetes

Early diagnosis of diabetes enables early treatment of the disease and less life-threatening complications. There are four different approaches for diagnosing diabetes, either by 1) measuring casual blood glucose levels or 2) measuring blood glucose levels in a fasted state or 3) two hours after a high glucose load or 4) measuring glycated haemoglobin levels (American Diabetes Association, 2014).

Table 2.1 indicates the cut-off blood glucose values for the diagnosis of diabetes mellitus, IGT and IFG given by the WHO (World Health Organization, 2006). The standard measurement sample is venous plasma blood. However, due to common practice of capillary blood sampling in countries which lack of resources, capillary plasma values are also used for diagnosis. The tests do not indicate the type of diabetes. To determine the type, other symptoms and background of the patient have to be considered. Usually, patients can be easily diagnosed with type 1 diabetes or type 2 diabetes. However, due to increased childhood obesity nowadays (Health and Social Care Information Centre, 2016; Ogden et al., 2015), the differentiation between the types of diabetes is more challenging.

*Table 2.1 Criteria for the diagnosis of diabetes mellitus, impaired fasting glucose and impaired glucose tolerances in the venous blood plasma (adapted from American Diabetes Association, 2013)*

	<b>Random plasma glucose</b>	<b>Fasting plasma glucose</b>	<b>2h plasma glucose after OGTT</b>	<b>HbA1c</b>
<b>Diabetes mellitus</b>	≥11.1 mmol/L	≥7.0 mmol/L	≥11.1 mmol/L	≥6.5 %
<b>Impaired fasting glucose</b>	-	5.6 – 6. mmol/L	-	-
<b>Impaired glucose tolerances</b>	-	-	7.8 – 11.0 mmol/L	-

### 2.3.3.1 Casual blood glucose measurement

If venous plasma glucose measurement at any time of the day is above 11.1 mmol/L and classic symptoms of diabetes mellitus are shown, the patient is considered as diabetic.

### 2.3.3.2 Fasting blood glucose measurement

The fasting blood glucose measurement is mostly performed in the morning after an overnight fast of at least eight hours. If the glucose concentration in the fasted state is above 7.0 mmol/L in the blood plasma and symptoms of diabetes are seen, the patient is seen will be considered as diabetic. If no symptoms are seen, the test needs to be repeated to be diagnosed with diabetes.

### 2.3.3.3 Oral glucose tolerance test (OGTT)

The oral glucose tolerance test was declared as means for diagnosing diabetes by the WHO in 1980. The glucose concentration of the plasma is measured two hours after having a 75 g of a high glucose drink mixed with approximately 300 ml of water. For children, the volume of the high glucose is calculated by multiplying their body weight with a factor of 1.75. The maximum amount of the glucose load is 75 g. If the glucose concentration of the venous plasma 2 hours after the glucose load exceeds 11.1 mmol/L in conjunction with symptoms of diabetes, the patient would be classified as diabetic. In case of elevated glucose levels without any kind of symptoms, the test needs to be repeated to confirm the diagnosis.

Figure 2.5 depicts the glucose curves after a high glucose drink from a non-diabetic, a patient with impaired glucose tolerances and a patient with diabetes.

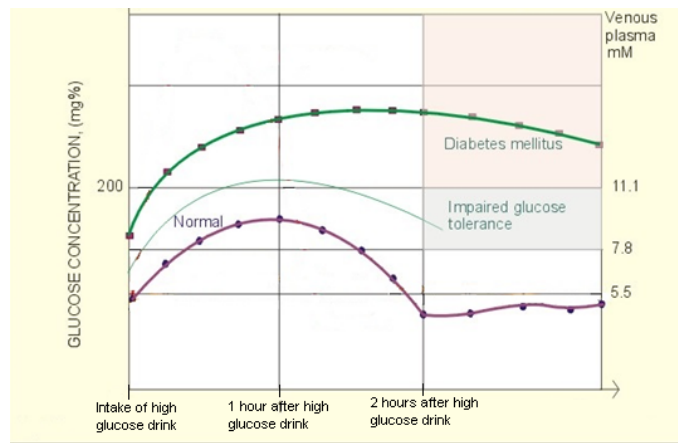


Figure 2.5 Examples of glucose profiles after an OGTT in a person with normoglycaemia (bold violet line), a person with IGT (green line) and a person with diabetes mellitus (bold green line) (adapted from Paulev & Zubieta-Calleja 2004)

### 2.3.3.4 HbA1c

In 2009, it was suggested to use glycated haemoglobin (HbA1c) values for diagnosing diabetes. Glycated haemoglobin is formed by the addition of glucose to haemoglobin via a non- enzymatic reaction. One of the advantages of using HbA1c, is that the patient does not need to be in a fasted state, which is especially beneficial for children. Furthermore, HbA1c samples can stay stable for up to a week, whereas glucose samples tend to undergo glycolysis. In addition, glucose values can easily be altered by changing your lifestyle, whereas HbA1c is less prone to short term changes and mirrors glycaemic values over eight to ten weeks. In comparison, the results from fasting blood glucose measurements and OGTT show only the real-time glucose values.

The downside of using this method is that there are conditions not related to glycaemia, which could result in alteration of the HbA1c value. For example, conditions such as kidney failure or pregnancy could lead to changes of HbA1c level. Furthermore, this method of diagnosis of diabetes requires the use of a well-equipped laboratory so that the results can be analysed using the International Federation of Clinical Chemistry (IFCC) developed standardised haemoglobin assay. However, this will be difficult to implement in developing countries. (Magliano et al., 2015)

In 2011, WHO approved glycated haemoglobin testing as an additional tool to diagnose diabetes (World Health Organization, 2011). If HbA1 levels exceed 6.5% and the patient is showing symptoms of diabetes, then the patients is classified as

diabetic (American Diabetes Association, 2014). The test needs to be repeated in case of absence of any diabetic symptoms to confirm the diagnosis.

HbA1c level measurements are not only for diagnosing purposes but it is also recommended to test glycated haemoglobin levels every six months from type 2 diabetes patients as it can indicate the effectiveness of the treatment plan as the HbA1c level mirrors the glycaemic levels over months (NHS Cambridgeshire and Peterborough Clinical Commissioning Group, 2016).

### 2.3.4 Treatment options

The major concern with diabetes is that till date there is no cure. The only treatment, which could be seen as a form of a cure would be pancreas transplantation or islet cell transplantation (Hönes et al., 2008). However, it is costly, there is deficiency in organs and the risks of organs transplants need to be carefully contemplated. Furthermore, the side effects from lifelong consumption of immunosuppressant need to be considered as well. Moreover, islet cell transplantations only provide temporary cure of the disease. Advancements in diabetes treatment forms also involve cell-based treatments. One idea is to regenerate respectively replace beta cells with stem cells (Ellis et al., 2017). Oggu et al. investigated in treatment of diabetes with the help of mesenchymal stem cell (MSC) therapy (Oggu et al., 2017). Madec et al. showed that MSC can protect beta cells from autoimmune destruction, which could ultimately prevent diabetes (Madec et al., 2009). Cell based therapies are an emerging field but it is still highly experimental and is not yet considered as a viable therapy form yet (Ellis et al., 2017; Oggu et al., 2017).

#### Treatment of type 1 diabetes:

In case of type 1 diabetes, the insulin producing cells are destroyed due to an autoimmune reaction. A big breakthrough with regards to treatment of diabetes occurred in 1921 when Frederick G. Banting, Charles Best and J. R. Macleod identified insulin as the hormone deficient in diabetes patients (Best & Scott, 1923). In 1922, scientists were able to extract and purify insulin from animals (cows and pigs) and successfully proved its effectivity by treating a type 1 diabetes patient with insulin injections (Quianzon & Cheikh, 2012).



Patients with type 1 diabetes are required to start daily insulin treatment promptly. There are three types of insulin: 1) animal insulin, which is extracted from animals, 2) human insulin and 3) analogue insulin (Diabetes.co.uk, 2017b). Human insulin as well as analogue insulin are both synthesised in a laboratory setting. Human insulin is prepared with the help of *Escherichia coli* (*E. coli*) bacteria and insulin proteins. It was first used in a clinical environment in 1982 (Quianzon & Cheikh, 2012). Analogue insulin undergoes the same preparation process as human insulin with an additional step of recombinant DNA. Here, the order of the amino acid chain is altered so that the body can take in the insulin quicker or in a more uniform manner.

Insulin can be also categorised depending on the rates they react in the body, such as fast acting insulin, intermediated acting insulin, or long acting insulin etc. Each vary in their onset, duration of activity and peak of activity.

In diabetic patients, insulin needs to be injected subcutaneously into the thighs, abdomen or buttocks with the use of insulin pens, syringes or insulin pumps (Holt & Kumar, 2010b). Insulin pumps are battery-operated and can deliver insulin as required via a cannula (flexible tube) which is inserted subcutaneously. The tube needs to be changed every two to three days.

Insulin is most effective for glycaemic control (Gough & Narendran, 2010). However, one limitation is its route of administration; Patients show reluctance to inject insulin. Therefore, alternative routes for insulin delivery were investigated such as orally, dermally or nasally (Heinemann et al., 2001). The Exubera system was the first inhaler which could be used in conjunction with dry-insulin powder and was brought to the market by Pfizer in 2006 (Harper et al., 2007). However, due to the lack of market acceptance it was withdrawn in 2008. It has to be noted that the use of inhaled insulin would not be sufficient to cover the body's full demand of insulin. The use the subcutaneous injection of long-acting insulin would still be required as part of the treatment regimen. Non-invasive routes for insulin administration is an emerging field (Heinemann, 2011; Mazzucchelli & Corsi, 2017; Thwala et al., 2017). Though, more research and time is required to achieve the required effectiveness and acceptance. The Technosphere® Inhaled Insulin is the latest advancement in terms of pulmonary insulin delivery systems (Heinemann et al., 2017). Further studies need to be

conducted to investigate the adverse effects and pulmonary safety in long-term use of these devices (Chan & Cheng-Lai, 2017).

Patients under insulin treatment are at high risk of hypoglycaemia. Therefore, self-monitoring of blood glucose (SMBG) is very important. They also have to maintain a healthy diet and perform physical activity regularly. This will help them to manage the disease and prevent complications.

#### Treatment of type 2 diabetes:

People diagnosed with impaired glucose tolerance have a high tendency to develop type 2 diabetes. Although, studies have proven that the further development to type 2 diabetes can be prevented in adults by lifestyle changes (Eriksson et al., 1999; Harland et al., 1999; Lindström et al., 2003; Oldroyd et al., 2001, 2006; Pan et al., 1997; Penn et al., 2009; Tuomilehto et al., 2001). Losing weight, increasing physical activity and change in dietary (less consumption of fat and increased up and increased intake of fibres) are some highly recommended aspects of life style changes (Penn et al., 2009). Initially as well as throughout the disease, dietary changes and regular exercise are required. These forms of treatment should help to control the glycaemic level. An additional oral drug therapy should be started to improve glycaemic control if blood glucose levels cannot be regulated with the latter form of treatment. Metformin is the most commonly used oral medication which has the ability to reduce gluconeogenesis in the liver, increase glucose uptake and reduce carbohydrate absorption for the gut lumen thus reducing blood glucose levels (Watkins et al., 2003). Gliclazide belongs to the group of sulfonylureas and is used to enhance insulin secretion. Metformin as well as Gliclazide have both been made accessible and available for type 2 diabetes patients all over the world by the WHO (International Diabetes Federation, 2019a). Other classes of medication for type 2 diabetes include thiazolidinediones, SGLT2i and GLP1-RA (DeFronzo, 2017).

Insulin therapy might be required in the later stage when the drug therapy and other means are insufficient to keep the glucose levels in normal glucose levels.

Weight loss surgeries are used as part of treating diabetes. Studies have shown its effectivity in obesity- induced type 2 diabetes patients (Buchwald et al., 2009; Schauer et al., 2017; Schauer et al., 2017). However, it has to be mentioned that this approach

can cause with a variety of adverse effects such as cardiopulmonary complications, haemorrhage or thromboembolic disease or even death (Schauer et al., 2017) .

The Diabetes Remission Clinical Trial (DiRECT) demonstrated that an intensive and structured weight loss management programme is a viable treatment form to reverse type 2 diabetes (Lean et al., 2018). In the trial, patients which were diagnosed with the type 2 diabetes (for less than six years) had to undergo a liquid formula diet with a dietary intake of 825-853 kcal per day for the first three to five months, followed by gradual food reintroduction in the following 2 to 8 weeks. Support and individual advice were given throughout the trial to maintain long-term weight loss. Antidiabetic and antihypertensive drugs were withdrawn during the study period. A reversal of type 2 diabetes was successful shown in 46 % of participants (68 participants out of 149) after 12 months (Lean et al., 2018). After two years, it was shown that the remission of type 2 diabetes could be sustained by 36% of the participants (53 participants out of 149) (Lean et al., 2019).

Poorly controlled diabetes can cause macrovascular and microvascular complications, kidney disease, eye disease, amputation, depression, neuropathy, sexual dysfunction and dementia (Diabetes UK, 2016). Diabetes patients need to be empowered to look after themselves properly so that long term complications from this disease can be delayed or prevented in the best-case scenario. It is important that the treatment plan is tailored for each patient individually depending on the type of diabetes, age, gender, lifestyle.

It was shown that tight control of glucose in normoglycaemic levels in the body can delay the onset and progression of secondary complications such as neuropathy, nephropathy and retinopathy in Type 1 diabetes patients (The Diabetes Control and Complications Trial Research Group, 1993) and microvascular complications in type 2 diabetes patients (UK Prospective Diabetes Study (UKPDS) Group, 1998). The evidence that good control improves macrovascular complications remains contentious at best. Tight control can be achieved by self- monitoring of blood glucose (SMBG) methods. This thesis focuses on self- monitoring of blood glucose (SMBG), which is one of the key routes in managing diabetes.

Figure 2.6 shows a summary of existing glucose sensing technologies used for SMBG. In principle, there are two main categories, point sample/intermittent glucose measurements and continuous glucose monitoring. The most commonly used intermittent glucose measurement, the finger-prick glucometer applies invasive means for glucose testing. The frequency of intermittent glucose measurements changes depending on the type of diabetes, age and severity of disease. For example, in type 1 diabetes patients who are undergoing insulin treatment, SMBG is an essential part of the treatment plan. They are strongly advised to check their glucose levels at least four times a day (NHS Cambridgeshire and Peterborough Clinical Commissioning Group, 2016). On the other hand, not all type 2 diabetes patients are required to perform SMBG. Only those under insulin therapy and those taking sulfonylurea or rapid acting insulin, are recommended to measure their glucose levels up to four times a day (NHS Cambridgeshire and Peterborough Clinical Commissioning Group, 2016).

Within continuous glucose monitoring, there are three approaches for glucose testing, 1) invasive 2) minimally invasive and 3) non-invasive. The focus of this thesis lies in a non-invasive glucose monitoring technique, called reverse iontophoresis (RI) (Section 2.8.2 Glucose monitoring using reverse iontophoresis).

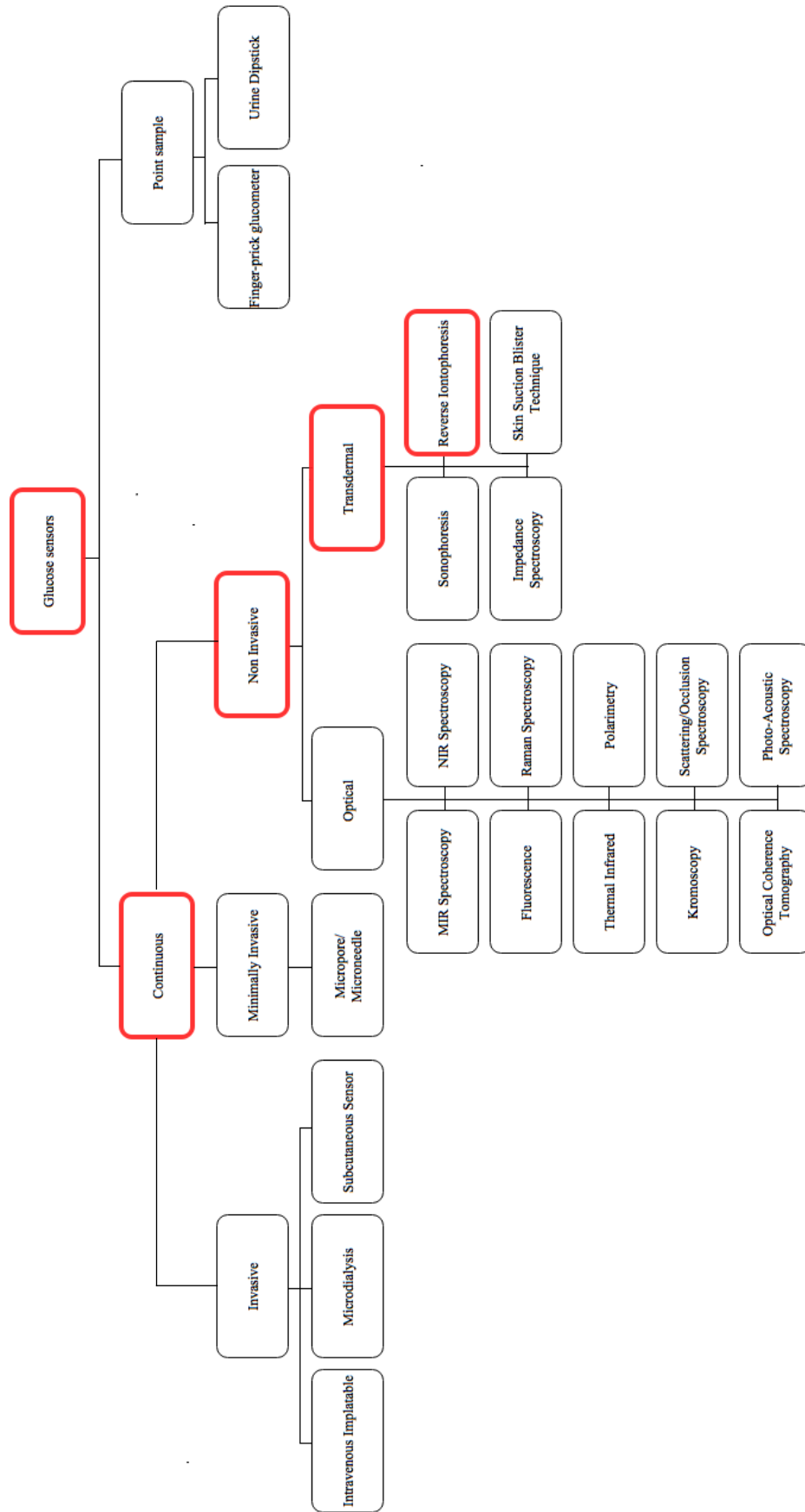


Figure 2.6 Overview of glucose sensing technologies for continuous and intermittent glucose monitoring (adapted from Oliver et al., 2009)

## 2.4 History of glucose monitoring

Managing diabetes started with glucose testing and monitoring in urine. In 1841, Trommer developed a urine test, which made use of the reaction between glucose and alkaline cupric sulphate reagents. Thereby, glucose was reduced and a coloured cuprous oxide was produced. The cuprous oxide was responsible for the colour change of the solution from green to yellow (Neisser et al., 2005). The colour change was assessed by the human eye.

In 1850, Jules Maumene devised a test strip for glucose quantification in urine. The strip of wool contained stannous chloride and if glucose was present in the urine, it would turn black (Neisser et al., 2005). In 1908, Stanley Benedict developed an improved method to monitor glucose through urine testing with a copper reagent (Benedict, 1909), a method which was used for 50 years (Simoni et al., 2002); however, this type of method showed practical difficulties for the use of self-monitoring as heat is required for the colour change to occur.

Elliot Joslin suggested that frequent self-monitoring of urinary glucose level, right diet and good exercise is crucial for managing diabetes (Joslin, 1918).

In 1945, Compton and Treneer from Ames introduced the Clinitest® Reagent Tablet, an improved copper reagent, which solved the heat problem from Benedict's method. The tablet was added to the urine sample in a test tube, which produced heat. Glucose was oxidised and the cupric sulphate was reduced which caused a colour change. Initially it is blue coloured, changing to green, then to yellow and finally to an orange colour. The glucose could be quantified by comparing the colour to the colour chart (Figure 2.7), which was a semiquantitative approach (Free & Free, 1984).



Figure 2.7 Colour chart to quantify the glucose using Clinistest® Reagent Tablet (adapted from Clarke and Foster, 2012)

In 1957, Clinistix, a test strip for urinary glucose was introduced by Ames. The method was improved by using filter paper, which was impregnated with glucose oxidase, peroxidase and orthotolidine. Glucose oxidase is an enzyme and was discovered and identified in 1928 (Muller, 1928), it catalyses the conversion of glucose to gluconolactone (Keilin & Hartree, 1948) whereby hydrogen peroxide ( $H_2O_2$ ) is produced (Franke & Deffner, 1939; Franke & Lorenz, 1937). Hydrogen peroxide in presence with peroxidase caused the oxidation of orthotolidine, which resulted in change of its colour to a deep blue chromogen. (Clarke & Foster, 2012).

Urine testing was the start of glucose monitoring for treating diabetes. However, it had its limitations. It had been proven that fluid intake and urine concentrations had an impact on the glucose results depending on the sensitivity of the strips (Goldstein et al., 2004). Moreover, the tests were only able to detect an excess of glucose in urine. Hence, a negative result meant that the patient could have been in state of hypoglycaemia, normoglycaemia or slightly enhanced hyperglycaemia (Goldstein et al., 2004). Besides, the obtained glucose concentrations were retrospective and it had been demonstrated that there was inconsistent correlation between plasma glucose concentration and urine glucose concentration (Hayford et al., 1983). Blood glucose measuring was introduced because of its easier accessibility and its ability to measure real time blood glucose concentrations which are very beneficial for self- monitoring.

The first test strip for glucose measurement in blood, called Dextrostix, was developed in 1965. These test strips were also based on an enzymatic reaction with glucose oxidase. The Dextrostix involved a semipermeable membrane, which would only pass through soluble glucose to react with the dry reagent. Glucose was determined by comparing the obtained colour change with a colour chart (Free & Free, 1984). A blood volume of 50-100  $\mu\text{L}$  was required for the Dextrostix test strips and the colour change occurred approximately one minute after. The difficulty to assess the colour change due to lighting conditions and subjective perception of the colour change was another problem of this method (Harvey et al., 1976). The Dextrostix was mainly used for surgeries and hospital wards, clinics, and intensive care units and was unsuitable for self-monitoring. To overcome the difficulties and inaccuracies of assessing colour change, the first automatic, electronic glucose test strip reader was introduced by Clemens Anton in 1970, the Ames Reflectance Meter (ARM) (Figure 2.8).



*Figure 2.8 First electronic blood glucose reader based on reflectance photometry by Clemens Anton in 1970  
(adapted from Mendosa, 2006)*

It enabled blood glucose measurement with the use of the Dextrostix but in combination with reflectance photometry-based ARM, which remedied the issues



concerning the assessment of the colour change. The ARM weigh approximately 1.2 kg because of the case and the rechargeable batteries, which consisted of lead acid, and cost around \$432 (Clarke & Foster, 2012). For calibration purposes, one reference strip was required. Studies have shown good correlation (around  $r=0.98$ ) between the results from the reflectance photometry and the applied laboratory methods in comparison (Cheah & Wong, 1974; Jarrett et al., 1970; Mazzaferri et al., 1970). This device was mainly used in the hospital wards or in doctor's offices. Common drawbacks of the ARM were its complex sampling and cleaning technique for each measurement and its heavy weight, making it not suitable as a portable device for self-monitoring purposes. In addition, it showed inaccuracies in detecting high blood glucose values above 180 mg per 100 ml (Junker & Ditzel, 1972) and over-diagnosis of hypoglycaemia by showing lower glucose levels than actual in newborns (Cavell et al., 1973).

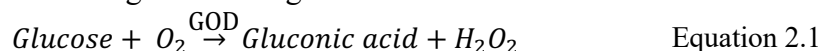
Few of the problems with the ARM were solved with the development of the Eytone blood glucose meter by the company called Kyoto-Daiichi in 1972. Eytone was also based on the use of the Dextrostix test strips and reflectance photometry. However, in comparison to ARM, it was lighter, cheaper and more accurate. The measurement range of the Eytone is 10 to 400 mg/ 100 ml. The accuracy was improved by calibrating the device at two blood glucose levels (Schersten et al., 1974). Studies showed good correlation between measurements from the Eytone and a laboratory method with  $R=0.97$  (Schersten et al., 1974) and  $R=0.99$  (Stewart, 1976).

Studies were conducted with the Ames Eytone meter for testing its use in monitoring glucose at home (Peterson et al., 1978; Sönksen et al., 1978). In Peterson's study, 10 diabetes type 1 patients were educated on how to use the meter. The glycated haemoglobin levels were recorded at the beginning of the study for each patient. After a check-up four to six months later, the mean HbA1c levels were decreased from 10.3% to 5.4%. Sönksen et al. tested the Ames Eytone on 64 patients (Sönksen et al., 1978). It was observable that 64% of the subjects were able to control 80% of their glucose levels below 10 mmol/l for more than a year. Another study with  $n=69$  showed that 50% of the subjects had capillary blood glucose level below 10.0mmol/l. Further studies confirmed the use of SMBG to improve glycaemic control (Danowski & Sunder, 1978; Ikeda et al., 1978; Skyler et al., 1978; Walford et al., 1978). The

combination of patient acceptance to self-monitoring and improvement of glycaemic control by SMBG led to expansion and further development of self-monitoring techniques. Alternative glucose quantification method apart from reflectance photometry was investigated in to offer faster and more accurate glucose measurements. The idea of using biosensors based on electrochemical principles for self- monitoring of blood glucose started with the development of the a biosensor electrode for pO<sub>2</sub> measurements by Clarke (Clarke, 1956).

## 2.5 Glucose biosensors for intermittent glucose monitoring

The first biosensor electrode for blood glucose measurement was proposed by Clarke and Lyons in 1962 (Clarke & Lyons, 1962). The enzyme, glucose oxidase (GOD), which can be extracted from *Aspergillus niger*, is ideal to be used in glucose sensors because of its specificity to glucose (Wilson & Turner, 1992). Glucose oxidase is a catalyst and oxidises glucose to gluconic acid where oxygen gets reduced. Equation 2.1 explains the reaction with glucose and glucose oxidase:



In the sensor, the glucose oxidase was entrapped in a thin layer in a dialysis membrane over the oxygen electrode. The sensors were based on monitoring the oxygen levels in blood. By applying a negative potential onto the working electrode, oxygen was reduced, which in turn was proportional to the glucose content.

Clarke and Lyons sensors were further developed by Updike and Hicks in 1967 (Updikes & Hicks, 1967). They made use of two oxygen electrodes, one was in combination with the glucose oxidase and the second electrode without the enzyme. This would aid to eliminate oxygen changes which were not caused by glucose oxidase.

In 1973, Guilbault and Lubrano devised the sensor further by applying an amperometric measurement method for glucose detection (Guilbault & Lubrano, 1973). This amperometric sensor measured the hydrogen peroxide produced when oxidising the glucose and reducing the oxygen. The amount quantified of hydrogen peroxide is in proportion with the glucose concentration.

Electrochemical detection of  $H_2O_2$  can be explained by the following equation (Equation 2.2).



This type of glucose sensor offers rapid electrochemical glucose measurements.

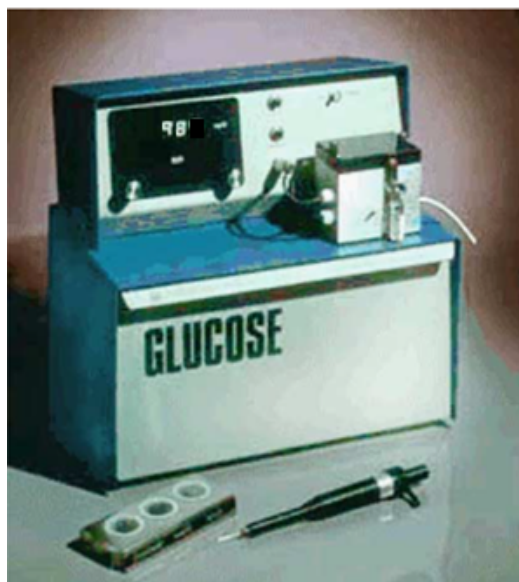


*Figure 2.9 The first glucose analyser Model 23A based on electrochemical glucose detection from YSI (adapted from Newman & Turner 2005)*

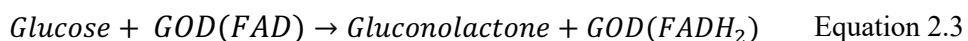
In 1975, based on the Clarke and Lyons technology, Yellow Spring Instrument (YSI) developed the glucose analyser Model 23A YSI analyser (Figure 2.9). It was able to measure glucose from a blood sample by detecting hydrogen peroxide amperometrically with a sample volume of  $25 \mu\text{L}$  (Wang, 2008). However, this device was expensive and was only used in clinical laboratories and was unsuitable to be used in self-monitoring.

Based on the method of glucose detection, following generations of glucose sensors were developed:

### 2.5.1 First generation glucose sensors

Glucose sensors which, are based on the hydrogen peroxide detection for glucose monitoring belong to the first-generation of glucose sensors.

The reaction can be summarised with the following equations (Equation 2.3, Equation 2.4 and Equation 2.2).



The flavin adenine dinucleotide (FAD) is the redox centre of the glucose oxidase, which gets reduced respectively reoxidised. The reduced form of glucose oxidase reacts with hydrogen and oxygen in blood and hydrogen peroxide is produced.



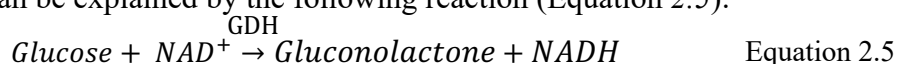
By applying a voltage of approximately +0.6V vs. Ag/AgCl on platinum electrode, the electron transfer occurs. A three-electrode system (see section 4.3.3) is used and the current between working electrode and counter electrode is measured. This current is proportional to the glucose concentration in blood.

The application of a potential is necessary for the electron transfer of the H<sub>2</sub>O<sub>2</sub> to occur so that an amperometric measurement can be performed. One of the problems with first generation glucose sensors is that there are also other electroactive species in blood such as ascorbic acid or uric acid, which can oxidise at the applied potential. The oxidation of the other electroactive compounds causes an increase of current, which is not in relation with the glucose concentration; hence the specificity and the accuracy of the measured signal towards glucose is compromised. Scientists have worked on different methods to minimise interferences due to the other electroactive species. One approach is by preventing access of interfering compounds to the sensing electrode surface. For example, integrating a cellulose acetate film inbetween the electrode and the enzyme layer have been shown to be beneficial due to its size exclusion properties. Thereby, it allows the transport of H<sub>2</sub>O<sub>2</sub>, which has a molecular weight (MW) of 34 Da to the electrode surface but blocks the transport of bigger interfering species such as acetaminophen (MW=151 Da), uric acid (MW=168 Da) or ascorbic acid (MW=176 Da) (Sternberg et al., 1988). Besides, Moussy et al. have shown that the negatively charged Nafion polymer coating helps to prevent interferences from negatively charged species such as uric acid and ascorbic acid. (Moussy et al., 1994).

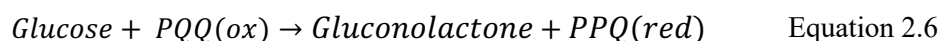
Another limitation of first-generation sensors is the oxygen dependency of glucose oxidase of this method. This reaction might be compromised due to changes in oxygen tension in the sample (Cass et al., 1984). One way to address this issue is with the

application of an oxygen enriched carbon paste onto the sensor electrode (Wang & Lu, 1998) thus providing another source for oxygen and allowing the oxygen- dependent enzymatic reaction with GOD to happen. Another approach is the use of an alternative enzyme for example glucose dehydrogenase (GDH). Instead of oxygen, this enzyme requires nicotinamide adenine dinucleotide (better known as  $NAD^+$  in its oxidised form) as a cofactor. It was shown that this enzyme was insensitive to oxygen fluctuations, which was one of the issues with using glucose oxidase. The disadvantage of this method is that it requires a soluble cofactor (Wilson & Turner, 1992) and  $NAD^+$  is costly and unstable (Newman & Turner, 2005).

The reaction can be explained by the following reaction (Equation 2.5):



Another enzyme, which can be used instead of GOD is the quinoprotein glucose dehydrogenase (GDH). Instead of oxygen or  $NAD^+$  as a coenzyme, this quinoprotein needs pyrroloquinoline quinone (PQQ) as a co-worker (D'Costa et al., 1986). Although, even this enzyme is also expensive (Newman & Turner, 2005) and unstable (Wilson & Turner, 1992). The following equation depicts the reaction (Equation 2.6).



## 2.5.2 Second generation glucose sensors

In order to eliminate the oxygen problem, the use of an artificial non-physiological mediator was suggested. Mediators have the responsibility to replace oxygen for electron transfer between working electrode and enzyme.

The requirements for the mediator are as follows (Cass et al., 1984):

- It should be able to react quickly with the enzyme.
- It should be stable in terms of pH sensitivity, redox state & dioxygen.
- It should be easily reduced but should also be easily re-oxidised.
- It should also be biocompatible with glucose oxidase

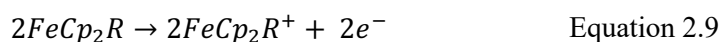
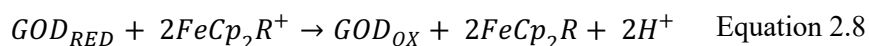
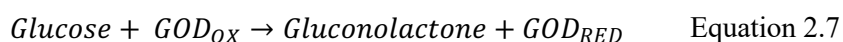
A variety of mediators, such as ferrocene, quinones, tetrathiafulvalene (TTF) or tetracyanoquinodimethane (TCNQ), were studied to be used in glucose sensors (Chaubey & Malhotra, 2002).

Ferrocene derivatives and ferrocyanide were suggested as good electron acceptors to be used in glucose sensors (Cass et al., 1984; Frew & Hill, 1987). Ferrocene is water

soluble and is commonly used for glucose sensors. Its rapidity and reversibility in redox reactions makes it ideal for glucose sensors. Cass et al. developed an amperometric enzyme electrode with ferricinium ion as a mediator. The sensor was tested and a linear response between current and glucose concentration was observable for a glucose concentration range between 1-30mM (Cass et al., 1984).

Chemical reaction in a glucose sensor with ferrocene as mediator:

Glucose oxidase facilitates the oxidation of glucose to gluconolactone (Equation 2.7). Glucose oxidase is reduced by accepting two electrons and two protons (Equation 2.7). The reduced enzyme is then oxidised by ferrocene, which acts as a mediator (Equation 2.8). The mediator is responsible for electron transfer between enzyme and working electrode. Once ferrocene gets reduced, it can be re-oxidised to ferrocinium ion at the electrode surface (Equation 2.9). A certain potential difference is needed for electron transfer to occur. The reduction of ferrocene is not a spontaneous reaction. (Cass et al., 1984).



The second-generation glucose sensor was applied in the ExacTech, the first personal blood glucose biosensor system for home glucose monitoring by Medisense. It was introduced in 1987 and consisted of a pen sized meter and was used in conjunction with disposable test strips (Figure 2.10) (Matthews et al., 1987).

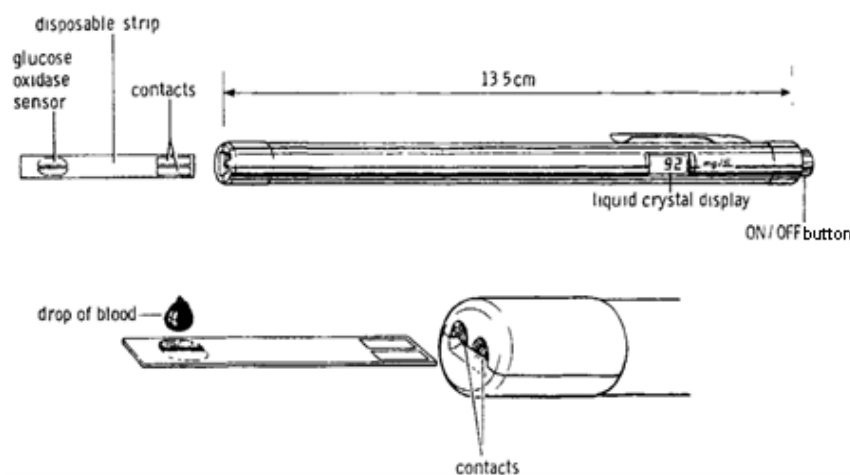


Figure 2.10 Pen-sized glucose meter and test strip (adapted from Matthews et al. 1987)

Glucose was measured electrochemically in 30 seconds in a blood sample of only 10  $\mu\text{L}$  using a single-use disposable test strip. The electrodes were screen printed and the test strip contained glucose oxidase and ferrocene as a mediator. Disposable screen printed electrodes are ideal to be used in glucose monitoring because of their low fabrication cost, rapid production and its capability to be mass produced (Hilditch & Green, 1991).

It was tested in a study by 51 diabetic patients (Matthews et al., 1987). Glucose reading from the device were compared with glucose readings from the YSI and a correlation of 0.985 was seen. Another study evaluated and confirmed the accuracy and reproducibility of the meter reading (Ross et al., 1990).

### 2.5.3 Third generation glucose sensors

In third generation glucose sensors, use of any form of mediators is avoided. The principle behind it is a direct electron transfer between enzyme and electrode (Ghindilis et al., 1997). The challenge in this type of sensors is the electron transfer between the electrode and the redox centre of the enzyme because of the thick protein layer around the FAD centre of the enzyme. The distance between the redox centre and the electrode should be as short as possible.

Problems were seen when using glucose oxidase as an enzyme in combination with conventional electrodes. Therefore, other electrode materials were investigated in. One attempt was to integrate conducting organic salts, such as tetrathiafulvalene-tetracyanoquinodimethane (TTF-TCNQ), a charge-transfer complex, into the electrodes (Palmisano et al., 2002).

Recent sensors belonging to the fourth-generation work with enzyme free glucose sensors. A lot of research and work is still required in this field to standardise it and to be used in glucose sensors (Toghill & Compton, 2010).

### 2.5.4 The Clarke Error Grid

The Clarke Error Grid introduced in 1987 (Clarke et al., 1987; Cox et al., 1985) is now considered as the golden standard to test accuracy of the blood glucose meter reading.

Reference glucose concentrations are applied on the x axis and measured glucose values are applied on the y axis (Figure 2.11). The error grid comprises of 5 zones namely, A, B, C, D and E. Results in zone A and zone B are seen as clinically acceptable. Overcorrect results fall in zone C and lead to hyperglycaemia or hypoglycaemia. zone D results are considered as failure to detect hyperglycaemia or hypoglycaemia and results zone E are erroneous outcomes.

It was proven as a useful tool to evaluate clinical significance and was used to assess many blood glucose meters (Gross et al. 2000; Tierney et al. 2001; Potts et al. 2002; Eastman et al. 2002; Clarke 2005; Harman-Boehm et al. 2009; Caduff et al. 2011; Keenan et al. 2012; Kovatchev et al. 2015; Fokkert et al. 2017) .

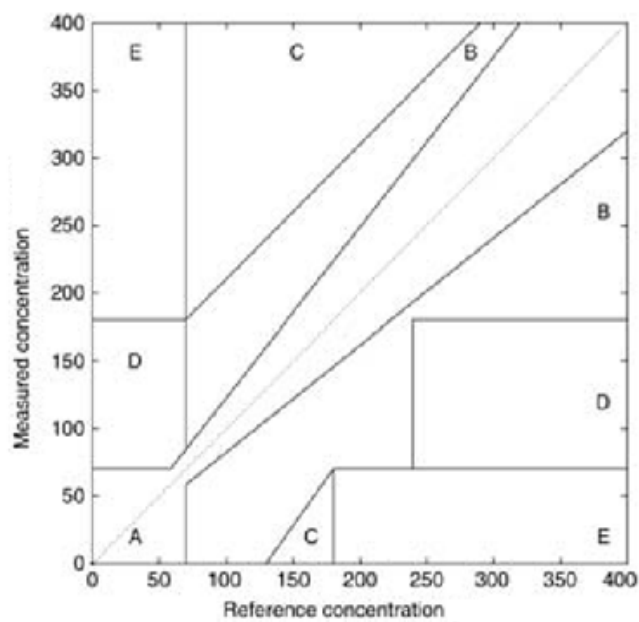


Figure 2.11 Example of Clarke Error grid with Zones A, B, C, D and E indicated (adapted from Oliver et al. 2009)

## 2.5.5 Commercially available blood glucose meters for intermittent glucose measurements

Over the past years, a lot of research and efforts have been made to improve user friendliness, performance and accuracy of blood glucose self-monitoring devices.

Figure 2.12 shows an example of a glucose meter with a test strip and a lancing device. The standard blood glucose meters nowadays are battery operated, easy to use, handheld, and contain top microelectronics and software which enable a range of



functions such as storing and retrieving your results. They have minimal operating steps, give an alarm if the blood sample is poorly filled and provide autocalibration. The test strips only require a 0.3-1  $\mu\text{L}$  of blood and lancing devices, which are used for collecting blood samples and are designed in a way where they are less painful. Abbott, Roche diagnostics, Lifescan and Bayer, are the key blood glucose meter developing companies. There is a high competition in this market where all companies try to succeed by improving their design and performance of the glucose meters.



*Figure 2.12 Example of a blood glucose meter with a test strip and a lancing device from Accu-Chek® Aviva (adapted from Healthcare4All, 2014)*

Most of the glucose meters for intermittent self-testing work in conjunction with electrochemical test strips with amperometric glucose measurements.

Table 2.2 shows examples of currently available glucose meters for intermittent glucose measurements. Different companies have brought different glucose meters to the market with different detection times, blood volumes, concentrations ranges and additional features such as ketone measurements. Abbott's product line for blood glucose meters is called FreeStyle, Roche diagnostics' Accu-Chek, LifeScan's OneTouch and Bayer's Contour.

Table 2.2 Selected currently available glucose meters for intermittent glucose monitoring for self-testing

Device	Company	Blood volume for measurement [ $\mu\text{L}$ ]	Detection time [s]	Glucose concentration range [mmol/L]
FreeStyle Optium Neo	Abbott	0.6	5	1.1 - 27.8
OneTouch UltraSmart®	Lifescan	1	5	1.1 - 33.3
Accu-Chek® Mobile	Roche diagnostics	0.3	5	unknown
Contour® Next	Bayer	0.6	5	1.1- 33.3

Electrochemical test strips for blood glucose meter vary in design, way of use and number of electrodes depending on the manufacturer. It has to be noted that they are for single use. Figure 2.13 shows a test strip used with the Freestyle Optium Neo blood glucose monitoring device from Abbott (Abbott, 2013).

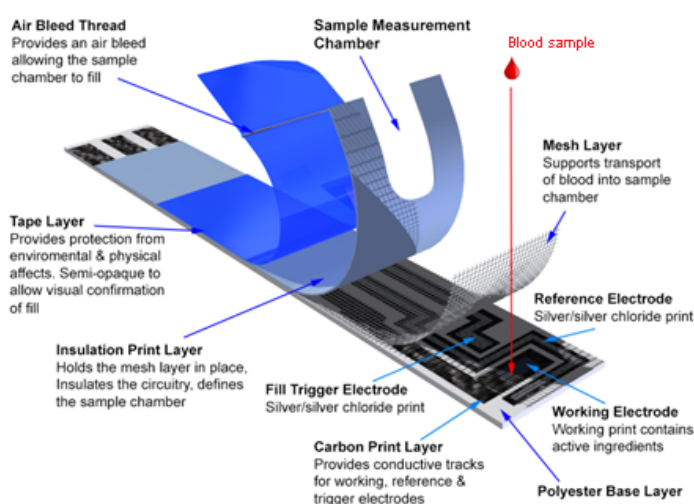
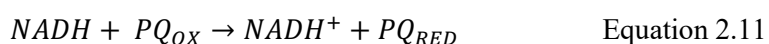
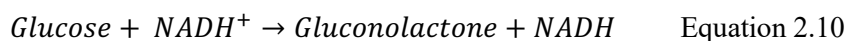


Figure 2.13 Example of a glucose test strip Freestyle (adapted from Abbott 2013)

The glucose sensor of the Freestyle Optium Neo is based on a mediated enzymatic reaction (Abbott, 2013). Glucose dehydrogenase (GDH) is used as the enzyme and nicotinamide adenine dinucleotide (NAD) was used as a coenzyme. Phenanthroline quinone (PQ) was the mediator for the sensor.

The enzyme and the mediator are placed on the working electrode of the test strip.

### Reactions in test strip:



Glucose is oxidised to gluconolactone by reaction with NAD. GDH acts as a catalyst in this reaction. The mediator acts with the reduced form of the coenzyme and gets reduced itself. The coenzyme oxidises back to  $\text{NADH}^+$ . When a voltage of 200 mV is applied between working electrode and reference electrode, PQ gets oxidised and loses its electron. The current, which is produced in that process, is proportional to the glucose concentration in blood. The glucose meter converts the current reading into a meaningful glucose concentration and displays it.

PQ is used as a mediator because it enables low potential oxidation. There is a risk that at higher potentials other substances might oxidise which can lead to measurement errors.

The glucose measurement is taken by a three-electrode system consisting of 1) the working electrode, 2) the reference electrode and a so-called 3) fill trigger electrode, which is an equivalent to a counter electrode. More details on the application of a three-electrode system for glucose quantification is given in the theory chapter (section 4.3.3)

The blood sample is applied onto the sample measurement chamber. The measurement starts automatically once the sample is in contact with all three electrodes. If there is insufficient amount of sample volume, the test will not start. This feature helps users to know if enough blood was sample and if not, they can add more blood onto the same test strip. In many devices, patients need to use a new test strip if insufficient blood volume was applied. Hence, this design of Freestyle electrodes helps to reduce wastage of test strips because insufficient blood volume.

It is crucial that all test strips meet the required standard so that glucose measurements are accurate and precise. A surveillance program tested different test strips randomly all over the world for a time period of seven years in terms of sensitivity and accuracy of the glucose measurements (Setford et al., 2017). Results showed that all test strips were in the clinical acceptable region and met the ISO 15197:2015 standards. All blood glucose monitoring systems for self-monitoring need to meet the requirements

of the EN ISO 15197:2015. ISO 15197:2015 is defined by the International Organisation for Standardisation and applies to “*In vitro diagnostic test systems – Requirements for blood-glucose monitoring systems for self- testing in managing diabetes mellitus.*” (International Organization for Standardization, 2017)

## 2.6 Continuous blood glucose monitoring

In contrast to intermittent glucose measurement systems, continuous glucose monitoring systems (CGMSs) are able to automatically provide glucose measurements in a certain time interval. CGMS enables monitoring blood glucose level trends and patterns and glucose fluctuations due to meals or oral medication or insulin therapy in diabetes patients. This information can improve treatment plan, which results in better glucose control in type 1 diabetes (Bode & Hirsch, 2000; Kaufman et al., 2001). It gives information of the diabetic status of the patients which motivates them for tight glycaemic control as well as educates them more about their disease (Boland & Tamborlane, 2000).

### Advantages of CGMS:

- It is a powerful tool to detect unrecognised hypoglycaemia especially during sleep or physical activity in type 1 diabetes and type 2 diabetes (Chico, Vidal-Rios, Subira, & Novials, 2003).
- Studies reported that continuous glucose monitoring helped to improve HbA1c levels to a greater extent compared to with just intermittent glucose measurements (Beck et al., 2017; Blevins et al., 2010; Bode et al., 1999; Deiss et al., 2006; Petrovski et al., 2005; Racciah et al., 2009; Rodbard, 2017; Šoupal et al., 2016).
- Allen et al. showed that CGMS enhances physical activity in type 2 diabetes patients (Allen et al., 2008).
- CGMS also helps to reduce the time spent in hypoglycaemia or hyperglycaemia due to quicker reaction and therapeutic intervention (Beck et al., 2017; Šoupal et al., 2016; Tamborlane et al., 2008).
- It was shown that 60% of hypoglycaemia were not detected by conventional finger pricking method (Pitzer et al., 2001). Figure 2.14 shows examples of

intermittent glucose readings over a three days' period. States of hypoglycaemia (circled areas in Figure 2.14b) were missed in the Figure 2.14a due to less frequency of testing. This shows the importance of tighter glycaemic control and CGMSs can provide several measurements in an hour depending on the manufacturer.

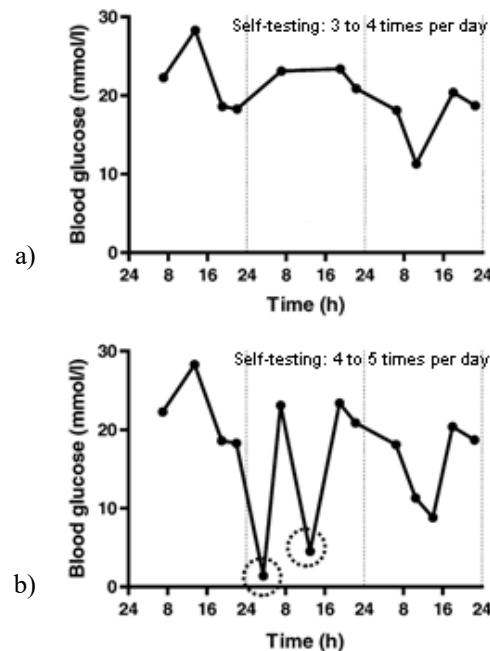


Figure 2.14 Example of intermittent glucose readings of a type 1 diabetes patient over three days. In 14a, three to four glucose readings were taken per day. In comparison in 14b, four to five readings were taken a day. The two circled areas in the bottom pictures indicate states of hypoglycaemia, which were missed in the top scenario due to less frequency of glucose measurement. (adapted from Pickup et al. 2005)

Glucose measurement from the interstitial fluid (ISF) is an alternative for blood glucose measurements and is commonly used in continuous glucose monitoring devices. ISF is part of the extracellular fluid amongst intravascular fluid (blood plasma) and cerebrospinal fluid. The glucose concentration in blood is an indicator of the overall glucose level in the body. Glucose molecules in the blood enter the ISF before taken up by the cells. The glucose in the ISF is depended on the site, how much glucose diffuses from the blood to the ISF and how much of the glucose is eventually metabolised by the nearby cells. Therefore, the glucose changes in the ISF are at slower rate compared to the glucose in blood. (Siegmund et al., 2017)

Good correlation between glucose concentration in ISF and capillary blood glucose concentration were identified in several studies (Bantle & Thomas 1997; Thennadil et al. 2001; Cengiz & Tamborlane 2009).17 patients with type 1 diabetes were subjects

in a study to test the correlation between dermal ISF and plasma glucose (Bantle & Thomas, 1997). Glucose levels were measured in plasma, capillary blood and ISF pre and postprandial period. The results from this study showed high correlation with  $R=0.95$  and  $p< 0.0001$  between plasma glucose and dermal ISF glucose.

It has to be noted that there is a physiological time lag of approximately six minutes between glucose in blood and in the ISF (Basu et al., 2015; Boyne et al., 2003; Kulcu et al., 2003). Therefore, it is crucial that the sensor used for ISF measurements is calibrated against a blood glucose values in a regular interval. Otherwise, in case of fast-changing glucose in patients, wrong treatment decisions might be made due to time-lagged glucose measurements

There is not only a difference in timing between glucose in ISF and blood but also in the magnitude. As mentioned, glucose molecules from the blood enter the ISF before taken up by the cells. This suggests that ISF glucose measurements can indicate earlier signs of hypoglycaemia than capillary glucose measurements (Thome-Duret et al., 1996).

ISF can be found in the subcutaneous tissue. In RI, the glucose from the ISF is extracted non- invasively and transdermally by applying a microampere current. Other continuous glucose monitoring devices insert a glucose sensor subcutaneously where in comes in contact with the glucose in the ISF. This method is considered as minimally- invasive as it involves puncturing the skin with a micro needle.

In general, CGMSs are seen as adjunct devices, which means that they are used as a supplement to the conventional finger pricking method. The glucose sensors in CGMS need to be calibrated against blood glucose values measured by intermittent glucose monitoring devices. It is also advised to confirm the reading of CGMS with a finger prick test before treating states of hypoglycaemia or hyperglycaemia. However, recent advances show the possibility of omission of the fingerstick glucose testing for treatment decisions with the use of the Dexcom G6 from Medtronic (see section Commercially available continuous glucose monitoring systems) (Castle & Jacobs 2016; Edelman 2017).

The first CGMS was introduced by Minimed Inc. in 1999, which is now part of Medtronic since 2001.

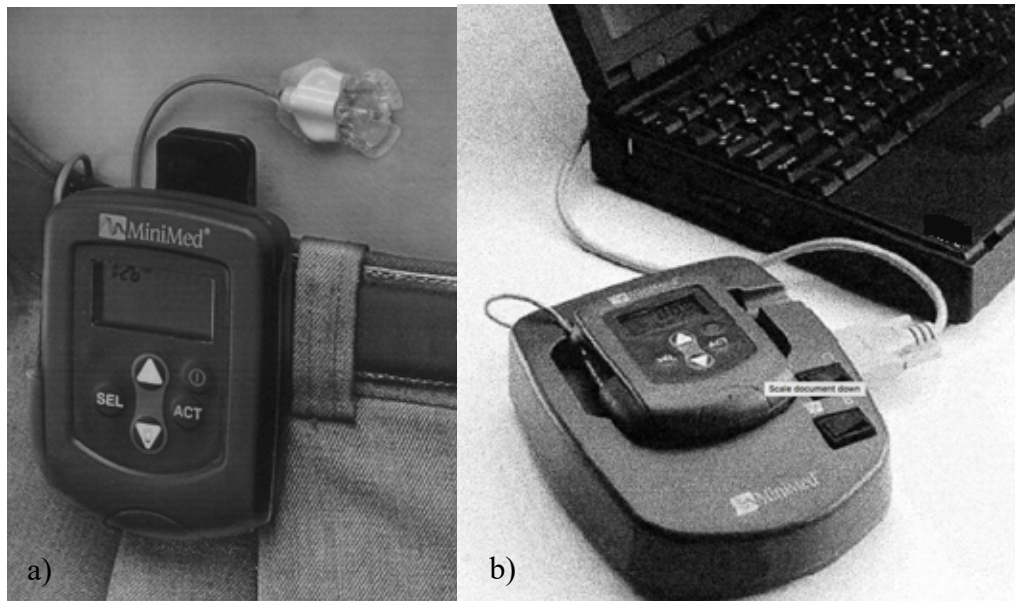


*Figure 2.15 Continuous glucose monitoring system from Minimed a) with the sensor attached to body and glucose meter (adapted from Bode et al. 1999) b) Glucose meter on the com-station for data transfer (adapted from Mastrototaro 2000)*

It was able to take glucose measurements from ISF every five minutes for 72 hours continuously in a range between 2.2 mmol/L and 22.2 mmol/L (Mastrototaro, 2000). After the three days, the data could be downloaded at the physician's office and discussed retrospectively.

The system consisted of a subcutaneous sensor, a connecting cable to the glucose meter (Figure 2.15a) and a com-station, which is a communication device to transfer data from the meter to the computer (Figure 2.15b). The disposable single use sensor was inserted subcutaneously and had a sensor life of three days. It was advised to calibrate the sensor four times a day to ensure sensor performance. Glucose oxidase was used an enzyme and glucose was measured by an amperometric measurement of the oxidation of  $H_2O_2$ . The amperometric measurement was in the nanoampere range. It was evaluated for home use by Gross et al in 2000 (Gross et al., 2000). 135 diabetes patients had to wear Minimed for at least three days and also take conventional finger prick blood glucose measurements. Both glucose results were compared and it showed a good agreement with a correlation of 0.91. It was a major breakthrough at that time. Although, measurement error of more than  $\pm 20\%$  was reported (Gross et al., 2000).

The CGMS nowadays have a reduced measurement error of approximately  $\pm 10\%$  (Damiano et al. 2014; Pleus et al. 2015; Nakamura & Balo 2015; Bailey et al. 2016).

## 2.6.1 Commercially available continuous glucose monitoring systems

The main companies focusing on CGMS now are Abbott, Dexcom and Medtronic. Most of the continuous glucose monitoring system in current use consists of implantable subcutaneous glucose sensor, which measures the glucose and a transmitter, which transfers the measured glucose measurements to a receiver. The receiver shows the glucose values on the display of the reader. The system can be further expanded with an insulin pump, which administers the adequate amount of insulin.

Glucose sensors for CGMS should have stability, high accuracy, rapid response, high selectivity to glucose and should be easy to implant and very importantly biocompatible.



*Figure 2.16 Medtronic's CGMS with a) Guardian 3 glucose sensor and Guardian 3 Link transmitter (adapted from Medtronic, 2019a) b) Minimed 670G pump (adapted from Medtronic, 2019b)*

Medtronic's most recent continuous glucose monitoring system is the Minimed 670G, which is used in conjunction with the Guardian 3 glucose sensor, the Guardian™ 3 Link transmitter and the MiniMed® 670G insulin pump. It is suitable for people above 14 years with type 1 diabetes. The sensor can be easily applied using a one-pressserter, which is a handheld device that can release the sensor onto the measuring site via a



single button press. (Food and Drug Administration, 2018). The sensor was successfully tested in terms of accuracy throughout the sensor shelf life of 7 days (Christiansen et al., 2017).

The Dexcom G5 was the first continuous glucose monitoring device developed by Dexcom, which was approved for non-adjuvant use by the FDA in 2016 (U.S. Food and Drug Administration, 2016). Hence, it does not need a confirmatory fingerpricking blood glucose measurement before taking action in case of hypoglycaemia or hyperglycaemia. That means that the insulin dosage adjustment is purely based on the glucose measurements from the CGMS.



*Figure 2.17 Dexcom G6 CGMS with a) the auto-applicator (adapted from Dexcom Inc., 2019) b) the Dexcom G6 glucose sensors with transmitter (adapted from Dexcom Inc., 2019) and c) the receiver in form of a smart phone (adapted from Dexcom Inc., 2019)*

The Dexcom G6 (Figure 2.17) is the latest CGMS developed by Dexcom, which has also been approved for non-adjuvant use by the FDA (U.S. Food and Drug Administration, 2018). In addition, no fingerstick calibration step is required either. It can be used by type 1 and type 2 diabetes patients and by adults as well as paediatrics older than two years. The Dexcom G6 is used in conjunction with the Dexcom G6 sensors, which have a sensor life of up to 10 days. It provides glucose measurements every five minutes and sends the readings directly to a smart device via the transmitter. The transmitter has a shelf life of three months and needs to be replaced after. The sensor is inserted into the body with an auto-applicator. The sensor is able to block any interferences caused by acetaminophen (Dexcom Inc., 2019). Accurate glucose

readings could be provided throughout the given sensor life of 10 days (Shah et al., 2018).

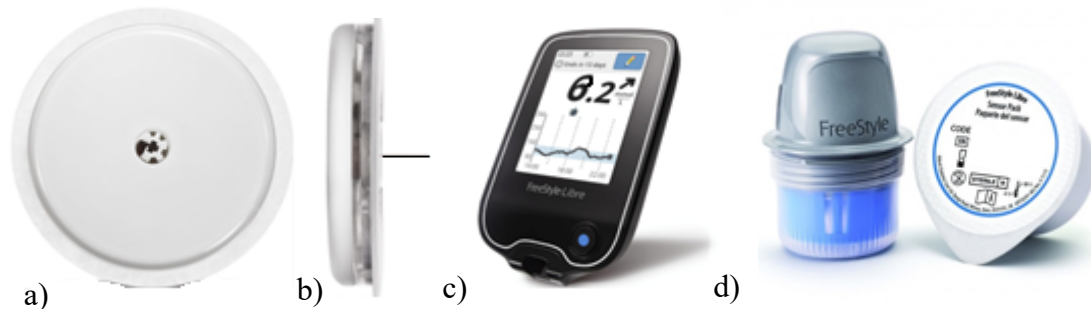


Figure 2.18 a) Glucose sensor for the Freestyle Libre (front view) (adapted from Abbott Laboratories Limited 2017b) b) Glucose sensor for the Freestyle Libre (side view) (adapted from Abbott Laboratories Limited 2017b) c) FreeStyle Libre glucose reader (adapted from Abbott Laboratories Limited 2017a) d) Glucose sensor applicator (left) with a new sensor in a package (right) (adapted from Children With Type 1 Diabetes 2016)

In 2015, Abbott laboratories introduced a flash glucose monitoring device the Freestyle Libre. The sensor (Figure 2.18a and Figure 2.18b) has the size of a £2 coin and is positioned in the back of the upper arm with the use of a so-called applicator (Figure 2.18d left). The sensor is located inside an applicator and by pushing the device down onto the skin, the sensor is applied. The sensor can stay up to 14 days in the body and measures glucose in ISF. In order to take a measurement, the patient only needs to scan the reader over the sensor within a distance between one and four centimetres. Abbott has also developed a free app for Android smartphones, the LibreLink, which can be used to take glucose measurements. By scanning the app on the glucose sensor, glucose readings can be taken instead of with the reader.

A big advantage of this device is that no calibration is required from the patient side. The data can be uploaded onto the FreeStyle Libre software for analysis.

Bailey et al. tested its usability and performance in 72 diabetes patients and the outcome was that the ISF glucose measurement corresponded well with the capillary blood glucose measurement in the time frame of 14 days (Bailey et al., 2016). A time lag of  $4.5 \pm 4.8$  minutes in average was identified between both measurements. Haak et al tested this flash glucose monitor in terms of safety and efficacy to compare it with current self-monitoring of blood glucose (Haak et al., 2017). 224 participants took part in the study. 149 subjects were using the flash glucose monitor and 75 subjects applied SMBG and followed their treatment regime. After six months, HbA1c levels were

measured from both groups and compared to each other. No differences were observable, which shows that the flash glucose monitor is as beneficial as conventional SMBG; however, without taking blood samples. The flash glucose monitoring device is highly favoured by the patients (Chaplin, 2016). On the downside, some users developed allergic contact dermatitis due to the isobornyl acrylate in the Freestyle Libre (Oppel et al., 2019).

Most recently, Senseonics developed the eversense CGMS (Figure 2.19) and received FDA approval to be used as a non-adjuvant device (Senseonics, 2019b). The big advantage of this CGM system is that the sensor has a shelf life of 90 days. Accurate glucose readings were shown throughout the given sensor life (Christiansen et al., 2019). The sensor, which has a size of 3.5 mm x 18.3 mm, needs to be implanted in the upper arm by a health care provider. Glucose measurements are taken with the implanted sensor, based on advanced fluorescence technology and sent via the transmitter, which has a dimension of 37.6 x 48 x 8.8 mm and is placed over the sensor on your upper arm to your smartphone.

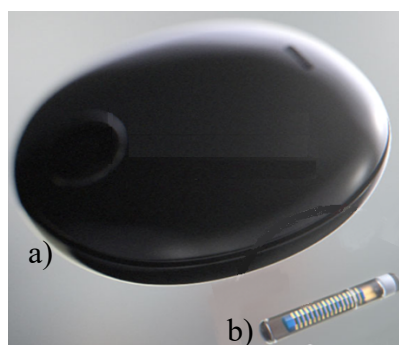


Figure 2.19 Senseonics' CGMS with a) the eversense transmitter and b) the implantable glucose sensor (adapted from Senseonics, 2019a)

Table 2.3 Technical details of selected commercially available glucose sensors for continuous glucose monitoring

Sensor	Company	Sensor measurement range [mmol/L]	Sensor lifetime	Number of calibrations per day
Freestyle Libre	Abbott	1.1 - 27.8	Up to 14 days	None
Dexcom G6	Dexcom	2.2 – 22.2	Up to 10 days	None
Guardian 3	Medtronic	2.2 – 22.2	Up to 7 days	3-4
Eversense	Senseonics	2.2 – 22.2	Up to 90 days	2

## 2.7 Problems with self- monitoring of blood glucose

Even though self-monitoring of glucose levels is very beneficial for glycaemic control, adherence to the treatment plan is a major concern. A variety of factors, such as demographic factors, physiological factors, social factors, health care provider and medical system factors, disease- and treatment-related factors have been listed as reasons for non- adherence (Delamater, 2006).

Vincze et al. conducted a study where they tested 933 diabetes patients and their adherence to self-monitoring of glucose (Vincze et al., 2004). It showed that only 52% of the patients followed the self-monitoring regime given by the healthcare provider. It was also shown that type 1 diabetes patients were more likely to adhere to SMBG. It was shown by Brindisi et al. that diabetes patients do not understand the importance of self-testing (Brindisi et al., 2007).

Polonski et al. tried to study factors for non-adherence by conducting a survey on 886 type 2 diabetes patients (Polonsky et al., 2014). The outcome of the survey revealed that the factors such as avoidance, pointlessness and burden are the main obstacles for self-monitoring of blood glucose. It was suggested that education by healthcare professional is a crucial factor in adherence.

A randomised clinical trial in India revealed that patient adherence to medication and frequency of blood glucose testing was increased using an m-health platform (Kleinman et al., 2017).

Wagner et al. reported that the invasiveness of self-monitoring of glucose is seen as a barrier for adherence (Wagner et al., 2005). It suggested that non-invasive methods would enhance the frequency of self-testing as well as improve quality of life.

## 2.8 Towards non- invasive glucose monitoring

In contrast to invasive glucose monitoring methods, non- invasive glucose monitoring devices do not breach the skin barrier. This emerging development is a big step towards pain free glucose monitoring and an immense improvement in quality of life in diabetes patients.

## 2.8.1 Currently/ Upcoming commercially available non-invasive glucose monitoring systems



*Figure 2.20 GlucoWise device from MediWise (adapted from MediWise 2017)*

Glucowise™ (Figure 2.20) from MediWise is a non-invasive blood glucose measuring device under development (MediWise, 2017). It offers real time capillary blood glucose monitoring and can send the results directly to the patients' smartphone or tablet via Bluetooth or transferred to their computers via a USB cable. By sending a high frequency radio wave in the range of 65 GHz, it measures glucose either on the ear lobe or on the skin between the thumb on index finger. Unlimited number of measurements can be taken by the device by placing it on the measurement sites. The sensor detects the transmitted waves which correlates with the glucose concentration. It further uses another method where they integrate a nano-composite film onto the sensor so that the skin is made transparent when applying the high frequency wave. This enables the use of the device by people with any skin colour or skin type or people at any age. Accuracy and sensitivity related data are not published yet. However, for the device to come to the market, the accuracy and performance levels of the device needs to be met according to the Class IIa medical device regulations. The development phase of the device is currently ongoing and after performing clinicals trials it will be available for public (META, 2021).



*Figure 2.21 GlucoTrack device by integrity applications (adapted from Integrity Applications 2017)). It consists of a main unit and a Personal Ear Clipper*

The GlucoTrack (Figure 2.21) by the company integrity applications is another non-invasive blood glucose monitoring device (Integrity Applications, 2017). This device measures glucose by independently applying ultrasonic, electromagnetic and thermal technologies at the same time and then applying a proprietary algorithm to give an average glucose reading from all three measurements techniques (Freger et al., 2005). The ultrasonic technique is based on the measurement of the velocity of the ultrasonic wave through tissue with the use of a ultrasonic transmitter and the use of an ultrasonic receiver at the other side of the tissue. There is a linear relationship between the propagation velocity and the glucose concentration. With increasing glucose concentration, the velocity of propagation increases as well.

The electromagnetic technology is based on detecting the changes in the electrical impedance of the tissue due to variations in the glucose concentration.

Glucose alterations has also an impact on the heat transfer characteristics of tissue. Therefore, changes in the blood glucose causes variations in the temperature in terms of magnitude and rate. With a thermal sensor a certain amount of energy is applied onto the tissue. Thereby, higher the temperatures in the tissue can be detected with increasing glucose concentration.

By combining three technologies, the errors from each method separately can be diminished, therefore increasing the overall accuracy. The mulitsensors is integrated in a personal ear clipper and then clipped onto the ear lobe to take readings.

Data is transferred through usb port. Same as with the GlucoWise device, unlimited glucose measurements can be taken with the device. Both cut the cost by not needing to buy further disposables sensors for measurement. The device needs to be calibrated against basal and postprandial glucose levels using fingerstick blood sample measurements.

This device has received CE mark for type two diabetes patients or prediabetes patients over 18 years for home glucose monitoring (Wilmington et al., 2017).

It was shown that by combining three technologies enhanced accuracy and precision in the glucose readings can be achieved (Harman-Boehm et al., 2010).

Horman et al. evaluated the device in terms of user experience and device performance over a six months period (Horman et al., 2016). The outcome of the study showed that 98% of the measurement results were in clinically acceptable zone A& B of the Clarke error grid and the device was highly accepted by diabetes patients.

EyeSense GmbH devised two devices for glucose monitoring, the Eyesense sensor which can take intermittent glucose measurements of the tissue fluid under the conjunctiva and the FiberSense-system, a device for continuous glucose monitoring in ISF.

Both sensors are based on fiber optic methods in combination with fluorescence photometry.

The chemical sensor is made of a hydrogel matrix which contains particles of dye labelled sensor molecule. The particles can measure glucose without changing any chemical properties of the glucose itself. It is the sensor particles which are changed by the glucose and hence causes a change of the dye, which can be detected by the fluorescence photometer. The intensity of the emitted fluorescence is in correlation with the glucose concentration.

By making a one to two-millimetre incision of the conjunctiva by the ophthalmologist, the sensor chip is implanted into the eye. The sensor can be kept in the eye for up to a year and can be inserted in either of the eye as many times as required. The glucose can be measured as many times as wanted by scanning a handheld photometer over the chip.

The sensor was tested on 28 subjects with diabetes in terms of sensor performance as well as safety of the implant in a time frame of 16 weeks (Hasslacher et al., 2012). The outcome of the study showed good correlation between sensor glucose measurements in ISF with capillary glucose measurements obtained by finger pricking method. Even though the sensor was well tolerated by the patients, a mild haemorrhage under the conjunctiva was experienced by most patients.

The FiberSense-system can be placed on the arm or on the abdomen and glucose measurements are sent continuously and wirelessly to the reader. Initial evaluation of the sensor showed good sensor performance for the first 14 days (Müller et al., 2013). This sensor has a shelf life of one month.

There are a variety of methods, which can be employed for non-invasive glucose monitoring but are still in the development phase or have not yet been used in a glucose monitoring device.

The Medical Diagnostics and Wearables Group at Strathclyde is working on devices for transdermal continuous monitoring of glucose using reverse iontophoresis (RI). RI is a process which enables transdermal extraction molecules by applying low current to the skin (Santi & Guy, 1996a).

## 2.8.2 Glucose monitoring using reverse iontophoresis

Iontophoresis is a widely used technique which enhances drug delivery across the skin by the application of current (Singh & Maibach, 1994). It is used for therapeutic, laboratory and diagnostics purposes.

RI can be used for a variety of applications such as detecting diagnostics markers, therapeutic drug monitoring and also glucose monitoring (Guy et al., 2000). RI for non-invasive glucose monitoring was first suggested by Rao et al in 1993 (Rao et al., 1993). To prove this concept, *in vitro* experiments on hairless mouse skin were performed. They successfully managed to extract glucose by the application of a current of  $0.34 \text{ mA/cm}^2$ . Rao et al also successfully proved that RI can be applied on humans to measure glucose levels (Rao et al., 1995). Tamada et al. tested the



relationship between extracted glucose via RI and blood glucose concentrations on five diabetic subjects and identified a time lag of 20 minutes and an average correlation coefficient of  $r=0.89$  (Tamada et al., 1995). In RI, an iontophoretic current is applied across the skin using two electrodes with a conducting gel, which facilitates the extraction of charged and neutral molecules and ions from the ISF into the gel reservoir. Three transport mechanisms are involved in RI, 1) electromigration, 2) passive diffusion and 3) electroosmosis which the main transport for glucose. As the human skin has net negative charge at physiological levels (Burnette & Ongpipattanakul, 1987), a solvent flow is created between the two electrodes (from anode to cathode). Glucose, which is an uncharged molecule, is carried along the solvent flow to the cathode. RI is explained in further detail in the theory chapter, section 4.2.

The use of RI for transdermal monitoring of molecules was further tested by other research groups. Sieg et al. extracted glucose and urea simultaneously (Sieg et al., 2004b) and Ching and Connolly successfully demonstrated the simultaneous extraction of glucose and lactate (Ching & Connolly, 2008c). The extracted analytes can be quantified with the help of biosensors (Kurnik et al., 1999).

RI was first successfully employed in the Glucowatch Biographer by Cygnus Inc, a wrist watch type of device for the use of continuous, non-invasive glucose monitoring (Figure 2.22a), which received FDA approval in 2000 (Sage, 2000).

The device was able to take transdermal glucose measurements every 20 minutes for up to 12 hours. For every 12 hours of measurement a three hours warming up period was required followed by a calibration of the devices with a fingerstick blood glucose level. The device was a supplement to conventional blood glucose measurements. It was able to give alarms in case of hypo- or hyperglycaemia or in case of fast falling glycaemic levels.

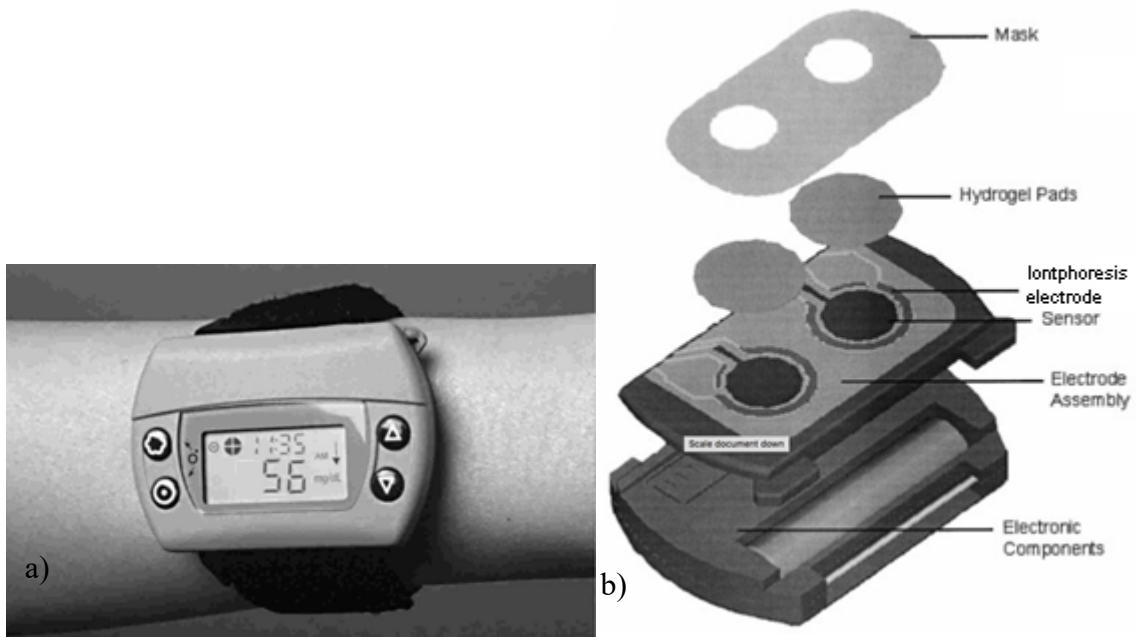


Figure 2.22 a) Glucosewatch in use (adapted from Tierney et al. 2001) b) Autosensor unit (adapted from Tierney et al. 1999)

The AutoSensor (Figure 2.22b) was disposable and needed to be replaced after every 15 hours of measurement cycle. It consisted of two iontophoresis electrodes, a biosensing unit, two hydrogel disks and an adhesive pad to secure the device onto the skin. The gel acted on one side as a conducting material and on the other side as a gel reservoir. A mask was used to direct diffused glucose to the glucose sensing unit.

When applying an iontophoretic current across the skin, the current will flow from one direction to the other. Therefore, two iontophoresis electrodes were needed to complete a circuit. One acted as a cathode (positively charged electrode) and one acted as an anode (negatively charged electrode). A solvent flow was created from anode to cathode by the application of an iontophoretic current, and glucose was extracted to the cathode via the electroosmotic flow. Hence, the glucose was extracted into a gel reservoir of the cathode, where the biosensing unit is integrated. After the application of a constant current of  $300 \mu\text{A}$  the glucose was quantified with an amperometric sensor. The sensor was designed by Tierney et al (Tierney et al., 1999). It was based on enzymatic reaction with glucose oxidase, which was dissolved in the gel, and the amount of hydrogen peroxide produced was measured on a platinum electrode.

The oxygen dependency was not a concern in this technology because of the low glucose concentration levels. Furthermore, the skin itself acted as a filter preventing larger molecules pass the skin pores and hence lowered electrode fouling. Moreover,

interferences from some electroactive species such as urate or ascorbate were eliminated as they were carried to the anode because of their charge. This sensor was operated at a voltage of 0.42 V (vs AgAgCl reference electrode) as compared to other H<sub>2</sub>O<sub>2</sub> measuring biosensor, which have an operating potential of approximately 0.6 V. The applied low potential avoided interferences of the higher voltage electroactive species such as tryptophan or tyrosine.

Around 50 picomol to 500 picomol of glucose was extracted after a 3 minutes' iontophoresis cycle. However, the amount of glucose extracted into the gel reservoir is between 2.5  $\mu$ M to 25  $\mu$ M, i.e. all the glucose extracted does not reach the sensor surface. Furthermore, the device was able to measure the temperature of the skin, which is an indicator about the patients' perspiration state and also skin conductance.

Good correlation between GlucoWatch readings and a reference glucose reading using standard fingerstick method were identified in various studies. In a clinical controlled setting, following correlation factors were reported:  $r=0.90$  (Garg et al., 1999),  $r=0.88$  (Tamada et al., 1999),  $r=0.85$  (Tierney et al., 1999) and  $r=0.90$  (Gandrud et al., 2004). In comparison, in the home environment lower correlation factors were identified  $r=0.85$  (Garg et al., 1999) and  $r=0.80$  (Tierney et al., 1999).

Nunnold et al. reported that the correlation between GlucoWatch readings and reference readings was compromised ( $r=0.81$ ) if subjects were performing physical activity with moderate or heavy sweating (Nunnhold et al., 2004).

In most of the studies, more than 93% of the measurements results were within the Region A and B of the Clarke Error Grid such as 96% (Garg et al., 1999), 96.8% (Tamada et al., 1999). and 94% (Tierney et al., 1999), 93% (Tierney et al., 2000) and 95% (Eastman et al., 2002).

A lag time of 17 to 20 minutes was identified between the glucose readings from the GlucoWatch and the corresponding blood glucose reading (Garg et al., 1999; Pitzer et al., 2001; Tamada et al., 1999; Tierney et al., 2000). As previously mentioned, there is a physiological time lag of approximately six minutes between glucose in blood and in the ISF (Basu et al., 2015; Boyne et al., 2003; Kulcu et al., 2003). This indicates a

time lag of around 11-14 minutes is due to the instrument for glucose measurement itself.

Chase et al proved that the GlucoWatch enhanced glycaemic control (Chase et al., 2003). HbA1c levels in 40 children were monitored for up to nine months. The glycated haemoglobin level decreased in average from 8.9% to 8.4% in the GlucoWatch group. In comparison, in the control group the HbA1c level was the same after nine months with conventional fingerstick blood glucose monitoring. It was shown that the GlucoWatch can detect hypoglycaemia effectively and due to the hypoglycaemic related alarms patients can intervene quicker (Pitzer et al., 2001).

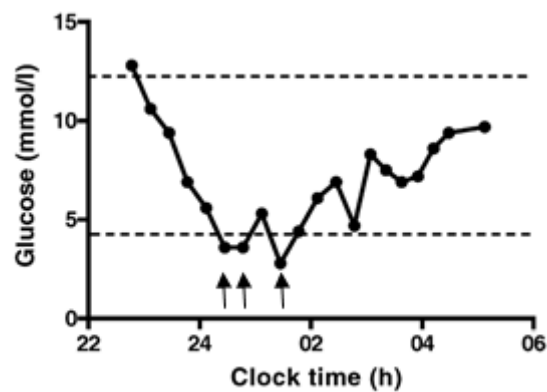


Figure 2.23 Example of glucose variation at night time measured with the GlucoWatch; The dashed lines indicate the thresholds for hyper- and hypoglycaemia. The arrows show alarms raised by the device because of hypoglycaemia. (adapted from Pickup et al. 2005)

In Garg's study, patients had to wear two GlucoWatches and glucose measurements were taken three times in an hour. When comparing the results of the two biographers worn simultaneously by the subjects, a correlation factor of 0.94 was identified. Eastman et al successfully tested the effectiveness and safety of GlucoWatch in 66 children and adolescents (Eastman et al., 2002). Various testing sites including lower and upper arm, leg and torso were investigated. The mean absolute relative difference (MARD) between GlucoWatch readings and reference readings was the lowest for the device on the lower arm with 21%, for upper arm it was 21.3%, for legs 21.8% and for torso it was 21.2%. Also, securing the device on upper arm, legs and torso was shown to be more difficult and led to skipping glucose reading. Furthermore, it is important for the user to see the display of the device for calibration purposes.

One limitation of this device is that even though glucose is extracted and quantified non-invasively, invasive means is still required for calibration. Scientists are looking are ways to omit fingerstick calibration procedure and instead having an internal standard such as sodium (Sieg et al., 2004a) or potassium (McCormick et al., 2012). However, more research has to be done to achieve clinical acceptance. Furthermore, temporary skin irritations such as edema or erythema were reported in many studies by the use of the GlucoWatch (Eastman et al., 2002; Gandrud et al., 2004; Garg et al., 1999; Tamada et al., 1999; Tierney et al., 1999). It took two to seven days for them to resolve. Moreover, in Gandrud's study it was shown that out of 1263 glucose readings in total from the GlucoWatch, in 33% of the measurement the reading was skipped due to either excessive sweat, or change in temperature and inconsistencies in the glucose measurements between the two measurement cycles, which can be caused by extreme movement or unwanted force exertion on the device itself. (Gandrud et al., 2004)



*Figure 2.24 SugarBeat® patch (red box) applied on an arm (adapted from Nemaaura 2016)*

Nemaaura Medical Inc. has devised a non-invasive continuous glucose monitoring system the SugarBeat® (Figure 2.24), which is also based on RI. It can be placed onto the arm, leg or abdomen and has a sensor life of 24 hours. It consists of a disposable needle-free 1 mm thick patch with a transmitter. Each patch needs a fingerstick calibration before use. After the calibration and a 30 minute warm up period, it can take glucose readings every five minutes and send the results directly to the

smartphone or a reader device via Bluetooth. It can be used by type 1 and type 2 diabetes patients as an adjunctive help to conventional fingerprick glucose monitoring. Glucose molecules are extracted from the ISF by applying a low electric current. And the extracted glucose is converted to a glucose concentration. It is expected to be brought to the market in 2019 in United Kingdom (SugarBEAT™, 2017).

Bandodkar et al. devised a flexible tattoo based glucose monitoring system based on reverse iontophoresis in 2014 (Bandodkar et al., 2014) (Figure 2.25).

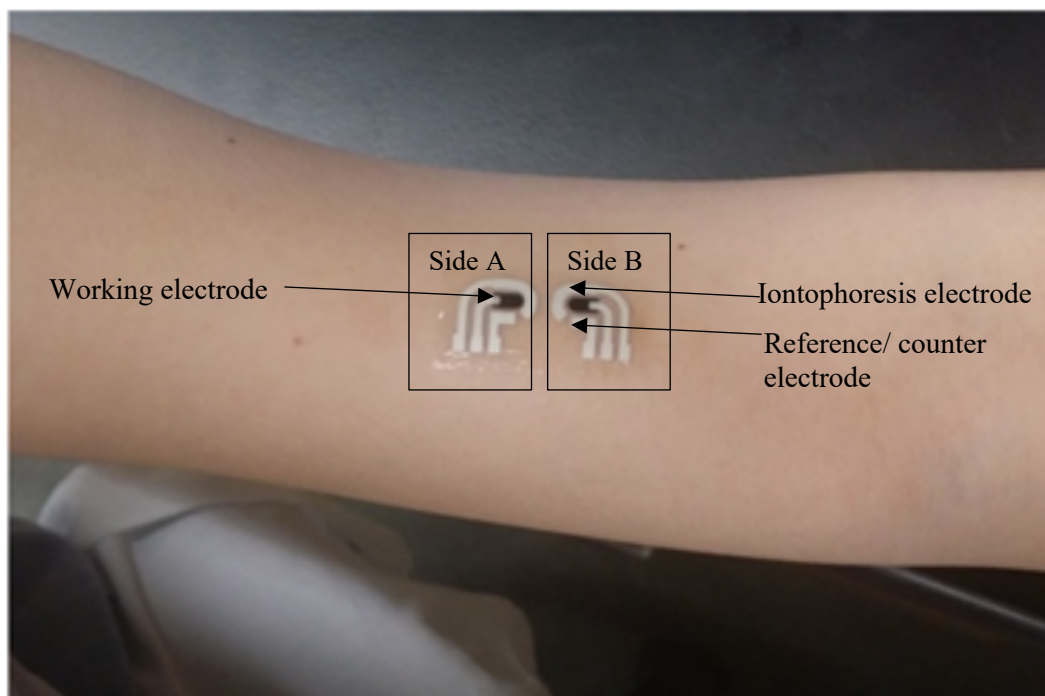


Figure 2.25 Tattoo sensor applied on forearm (adapted from Bandodkar et al. 2014)

They addressed the skin irritations, which were reported by using the Gluowatch with lowering the iontophoretic current to  $0.2 \text{ mA/cm}^2$ . The sensor consists of two iontophoresis electrodes to complete a circuit. A solvent flow was created from anode to cathode by the application of an iontophoretic current, and glucose was extracted at the cathode.

A hydrogel layer was applied between the electrodes and the skin. It was shown that the use of the hydrogel layer prevents skin irritations and is efficient for glucose extraction.

The iontophoresis and reference/counter electrode were printed using Ag/AgCl ink and for the working electrode, Prussian Blue conductive carbon ink was used. Prussian Blue is a mediator and can be used to detect H<sub>2</sub>O<sub>2</sub>.

Two sensing units were integrated in the sensor, side A and side B: The glucose oxidase layer was embedded onto the working electrode of the cathodal side of the iontophoresis electrode with the help of a polymer, called chitosan. The cathodal side is responsible to detect any glucose related current changes. The anodal side of the glucose sensor not coated with any enzyme and it is intended to identify any background current or any current caused by any interfering species. This method helps to increase the specificity of the sensors towards glucose measurements.

Glucose in the ISF was quantified using an amperometric measurement at a potential of -0.1V vs Ag/AgCl.

The sensor showed linear response to glucose concentrations for up to 100  $\mu$ M with a lower detection limit of 3  $\mu$ M in an *in vitro* environment.

The preliminary study proved the concept of skin worn tattoo-based biosensor to be used for glucose monitoring. However, more research has to be conducted for it to be used as part of diabetes management.

Kim et al developed a wearable biosensor which has the ability to simultaneously measure glucose from the ISF and sweat extracted via RI (Kim et al., 2018).



1	Counter electrode
2	Iontophoresis electrode
3	Working electrode
4	Reference electrode

Figure 2.26 Panda-shaped screen-printed three electrode system with iontophoresis electrodes (adapted from Kim et al., 2018)

The panda-shaped sensor (Figure 2.26) consists of an anodal and a cathodal side and for both sides a three-electrode system with an iontophoresis electrode for the application of an iontophoretic current of 300  $\mu$ A/cm<sup>2</sup> can be seen. The anodal side is intended for measuring sweat and glucose is measured at the cathodal side.

The working electrode and the counter electrode consist of a Prussian blue modified carbon ink and the reference and iontophoresis electrodes were prepared using Ag/AgCl ink. For the biosensing unit of glucose, glucose oxidase was immobilised

onto the working electrode with the help of chitosan. Glucose was measured electrochemically at a voltage of -0.2V at the cathodal side using enzymatic glucose electrode. A linear current response was observable with increasing the glucose concentration from 0  $\mu\text{M}$  to 160  $\mu\text{M}$ . A healthy volunteer study was conducted with 11 subjects to test the performance of the wearable sensor. Good correlation between the sensor results and measurements using a commercially available blood glucose meter could be identified.

## 2.9 Factors, which have an impact on RI of human skin for molecular and ionic extraction

The aim of the project was to improve transdermal extraction and sensing of glucose linked to RI. This was done by conducting *in vitro* RI experiments using a diffusion cell with an artificial membrane. The applied experimental setup to perform RI experiments is shown in detail in section 5.6. There are a variety of biological and operational factors, which have an impact on the extraction of glucose via RI and are discussed here:

### 2.9.1 Biological factors

#### Skin:

The skin is the largest organ of the human body with an area of 1.5 to 2  $\text{m}^2$  and accounts of approximately 16% of the body weight. It is a versatile organ and responsible for a variety of functions. It protects underlying tissues and organs from any sort of impact, chemical attack, abrasion or fluid loss. It regulates and maintains body temperature. It is responsible for the removal of salt, water and any organic waste products. It is one of the sensory organs and responsible for sensing pressure, pain, touch and temperature stimuli and transfer of information to the nervous system.



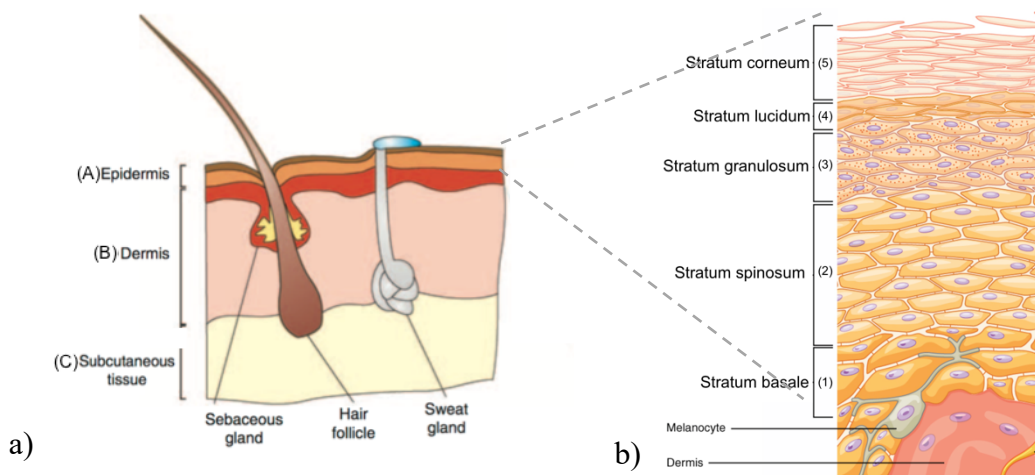


Figure 2.27 a) Structure of skin with the three layers A) epidermis, B) dermis and C) subcutaneous tissue (adapted from Kern et al. 2011) b) Layers of epidermis stratum basale (1), the stratum spinosum (2), the stratum granulosum (3), then the stratum lucidum (4) and the stratum corneum (5) (adapted from Betts et al., 2017b)

The skin has a thickness of 4 mm (Wood & Bladon, 1985) and consists of the following three layers: the epidermis (A), the dermis (B) and the subcutaneous tissue (C) (Figure 2.27). Each layer has its own purpose and characteristics. The cells in the epidermis are called keratinocytes and contain the protein keratin. The total thickness of the epidermis is 100  $\mu\text{m}$  (Wood & Bladon, 1985) and the epidermis is avascular. It is supplied with oxygen and nutrients by diffusion from the capillaries within the dermis. The epidermis consists of five layers containing keratinocytes, the stratum basale (1), which is the innermost layer, then the stratum spinosum (2), followed by the stratum granulosum (3), then the stratum lucidum (4) and the outermost layer is the stratum corneum (5) (Betts et al., 2017b; Martini et al., 2014b). The skin has the ability of constant self-renewal. It takes about 15 to 30 days for a cell to move from the innermost layer of the epidermis to the outermost layer of the epidermis. The stratum corneum has a thickness of roughly 15 to 40  $\mu\text{m}$  (Coston & Li, 2002) and provides the primary barrier between the body and the environment. Corneocytes are a type of keratinocytes, which you can find in the stratum corneum. These corneocytes are enclosed in lipid by layer, which creates a brick and mortar structure (Figure 2.28) (Elias, 1983).

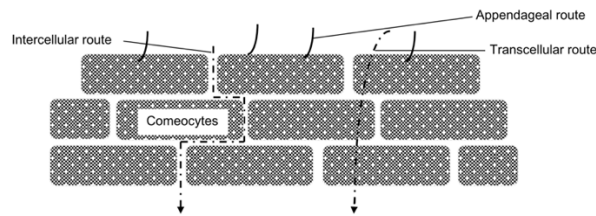


Figure 2.28 Stratum corneum with corneocytes in a brick and mortar structure.(adapted from Dhote et al. 2012)

The dermis (B) consists of two layers the papillary layer and the reticular layer. It encloses the capillaries and lymphatics as well as the sensory neurons, which is responsible for the surface of the skin placed within the dermis. Sweat glands and hair follicles are also part of the dermis. The subcutaneous tissue (C) mainly consists of adipose tissues and the large blood vessels can be found it in this part. (Martini et al., 2014b)

### Pathways of ions and molecules across the skin

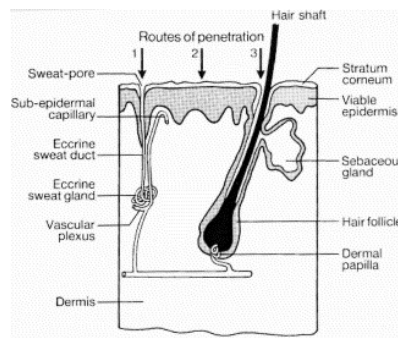


Figure 2.29 Routes of penetrations across the skin (adapted from Barry 2002) 1) via sweat pores, 2) through the skin and 3) via hair follicles

There are mainly two pathways, 1) the appendageal pathway and 2) the non-appendageal pathway (Cullander, 1992). In the first pathway, the molecules follow the path of hair follicles, sweat glands or secretory glands. In the second, molecules can cross the skin either intercellularly or transcellularly (intracellularly) (Figure 2.29). Intercellularly means that the molecules take the route between the corneocytes. In contrast, transcellular movement indicates that the molecules cross the corneocytes. It was shown that the appendageal pathway predominates, as molecules prefer the path of least resistance (Burnette & Marrero, 1986; Burnette & Ongpipattanakul, 1988; Del Terzo et al., 1989).

The properties of the skin vary from person to person depending on a variety of factors such as gender (Giacomoni et al., 2009), ethnicity (Wesley & Maibach, 2003) and age

(Sugihara et al., 1991). It was reported that skin thickness varies depending of the site of the skin on the human body. For example the skin on the forehead is thicker than of the ventral forearm (Diridollou et al., 2000). The skin itself acts as a barrier and limits the extraction of all molecules across the skin when applying RI. It is reported that additional permeation enhancers are required to enable the extraction of molecules with a higher molecular weight than 500 Da (McCormick et al., 2012) (1 Dalton equals to 1 g/mol) when applying an iontophoretic current. Glucose having a molecular weight of 180 Da, is able to penetrate the skin without any additional enhancers. The pore size of the human skin varies from 10 Å to 25 Å (Ching, 2005) (1 Å equals to 0.1 nm).

In this project, a commercially available membrane was used to mimic the stratum corneum due to ethical, safety and legal reason. Furthermore, this also helped to avoid any sample to sample variation. Eventually for the device to be part of a wearable sensor for continuous glucose monitoring the variability in skin and therefore the variation in the glucose flux rates depending on patient and anatomical needs to be addressed. Skin variability can be considered by for example measuring skin impedance as it correlates well with skin permeability (Li et al., 2015). Therefore, integrating an electrode system to the device, which allows skin impedance measurement and make it part of the calibration process of each individual can help to account for skin variability.

## 2.9.2 Operational factors

A variety of experimental conditions have an impact on efficiency of the glucose extractions from RI systems. Three transport mechanism are involved in RI: 1) electromigration, 2) passive diffusion and 3) convection due to electroosmosis, which is the main transport mechanism for glucose. Convective flow caused by electroosmosis is induced by the application of an electric field across a charged membrane. Thereby, a solvent flow is created in the same direction as the flow of counterions. As the human skin has net negative charge at physiological levels (Burnette & Ongpipattanakul, 1987), a solvent flow is created between the two

electrodes (from anode to cathode). Glucose, which is an uncharged molecule, is carried along the solvent flow to the cathode.

The parameters, which have an influence on glucose extraction via RI are discussed here:

#### 2.9.2.1 pH of the buffer solution, which simulates the ISF

In the *in vitro* RI experiments, the diffusion cell is filled with a buffer, which simulates the ISF. Santi and Guy showed that the pH of the buffer solution in the diffusion cell has an impact on RI (Santi & Guy, 1996b). They reported that the cathodal extraction was improved by increasing the pH in the buffer solution. This can be explained by the isoelectric point of skin, which is approximately at a pH of 4. The isoelectric point is the pH where there is electroneutrality. When increasing the pH, the negative charge of the skin increases, which in turn leads to improved electroosmotic flow from the positive pole to the negative pole. In contrast, lowering the pH of the buffer leads to improved anodal extraction. When decreasing the pH, the negative charge from the skin declines, which causes less electroosmotic flow from anode to cathode. It was shown too high or too low pH levels can cause skin irritations. Under physiological condition, the skin has a pH of 7.4, hence the buffer solution for the diffusion cell in this project was adjusted to the same pH.

#### 2.9.2.2 Current intensity

The application of a low current to the skin, enables the transdermal extraction of molecules and ions across the skin. It has to be taken into account that the intensity of the applied current is limited as it was reported that applying high current across to skin can cause a variety of adverse effects such as tingling, pricking, itching, irritations or high pain or discomfort depending on the current density (Ledger, 1992). A maximum current density of 0.5 mA/cm<sup>2</sup> was identified as tolerable with respect to human safety (Banga & Chien, 1988; Burnette & Ongpipattanakul, 1988; Ledger, 1992). Delgado-Charro and Guy reported that the convective flow from anode to cathode did increase with higher current density. They also mentioned that the electroosmotic flow from cathode to anode decreased with higher current density (Delgado-Charro & Guy, 1994). Santi and Guy performed RI experiments with current densities of 0.3 mA/cm<sup>2</sup> and 0.5 mA/cm<sup>2</sup>. They were able to extract more mannitol

when applying the higher current, however, there was no significant difference between both current densities (Santi & Guy, 1996b). Few studies were reported where RI experiments were conducted on humans (Bandodkar et al., 2014; Ching, 2005; McCormick et al., 2012; Rao et al., 1995; Sieg et al., 2004a; Tamada et al., 1995). In these studies, they applied a current density ranging from 0.1 mA/cm<sup>2</sup> to 0.35 mA/cm<sup>2</sup>. To-date, McCormick et al. applied the least amount of current. They only applied a current of 0.1 mA/cm<sup>2</sup> and were able to extract on average  $25.9 \pm 5.4$   $\mu$ M of glucose across both iontophoresis electrodes from human subjects in the fasted state. The *in situ* glucose sensor used in the Gluowatch was able to quantify glucose concentrations down to 5  $\mu$ M (Tierney et al., 1999, 2001). This shows that it is possible to detect the glucose concentrations obtained via RI with 100  $\mu$ A/cm<sup>2</sup> with a similar *in situ* sensor and the potential of the low current to be used for continuous glucose monitoring. Lowering the iontophoretic current to 100  $\mu$ A/cm<sup>2</sup> is beneficial as it is associated with lower pain, hence it will increase the acceptance level of user (Ledger, 1992). Furthermore, the amount extracted by McCormick et al was comparably even higher than in Rao et al's work, even though the latter applied a current of 0.25 mA/cm<sup>2</sup>. Rao et al. were able to extract approximately 5.8 nmol of glucose across the human skin to the cathodal chamber when applying RI for one hour (Rao et al., 1995). In contrast, McCormick et al. extracted on average 11 nmol of glucose after one hour of RI. The average glucose flux was identified as 3.8 nm/cm<sup>2</sup>h by McCormick et al. This value corresponds well with the fluxes of 1-8 nm/cm<sup>2</sup>h obtained by Tamada et al. (Tamada et al., 1995). The aim is to apply a current as low as possible to avoid any discomfort or pain to the patients. Due to the successful extraction of glucose in such low current density, a current density of 0.1 mA/cm<sup>2</sup> was also used for this project.

### 2.9.2.3 Current waveform

The applied current waveform plays a crucial role in RI. The application of a direct current (DC) during RI leads to the accumulation of hydroxyl ions and hydrogen ions at the anode respectively cathode. Thereby the local pH changes which in return cause erythema, stinging and can also lead to electrochemical burns on the skin underneath the electrodes (Howard et al., 1995).

The application of a pulsed DC was tested and it was shown that it reduces pH alterations. Skin polarisation, which is the charge build-up at the skin is prevented as during pulsed DC the skin has time to depolarise (Chien et al., 1987, 1990).

Another possibility is the use of a bipolar current. Thereby, a direct current is applied for a specific time and the direction of current flow is switched periodically. Due to the change of polarity, skin polarisation is prevented and pH alterations are minimised. The theory behind that is the build-up of hydrogen at the initial anode and a hydroxyl-build up at the initial cathode. When switching polarities, the initial anode becomes the cathode and hydroxyl ions start accumulating at the cathode. And when the initial cathode becomes the anode, the hydrogen ions start accumulating. Hence, the change in direction of current allows the skin to depolarise. Tomohira et al. tested the bipolar current profile with and without switching polarities on rats. Thereby iontophoresis was applied to deliver insulin and calcitonin across the skin. It was reported that an increased output of drugs can be achieved with switching of polarities. (Tomohira et al., 1997). Hirvonen et al studied the application of different current waveforms in with an in-vitro system for delivering of amino acids via iontophoresis. It was shown that bipolar current had improved transport rates more than pulsed current. In addition, the transport rate of direct current and bipolar current were comparable (Hirvonen et al., 1995).

Ching and Connolly investigated the effect of direct current with switching polarities at different time intervals on transdermal glucose extraction in in-vitro RI experiments. They tested 1) direct current for 60 minutes, 2) direct current with switching polarities every 5 minutes for a total RI duration of 60 minutes, 3) direct current with switching polarities every 10 minutes for a total RI duration of 60 minutes and 4) direct current with switching polarities every 15 minutes for a total RI duration of 60 minutes. It was shown that the last current waveform showed the highest amount of glucose extracted (Ching & Connolly, 2008c). Furthermore, it was also shown that switching polarities minimises skin irritations in humans (Ching & Connolly, 2008b). Therefore, a bipolar current with switching polarities every 15 minutes was used in this project.

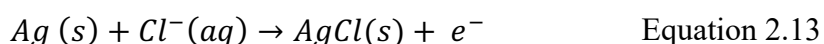
#### 2.9.2.4 Medium for current passage from electrode to skin

A conducting medium is required for the current to pass from the electrode to the skin. Gels or liquids can be used for this purpose. It was shown that gels have more

advantages than aqueous solution because 1) they provide good stability, 2) they can be used with a variety of electrode designs, 3) they provide improved occlusion, 4) they can be easily deformed to the skin structure and 5) they provide good conductivity for current transfer due to the high-water content in the gel. Several studies have used gel as a medium for iontophoresis experiments (Alvarez-Figueroa & Blanco-Méndez, 2001; Bandodkar et al., 2014; Banga & Chien, 1993; Phipps et al., 1989). In this project, the gel was prepared using methylcellulose powder. It is a non-toxic carbohydrate polymer. It has been used in the food and pharmaceutical industry (DOW, 2013). Research groups have used methylcellulose gel in some iontophoresis experiments (Calkin et al., 2002; Noon et al., 1998; Schmelz et al., 1997) and also in RI experiments (Arias, 2011; Ching & Connolly, 2008c; Mackinnon, 2004; McCormick et al., 2012). As RI experiments are pH sensitive, it is important for the gel to be able to maintain its pH level. Phosphate buffer was added to the methylcellulose gel for that purpose as it helps to maintain the pH level stable and it is also non-toxic to humans.

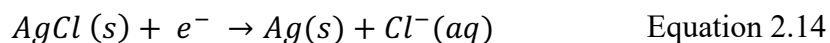
#### 2.9.2.5 Electrode material for RI experiments

The type of electrode used for RI does also have an impact on the process of RI. There are polarisable and non-polarisable electrodes. In an ideally polarisable electrode there is no current flow between the electrode-electrolyte interface and the electrode. The electrodes act as a capacitor and there will be no charge transfer. Platinum electrodes belong to this group of electrodes. In contrast, with non-polarisable electrodes, there will be free current flow in the electrode-electrolyte interface. An example for non-polarisable electrode is Silver/Silver chloride (Ag/AgCl). For RI experiments, it is recommended to use non-polarisable electrodes (Ching, 2005). Ag/AgCl electrodes, which are biocompatible, have the ability to deliver high amounts of current without causing any pH changes in the buffer solution in the diffusion cell (Jahn, 1900). This can be explained by the redox potential from the Ag/AgCl being lower than water. Hence, it is possible to maintain electroneutrality at both sides of the electrodes, the anode and cathode. During RI, following reaction at the anode can be observed:



At a potential of  $E_0 = -0.22V$ , silver gets oxidised to silver chloride after reacting with the chloride in the solution. In contrast, at the cathode, silver chloride gets reduced to

silver at a potential of  $E_0=0.22\text{V}$  and thereby the chloride ions are liberated. The following equation expresses the reaction at the cathode:



Section 5.5 explains how the electrodes were prepared using the screen-printing method.

The advantage of RI compared to other existing methods of commercially available devices is that it does not involve the use of any needles nor any implantable sensors. In addition, it can provide continuous, real time glucose monitoring with little user participation. The GlucoWatch is an example for RI having the potential to be viable method for glucose monitoring. However, none of the RI based devices have sustained long term acceptance in healthcare due to calibration issues, skin irritation and variabilities in measurement results. For RI to become a sustainable method further improvement are needed.

The Medical Diagnostics and Wearables Group at Strathclyde has been working on ways to address these problems with RI based glucose sensing devices.

One of the problems is that once glucose enters the sensors, it accumulates in the gel reservoir and it does not reach the back of the sensor, where the sensing takes place. This causes that all glucose extracted via RI cannot be quantified hence, resulting in inadequate quantification of the glucose. Furthermore, it leads to glucose accumulation on the sensor surface prevents further extraction of glucose from ISF. The build-up of glucose within a wearable transdermal sensor has to be addressed otherwise results obtained cannot be time correlated to the patient blood levels. In the GlucoWatch all glucose was eventually converted to  $\text{H}_2\text{O}_2$  in the gel electrode system but this itself can be a source of skin irritation.

## 2.10 Means to control glucose flux

The integration of a trapping/binding agent in the sensor can help to control the glucose once it is extracted into the gel reservoir of the sensor. One approach is to integrate glucose binding proteins such as concanavalin A (Con A) in the glucose sensor.



Studies have successfully shown the effectivity, accuracy and reproducibility of glucose measurements with the use of con A in the (Cummins et al., 2013; Kuenzi et al., 2010; Russell et al., 1999; Srinivasan et al., 1986). Con A belong to the group of lectins amongst lens culinaris, pisum sativum and concanavalin gladiata. Lectins are a type of proteins which can bind to carbohydrates. Lens culinaris and pisum sativum are known for their fructose specificity (Tateno et al., 2009). One major concern with Con A is the toxicity associated with it. Andersson et al. and Gunther et al. showed that con A induced mitogenesis in cell culture experiments (Andersson et al., 1972; Gunther et al., 1973). Gunther et al and Phillips et al found cytotoxic effects of Con A in cell culture experiments (Gunther et al., 1973; Phillips & Lanier, 1986). Hepatotoxic effects in mice (Leist & Wendel, 1996) and teratogenic effects in rat embryos (Nishida et al., 1997) were also seen with the use of Con A. However, Ballerstadt et al. detailed that the route of administering Con A and the dosage of Con A have an impact on the toxicological side effect (Ballerstadt et al., 2006). Furthermore, they have identified that the usage of Con A less than 10  $\mu\text{g}/\mu\text{l}$  is considered as acceptable amounts in implantable glucose sensor and does not pose any health risks.

Another protein, which has been commonly integrated in glucose sensors is the glucose/galactose binding protein (GGBP) from *E. coli* (Salins et al., 2001; Scognamiglio et al., 2007; Tolosa & Rao, 2006). By glucose/galactose binding to the GGBP, the conformation of the protein changes. The glucose can be monitored by adding a fluorophore to a particular site of the protein, and then by measuring the change of emission of the fluorophore upon the binding of the glucose/galactose. Salins et al. were able to detect glucose concentrations in yeast fermentation in the submicromolar range. It should be noted that GGBP is selective to glucose as well as galactose. Tolosa and Rao identified a lower detection limit of 0.3  $\mu\text{M}$  – 0.5  $\mu\text{M}$  using their glucose sensor.

The preparation of glucose specific polymers is another approach to replace the need of an enzyme or to enhance glucose detection. Chen et al devised a metal-complexing polymer for glucose monitoring in biological samples (Chen et al., 1997). They prepared a Triazacyclononane chelate (TANCN)  $\text{Cu}^{2+}$  metal ion complex, which had the ability to bind to glucose molecules and in return release protons proportional to the glucose concentration. The glucose selective polymer was successfully tested in

porcine plasma and a linear relationship between proton release and glucose concentration was seen in a concentration range between 0 mM and 25 mM.

Li et al. studied the interactions between glucose and five glucose specific proteins such as 1) human beta-cell glucokinase, 2) d-xylose isomerase 3) lectins such as lathyrus ochrus isolectin 4) Con A and 5) GBP (Li et al., 1998). This helped to identify binding sites between protein and glucose molecules. It was shown that the binding occurs between the hydroxyl group (OH) of the glucose molecules and the hydrogen bondings from the proteins. This revelation was considered when developing molecularly imprinted polymers (MIPs) with integration of glucose specific recognition sites in the polymer itself using monomers, that can mimic protein interactions (Seong et al., 2002).

The Medical Diagnostics and Wearables Group at Strathclyde has a patent on methods to control the glucose concentration once it is extracted across to the skin into the gel reservoir by the application of reverse iontophoresis (Connolly, 2014). It discusses the use of different binding/trapping agents such as polymers (for example nylon and nitrocellulose), proteins (for example Con A and antibodies) or porous charcoal to be used in transdermal devices to create a controlled glucose flux. In this project, the use of activated carbon (AC) was explored for glucose control. AC has adsorption properties to organic compounds due to its high surface area and highly developed micropore structure (Aygün et al., 2003; Wang et al., 2010). Therefore, it has the potential to be used as a glucose binding agent in a wearable sensor. The integration of AC in the outer layer of the sensor ensures the transport of glucose across the gel towards the vicinity of the electrode where the glucose detection takes place (Figure 2.30). Thereby, a uniform transdermal glucose profile within the sensor is allowed.

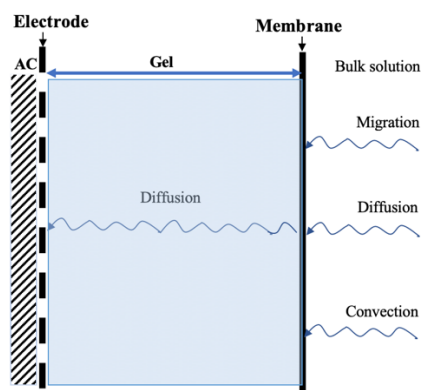


Figure 2.30 Schematic view of wearable sensor with AC in the outer layer. There are three mechanisms (migration, diffusion and convection) for molecules and ions to be transported from the bulk solution across the membrane. Due the adsorption capabilities of AC to organic compounds, glucose transport is further ensured across the gel layer towards the electrode vicinity, where the glucose detection takes place.

The novelty of this project is that glucose control is attempted using glucose adsorption to AC, which is reagentless and does not create any secondary chemicals compared to other means of control. Integrating AC in the device will enhance accuracy, hence providing RI based devices more reliable glucose results.

The following section discusses fundamentals of adsorption and factors which have an impact on the adsorption process.

## 2.11 Adsorption

Adsorption is a surface phenomenon, where Substance A (adsorbate) in gaseous or liquid form (for example molecules, atoms or ions) adhere to the surface of Substance B (adsorbent). In this project, activated carbon (AC), which is also called activated charcoal was used as the adsorbent and glucose as the adsorbate.

The adsorption process is a spontaneous reaction at constant pressure and temperature provided that there is negative Gibbs free energy ( $\Delta G < 0$ ) (Bolis, 2013; Moreno-Castilla, 2004; Wang et al., 2019). The change in Gibbs energy can be calculated with the Equation 2.15 based on the laws of thermodynamics.

$$\Delta G^\circ = \Delta H^\circ - T\Delta S^\circ \quad \text{Equation 2.15}$$

$\Delta G^\circ$  ... Change in Gibbs free energy [J]

$\Delta H^\circ$  ... Change in enthalpy

$T$  ... Absolute temperature [K]

$\Delta S^\circ$  ... Change in entropy

Enthalpy is defined as the heat that is released during the adsorption of one mole of adsorbate.

During the adsorption process, the movement of the molecules becomes limited once adhered to the surface and hence the entropy is decreased ( $\Delta S^\circ < 0$ ). Therefore, the enthalpy must be also negative ( $\Delta H^\circ < 0$ ) for a spontaneous reaction to happen. This in turn results to the adsorption to be an exothermic process, and releases heat during adsorption. (Bolis, 2013)

### Forms of Adsorption

Depending on the type of adsorbate and adsorbent involved, the adsorbate can adhere to the adsorbent via two mechanisms: Either via physical adsorption (physisorption) or via chemical adsorption (chemisorption) (Ruthven, 2008). Physisorption involves the adherence of the adsorbate to the surface via Van der Waals interactions. It is non-specific and can occur on monolayers as well as multilayers. This form of adsorption occurs at low temperatures and it is a reversible process. It is a pressure and temperature dependent reaction and low heat is released (2-25 kJ/mol) during physisorption (Ghosh, 2014). In contrast, during chemisorption the adsorbate adheres to the surface of the adsorbent via establishing a chemical bonding. It is a highly specific process and only occurs on monolayers. It happens on relatively high temperatures and it is an irreversible process. Chemisorption releases a high heat of adsorption (50-500 kJ/mol) (Ghosh, 2014).

### Adsorption isotherms

An adsorption isotherm helps to understand the adsorption behaviour and gives information about the equilibrium relationship between adsorbate and adsorbent. When adsorbate and adsorbent are in contact for a sufficient time period, an equilibrium is created between the amount of adsorbate remaining in the solution and the amount of the adsorbate adsorbed by the weight of the adsorbent. In general, the

adsorbate and the adsorbent try to reach the equilibrium stage. Adsorption isotherms are expressed in form of a curve (Figure 2.31). On the x-axis the remaining concentration in the solution after the adsorption ( $c_e$ ) (which is also called the equilibrium concentration) is applied and on the y-axis the amount of adsorbate adsorbed per unit weight of the adsorbate ( $q_e$ ) can be seen. There are five commonly observed models which are used to identify the adsorption capacity of AC (Moreno-Castilla, 2004), 1) the linear model 2) the Langmuir model (Langmuir, 1918), 3) the Freundlich model (Freundlich, 1906), 4) the high- affinity model and 5) the sigmoidal model. A linear relationship can be seen for the Freundlich and Langmuir models only for very low concentrations. A non-linear behaviour can be seen with higher concentrations. Adsorption isotherms are expressed in form of equations based on the curves seen in Figure 2.31.

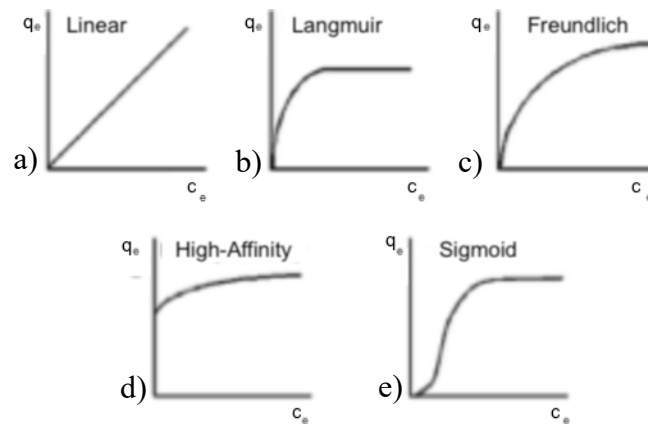


Figure 2.31 Types of adsorption isotherms (a) linear, b) Langmuir, c) Freundlich d) high- affinity and e) sigmoidal (adapted from Moreno-Castilla, 2004)

#### Factors affecting the adsorption process:

The adsorption process in a liquid-phase depends on a variety of factors related to 1) the adsorbent, 2) the adsorbate and 3) the solution where the adsorption occurs (Haghseresht et al., 2002):

#### 2.11.1 Adsorbent

AC has been used for wide range of applications such as air purification (Wang et al., 2019), removal of contaminants in drinking water and treating waste water (Herrera-González et al., 2019; Hsu et al., 2019; Mohan & Singh, 2002; Namasivayam &

Kavitha, 2002). Furthermore, it is also applied for a variety of medical purposes such as lowering cholesterol levels and treating cholestasis in pregnant women (Jacobi The Carbon Company, 2015). It is used for blood purification (Howell et al., 2016), wound healing (Lin et al., 2012) and as decontaminant agent to remove any toxins or chemicals in the body in the gastrointestinal tract (Juurlink, 2016). And more research is underway to expand the usability and applications of AC.

AC is a flexible material and can be modified to enhance adsorbate- specific adsorption characteristics. For example, magnetic properties were added to AC to enhance its adsorption to metal ions (Adio et al., 2019). In a different study AC was treated with sulphur to improve aqueous mercury adsorption to AC (Hsu et al., 2019). There are many different forms of AC such as pellets, granules, spherical beads, powder or fibers (Axtell et al., 2008). Granular activated carbon (GAC) is made of a base material such as coconut shells, charcoal, wood or lignite and activated carbon fibers (ACF) are made of cellulose, polyacrylonitrole or phenolic resins (Kasaoka et al., 1987). Research is also conducted to explore adsorption characteristics of AC made of low-cost base materials such as bagasse (agricultural waste) (Mohan & Singh, 2002) or coir pith (Namasivayam & Kavitha, 2002) or date stones (Belhamdi et al., 2016) for economic reasons.

AC varies in its chemical and physical characteristics depending on its manufacturing process.

#### 2.11.1.1 Pore structure and surface area of AC

The porous structure in the AC is created by either (1) physical activation via thermal oxidation or (2) chemical activation via chemical oxidation (Ahmadpour & Do, 1996). In the physical activation process, the base material needs to be carbonised first in an inert atmosphere before being oxidised using steam or CO<sub>2</sub>. In contrast, in the chemical activation process, the base material is first impregnated with an oxidising and dehydrating chemical before undergoing chemical oxidation using bases, acids (e.g. phosphoric acid) or any other chemicals (Li et al., 2002). The chemical activation process is more advantageous a) due to better developed pore structure. b) lower activation temperatures ranging from 400 to 700 °C compared to physical activation, which is in the range of 500 to 900 °C and c) because it is only a one-step process as

the carbonisation of the base material and the chemical activation is usually done simultaneously (Rodriguez-Reinoso, 1997).

The pore volume and the surface area depend on the base material and the activation process (Çeçen, 2014). AC can have a surface area ranging from approximately 500 to 1500 m<sup>2</sup>/g and the apparent density, which includes the pore structure but not the interparticle voids of AC can vary from 0.29 to 0.8  $\frac{g}{cm^3}$  (Çeçen, 2014). The surface site density describes the number of available sites for adsorption. Chen et al. calculated a surface site density of 0.18 sites/nm<sup>2</sup> for copper adsorption to GAC (Chen et al., 2003). The surface area of AC can be determined using established techniques such as the nitrogen adsorption at 77K (Sing, 1995) or the iodine number (Mianowski et al., 2007). In addition the pore size distribution and the micropore volume can be also identified with the nitrogen adsorption at 77K (Haghseresht et al., 2002; Li et al., 2002).

It was shown by Kasaoka et al. that GAC have a multidisperse pore structure consisting of micropores, mesopores and macropores. According to the IUPAC recommendations micropores are defined as having a width diameter of less than 2 nm, mesopores have a width diameter between 2 – 50 nm and macropores have width diameters bigger than 50 nm (Rouquerol et al., 1944; Sing et al., 1985). An example of the surface structure of AC with micropores and mesopores can be seen in Figure 2.32.

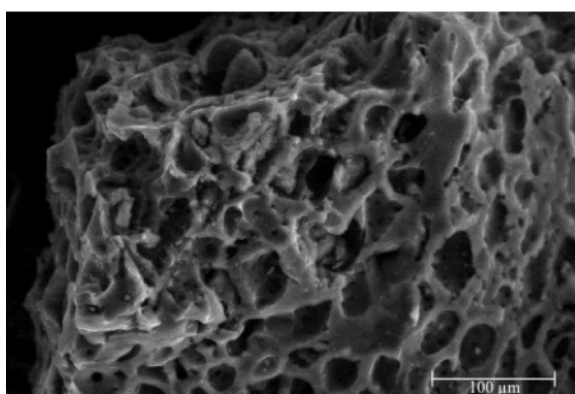


Figure 2.32 Example of surface structure of AC with micropores and mesopores acquired using scanning electron microscopy (adapted from Belhamdi et al., 2016)

In contrast, for ACF a homogenous pore structure consisting of micropores was seen by Kasaoka et al and by Moreno-Castilla (Kasaoka et al., 1987; Moreno-Castilla,

2004). The homogenous pore structure was confirmed by Daley et al. using a scanning tunnelling microscope (Daley et al., 1996).

The pore size of the adsorbent has the following effects on the adsorption process of organic compounds to AC.

- (1) The strength of the adsorption increases with smaller pore size. This is due the fact that there are more contact points between adsorbate and adsorbent in case of smaller pore sizes (Newcombe et al., 1997). In addition, with the condition that the micropore size is less than double of the adsorbate diameter, the adsorption strength increases as well due to overlap of opposing pore walls (Dubinin, 1960; Sing, 1995).
- (2) Adsorption is limited if the size of the adsorbate is bigger than the pore size of the adsorbent. For effective adsorption, it was recommended that the pore width of the adsorbent should be 1.3-1.8 times bigger than the width of the adsorbate (Li et al., 2002). Nonetheless, it is not only the pore size of the AC, which has an impact on the adsorption capacity of AC but it is also the accessibility of the compounds to the inside of the adsorbent, which can be restricted by size of the adsorbate (Moreno-Castilla, 2004).

#### 2.11.1.2 Surface chemistry of AC:

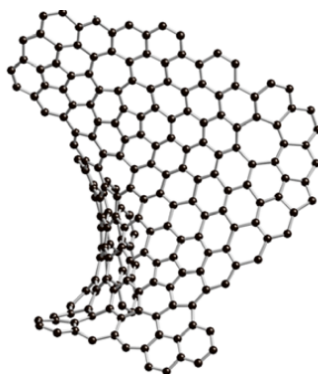


*Figure 2.33 Atomic structure from AC (adapted from Harris, Liu and Suenaga, 2008)*

Figure 2.33 shows an example of the atomic structure of AC consisting of carbon rings. At the edges of the AC heterogeneity is identified, which can be caused by 1) due to for example different pore size, pore shapes or cracks (geometrical heterogeneity) 2) by chemical heterogeneity (Dąbrowski et al., 2005). Chemical heterogeneity is caused by heteroatoms such as oxygen, which can be found in e.g. carboxylic acid,



hydroxyl groups, or quinone groups (Figure 2.34) due to the oxidation procedure of the carbon.

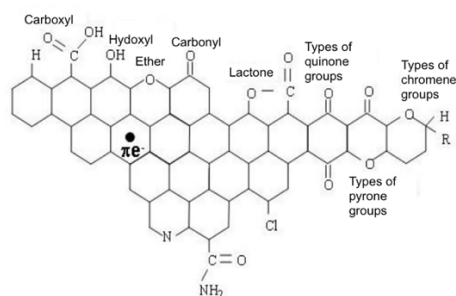


Figure 2.34 Heteroatoms at the edges of the atomic structure of AC (adapted from Cárdenas-López et al., 2007)

The heteroatoms constitute to the chemical characteristics of the AC and have an impact on the hydrophobicity of AC, the electronic density of the AC's graphene layer and the surface charge of the AC; whereby the surface charge also depends on the pH of the solution, in which the adsorption takes place (Biniak et al., 2001). The oxidation of AC by certain oxidants (e.g. hydrogen peroxide or nitric acid) or exposing AC to oxygen in the temperature range of 200 °C to 700 °C creates an acidic nature of the AC. It is caused by the formation of acidic oxygen-containing groups such as carboxylic acid and phenolic hydroxyl (León & Radovic, 2001). Studies showed that increased oxygen and acidic functional groups have a negative impact on the adsorption of organic compounds in the liquid phase (Considine et al., 2001; Franz et al., 2000; Kaneko et al., 1989; Karanfil & Kilduff, 1999; Pendleton et al., 1997). However, in the gaseous phase the adsorption of organic compounds is promoted by oxidation of AC (Dimotakis et al., 1995; Mangun et al., 1999). It was shown by Kaneko et al that removing the acidic groups from the AC did improve the adsorption of relatively polar/relatively nonpolar organic compounds (Kaneko et al., 1989). The oxygen-containing acidic groups were removed with heat treatment in a hydrogen atmosphere. During the heat treatment, the delocalised  $\pi$ -electrons arise due to the removal of oxygen and create the basic nature of the AC.

### 2.11.1.3 Mineral matter content of AC

Approximately 20% of the AC consists of mineral matter, which is shown in form of ash content (Dąbrowski et al., 2005). The mineral matter content in the AC has a negative impact on the adsorption process as they obstruct the porosity of the AC

(Moreno-Castilla, 2004). In addition, due to the hydrophilic character of mineral matters, AC with higher mineral matter content prefer adsorption to water hence, limiting the adsorption of the adsorbate.

### 2.11.2 Adsorbate

Following characteristics of the adsorbate affect the adsorption process: 1) Molecular size: The molecular size of the adsorbate determines the accessibility to the AC pores. 2) Solubility: It defines the hydrophobic interactions 3)  $pK_a$ : In case that the adsorptive is an electrolyte, the  $pK_a$  – value determines dissociation of the adsorbate (Moreno-Castilla, 2004).

Glucose is a neutral and polar molecule and has a MW of 180 Da. It is a water-soluble compound and has a kinetic diameter of 8.6 Å (Lourvanji, 1995; Weng et al., 2015). It was reported that glucose acts as weak acid in the solutions with a  $pK_a$  value of 12.87 (Britton, 1955; Singh & Mohan, 2004). Organic molecules attach to the surface via physisorption via to Van der Waals interactions (Moreno-Castilla, 2004). The  $\pi$ -electrons of the aromatic ring of the organic molecule interact with the  $\pi$ -electrons of the graphene layer of the AC (Moreno-Castilla, 2004).

### 2.11.3 Solution chemistry

The pH of the solution, the concentration of the adsorbate in the solution and the ionic strength play a role in the adsorption process. It was observable that increasing the ionic strength in the solution improves the adsorption by adsorbents, which are negatively charged. However, it decreased adsorption capabilities of positively charged adsorbents. (Summers & Roberts, 1988)

In addition, also the surface charge of AC in combination with the pH of the solution affect the adsorption process. Moreno-Castello stated that if the pH of the solution is lower than the pH at which the total surface charge of the AC is zero, then total surface charge will be positive. However, if the pH of the solution is higher than the pH at which the total surface charge is zero, then the total surface charge of the AC will be negatively charged (Moreno-Castilla, 2004).

In one study adsorption of the dye Congo red was tested onto AC at different pH levels (Namasivayam & Kavitha, 2002). They identified that adsorption decreased when the pH was increased from pH of 2 to pH of 4. Adsorption remained the same in the pH range between 4 and 10. These mechanisms can be explained due to the fact that at acidic pH levels, there was high electrostatic attraction between the surface of the AC, which was positively charged and the dye, which was negatively charged. With increasing pH, the negatively charged sites on AC increased, which lead to less adsorption due electrostatic repulsion between the negatively charged sites and the anionic dye. In addition, with increasing pH levels, there were more OH<sup>-</sup> ions in the solution, with which the anionic dye had to compete for the available adsorption sites. In this project the pH of the buffer solution was set at 7.4 corresponding to the physiological pH in the body is 7.4.

#### 2.11.4 Temperature and pressure

Adsorption is a temperature- and pressure- dependent process. Based on Equation 2.15, the adsorption capabilities increases with decreasing temperature (Dąbrowski et al., 2005). However, the exact impact of temperature and pressure depends on the type of adsorbate and the adsorbent involved. In Wang et al.'s study, the adsorption of acetaldehyde and acetone (both in gaseous form) on AC was decreased when increasing the temperature from 24.85 °C to 64.85 °C (Wang et al., 2019). By increasing the temperature the adsorbed compounds have more energy and are able to withstand the attractive forces to the surface of AC and go back to the gaseous state (Zhou et al., 2012). In a different study mercury adsorption to AC was tested and they identified that decreasing temperature and increased adsorbate concentration led to an increase of adsorption (Hsu et al., 2019). But Namasivayam and Kavitha stated the adsorption of the dye Congo red to AC was slightly increased when increasing the temperature (Namasivayam & Kavitha, 2002). This could be due to the way the adsorbate adhered to the surface. In chemisorption it is observable that with increasing temperature adsorption increases up until a certain point is reached. Namasivayam and Kavitha also showed that at a temperature of 60 °C,  $\Delta G < 0$  was established, indicating that the adsorption process occurred spontaneously. However,  $\Delta G > 0$  was identified at

lower temperatures (35 °C, 40 °C and 50 °C), which indicates that spontaneous reactions are not preferred at lower temperatures.

All the adsorption experiments in this project were performed at room temperature to match the potential use for glucose adsorption to AC in RI experiments.

## 2.12 Summary

- This chapter began with anatomical and physiological aspects of the pancreas. Furthermore, the blood glucose regulation in a healthy body with the help of the hormones, insulin and glucagon was explained.
- It then discussed the causes, symptoms, complications, diagnosis and treatment options of type 1 and type 2 diabetes.
- The focus of the thesis is in SMBG, which is one of the main means of diabetes management.
- The history of glucose monitoring was elucidated with initially using urine samples for glucose testing and later blood samples were used. Glucose was initially quantified using devices based on reflectance photometry.
- This was followed by the development and use of glucose biosensors for intermittent glucose measurements based on electrochemical principles.
- CGMS, which offers tighter glycaemic control in comparison to intermittent glucose measurements, was then explained.
- This chapter provided a comprehensive review of the existing glucose monitoring technologies and devices for intermittent and continuous glucose monitoring.
- The need for non-invasive glucose monitoring is considered to be very beneficial, as it can increase patients' compliance to treatment plans.
- The focus of this thesis is in improving transdermal sensing linked to reverse iontophoresis, which has been proposed as means for non-invasive monitoring of glucose. The use, the limitations, biological and operational factor having an influence on RI for glucose monitoring were discussed.
- Means for improved and controlled glucose flux in RI devices is a key part of the work described in this thesis, in particular the use of activated carbon (AC)

as a glucose binding agent which will remove excess glucose from a transdermal sensor and permit more uniform transdermal profiles of glucose within a wearable sensor.

- Glucose control is attempted using AC, which has adsorption characteristics to organic compounds. Therefore, the fundamentals of adsorption and factors which have an impact on the adsorption process were discussed.

### 3 Study design

This chapter highlights the rationale of the study, the key aim and the objectives of this research. In addition, the research questions, which were addressed in the course of this project are listed.

#### 3.1 Rationale of the study

- Self-monitoring of blood glucose plays a crucial role in diabetes care. Currently, the most commonly used methods work in an invasive manner for blood glucose monitoring, which causes pain and discomfort to the patients.
- Reverse iontophoresis (RI) has been proposed as means for non-invasive, transdermal diagnostics for the monitoring of many small circulating molecules and ions (e.g. glucose). In this technique, electric current is applied across the skin to extract a substance of interest across the skin via gel electrodes. The gel facilitates electrical conductance and also serves as a receptacle to collect the extracted molecules and ions.
- To date, few working examples of diagnostic devices have been produced as discussed in Section 2.8.1; but none have sustained long term acceptance in healthcare.
- One of the problems in wearable sensors for glucose monitoring based on RI, is the glucose build-up in the gel reservoir of the sensor. This in turn 1) prevents further glucose extraction from the interstitial fluid 2) leads to inaccurate glucose quantification, as not all the extracted glucose reaches the sensor surface where glucose detection takes place and 3) causes time lags in the correlation between glucose concentrations in interstitial fluid and blood.
- The Medical Diagnostics and Wearable Group at Strathclyde has a patent on methods to control glucose (once it is in the gel reservoir) by the use of different binding/trapping agents such as porous charcoal (Connolly, 2014).
- Activated carbon (AC) has adsorption characteristics to organic molecules and could therefore, act as a glucose binding agent. Thereby, it could remove excess glucose from the sensor and hence allow a more uniform transdermal glucose profile within a wearable sensor.

- The novelty in this project is that the glucose control is attempted using AC, which is reagentless and does not create any secondary chemicals compared to other means of control such as the deployment of glucose oxidase in the gels (see Section 2.8.1 for description of some such systems).

## 3.2 Aim of the investigation

The overall aim of this project was to test the concept of glucose adsorption to AC and to evaluate the suitability of AC as a glucose binding agent for a better controlled and uniform glucose flux in wearable sensors in the RI environment. In addition, this study involved embedding a biosensor in the electrode system to allow direct glucose measurements, which could also be part of a wearable sensor in the future.

## 3.3 Research objectives

- To compare two commercially available glucose enzyme kits in terms of sensitivity and limit of detection (GLUC-PAP from Randox Laboratories and GAHK20-1KT from Sigma Aldrich)
- To evaluate the use of the Genova Nano, a micro- volume spectrophotometer for glucose quantification in comparison with the standard method using the plate reader
- To study the flux of glucose molecules in RI experiments using an *in vitro* diffusion cell
- To test and compare two commercially available artificial skin membranes on its ability to mimic human skin in RI experiments (Spectrapore membrane from Spectrum Laboratories and Vitro-Skin from IMS Inc.)
- To establish proof of concept of glucose adsorption to AC
- To design an AC integrated gel electrode system
- To study glucose flux in *in vitro* RI experiments using AC integrated electrodes and compare it with the results obtained via the standard gel electrodes without AC
- To include a biosensor in the electrode system for direct glucose quantification in the gel

- To study the biosensor performance in the gel environment using cyclic voltammetry
- To perform *in vitro* RI experiments using glucose biosensors and compare the electrochemical glucose detection method using the biosensor with the standard method using laboratory kits
- To design an AC integrated glucose biosensor
- To perform *in vitro* RI experiments using AC integrated glucose biosensors and compare the electrochemical glucose detection method using the AC integrated biosensor with the standard method using laboratory kits

### 3.4 Research questions

- Which glucose assay kit is more suitable to quantify glucose in the required glucose concentration range?
- Is the level of sensitivity of the Genova Nano, micro-volume spectrophotometer sufficient to quantify glucose in samples if only very small sample volumes are available?
- Which of the tested artificial skin membrane mimics the human skin better in RI experiments?
- Proof of concept: Does glucose adsorb to AC?
- Can AC be used as a glucose binding agent in a wearable sensor in the RI environment and allow a more uniform transdermal glucose profile?
- How does the biosensor operate in the gel environment?
- Can the embedded glucose biosensor quantify glucose in the required glucose concentration range?
- Is it possible to electrochemically quantify the extracted glucose via RI with the glucose sensor?



## 4 Theory

As discussed, the application of Reverse Iontophoresis (RI) in combination with sensor technology can have a great promise for non-invasive glucose monitoring in diabetes care. The use of Activated Carbon (AC) as a glucose binding agent could help to improve and better control glucose flux in wearable sensors in the RI environment. In addition, embedding a glucose sensor in the electrode system would allow direct glucose measurements.

This chapter aims to provide relevant background theory for the development of a mediated amperometric glucose sensor with AC as a glucose binding agent to overcome the limitations of previous devices based on RI.

This chapter introduces theory on glucose detection and quantification methods via colorimetric assays and optical spectrophotometer, a method commonly used in laboratory settings. Moreover, glucose detection methods using electrochemical means are elucidated, which is the basis of glucose sensors. Electrochemistry is the field of study which relates electron transfer processes to chemical changes. Electrochemical fundamental processes occurring at the electrode-solution interface are introduced in this chapter. The operation of an electrochemical glucose sensors is discussed and the principles of Cyclic Voltammetry (CV), the electroanalytical technique applied for glucose detection in this study, is explained.

In addition, the principles of RI and the transport mechanisms involved during RI are described.

Finally, statistical analysis approaches, which were applied to evaluate the results, are provided.

## 4.1 Glucose detection techniques

Glucose (Figure 4.1) belongs to the group of carbohydrates and is a neutral and polar molecule. It has a molecular weight (MW) of 180 Da and its molecular formula is  $C_6H_{12}O_6$ . It is a water-soluble compound.

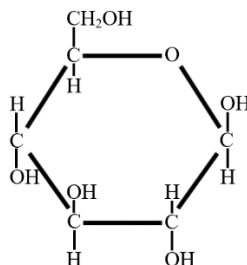


Figure 4.1 Molecular ring structure of glucose

As discussed in section 2.3.4, self-monitoring of glucose in the body is one of the key routes in managing diabetes. The most common method to detect glucose is based on enzymatic reactions. An enzyme acts as a catalyst and can accelerate chemical reactions, without consuming itself. It reacts with the analyte of interest and causes a detectable substance to be formed. The detectable substance can then be quantified using for example 1) an optical spectrophotometer or 2) with electroanalytical methods. Both methods were used in this study for quantitative analysis of glucose and are explained more in-depth in section 4.2 and section 4.3.

### 4.1.1 Enzyme kinetics

Equation 4.1 shows the general principle of an enzymatic reaction with a substrate (Bisswanger, 2008).



*E*...Enzyme

*S*...Substrate

*ES*...Enzyme-substrate complex

*P*...Product

*k*<sub>1</sub>...Rate constant of the formation of *ES* complex

*k*<sub>2</sub>...Rate constant for the formation of *P*

The product formation occurs in two steps: First the enzyme (*E*) binds with the substrate (*S*) and creates an intermediate enzyme-substrate complex (*ES*). In the

second reaction, the  $ES$  complex dissociates, regenerating free enzymes ( $E$ ) and a forming product ( $P$ ).

The changes of the concentrations of the reactants in an enzymatic reaction over time can be seen in Figure 4.2.

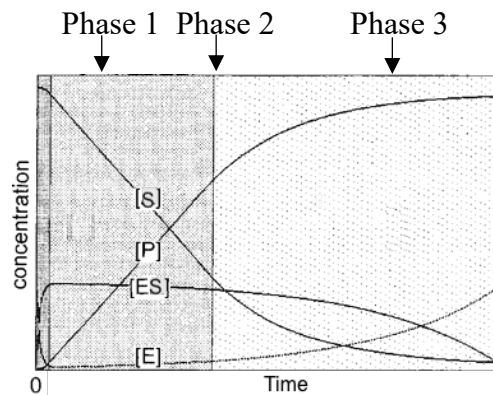


Figure 4.2 Changes of the concentration of the enzyme ( $E$ ), substrate ( $S$ ), enzyme-substrate ( $ES$ ) and product ( $P$ ) over time during an enzymatic reaction (adapted from Bisswanger, 2008)

In Phase 1, an increase of the concentration of the  $ES$  complexes is observable due to the binding of the free enzymes to the substrate. This in turn leads to the decrease of the concentrations of free  $E$  and free  $S$ . In Phase 2, while the concentration of the  $ES$  complex remains constant, the concentration of the product is increasing linearly; whereas the substrate concentration is further decreasing. A slow increase in the enzyme concentration can be seen due to the decomposition of the  $ES$  complex and the regeneration of the free enzymes and the formation of the product. In Phase 3, the depletion phase, the substrate is getting fully exhausted and the  $ES$  complexes decay over time until they are fully depleted. The duration of each phase changes depending on the rate constants of the enzymatic reaction (Bisswanger, 2008).

The Michaelis Menten equation (Bisswanger, 2008) relates the substrate concentration with the reaction velocity ( $V$ ), which is the speed to form the product ( $P$ ). It is defined as change of the product concentration over time and can be expressed with

$$V = \frac{V_{MAX}[S]}{K_M + [S]} \quad \text{Equation 4.2}$$

$V$ ...Reaction velocity

$V_{MAX}$ ...Maximum reaction rate

$K_M$ ...Michaelis constant

[S]...Initial concentration of the substrate

Considering a constant enzyme concentration in a reaction, an increasing substrate concentration results in the increase of the reaction rate until  $V_{MAX}$  is reached. This is the point where the enzyme has achieved its maximum reaction rate and gets saturated. The Michaelis constant ( $K_M$ ), is the concentration of the substrate, where the reaction rate is  $V_{MAX}/2$ . When plotting the velocity of the reaction versus the substrate concentration, a hyperbolic relationship can be seen Figure 4.3.

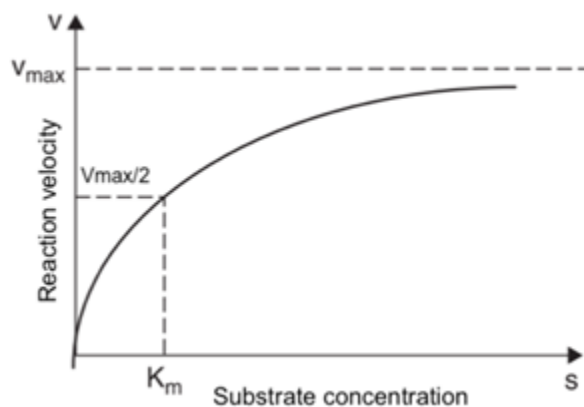


Figure 4.3 Function of reaction velocity over substrate concentration (adapted from Berk, 2009)

A high  $K_M$  value indicates a low affinity to the substrate, which in turn results in higher substrate concentrations to reach  $V_{MAX}$ . In contrast, a low  $K_M$  value implies a high affinity to the substrate. Hence, lower concentrations of substrate are needed to reach  $V_{MAX}$ .

## 4.2 Colourimetric assay and optical spectrophotometer

Colourimetric assays are based on the principles that a chromogenic response in relation to the analyte concentration is developed after an enzymatic reaction, which can be measured using an optical spectrophotometer at a particular wavelength (Porstmann & Kiessig, 1992). The spectrophotometer emits light at a specific wavelength and the light absorbed by the sample is related to the analyte concentration.

The Beer Lambert law defines that the absorbed light is directly proportional to the analyte concentration in low concentrations (Swinehart, 1962) and it is expressed with the:

$$A = \epsilon \times l \times c \quad \text{Equation 4.3}$$

$A$ ...Absorbance

$\epsilon$ ... Molar absorption coefficient [ $\frac{L}{mol \cdot cm}$ ]

$l$ ...Path length [cm]

$c$ ...Analyte concentration [ $\frac{mol}{L}$ ]

The molar absorption coefficient gives information about the tendency of a substance to absorb light at a given wavelength. It is constant for a given substance in a given solute at a specific wavelength. The linearity in Beer Lambert's law can be impaired due to instrumental or chemical factors, or due to high analyte concentration (Vitha, 2019).

Experimentally, the absorbance can be identified by measuring the transmittance using an optical spectrophotometer. Transmittance is defined as the proportion of light which can pass through the sample.

A basic optical spectrophotometer consists of four essential parts, a light source (1), a monochromator (2), a sample holder (3) and a detector (4) (Figure 4.4).

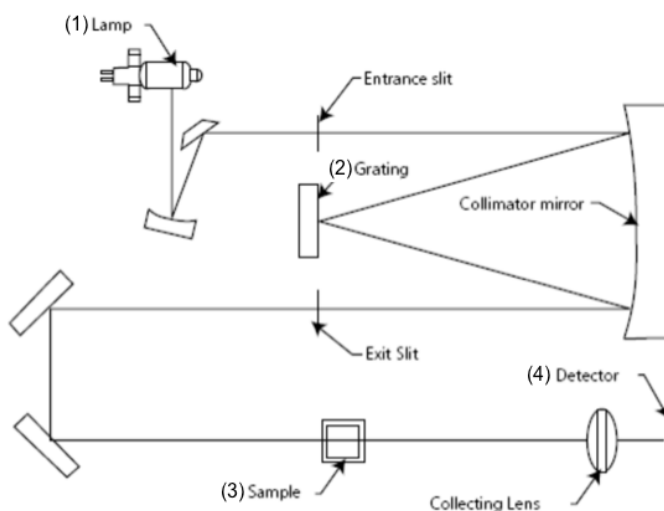
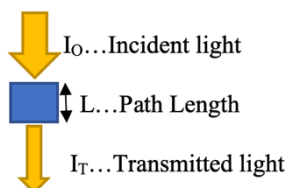


Figure 4.4 Schematic design of the spectrophotometer (adapted from Bibby Scientific 2012)

The light source, for example a Xenon lamp, produces light. The monochromator has the responsibility to separate the light into discrete wavelengths. This can be done using a grating or a prism. In the device used in this project a grating was used for that

purpose. The exit slit only transmits the desired wavelength and it will hit the sample. Some light will be absorbed by the sample and some light will be transmitted. The transmitted light ( $T$ ) is detected with the signal detector, which is in this case a photomultiplier (Poole & Kalnenieks, 2000) and is expressed with:



The diagram shows a blue rectangular sample cell. A yellow arrow labeled 'I<sub>0</sub>... Incident light' points downwards into the top of the cell. A double-headed vertical arrow next to the cell is labeled 'L... Path Length'. A yellow arrow labeled 'I<sub>T</sub>... Transmitted light' points downwards from the bottom of the cell.

$$T = \frac{I_T}{I_0} \quad \text{Equation 4.4}$$

Absorbance has an inverse relationship with transmittance and is described with Equation 4.5:

$$A = \frac{\log 1}{T} \quad \text{Equation 4.5}$$

- Establishment of a glucose calibration curve using colorimetric assay and an optical spectrophotometer

Glucose calibration curves can be established with the help of colorimetric assays. They are required to quantify unknown glucose concentrations from samples by the means of comparing them to a set of standards with known concentrations. In this project calibration curves were established for glucose assay kits in order to quantify unknown concentrations of glucose samples extracted from RI experiments. More details of the glucose assay kits, which were used in this project, can be found in section 5.3. The enzymes in the glucose assay kit catalyse chemical reactions with the glucose in the standard samples. The chromogenic response was then measured by taking absorbance reading with the spectrophotometer at a specific wavelength. The wavelength of each assay kit is indicated on its product information sheet. Glucose concentrations of standards are plotted against absorbance readings from the spectrophotometer. A linear response is expected between a limited range of the standard glucose concentrations and the respective absorbance reading from the spectrophotometer and is expressed with the linear function equation (Equation 4.6).

$$y = bx + a \quad \text{Equation 4.6}$$

$y$ ... Instruments' response (absorbance reading taken by the spectrophotometer),

$x$ ... Standard glucose concentration

$b$ ... Slope of the line or gradient; it indicates the sensitivity of the measurement

a... Intercept with the y-axis of the standard calibration curve

### 4.2.1 Limit of detection and Limit of Quantification

The limit of detection (LOD) and limit of quantification (LOQ) are measures to identify the lower limit of the linear range of a calibration curve.

The LOD indicates the lowest value that is significantly higher than the background reading and therefore, can be reliably detected by an analytical process (MacDougall & Crummett, 1980). The LOD is calculated with Equation 4.7, whereby  $\sigma_b$ , is the standard deviation of the blank solution and  $x_b$  is the mean of the blank solution (MacDougall & Crummett, 1980; Shrivastava & Gupta, 2011). The blank solution is the sample, which does not have the analyte of interest. Any concentrations below the LOD cannot be quantified and are considered as noise. A multiplication factor of  $k = 3$  was chosen for analysing purposes in this study as it is recommended as a minimum multiplication factor in the guidelines from MacDougall et al. and Eurachem 2014 (Eurachem, 2014; MacDougall & Crummett, 1980).

$$LOD = x_b + k \times \sigma_b \quad \text{Equation 4.7}$$

The LOQ implies the lowest value, which can be precisely quantified. It is the value at which the unknown sample can be quantified with an acceptable level of precision and accuracy by the instrument. It can be determined with Equation 4.8 whereby  $\sigma_b$ , is the standard deviation of the blank solution and  $x_b$  is the mean of the blank solution (MacDougall & Crummett, 1980; Shrivastava & Gupta, 2011). A minimum multiplication factor of 10 was suggested (Eurachem, 2014; MacDougall & Crummett, 1980) and therefore chosen in this study.

$$LOQ = x_b + k \times \sigma_b \quad \text{Equation 4.8}$$

Figure 4.5 illustrates an example of a possible calibration curve obtained (left side). The absorbance is applied on the y-axis and the standard concentrations on the x-axis. The region between LOD and LOQ is referred to as the region of detection. The right side of Figure 4.5, shows the limited linear range, which is ultimately used to quantify unknown concentrations in the sample. It can be seen how the linear range starts from the LOQ to the value, where the calibration curve goes non-linear (Gaines, 2018). Non-linear behaviour can be seen as higher analyte concentrations can cause changes in the molar absorptivity of the analyte or in the refractive index thus leading to

deviations from Beer Lambert's law (Vitha, 2019). The region above the LOQ is indicated as the region of quantification.

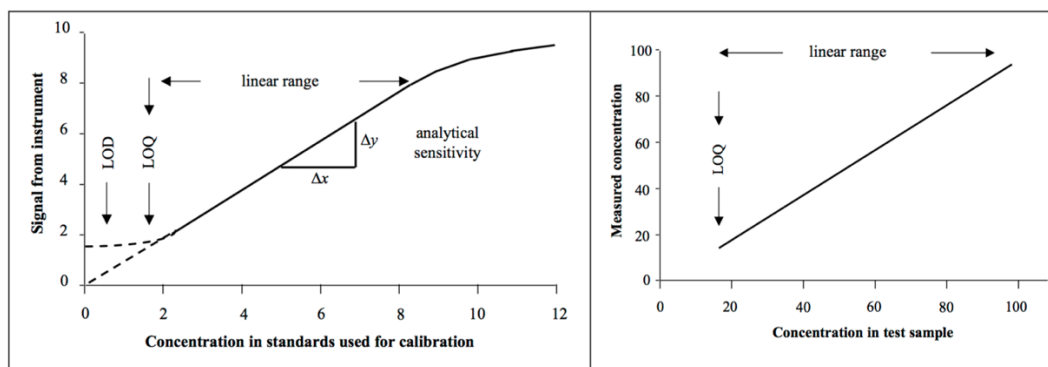


Figure 4.5 Example of a calibration curve obtained with LOQ, LOD, linear range, sensitivity indicated (left side) Linear range of the calibration curve starting from the LOQ (right side). (adapted from Eurachem 2014)

## 4.3 Electrochemical detection of glucose

Glucose can also be detected using electrochemical techniques employing enzymes and electrodes. The enzyme catalyses reduction-oxidation (redox) reactions of electroactive species. And the current produced via the electron transfer processes across the electrode-solution interface is related to the concentration of the analyte of interest and can be measured with an electrode system. This method is commonly used in glucose biosensors.

Electrochemical fundamental processes occurring at the electrode-solution interface are discussed in this section first before elucidating the operation of an electrochemical glucose sensor.

### 4.3.1 Electrode - electrolyte interface

Electrodes were used in this study for the application of current to an electrochemical cell and for the application of the iontophoretic current to perform RI experiments. An electrolyte, which is a conducting medium, can pass the current from the electrode by the movement of the charged ions. In this study gel was used as an electrolyte.



Once an electrode is immersed into a solution, a potential is developed, which is called the half-cell potential,  $E_0$ . The developed potential can be measured with a voltmeter; however, it requires the introduction of a reference electrode (RE) whose potential difference to the solution is known. The use of a RE enables the measurement of any half-cell potentials with respect to the RE. The standard hydrogen electrode (SHE) is seen as the ideal RE as its half-cell potential is considered to be  $E_0 = 0$  V (Bard & Faulkner, 2001b). The disadvantage of SHE reference electrodes is that they are fragile and cumbersome to assemble. Alternatively, standard calomel electrode (SCE) or the silver/silver chloride electrode (Ag/AgCl) can be used as RE, which are durable and less cumbersome to assemble. For this project screen printed pseudo Ag/AgCl electrodes were used as RE as discussed in section 2.9.2.

#### 4.3.1.1 Faradaic and non-faradaic processes

Faradaic and non-faradaic processes can be seen on the electrode-electrolyte interface when a reaction takes place on an electrode.

Faradaic processes involve electron transfer processes across the electrode-electrolyte interface and they occur via redox reactions. Oxidation is defined as the loss of an electron and reduction is described as the gain of an electron. Energy level differences are the driving forces for electron transfers between solution and electrode. When applying a potential at the electrode, the energy level of the electrons of the electrode changes. For example, with increasing potential at the electrode, the energy level of the electrons in the electrode decreases. Hence, if the energy level of the electrons in the electrode is lower than the highest occupied molecular orbital (MO) of the electroactive species in the solution, then an electron transfer will occur from the solution to the electrode, causing the oxidation of the species (Figure 4.6a). Oxidation potential is referred to as the potential where the oxidation of the species occurs. And the oxidation current is the current due to the electron transfer process from the solution to the electrode. The oxidation potential and oxidation current play an essential in the detection of glucose (see section 4.3.2).

In contrast, with decreasing potential at the electrode, the energy level of the electrons at the electrode increases. And if the energy level of the electrons at the electrode is higher than the lowest vacant MO of the electroactive species in the solution, an

electron transfer will occur from the electrode to the solution causing the reduction of the species (Figure 4.6b).

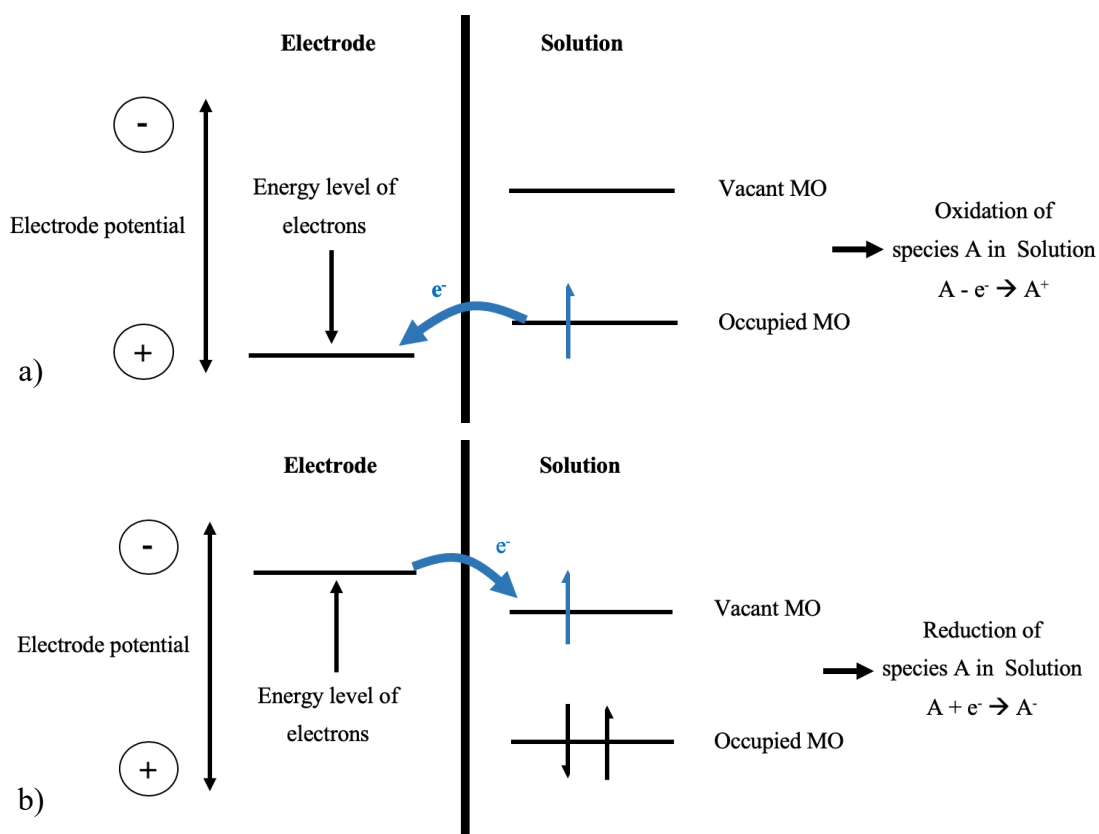


Figure 4.6 Schematic representation of redox reaction at an electrode-solution interface. a) Oxidation of species A in a solution b) Reduction of species A in a solution. The molecular orbits (MO) shown in this figure are the lowest vacant molecular orbital and the highest occupied molecular orbital of species A (adapted from Bard & Faulkner, 2001b)

Faradaic processes follow Faraday's law, which states that the amount of an electroactive species produced or consumed in electrochemical reactions in an electrochemical cell is proportional to the total amount of charge applied to the cell (Bard & Faulkner, 2001b).

The current passing through an interface is equal to the flow of charge per unit time and is expressed with the following equation:

$$i = \frac{dQ}{dt} \quad \text{Equation 4.9}$$

$i$ ...Current [A]

$Q$ ...Charge [coulomb]

$t$ ...Time [s]

The number of moles of a chemical compound electrolysed ( $N$ ) in a reaction relates to the charge with

$$N = \frac{Q}{n * F} \quad \text{Equation 4.10}$$

$n$ ...Number of electrons consumed in the reaction at the electrode

$F$ ...Faraday's constant 95484.56 C/mol; it is defined as the charge of one mole of electron.

Based on Equation 4.9 and Equation 4.10, the rate of an electrode reaction ( $v$ ) is given by:

$$v = \frac{dN}{dt} = \frac{i}{n * F * A} \quad \text{Equation 4.11}$$

$A$ ...Electrode area [ $\text{cm}^2$ ]

Non-faradaic processes do not involve any charge transfer across the electrode-electrolyte interface. However, non-faradaic current can flow transiently due to changes in the electrode structure (e.g. due to variation in the potential or solution composition or due to adsorption of proteins).

#### 4.3.1.2 Electrical double layer

When you immerse an electrode into an electrolyte, the formation of an electrical double layer (EDL) on the electrode-solution interface can be observable. The EDL is a charge build-up at the electrode- solution interface and it is considered to behave like a capacitor. According to the first EDL model by Helmholtz, it is made up of a layer of charge on electrode surface and layer of opposite charge on the solution side; whereby the charge on the solution side comprises of a compact layer (consisting of the inner Helmholtz plane (IHP) and the outer Helmholtz plane (OHP)) and a diffuse layer. Figure 4.7 shows the proposed model of an EDL by Helmholtz.

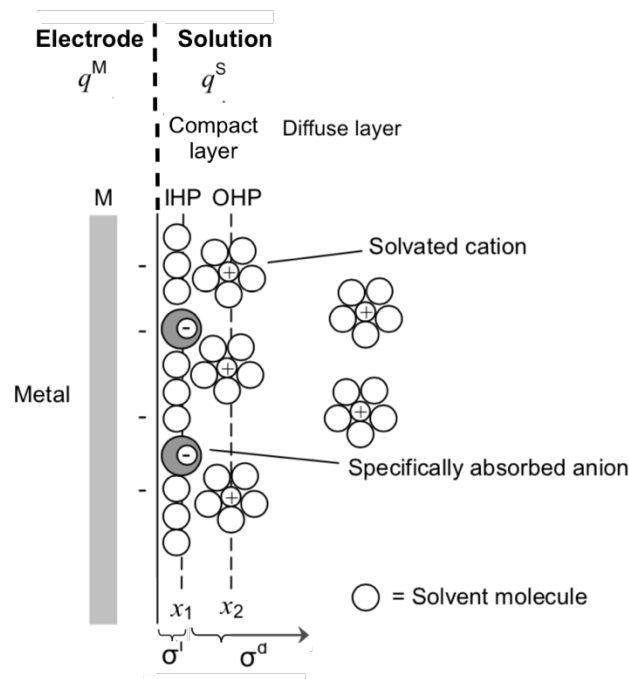


Figure 4.7 Electrode double layer according to Helmholtz model. A metal electrode with a negative charge  $q^M$  immersed in a solution with charge  $q^S$  (adapted from Bard & Faulkner, 2001b)

$q^M$  is defined as is the charge at the metal electrode and  $q^S$  is defined as the charge in the solution at a given potential. Depending on the composition of the solution and the applied potential, the charge at the metal electrode is either positive or negative.  $q^M$  resides in thin layer ( $< 0.1 \text{ \AA}$ ) and is made up of either a deficiency of excess of electrons. In contrast,  $q^S$  represents an excess of either of cations, which are positively charged ions or anions, which are negatively charged ions in the vicinity of the electrode. Charges are commonly expressed in form of charge densities ( $\sigma$ ), which is defined as the charge by the electrode area:

$$\sigma^M = \frac{q^M [\mu C]}{A [cm^2]} \quad \text{Equation 4.12}$$

The IHP consists of specifically adsorbed ions and molecules with a charge density of  $\sigma^I$  at a distance of  $x_1$  from the electrode. Solvated ions can be found in the OHP at a distance of  $x_2$  from the electrode. They are considered to be non-specifically adsorbed as they only interact via long-range electrostatic forces to the metal surface, where the chemical properties of ions are not relevant. The diffuse layer is the region between OHP and bulk solution and solvated ions can be found throughout this layer. The total density of the solvated ions in the diffuse layer is expressed with  $\sigma^D$ . The thickness of the diffuse layer is dependent on the ion concentration in the solution. The total charge

density in the solution interface  $\sigma^S$  is made of the charge of the inner layer  $\sigma^I$  and the diffuse layer  $\sigma^D$ .

$$\sigma^S = \sigma^I + \sigma^D = -\sigma^M \quad \text{Equation 4.13}$$

At all times, it is said that the charge density at the solution side of the EDL is opposite and equal to the charge density of the electrode side  $\sigma^M$ .

It is very important to consider the EDL capacitance in electrochemical measurements due to the charging current caused by the charging and discharging of the double layer. The EDL can influence faradaic processes on the electrode by the adsorption of electroactive species onto the electrode. Especially in electrode reactions, which involve redox reactions of electroactive species at low concentrations, there is the chance that the non-faradaic current caused by the EDL charging is higher than the faradaic current (Bard & Faulkner, 2001b).

#### 4.3.1.3 Polarisable and non-polarisable electrodes:

Polarisation is described as the change of the electrode potential from its equilibrium potential due to the passage of a faradaic current.

Electrodes, which allow free electron transfer processes are called non-polarisable electrodes. Non-polarisable electrodes do not change their equilibrium potential upon applying a current. In contrast, in ideal polarisable electrodes, already large changes the potential are observable upon the application of a small faradic current. They do not allow any charge transfer. However, it has to be mentioned that no electrode can be completely categorised into polarisable and non-polarisable electrodes. The ability of an electrode to polarise depends on a variety of factors with respect to the properties of the electrode, such as the electrode potential or electrode material, as well as the properties of the electrolytic solution, such as the presence of electroactive species. In most electrodes, faradaic and non-faradaic processes are observable (Bard & Faulkner, 2001b).

### 4.3.2 Operation of a mediated amperometric glucose sensor

In section 2.5, an overview of different generations of glucose sensors was given. Glucose sensors with a mediated electron transfer belong to the second generation of glucose sensors.

The main responsibility of a mediator is to transfer electron(s) between the enzyme and the working electrode. In this study glucose oxidase (GOD) was used as the enzyme and 1,1 dimethylferrocene (DMFc) was used as a mediator. A mediated enzymatic reaction in a glucose sensor with GOD and DMFc can be seen in Figure 4.8.

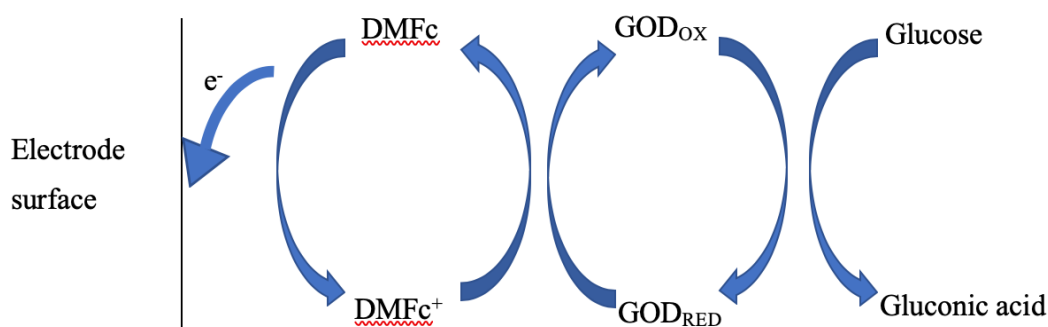


Figure 4.8 Redox reaction at electrode surface of a mediated glucose sensor (adapted from Hsueh *et al.*, 2014)

Glucose gets oxidised to gluconic acid, a reaction catalysed by glucose oxidase. Thereby, the glucose oxidase gets reduced itself and reacts with the oxidised form of the mediator. In this process the enzyme gets oxidised and gives away the electron to the mediator, which in turn gets reduced. By application of a particular potential at the electrode, the mediator gets oxidised and gives an electron to the electrode. The current produced due to the oxidation reaction of the mediator in the solution (oxidation current), is proportional to the glucose concentration. The potential at which the oxidation of the mediator occurs is called the oxidation potential.

Cyclic voltammetry (CV) is an electroanalytical technique, which was used in this study to identify the oxidation potential. The equipment and experimental setup needed to perform electrochemical glucose detection is explained in following section.

### 4.3.3 Three- electrode system and potentiostat

To perform electroanalytical measurements such as cyclic voltammetry, an electrochemical cell with a three-electrode system is required. A three-electrode system consists of a working electrode (WE), a reference electrode (RE) and a counter electrode (CE) in an electrolytic solution. Each electrode has a specific function, which is controlled by a potentiostat.

In a three-electrode system, a flow of charge across the electrode- solution is induced from CE to WE by creating a potential difference across the CE and WE with respect to the RE. The WE provides the surface for the chemical reaction to happen without taking part in the reaction with the bulk solution. The RE is a non-polarisable electrode and has the responsibility to provide a stable reference voltage against which the potential at the WE can be controlled and measured. At no point does the RE draw any current. This ensures that all the current in the cell flows through the WE and it can be measured with a potentiostat. The CE is required to control and adjust the current flow in order to keep the desired potential at the WE relative to the RE. The CE and WE are made of inert electrode so that they serve as good electron conductors and do not participate in any chemical reactions with the bulk solution.

Charge is carried in form of electrons in the electrode and in form of ions in the solution. The chemical reactions (eg. oxidation of a species) occurring at the WE can cause increases in electron flow leading to an increased flow rate of charge. This in turn leads to a higher current, which can be measured by the potentiostat.

#### Potentiostat

A potentiostat is a device, which is used to control the three-electrode system. It supplies and maintains the desired potential at the WE with respect to the RE and takes current measurements caused by chemical reactions. The circuit diagram of a potentiostat with a three-electrode system can be seen in Figure 4.9.

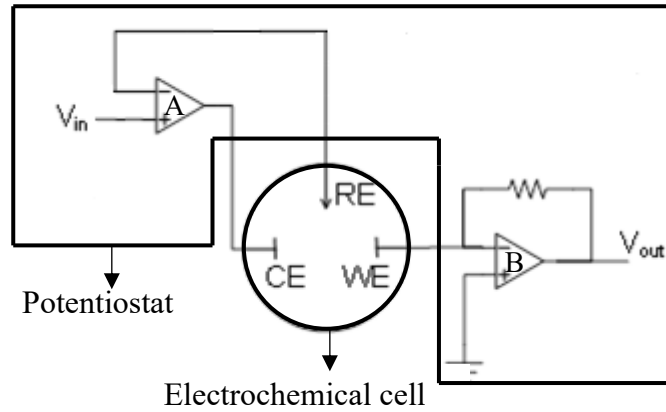


Figure 4.9 Circuit of a basic potentiostat with an electrochemical cell consisting of a three electrode system; opamp A works as a voltage follower and opamp B works as a current to voltage converter (adapted from Allen, Hill and Sanghera, 2011)

Operational amplifiers (op-amps) are required to ensure the functionalities of a potentiostat to carry out electrochemical measurements.

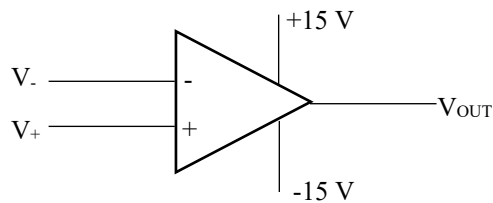


Figure 4.10 Diagram of an opamp

Op-amps (Figure 4.10) need their own power supply (e.g.  $\pm 15\text{V}$  with respect to a common ground). They have an inverting input ( $V_-$ ) and a non-inverting input ( $V_+$ ) and one output ( $V_{out}$ ).  $V_S$  is the supply voltage and is defined as the potential at  $V_-$  relative to the potential at  $V_+$

$$V_S = V_- - V_+ \quad \text{Equation 4.14}$$

The output voltage ( $V_{out}$ ) of an opamp is expressed with

$$V_{out} = -A * V_S \quad \text{Equation 4.15}$$

A...Open gain loop

In the ideal case op-amps have infinite input impedance, infinite open loop gain and zero output impedance and infinite bandwidth. The devices used for electrochemical applications are said to perform so well so that the nonidealities are considered to be negligible (Bard & Faulkner, 2001a).



Opamps can be used in different configurations depending on the intended use. For potentiostatic purposes, they were used in the form of a voltage follower (opamp A in Figure 4.9) and a current to voltage converter (opamp B in Figure 4.9).

Voltage followers are also called unity gain amplifier and their circuit design can be seen in Figure 4.11. In this configuration, there is no amplification of the input signal and  $V_+$  equals to  $V_{out}$ .

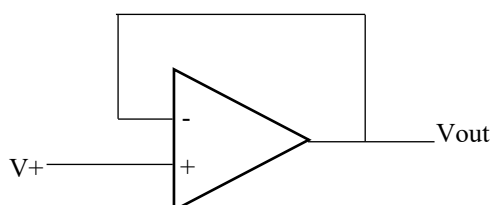


Figure 4.11 Circuit of a voltage follower

In electrochemical systems it is challenging to maintain the potential at WE at the desired value due to the constant changes in resistance and solution current. But it can be achieved with the help of a voltage feedback mechanism provided by the RE. The RE electrode is connected to the inverting input of the voltage follower. This on one side ensures that no respectively negligible amount current will be drawn by the RE due to the high input impedance of the opamp. In addition, it allows for the measured voltage difference between the WE and RE to be reflected in the output of the opamp A, which supplies the WE with the desired potential. The opamp aims to maintain the same potential at both of its inputs. Therefore, opamp A compares the measured potential to the desired potential and adjusts the output current accordingly so that both are the same (Bard & Faulkner, 2001a)..

Current to voltage converter work effectively on the same principles as voltage followers. However, they have additionally a feedback resistor, see circuit in Figure 4.12.

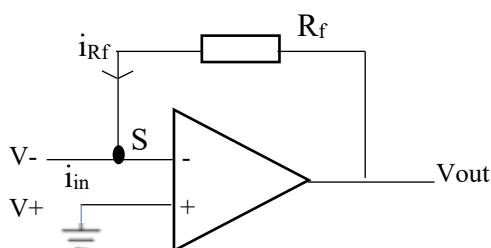


Figure 4.12 Circuit of a current to voltage follower

As discussed, in an ideal opamp, the voltage at the positive and negative input are virtually the same. As the non-inverting input of the op-amp is connected to the ground, node S is considered as a virtual ground. Based on Kirchoff's law, following relationship at node S can be determined

$$i_{in} = -i_{Rf} \quad \text{Equation 4.16}$$

Whereby  $i_{Rf} = \frac{V_{out}}{R_f}$  based on Ohm's law;

$$i_{in} = -\frac{V_{out}}{R_f} \quad \text{Equation 4.17}$$

$$V_{out} = -i_{in} * R_f \quad \text{Equation 4.18}$$

Equation 4.18 indicates that  $V_{out}$  is proportional to the input current  $i_{in}$  by a factor defined by  $R_f$ .

The WE is connected to the inverting output of current to voltage follower. It provides the input current  $i_{in}$ , which is the current flowing through the cell and can be obtained with  $V_{OUT}$  based on Equation 4.18.

#### 4.3.4 Cyclic voltammetry

Cyclic voltammetry (CV) is an electroanalytical technique, which allows the monitoring of the current produced via a redox reaction of the mediator on the electrode surface as a function of potential. This method was used to identify the oxidation potential of the mediator. CV is employed using a three-electrode system and a potentiostat, which was explained in Section 4.3.3.

In CV, the potential applied to the WE relative to the RE is also called potential excitation signal. For CV, the excitation signal has a linear triangular shape (Figure 4.13); Thereby, the excitation signal is swept between two values, which are also called the switching potentials. In the forward scan, the potential will be increased until the switching potential  $E_\lambda$  is reached and in the reverse scan it will be decreased until the second switching potential is reached. One full cycle consists of a forward and a reverse scan. The cycle can be repeated multiple times. The scan rate (SR) indicates how fast the potential changes with regards to time and its unit is V/s.

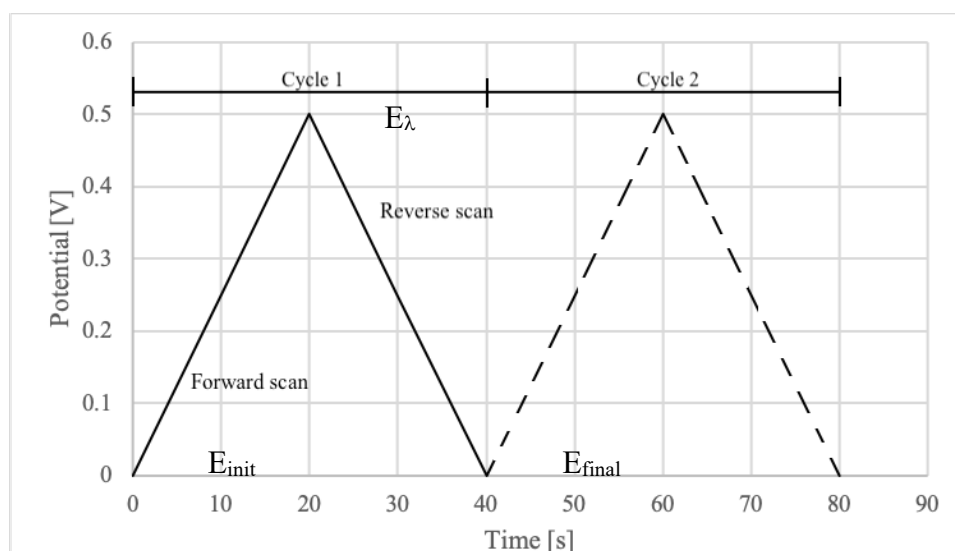


Figure 4.13 Typical excitation signal for cyclic voltammetry

During the potential scan, the current at the WE is measured. Figure 4.14 shows a voltammogram, which is a graph that shows the applied potential at the WE with respect to the RE on the x-axis and the resulting current y-axis.

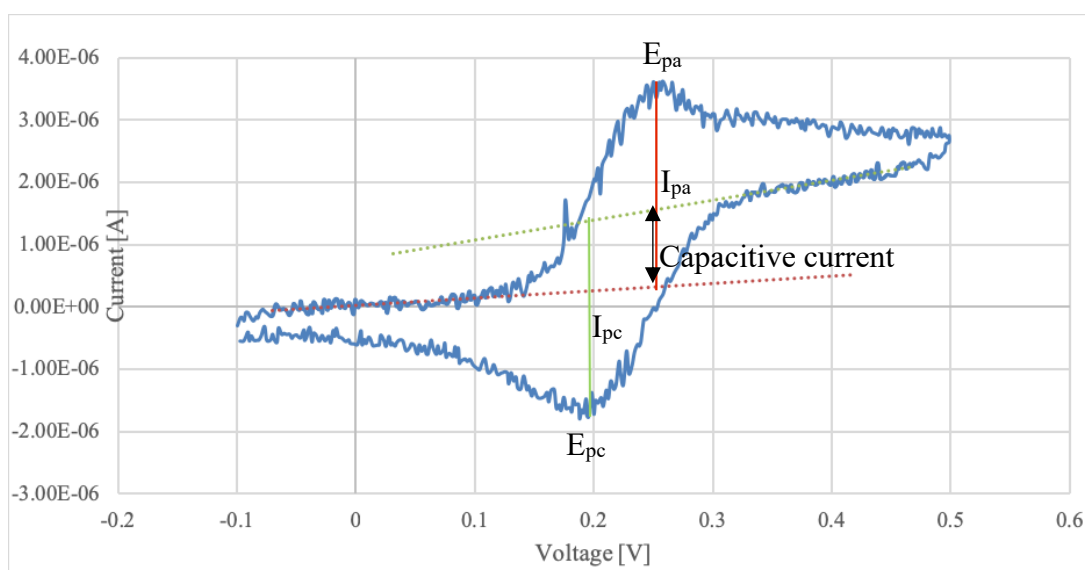


Figure 4.14 Example of a cyclic voltammogram of a ferrocene derivative: 0.5 mM ferrocenemonocarboxylic acid ( $\text{Fcpc}_2\text{R}$ ).  $E_{pa}$  and  $E_{pc}$  being the anodic peak potential and cathodic peak potential respectively and  $I_{pa}$  and  $I_{pc}$  being the anodic peak current and cathodic peak current respectively;

The forward scan starts at the excitation potential (-0.1 V) and ends with the switching potential (0.5 V). At the beginning, only a non-faradaic capacitive current is observable due to the electrode double layer.

The electroactive species on the electrode surface are able to undergo electrochemical conversions at certain potentials. Once the potential is sufficiently positive to oxidise ferrocene ( $\text{Fcpc}_2\text{R}$ ) to ferricinium ion ( $\text{Fcpc}_2\text{R}^+$ ), an increase of current is seen, which is a faradaic current. The faradaic current continues to increase until ferrocene gets fully depleted on the electrode surface causing a current peak ( $I_{pa}$ ). The potential, where the current reaches its maximum is called anodic peak potential ( $E_{pa}$ ). Subsequently, the current decays as the concentration of the ferrocene diminish from the surrounding of the electrode surface and the rate of oxidation occurs faster than the mass transport of the analyte from the bulk solution to the electrode surface. At the same time an increase of ferricinium concentration at the electrode surface occurs. As soon as the switching potential is reached, the reverse scan begins and the potential gradually decreases. Once the potential is sufficiently negative to reduce ferricinium ions to ferrocene, the cathodic current starts flowing until the concentration of the ferricinium ion is depleted in the vicinity of the electrode surface and a cathodic current peak ( $I_{pc}$ ) is produced. The voltage, where the cathodic current reaches its maximum is called the cathodic peak potential. After that the current decays, as there is no more ferricinium in the surrounding of the electrode surface. One full cycle has been completed, once the potential reaches the excitation voltage (Kissinger & Heineman, 1983).

Only the faradaic current is the result of the electron transfer and is proportional to the analyte concentration. It has to be taken into account that the capacitive current is constantly flowing due to the rearrangements of ions in electrode double layer caused by the changes in applied potential in CV. The capacitive current can be determined by extrapolating the baseline current (Kissinger & Heineman, 1983) and subsequently deducted from total current to identify  $I_{pa}$ .

The Nernst equation relates the cell potential to the standard cell potential and the concentrations of the oxidised species/reduced species in a system. At a temperature of 25 °C and a reversible electron transfer system it is expressed with:

$$E = E^0 - \frac{0.0592}{n} * \log \frac{[\text{concentration of oxidised species}]}{[\text{concentration of reduced species}]} \quad \text{Equation 4.19}$$

$E$ ... Cell potential [V]

$E^0$ ...Standard reduction potential [V]

$n$ ...Number of electrons

It helps to predict the response of a system caused by concentration changes of the oxidised/reduced species or by altering the excitation potential. For example, the excitation potential equals to the standard reduction potential, when the ratio of the concentration of oxidised species by the concentration of the reduced species equals to one.

The peak current changes with respect to the scan rate. With an increased scan rate, the diffusion layer decreases, which in turn leads to higher peak currents. Randles-Sevcik equation (Equation 4.20) relates the peak current with the scan rate in a reversible system.

$$I = 0.446 * n * F * A * c \left( \frac{n * F * SR * D}{R * T} \right)^{1/2} \quad \text{Equation 4.20}$$

$I$ ...current [A]

$n$ ...Number of electrons transferred

$F$ ...Faraday's constant [ $\frac{C}{mol}$ ]

$A$ ...Area of electrode [cm<sup>2</sup>]

$D$ ...Diffusion coefficient of mediator [ $\frac{cm^2}{s}$ ]

$c$ ...Concentration of analyte of interest in bulk solution [ $\frac{mol}{cm^3}$ ]

$SR$ ...Scan rate [ $\frac{V}{s}$ ]

$R$ ...Gas constant [ $\frac{J}{K * mol}$ ]

$T$ ...Temperature [K]

It is known that ferrocene and ferrocene derivatives undergo a reversible one electron transfer indicating a good stability of the mediator (Cass et al., 1984). In a reversible

system an anodic and a cathodic peak should be observable in the cyclic voltammogram. A stable species will stay close to the electrode surface and in the reverse scan a current wave of the opposite polarity of the forward scan will be seen. An unstable species will show no current wave in the reverse scan.

Reversible systems can be determined by analysing the voltammogram and the following conditions apply (Hill & Sanghera, 1990):

- 1) There should be a peak separation of 57 mV between the anodic and cathodic peak potential.
- 2) The peak current, which was obtained from the potential scan, should be proportional to the square root of the scan rate

$$i_p = A * v^{1/2} \quad \text{Equation 4.21}$$

- 3) The ratio between the anodic peak current ( $i_{pa}$ ) and cathodic peak current ( $i_{pc}$ ) should equal to 1

$$\frac{i_{pa}}{i_{pc}} = 1 \quad \text{Equation 4.22}$$

- 4) The anodic peak potential is independent of the applied scan rate.

In case of a reversible system, the redox potential can be identified with Equation 4.23, whereby  $E_{pa}$  is the anodic peak potential and  $E_{pc}$  is the cathodic peak potential.

$$E = \frac{E_{pa} + E_{pc}}{2} \quad \text{Equation 4.23}$$

- Establishment of a glucose calibration curve using electrochemical glucose detection techniques

Glucose calibration curves based on electrochemical glucose detection can be established with the help of the anodic peak currents. Glucose concentrations of standards are plotted against the anodic peak currents obtained via CV using the glucose sensors. A linear response is expected between a limited range of the standard glucose concentrations and the respective oxidation current and can be expressed with the linear function equation (Equation 4.6).

### 4.3.5 Reference electrodes

As discussed, the potential applied to the WE in an electrochemical system is relative to a RE. For this project screen printed pseudo Ag/AgCl electrodes were used as RE. For comparison purposes to existing literature, there is the possibility to convert potentials which was acquired relative to one type of RE to a potential relative to another type of RE (Research Solutions & Resources LLC., 2014). The reference potential of the screen-printed pseudo Ag/AgCl electrodes were tested relative to a standard Ag/AgCl (3M KCl) references electrode. Therefore, redox potentials of ferrocene derivatives found in literature were converted with respect to Ag/AgCl (3M KCl) references electrode.

From literature it is known that Ag/AgCl (3M KCl) vs. NHE has a potential of 0.210 V and a potential of -0.032V vs. SCE (Friis et al., 1998).

Table 4.1 shows a list of selected mediators with their redox potentials from the literature and the converted potential vs Ag/AgCl (3 M KCl) reference electrode.

Table 4.1 Mediators with redox potentials from literature

<b>Electroactive species</b>	<b>Redox potential from literature</b>	<b>Converted redox potential vs Ag/AgCl</b>	<b>Reference</b>
DMFc	0.100 V vs SCE	0.132 V vs Ag/AgCl (3M KCl)	(Cass et al., 1984)
Ferrocene	0.165 V vs SCE	0.197 V Ag/AgCl (3M KCl)	(Cass et al., 1984)
Ferrocene	0.4 V vs SHE	0.190 V vs Ag/AgCl (3M KCl)	(Sharpe & Housecroft, 2005)
Ferrocene	0.2 V vs Ag/AgCl		(Gray, 2008)

From theory it is known that in case of a one-electron reversible system, following formula applies for the difference in peak potentials (Kissinger & Heineman, 1983):

$$\Delta E = E_{pa} - E_{pc} \cong \frac{0.059}{\text{number of electrons transferred}} \quad \text{Equation 4.24}$$

Based on Equation 4.24, the anodic and cathodic peak potential of dimethyl ferrocene, which undergoes a one-electron transfer, should be situated  $\pm 0.0295$  V (0.059/2) from the redox potential of DMFc. Therefore, an anodic peak potential of 0.1615V

(0.132 V + 0.0295) and a cathodic peak potential of 0.1025 V (0.132V- 0.0295V) were calculated from the redox potential of DMFc given by Cass et al's research (Cass et al., 1984).

## 4.4 Reverse iontophoresis

Reverse iontophoresis (RI) enables non-invasive transdermal extraction of glucose molecules across the skin by applying a low level current. The skin structure and pathways for molecules to cross the skin barrier were discussed in detail in section 2.9.1. This section explains the mass transport mechanisms involved in RI.

As discussed, non-polarisable electrodes, such as Ag/AgCl electrodes enable free current flow in the electrode-electrolyte interface. Therefore, this type of electrode was used to apply the iontophoretic current. When applying the iontophoretic current across the skin, the current will flow from one direction to the other. Therefore, two iontophoresis electrodes are required to complete a circuit, an anode, which is the positively charged electrode and a cathode, which is the negatively charged electrode. The applied iontophoretic current is carried by electrons in the metallic part of the circuit and in solution the current is carried by the ions (cations or anions). For the continuous flow of current in the circuit, the same amount of charge has to leave and reach the electrode.

In addition, a third electrode was used in the RI setup as a control electrode where no current was passed through. In the configuration used in this project gel is applied onto the electrode for electrical conductance. It is also used as a receptacle for the glucose to accumulate.

Three transport mechanisms contribute to the mass transfer during the process of RI 1) electromigration 2) convection due to electroosmosis and 3) diffusion; whereby electromigration and electroosmosis are a direct result of RI and diffusion occurs indirectly. Figure 4.15 shows a schematic view of the RI process and the involved transport mechanisms at each electrode.



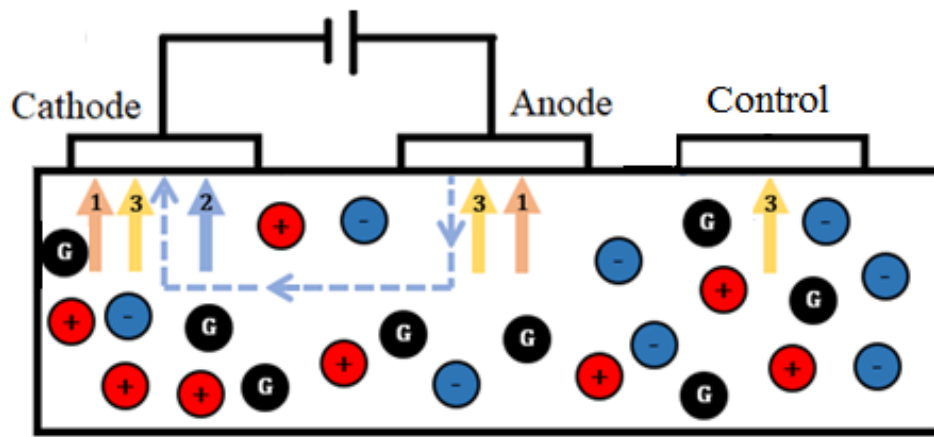


Figure 4.15 Schematic view of reverse iontophoresis with the transport mechanisms indicated with the arrows (1= electromigration, 2= electro-osmotic flow and 3= passive diffusion) at each electrode. Three transport mechanisms are active on the cathodal side of electrodes, two are active on the anodal side and one is active on the control electrode.

Electromigration is the main transport mechanism of charged particles and is induced by an electric field. Thereby, charged species migrate towards the electrode with opposite polarity. Convective flow caused by electroosmosis is induced by the application of an electric field across a charged membrane. Thereby, a solvent flow is created in the same direction as the flow of counterions. Diffusion is the movement of particles along a concentration gradient across a membrane. It occurs mainly in the electrode-solution interface as the concentration gradient within the bulk solution is usually small. Compared to electromigration and electroosmotic flow, passive diffusion extracts the least amount of solute.

The total flux of a charged species  $i$  ( $J_i$ ) during RI is defined as the sum of flux caused by diffusion ( $J_{D,i}$ ), electromigration ( $J_{M,i}$ ) and convective flow due to electroosmosis ( $J_{C,i}$ ) and can be characterised with a modified Nernst-Planck expression (Bard & Faulkner, 2001c):

$$J_i = \underbrace{-D_i \frac{dc_i}{dx}}_{J_{D,i}} + \underbrace{\frac{z_i F D_i}{RT} c_i * X}_{J_{M,i}} + \underbrace{v * c_i}_{J_{C,i}} \quad \text{Equation 4.25}$$

$J_i$ ...Flux of species  $i$  [ $\frac{mol}{s*cm^2}$ ]

$D_i$ ...Diffusion coefficient of species  $i$  [ $\frac{cm^2}{s}$ ]

- $c_i$ ... Ion concentration of species  $i$  [ $\frac{mol}{cm^3}$ ]
- $x$ ... Distance [cm]
- $z_i$ ... Charge number of species  $i$
- $F$ ... Faraday's constant [ $\frac{C}{mol}$ ]
- $X$ ... Applied electric field
- $v$ ... Average electroosmotic solvent flow velocity [ $\frac{cm}{s}$ ]

For a charged species, the flux of the species ( $J_i$ ) equals to the current density with the following equation (Bard & Faulkner, 2001c):

$$J_i = \frac{i_i}{z_i F A} \quad \text{Equation 4.26}$$

- $i_i$ ... Current [A]
- $A$ ... Electrode area [cm<sup>2</sup>]

The flux of a charged species ( $J_i$ ) during RI can be translated into a current carried by an ion ( $i_i$ ) with the help of Equation 4.25 and Equation 4.26:

$$i_i = \boxed{z_i F A * J_{D,i}} + \boxed{z_i F A * J_{M,i}} + \boxed{z_i F A * J_{C,i}} \quad \text{Equation 4.27}$$

Diffusion	Migration	Convection
└─┘	└─┘	└─┘

The diffusion coefficient  $D$  is expressed with the Einstein-stokes equation (Equation 4.28) and it relates the diffusion and viscous flow in a system (Bockris & Reddy, 1998). It is observable how the diffusion coefficient depends on the radius of the ion.

$$D = \frac{k * T}{6 * \pi * r * \eta} \quad \text{Equation 4.28}$$

- $k$ ... Boltzmann constant [ $\frac{J}{K}$ ]
- $T$ ... Temperature
- $r$ ... Radius of ion
- $\eta$ ... Viscosity of the solution

#### 4.4.1 Electromigration

Electromigration is defined as the movement of charged ions across the skin under the influence of an electric field. As discussed, the flow of electrons caused by the application of the iontophoretic current is exchanged to a flow of ions in the ionic solution. There is a balance between the number of electrons moving in the external circuit and the number of ionic charges moving through skin (Sage & Riviere, 1992). The flow of charge in the solution is carried out by all the ions present in solution i.e. each ion carries a fraction of the total charge. The total current ( $i$ ) in migration is defined as the sum of currents carried by each ion ( $i_i$ ):

$$i = \sum_i i_i = F * A * X * \sum_i z_i * \mu_i * c_i \quad \text{Equation 4.29}$$

$i$ ...Total current [A]

$i_i$ ...current by ion I [A]

$F$ ...Faraday's constant

$A$ ...Electrode surface [cm<sup>2</sup>]

$X$ ...Applied electric field

$z_i$ ...Charge number of ion i

$\mu_i$ ...Mobility of ion i [ $\frac{cm^2}{s*V}$ ]

$c_i$ ...Concentration of ion i [ $\frac{mol}{cm^3}$ ]

The Einstein-Smoluchowski equation relates the mobility of an ion with the diffusion coefficient (Bard & Faulkner, 2001c). The transport of charge of an ion increases with higher mobility of the ion.

$$\mu_i = \frac{z_i * F * D_i}{R * T} \quad \text{Equation 4.30}$$

$R$ ...Gas constant

$T$ ...Temperature

The transport number ( $t_i$ ) indicates the fraction of current carried by an ion relative to the total current and is expressed with (Bard & Faulkner, 2001c)

$$t_i = \frac{i_i}{i} = \frac{z_i * \mu_i * c_i}{\sum_k z_k \mu_k c_k} \quad \text{Equation 4.31}$$

The total charge transfer is depended on several factors: The current intensity, the duration of RI, the transport number of the ion of interest (Leboulanger et al., 2004). Due to safety concerns, the current intensity should not exceed 500  $\mu\text{A}/\text{cm}^2$ . The extraction time should be sufficiently long so that enough amount of the substance of interest has been extracted for detection.

Depending on the charge of the particles in the solution, they will migrate to the oppositely charged electrode under the influence of an electric field, i.e. positively charged molecules, such as sodium and potassium flow to the cathode and negatively charged ions such as chloride to the anode.

$\text{Na}^+$  and  $\text{Cl}^-$ , being the main extracellular electrolytes in the body (Terry, 1994), are the principle carriers of the iontophoretic current due to their small size and their high mobility (Merino et al., 1997). Their average ionic mobility was estimated to be  $1.5 \cdot 10^{-8} \frac{\text{cm}^2}{\text{V} \cdot \text{s}}$  in the stratum corneum (Guy et al., 2000). The higher the molecular weight of the ion, the more restricted is its mobility, which in turn compromises electromigration. It was shown that for cations with increasing ion size such as cation peptides (>1000 daltons), the ionic mobility decreases and therefore, the principle transport mechanism changes from electromigration to electroosmosis (Guy et al., 2000).

#### 4.4.2 Convection due to electroosmosis

In electroosmosis a solvent flow is created due the influence of an electric field on a charged membrane. The electroosmotic flow (EOF) plays an essential role in separation techniques such as capillary electrophoresis where charged species are separated based on their charge and size. It is also one of the transport mechanisms involved in RI.

Figure 4.16 shows a schematic view of the EOF occurring in glass capillary filled with an electrolytic solution under the influence of an electric field.

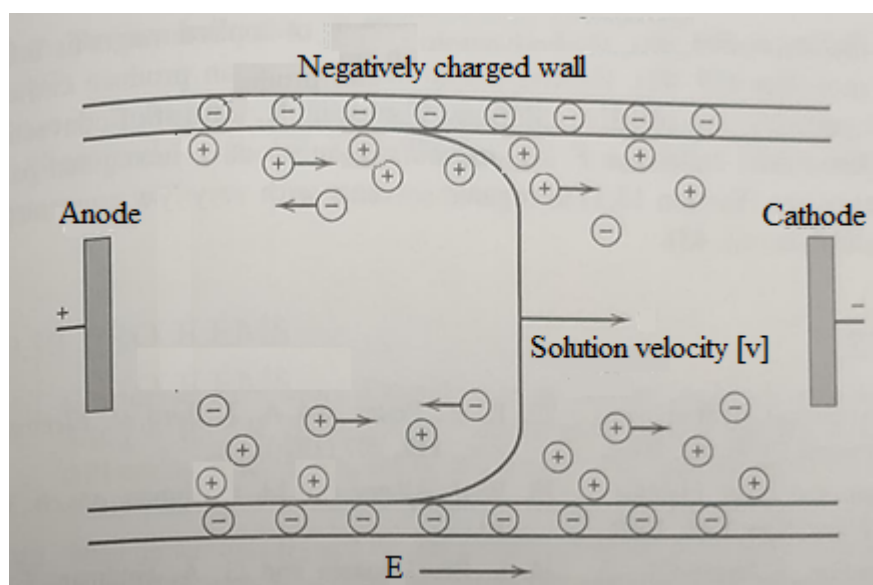


Figure 4.16 Schematic view of the electroosmotic flow in a glass capillary (adapted from Bard & Faulkner, 2001d)

The wall of the glass capillary has a net negative charge at a pH of 3. When a membrane is in contact with a solution, an electrical double layer is observable at the membrane-solution interface (similar to one at an electrode-solution interface). As discussed, an electrical double layer is a charge build-up and it is made up of a layer of charge on membrane surface and layer of opposite charge on the solution side. It consists of a compact and a diffuse layer.

Due to the net negative charge of the membrane, the anions in the solution are repelled from the membrane. However, cations from the bulk solution are strongly attracted to the negatively charged membrane, creating the compact layer of the double layer. Solvated cations are free to move and can be found in the diffuse layer of the double layer. Under the influence of an electric field, the movement of the cations in the diffuse layer create a solvent flow from the anode (+) to cathode (-) and thereby assists the transport of cations and neutral species along the solvent flow. In contrast, anion transport is hindered. (Bard & Faulkner, 2001d)

This behaviour can be also seen in RI experiments. As discussed, the isoelectric point of the skin is 4. Therefore, at physiological pH, the skin carries a net negative charge (Burnette & Ongpipattanakul, 1987). Under the influence of an electric field, a solvent flow is created from the anode to the cathode by the movement of the cations in the

diffuse layer. The  $\text{Na}^+$  ions are the main electrolytes responsible for creating the solvent flow and enable uncharged molecules to be transported to the cathode via the electro-osmotic flow (Pikal, 1990, 1992). The main transport mechanism for glucose in RI is the electroosmotic flow. In addition, passive diffusion also contributes to the transport of glucose across the skin (Sieg et al., 2004b). The electroosmotic flow supports the transport of cations and neutral compounds to the cathode but hinders anion transport to the anode.

The average velocity ( $v$ ) of the electroosmotic flow is proportional to the applied electrical field and can be described with (Bard & Faulkner, 2001d):

$$v = \frac{-\varepsilon * \varepsilon_0 * \xi * E}{\eta} \quad \text{Equation 4.32}$$

$v$ ...Average electroosmotic flow velocity

$\varepsilon$ ...Permittivity of the medium

$\varepsilon_0$ ... Permittivity of free space

$\xi$ ...Zeta potential, which is the potential at the shear plane between the compact and diffuse layer of the electrical double layer

$E$ ...Applied electrical field strength

$\eta$ ...Viscosity

The velocity of a neutral species or an ion ( $v_1$ ) with respect to the membrane is expressed as the sum of the velocity of the neutral species or ion relative to the solvent flow ( $v_1^0$ ) and the velocity of the solvent flow relative to the membrane ( $v$ ) (Pikal, 1992):

$$v_1 = v_1^0 + v \quad \text{Equation 4.33}$$

A neutral compound has a  $v_1^0 = 0$ , therefore it would be carried along the solvent flow with a velocity of  $v$ . In contrast, charged species have a  $v_1^0 \neq 0$ , due to their interaction with the electric field. Depending on the charge and hence direction of movement, the velocity of the solvent flow will either assist or hinder their transport.

The total current ( $i$ ) in electroosmosis could be expressed with

$$i = F * A * v * \sum_i z_i * c_i \quad \text{Equation 4.34}$$

However, due to the principles of electroneutrality in the bulk of a conducting solution ( $\sum_i z_i * c_i = 0$ ), the total convection current density in a system equals to zero (indicated with the dashed line in Equation 4.34) (Lefrou et al., 2012).

Factors, which have an influence on electroosmosis are current density, ionic strength and the pH value (Santi & Guy, 1996b).

The ionic strength gives information on the concentration of ions present in the electrolyte. It was shown that with lowering the ionic strength in the electrode chamber (which is filled with gel), the electroosmotic flow towards the cathode was enhanced (Merino et al., 1999; Santi & Guy, 1996b). This is due to that fact that, with decreasing ionic strength in the electrode chamber, the charge carriers in the chambers reduces. This forces the ions in the solution (in vivo: the ions in the subdermal region; in vitro: the ions in the buffer solution in the diffusion cell) to carry more of the total charge and hence electroosmotic flow from the solution to the skin surface or to membrane surface respectively is elevated. However, sufficient level of electrolyte must be present in the chamber to allow and support the necessary electrochemical reactions on the Ag/AgCl electrode (Santi & Guy, 1996b). In contrast, with increasing the ionic strength, the electroosmotic flow was decreased. With increased number of ions in the system, the fixed charges of the skin are effectively shielded causing a reduction of the electric field in the iontophoretic pathways. This in turn impairs the migration of counterions and therefore, the electroosmotic flow (Santi & Guy, 1996b).

It was shown that with decreasing pH in the electrode chamber, the electroosmotic flow towards the cathode was impaired. This could be due the neutralisation of the net negative charge of the skin with the hydrogen ions. In contrast, an improved electroosmotic flow towards the cathode was observable due increased net negative charge density at higher pH (Santi & Guy, 1996b).

Pikal stated that the molecular size of the solute does hardly have an impact on the flux of solutes during electroosmosis with the condition that the size of the solute does not interfere with the transport pathway (Pikal, 1992).

### 4.4.3 Diffusion

Diffusion is the movement of particles due to a concentration gradient. Diffusion in a steady state system can be characterised with Fick's first law of diffusion, which is expressed in the following equation (Equation 4.35)(Bard & Faulkner, 2001c). Diffusion of an analyte ( $J_i$ ) is proportional to the concentration gradient between two points.

$$J_i = -D * \frac{dc}{dx} \quad \text{Equation 4.35}$$

Diffusion in a non-steady state is governed by Fick's second law of diffusion. The change of concentration of a substance over time and space is expressed with the following equation

$$\frac{\partial c}{\partial t} = D \frac{\partial^2 c}{\partial x^2} \quad \text{Equation 4.36}$$

The total diffusion current can be expressed as the sum of currents carried by each ion ( $i$ ):

$$i = F * A * \sum_i z_i * D_i * \frac{dc_i}{dx} \quad \text{Equation 4.37}$$

The number of molecules transported via passive diffusion increases with the given diffusion area. Furthermore, passive diffusion also depends on the size of the molecule to diffuse as it was seen in Equation 4.28 that the diffusion coefficient depends on the radius of the ion (Kasting et al., 1987). Na<sup>+</sup> ions have a diffusion coefficient of  $D_{Na}=1.334*10^{-5} \text{ cm}^2/\text{s}$  in aqueous solution and Cl<sup>-</sup> ions  $D_{Cl}=2.032 *10^{-5} \text{ cm}^2/\text{s}$  (Bockris & Reddy, 1998). In comparison, glucose, which is the analyte of interest in this study has a diffusion coefficient of  $D=0.6*10^{-5} \text{ cm}^2/\text{s}$  in aqueous solution (Stein & Litman, 2015).

Glucose is extracted via electroosmosis and diffusion, whereby the contribution of passive diffusion is small compared to the electroosmotic flow. Figure 4.17 shows the iontophoretic solution flux in comparison to the passive solution flux of glucose across a hairless mouse skin using a permeation cell (Pikal & Shah, 1990).



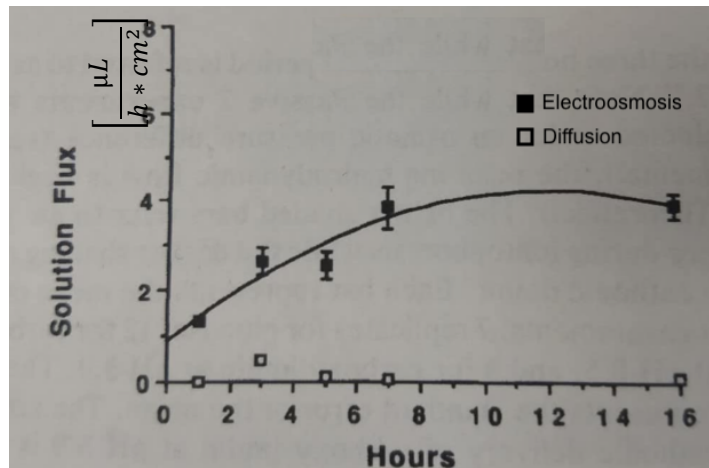


Figure 4.17 Contribution of diffusion and electroosmosis to glucose flux across hairless mouse skin over time with an iontophoretic current of  $0.32 \text{ mA/cm}^2$ . The glucose concentration in the donor cell was  $0.05 \text{ M}$ . (adapted from Pikal and Shah, 1990)

The passive diffusion flux of glucose was on average  $0.1 \frac{\mu\text{L}}{\text{h}\cdot\text{cm}^2}$ , whereas via electroosmosis higher glucose flux were observable (up to approximately  $4 \frac{\mu\text{L}}{\text{h}\cdot\text{cm}^2}$ ). In addition, it was shown that the application of an iontophoretic current enhances skin permeability due to the changes in the skin structure (Pikal, 1992; Srinivasan et al., 1988; Srinivasan et al., 1989). Pikal and Shah showed that the glucose flux via diffusion increased from  $0.2 \frac{\mu\text{L}}{\text{h}\cdot\text{cm}^2}$  by a factor of 10 after the application of an iontophoretic current (Pikal & Shah, 1990).

## 4.5 Integrating a glucose binding agent in the sensor in the RI environment

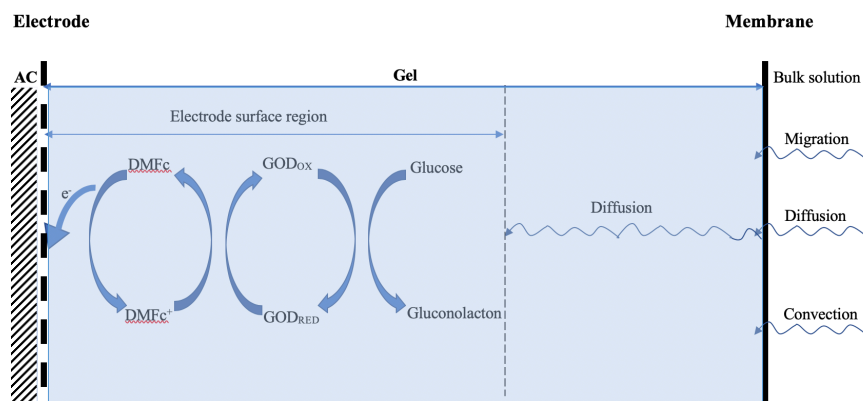


Figure 4.18 Transport mechanisms of molecules and ions from the bulk solution across the membrane to the mediated glucose sensor with AC as a glucose binding agent in the outer layer of the sensor.

Figure 4.18 shows a schematic view of a mediated amperometric glucose sensor with AC in the outer layer of the sensor and the transport mechanisms involved in RI. The mass transport mechanisms via RI across the membrane to the gel reservoir were discussed in section 4.4. Once glucose is in the gel reservoir via the application of RI, diffusion is the only transport mechanism for the glucose molecules to move across the layer gel to the electrode surface where the redox reaction of the mediator takes place.

With the condition that only one reaction occurs at the electrode-solution interface (i.e.  $A + e \rightarrow A^+$ ), the current related to the diffusion flux of the analyte of interest at the electrode surface is expressed with

$$J_o(0, t) = \frac{i}{n * F * A} = D_o \times \left[ \frac{dc(0, t)}{dx} \right]_{x=0} \quad \text{Equation 4.38}$$

The integration of a glucose binding agent in the outer layer of the sensor, can facilitate to draw the analyte of interest continuously out of the gel layer into the binding agent and it will prevent the accumulation of the analyte in the gel reservoir. Hence, it can create a uniform diffusion profile of glucose in the gel to the outer layer, governed by Fick's first law of diffusion. By the binding of the glucose to the binding agent in the outer layer, a local concentration of zero or near zero can be found. The concentration gradient in Fick's first law of diffusion can then be rewritten to

$$\frac{dc}{dx} = \frac{c_1 - c_0}{x_1 - x_0} = \frac{C_{skin} - 0}{x} \quad \text{Equation 4.39}$$

$C_{skin}$ ...glucose concentration at the skin barrier

$x$ ...thickness of the gel layer

The glucose concentration at the skin barrier will be depended on the glucose concentration in the interstitial fluid. Therefore, if the glucose concentration in the interstitial fluid changes, the glucose concentration at the skin barrier and the diffusion flux of glucose will change accordingly provided a controlled and uniform diffusion is present. (Connolly, 2014)

## 4.6 Statistical analysis

The standard error of mean (*SEM*) was used to show the sample distribution of the datasets and this was calculated with the following equation:

$$SEM = \frac{\textit{standard deviation}}{\textit{number of samples}} \quad \text{Equation 4.40}$$

### Statistical significance:

To analyse statistical significance of the obtained results, SPSS Statistics from IBM was used to perform statistical tests. When comparing two populations with a normal distribution, the two-independent sample t-tests were applied. In contrast, in the case of non-normal datasets, the Mann Whitney U test was applied to determine the statistical significance between two populations. In case of three or more than three populations with normal distribution, the one-way ANOVA test was used. A significance level of 0.05 was chosen for all statistical tests. P-values less than or equal to 0.05 indicate that the difference between both groups is enough to reject the null hypothesis. The null hypothesis states that there is no significant difference between both populations. In contrast, p-values higher than 0.05 indicate that there is no significant difference between the datasets.

## 5 Materials and Methods

The main aim of this study was to evaluate the suitability of AC to act as a glucose binding agent in wearable sensors in the reverse iontophoresis (RI) environment. This could help for better controlled and more uniform glucose flux across iontophoresis devices. For further improvement of the device, the integration of a biosensor in the electrode was investigated to provide direct glucose measurements in the gel electrode itself. This chapter reviews the key materials, methods and related experimental details that underpin this study.

In the first part of this chapter, all the materials and devices used in this project are listed followed by the preparation of basic buffer solutions and hydrogel. Details and the protocols of the used glucose assay kits are described here.

The electrodes, which were used to perform RI experiments were manufactured in the laboratory using screen-printing methods. *In vitro* RI experiments were then carried out to study the flux of glucose molecules during RI using a diffusion cell.

Preliminary experiments were performed to prove glucose adsorption to AC from glucose solution samples as well as glucose gel samples. Once glucose adsorption to AC was successfully shown, a prototype of an AC foam integrated electrode was developed and tested in the *in vitro* RI setup.

In the final section of the chapter, the fabrication of the glucose sensors, which were used for direct glucose measurements in the RI experiments, is explained. A series of experiments were carried out to assess sensor performance and its potential to be used in the RI environment. In addition, AC foam was also integrated in the biosensor and tested in the *in vitro* RI setup.

### 5.1.1 Materials

### 5.1.2 Chemicals

Methylcellulose powder (Methocel A4M Premium USP/EP – Lot# UJ24012N02) was purchased from Colorcon limited. Sodium phosphate monobasic (S2554 – Lot# 023K0049), Glucose (G8270), potassium chloride (P5405), sodium chloride (S7653), HEPES (H3375), 1,1'-dimethylferrocene, (DMFc) (109576), 1-cyclohexyl-3-(2-morpholinoethyl)-carbodiimide metho-p-toluenesulfonate crystalline (carbodiimide) (C1011), sodium acetate (S2889), potassium phosphate (P5379), ethanol (32221), sodium azide (S2002), sodium perchlorate (410241), potassium phosphate (P5379), standard Ag/AgCl (3M KCl) reference electrode and glycerol (G5516 – Lot# SHBC6976V) were purchased from Sigma Aldrich.

Glucose Oxidase (GOD) (*Aspergillus niger*) (G03A) was purchased from Biozyme Laboratories and asetic Acid (27013) was purchased from BDH, UK.

The silver/silver chloride ink (LOCTITE EDAG 6037 SS E&C – Batch No: OW62413025) and the carbon ink (LOCTITE EDAG PF 407A E&C) were both purchased from Henkel electronic materials.

The Elga Purelab system was used to purify water to distilled water.

### 5.1.3 Other materials

Glucose assay kit, GLUC-PAP (GL2623) was purchased from Randox Laboratories Limited.

Glucose (HK) Assay Kit (GAHK20-1KT) was purchased from Sigma Aldrich. The Spectrapore membrane (131060) was purchased from Spectrum Laboratories Inc. The Vitro-Skin® was purchased from IMS Inc. The Micropore Surgical Tape was purchased from Boots and the double-sided tape 1” inch red was purchased from Hair Direct.

The Betta Activated Filter Carbon was purchased from J&K Aquatics Ltd and the Compost caddy odour filters was purchased from Garland Products Limited.

The EuroPunch Pliers (Round 1.25 mm – PLR 133.60) for Sheet Metal was purchased from Eurotool punchhole.

The masks for the screen printing were purchased from MCI Precision Screens Ltd.

The acetate sheets were purchased from MA10 Niceday.

#### 5.1.4 Other devices

- Multiskan Ascent 96/384 Plate Reader from MTX Lab Systems Inc.
- Multiskan go from Thermo Scientific
- Genova Nano Spectrophotometer from Jenway
- Constant current source designed and constructed in the Biomedical Engineering Department, University of Strathclyde
- Electrochemical interface SI1268 from Schlumberger (University ID: INV017206)
- Diffusion cell from Biomedical Engineering Department, University of Strathclyde
- Screen exposure unit from Dek (University ID: INV017009)
- Semiautomatic screen printer Model 247 from Dek
- Carl Zeiss Axio Imager microscope

## 5.2 Methods

### 5.2.1 Preparation of 0.1 M phosphate buffer solution

0.1 M phosphate buffer solution was prepared by dissolving 2.9975 g of sodium phosphate monobasic in 250 ml distilled water. The pH was then adjusted to 7.4 by adding drops of 5 mM sodium hydroxide solution.

### 5.2.2 Preparation of 5 mM sodium hydroxide solution

5 mM sodium hydroxide solution was prepared by dissolving of 20 g of sodium hydroxide in 100 ml of distilled water.

### 5.2.3 Preparation of 3% w/v of methylcellulose hydrogel

The hydrogel was prepared by dissolving 3 g of methylcellulose powder in 80 ml of 0.1 M phosphate buffer solution, which had a pH of 7.4. 30 ml of the buffer was heated up to 80 °C and mixed with the powder with a battery-operated stirrer. Once the powder was completely dissolved, the remaining phosphate buffer was added and

mixed until an even paste was seen, and the temperature of the gel was brought down to room temperature. Finally, 20 ml of ethanol was added to the gel and again mixed properly. The hydrogel was then transferred to syringes and the tip was covered with para-film to prevent dehydration of the gel. It was stored in the fridge at a temperature of 4 °C.

## 5.2.4 Glucose sample preparation for calibration curve

Glucose solutions with a range of different concentrations were prepared in order to capture the range of the glucose concentrations expected to be observed during *in vivo* glucose extraction studies. Glucose was diluted with a 0.1 M sodium phosphate solution (pH 7.4). Existing literature, which involved RI experiments on humans, demonstrated that the glucose extraction level for humans is in the  $\mu\text{M}$  range (McCormick et al. 2012, Tamada et al. 1999). Hence, the following concentrations for the calibration curve were produced: 1000  $\mu\text{M}$ , 500  $\mu\text{M}$ , 250  $\mu\text{M}$ , 125  $\mu\text{M}$ , 62.5  $\mu\text{M}$ , 31.25  $\mu\text{M}$ , 15.625  $\mu\text{M}$ , 7.8125  $\mu\text{M}$ , 3.906  $\mu\text{M}$  and 0  $\mu\text{M}$ .

Table 5.1 Preparation of the standard glucose solution samples

Required glucose solution concentration [ $\mu\text{M}$ ]	Sample preparation for required glucose solution concentration:
1000	0.0036 g of glucose powder in 20 mL of phosphate buffered solution
500	10 mL from 1000 $\mu\text{M}$ glucose solution + 10 mL of phosphate buffered solution
250	10 mL from 500 $\mu\text{M}$ glucose solution + 10 mL of phosphate buffered solution
125	10 mL from 250 $\mu\text{M}$ glucose solution + 10 mL of phosphate buffered solution
62.5	10 mL from 125 $\mu\text{M}$ glucose solution + 10 mL of phosphate buffered solution
31.25	10 mL from 62.5 $\mu\text{M}$ glucose solution + 10 mL of phosphate buffered solution
15.63	10 mL from 31.25 $\mu\text{M}$ glucose solution + 10 mL of phosphate buffered solution
7.81	10 mL from 15.63 $\mu\text{M}$ glucose solution + 10 mL of phosphate buffered solution
3.91	10 mL from 7.81 $\mu\text{M}$ glucose solution + 10 mL of phosphate buffered solution
0	10 mL of phosphate buffered solution

## 5.2.5 Glucose sample preparation in gel format

As the samples from experiments involving- *in vivo* glucose extraction via RI were in gel format, a glucose concentration range was also prepared in gel format. This was achieved by mixing the 3% w/v methylcellulose gel with the previously prepared glucose solution samples (Section 5.2.4) in a ratio of 1 to 10. This provided glucose in gel concentration range of 900  $\mu\text{M}$ , 450  $\mu\text{M}$ , 225  $\mu\text{M}$ , 125  $\mu\text{M}$ , 112.5  $\mu\text{M}$ , 56.25  $\mu\text{M}$ , 28.125  $\mu\text{M}$ , 14.063  $\mu\text{M}$ , 7.031  $\mu\text{M}$ , 3.516  $\mu\text{M}$  and 0  $\mu\text{M}$ . The 1 to 10 ratio is in keeping with the dilution of the gel retrieved from human samples before assaying.

Table 5.2 Preparation of standard glucose gel samples

Required glucose gel sample concentrations [ $\mu\text{M}$ ]	Sample preparation for required glucose gel sample concentrations:
900	0.5 mL of gel + 4.5 mL of 1000 $\mu\text{M}$ glucose solution
450	0.5 mL of gel + 4.5 mL of 500 $\mu\text{M}$ glucose solution
225	0.5 mL of gel + 4.5 mL of 250 $\mu\text{M}$ glucose solution
112.5	0.5 mL of gel + 4.5 mL of 125 $\mu\text{M}$ glucose solution
56.25	0.5 mL of gel + 4.5 mL of 62.5 $\mu\text{M}$ glucose solution
28.13	0.5 mL of gel + 4.5 mL of 31.25 $\mu\text{M}$ glucose solution
14.06	0.5 mL of gel + 4.5 mL of 15.63 $\mu\text{M}$ glucose solution
7.03	0.5 mL of gel + 4.5 mL of 7.81 $\mu\text{M}$ glucose solution
3.52	0.5 mL of gel + 4.5 mL of 3.91 $\mu\text{M}$ glucose solution
0	0.5 mL of gel + 4.5 mL of phosphate buffer

## 5.2.6 Preparation of the buffer solution for the diffusion cell

A buffer solution with a pH of 7.4 was prepared for use in the diffusion cell to perform *in vitro* RI experiments. The buffer simulated the interstitial fluid in the human body. HEPES was used to maintain the physiological pH level of 7.4. In addition, the buffer consisted of the solutes (Arias, 2011) given in Table 5.3:

Table 5.3 Required quantities of solutes for making up 500 mL of the buffer solution

Solute	Desired concentration [mM]	Required quantity of solute [g]
Glucose	0/5/10/15/20	0/0.45/0.9/1.35/1.8
Potassium chloride (KCl)	4	0.298
Sodium chloride (NaCl)	133	7.77
HEPES	25	5.96



## 5.3 Glucose quantification method using glucose assay kits

Glucose calibration curves were established with the help of glucose assay kits. They were required to determine glucose concentrations from samples with unknown concentrations.

This section describes the principles of glucose detection and the protocols of two commercially available glucose assay kits which were used in this project, the GLUC-PAP GL2623 from Randox Laboratories and the GAHK20-1KT from Sigma Aldrich. Both glucose assay kits were tested and compared in terms of sensitivity and limit of detection to be able to fully analyse the gels collected after the RI experiments.

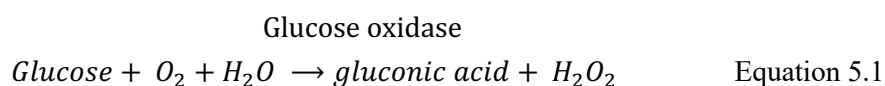
### 5.3.1 Randox Assay Kit

#### 5.3.1.1 Glucose Reagent Composition of Randox assay kit

- Phosphate Buffer: 50 mmol/l, pH 7.0
- MOPS Buffer: 50mmol/l, pH 7.0
- Phenol: 11 mmol/l
- 4-aminophenazone: 0.77 mmol/l
- Glucose oxidase:  $\geq 1.5$  kU/l
- Peroxidase:  $\geq 1.5$  kU/l

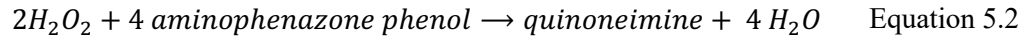
#### 5.3.1.2 Principles of glucose detection

*Glucose* gets oxidised in the presence of *glucose oxidase* (Equation 5.1). This reaction releases *gluconic acid* (which is also called gluconolactone) and *hydrogen peroxide*.



*Hydrogen peroxide* reacts with *4-aminophenazone* and *phenol*, whereby *peroxidase* acts as a catalyst. This reaction leads to the formation of the reddish *quinoneimine* dye. (Equation 5.2)

## Peroxidase



The increase of  $H_2O_2$  is directly proportional to the glucose amount and is ultimately identified by measuring the absorbance of the quinoneimine dye. The dye has a reddish colour, so the intensity of the dye indicates the glucose concentration in the sample (Randox Laboratories Limited, 2008).

### 5.3.1.3 Sample preparation with Randox assay kit

- 1) 80  $\mu$ L of the glucose sample were dispensed into a 96 well plate and 80  $\mu$ L of the glucose reagent were added to the glucose sample.
- 2) The 96 well- plate was put into Multiskan Ascent 96 Plate Reader and incubated for 90 minutes at a temperature of 36.9 °C.
- 3) The suggested wavelength for absorbance measurement from the Randox product information sheet was at 500 nm. Using the Multiskan Ascent 96 Plate Reader, the absorbance was measured at a wavelength of 492 nm, which was the closest option from the given wavelength range of the device to the suggested wavelength.
- 4) An example of the well plate layout can be seen in Figure 5.1. From each sample five replicates were made and then the average was taken.

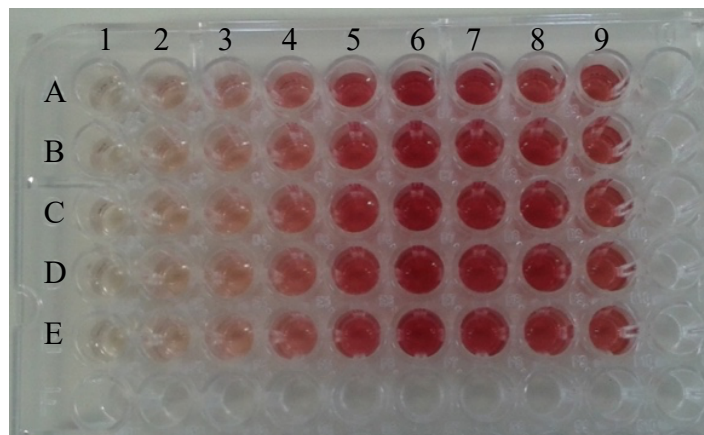


*Figure 5.1 Example of a well plate layout with glucose samples for establishing a calibration curve after the incubation of 90 minutes with the Randox reagent. Standard glucose samples with increasing concentrations were dispensed to columns 1 to 9 with five replicates for each concentration (rows A to E) Column 1 is filled with the Control*

#### 5.3.1.4 Establishment of the calibration curve

In order to establish the calibration curve, the absorbance values obtained via the plate reader were plotted against the glucose concentrations from the standard samples. A linear response was seen between a limited range of the standard glucose concentrations and the respective absorbance reading from the plate reader. Microsoft Office Excel 2017 was used to apply a straight-line fit on the dataset and to express the linear relationship in the form of the linear function equation by the method of least square fitting.

#### 5.3.1.5 Quantification of unknown glucose concentrations using the established calibration curve

To calculate the unknown glucose concentration, the linear function equation (Equation 4.6) was first rearranged to express  $x$  (Equation 5.3).

$$x = \frac{y}{k} - d \quad \text{Equation 5.3}$$

$x$ ...Unknown glucose concentration

$y$ ...Obtained absorbance value from the plate reader from the sample with the unknown glucose concentration

$k$ ...gradient of the linear equation obtained from the established calibration curve

$d$ ... slope of the linear equation obtained from the established calibration curve

Then, the obtained absorbance value of the unknown glucose concentration was inserted into the  $y$ -variable of the equation of the established calibration curve.

### 5.3.2 Sigma Aldrich Assay Kit

#### 5.3.2.1 Glucose Reagent Composition of Sigma Aldrich Glucose assay kit (Sigma Aldrich, 2004)

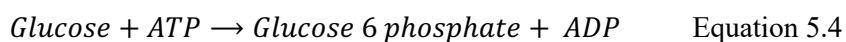
- Distilled H<sub>2</sub>O: 20 ml
- Nicotinamide adenine dinucleotide (NAD): 1.5 mM
- Adenosine triphosphate (ATP): 1.0 mM
- Hexokinase: 1.0 unit/ml
- Glucose-6-phosphate dehydrogenase (G6PDH): 1.0 unit/ml

- Sodium benzoate and potassium sorbate.

### 5.3.2.2 Principles of glucose detection

*Glucose* reacts with *ATP* in presence of *hexokinase* and forms *glucose-6-phosphate* (Equation 5.4).

Hexokinase



In the second step (Equation 5.5), *glucose-6-phosphate* is oxidised by *G6PDH* and *NAD* is reduced to *NADH*, which is ultimately measured and corresponds to the glucose concentration.

G6PDH



Sodium benzoate and potassium sorbate act as preservatives. (Sigma-Aldrich Inc., 2004)

### 5.3.2.3 Sample preparation with Sigma Aldrich assay kit

- To each of the glucose samples, 1 mL of the glucose reagent was added.
- Furthermore, a sample blank and a reagent blank were prepared.
- The sample blank consisted of 1 mL of deionised water and 100  $\mu\text{L}$  of the glucose gel sample.
- The reagent blank consisted of 1 mL of the glucose reagent and 100  $\mu\text{L}$  of the glucose gel sample.
- After 15 minutes of incubation, the absorbance was measured at a wavelength of 340 nm as given in the product information sheet.
- Five replicates were made to each sample.

### 5.3.2.4 Establishment of the calibration curve

In order to establish the calibration curve, the same approach as for the Randox assay kit was applied. The absorbance values obtained via the plate reader were plotted against the glucose concentrations from the standard samples. Microsoft Office Excel 2017 was used to apply a straight-line fit on the linear range of the standard glucose concentrations and the respective absorbance readings from the plate reader and the

linear relationship in the form of the linear function equation was expressed by the method of least square fitting.

#### 5.3.2.5 Quantification of unknown glucose concentration using the established calibration curve

To calculate the unknown glucose concentration, first the linear equation was rearranged to express  $x$ . By inserting the obtained absorbance value of the unknown glucose concentration into the equation of the established calibration curve, the unknown glucose concentration was calculated.

### 5.4 Investigation of glucose quantification method using the Genova Nano spectrophotometer (GNSPM)

Genova Nano from Jenway is a micro- volume spectrophotometer and has the ability to perform a variety of measurements such as standard spectroscopic measurements using only 2  $\mu\text{L}$  of sample volume per reading. In this project Genova Nano was used to evaluate the method of analysis for glucose quantification. The advantage of the Genova Nano is that it only requires a volume of 2  $\mu\text{L}$  per measurement; whereas most of the standard measurement techniques such as plate reader needs at least 80  $\mu\text{L}$  for glucose quantification. In case of clinical studies only limited amount of patient samples are available. So, more dilutions would be needed to run a colorimetric assay which lead to errors and imprecisions in concentration calculations.

To assess the suitability of the Genova Nano for glucose quantification, a calibration curve was established with glucose assay kit from Randox Laboratories to identify the lower limit of detection. The Randox assay kit was used as it showed better suitability for the required concentration range (see Section 6.1). For comparison purposes measurements were also done with a commonly used microplate reader.

Glucose gel samples were prepared in a 1 to 10 ratio with glucose samples as explained in Section 5.2.3 in the following glucose concentrations 900  $\mu\text{M}$ , 450  $\mu\text{M}$ , 225  $\mu\text{M}$ , 112.5  $\mu\text{M}$ , 56.25  $\mu\text{M}$ , 28.125  $\mu\text{M}$ , 14.063  $\mu\text{M}$ , 7.031  $\mu\text{M}$ , 3.516  $\mu\text{M}$  and 0  $\mu\text{M}$ .

Following procedure was followed:

80  $\mu\text{L}$  of the glucose gel samples were dispensed into the 96 well plates and 80  $\mu\text{L}$  of the glucose reagent from Randox were added to the glucose gel sample. After incubating that mixture for 90 minutes at a temperature of 36.9  $^{\circ}\text{C}$ , the glucose gel samples were ready to undergo the absorbance readings.

To measure the absorbance using the plate reader, measurements were taken at a wavelength of 492 nm.

With the Genova Nano, it was possible to select any wavelength of choice to perform the absorbance readings. Therefore, measurements were performed in the Photometrics measurement mode at the wavelength of 500 nm as it was suggested from the Randox product information sheet.

First, 2  $\mu\text{L}$  of the gel sample with 0  $\mu\text{M}$  glucose concentration with the Randox reagent was put onto the read head of the Genova Nano and calibration was performed at a wavelength of 500 nm. This step is needed for calibration of the device and the absorbance of the blank solution will be automatically deducted from the sample absorbance. Once the calibration was done, different glucose sample with increasing concentrations in presence with the Randox enzyme were measured. After each concentration, the read head was cleaned properly with a cloth to prevent any cross-contamination.

Two calibration curves were established, one from the standard measurements using the Multiskan Ascent 96 Plate Reader and one from using the Genova Nano. The results of the calibration curve showed that the absorbance values for the chosen glucose gel sample range were too low to be detected by the Genova Nano. Low absorbance values are caused by low glucose concentrations in the sample itself. Therefore, different dilution factors were analysed to see if it improves the results. Following gel to glucose solution ratios were tested: 1 to 6, 1 to 5 and 1 to 4. The standard glucose concentration range for each ratio can be seen in Table 5.4.

Table 5.4 Standard glucose concentration range for different gel to glucose solution ratios

<b>Standard glucose concentrations from samples with gel to glucose solution ratio of 1 to 10 [<math>\mu\text{M}</math>]</b>	<b>Standard glucose concentrations from samples with gel to glucose solution ratio of 1 to 6 [<math>\mu\text{M}</math>]</b>	<b>Standard glucose concentrations from samples with gel to glucose solution ratio of 1 to 5 [<math>\mu\text{M}</math>]</b>	<b>Standard glucose concentrations from samples with gel to glucose solution ratio of 1 to 4 [<math>\mu\text{M}</math>]</b>
1800.00	1666.67	1600.00	1500.00
900.00	833.33	800.00	750.00
450.00	416.67	400.00	375.00
225.00	208.33	200.00	187.50
112.50	104.17	100.00	93.75
56.25	52.08	50.00	46.88
28.13	26.04	25.00	23.44
14.06	13.02	12.50	11.72
7.03	6.51	6.25	5.86
3.52	3.26	3.13	2.93
1.76	1.63	1.56	1.46
0.00	0.00	0.00	0.00

Absorbance readings were taken with the Genova Nano and the plate reader for all three dilution factors. It was shown that the calibration curve obtained with a gel to glucose sample ratio of 1 to 4 had the lowest limit of detection. The acquired calibration curve was then further evaluated by experimentally identifying the glucose concentrations of two samples with known concentrations. Therefore, two glucose gel samples with known concentrations (204  $\mu\text{M}$  and 408  $\mu\text{M}$ ) were prepared and quantified using the calibration curve acquired using the Genova Nano and the plate reader. The focus of the experiment was to evaluate the accuracy of the glucose quantification method using the GNSPM with using a sample volume of only 2  $\mu\text{L}$ . Therefore, two concentrations were selected, which lie well in the linear range of the calibration curve.

## 5.5 Fabrication of screen-printed electrodes

Screen printed electrodes were used to perform RI experiments because of their low fabrication cost and fast production of a large number of electrodes.

Screen printing is a type of printing which is used in diverse applications such as for T- shirt and posters but it can be also used for biosensors. Screen-printed biosensors have been used in a variety of fields such as medicine, pharmaceuticals or the environment (Cooper & Cass, 2004) .

### 5.5.1 Electrode design

Two electrode designs were used in this project.

#### 1) Potassium electrodes

The electrode design shown in Figure 5.2 was developed by the Medical Devices Group in the Biomedical Engineering Department for a different research project in the field of RI. The RI electrode (indicated with the arrow) was used in this project to apply the iontophoretic current during RI experiments. As discussed in Section 2.9.2, for RI electrode, it is recommended to use non-polarisable electrodes (Ching, 2005). Ag/AgCl electrodes, which are biocompatible, have the ability to deliver high amounts of current without causing any pH changes in the buffer solution in the diffusion cell (Jahn, 1900). Therefore, the RI electrode was made of Ag/AgCl ink and it has a surface area of 0.82 cm<sup>2</sup>. Basic RI experiments were conducted with this type of electrode. Glucose quantification from RI samples obtained with this type of electrodes, was performed using laboratory assay kits.

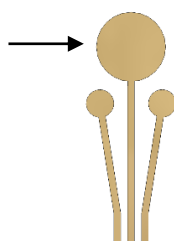


*Figure 5.2 Potassium electrode design*

#### 2) Three electrode system with iontophoresis electrode

The electrode design shown Figure 5.3 was developed by Medical Devices group in the Biomedical Engineering Department at the University of Strathclyde. A three-



electrode arrangement was integrated to the iontophoresis electrode to allow direct and rapid glucose quantification in the gel electrode instead of using laboratory glucose kits. The fabrication of the mediated glucose sensor is described in Section 5.9.

The principle of a three-electrode system is explained in Section 4.3.3. The working and counter electrode are usually made of an inert material, in this project it consists of carbon. The reference electrode is made of Ag/AgCl ink.

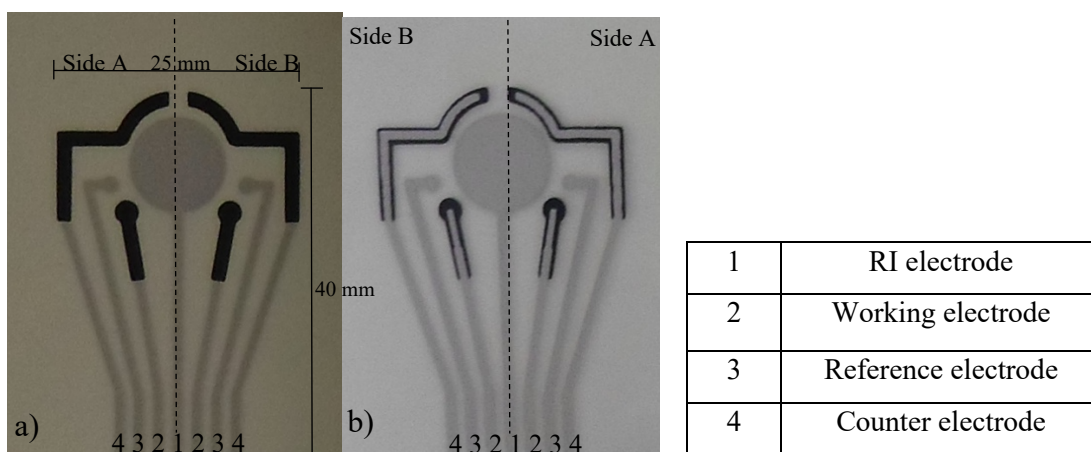


Figure 5.3 Electrode with three electrode arrangement and iontophoresis electrode a) Front view b) Back view

Table 5.5 Electrode area of the final device exposed to the test solution

Electrode	Surface area of electrode [cm <sup>2</sup> ]
RI electrode	0.82
Working electrode	0.12
Reference electrode	0.017
Counter electrode	0.16

### 5.5.2 Preparation of well in electrode to contain skin contact gel

For the gel or test solution to stay on the electrode, an electrode well was required. The well was made of 1 mm thick Polytetrafluoroethylene (PTFE) sheets. Double sided tape was applied on both sides of the PTFE sheets with the dimension of 21 x 0.1 x 29.7 cm. The sheets were then cut to strips with a dimension of 21 x 0.1 x 2.5 cm. Using a hand punch press, a 20 mm diameter hole was made on the PTFE strip. Sufficient space had to be kept between the holes to ensure adequate amount of tape around each well. One side of the double-sided tape permitted the well

to be attached to the electrode and the other side of the double-sided tape enabled the adhesion of the electrode onto the artificial membrane for the RI experiments. An example of the final device can be seen in Figure 5.4.

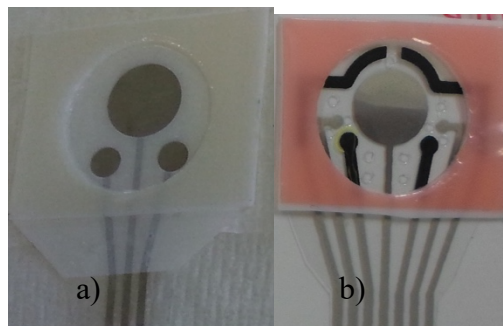


Figure 5.4 a) Potassium electrode design with electrode well b) Three-electrode design with iontophoresis electrode with well

### 5.5.3 Procedure for screen printing electrodes:

- 1) First a “Positive” design was produced. The electrode design consisted of 2 layers, the first layer was printed with Ag/AgCl ink (Figure 5.5a) and the second layer with carbon ink (Figure 5.5b). The “Positive” design was produced by printing each layer on separate acetate sheets.

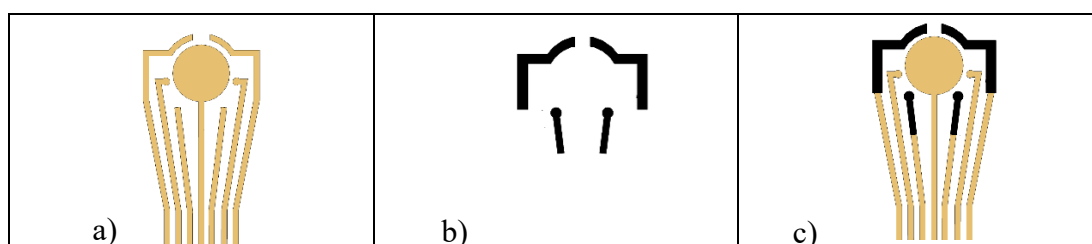


Figure 5.5 Electrode design for three electrode system with iontophoresis electrode. a) Ag/AgCl ink design for the first layer b) Carbon ink design for second layer c) The final electrode design.

- 2) The next step was to transfer the electrode design onto the mask, which was used to print the electrodes ultimately. The mask, which is also called the screen, consists of a mesh with either a plastic or a metallic frame. The mask with a metal frame was purchased from MCI and it was already covered with a light sensitive emulsion on both sides.
- 3) Using a sheet of glass, the positive design was secured onto the mask and left in the DEK exposure unit for UV light exposure for 20 minutes. The UV light reacted with the emulsion on the mask respectively did not react with the part

of the mask which was covered with the positive design. Through the reaction with the UV light, the emulsion solidified and became water insoluble; however, the protected part stayed water soluble.

- 4) After the 20 minutes of UV exposure, a hose with high pressure was used to wash out the emulsion on the mask which was water soluble which then left us with the desired pattern (Figure 5.6). The mask was left to dry overnight. Two separate screens were produced, one for the Ag/AgCl layer and one for the carbon layer.

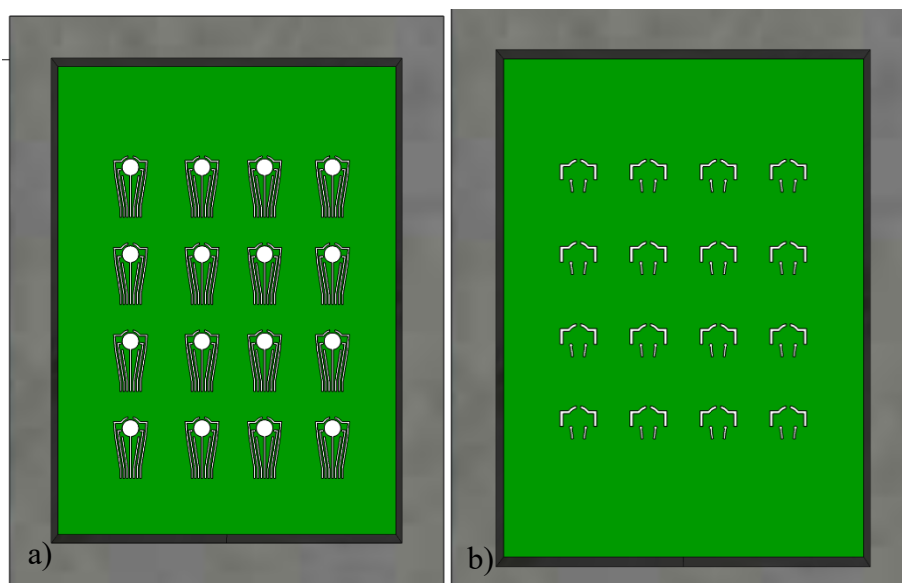


Figure 5.6 Screen mask for the a) Ag/AgCl ink printing and b) Carbon ink printing

- 5) Once both masks were ready, the electrodes were ready to be printed on the substrate. Acetate sheets were chosen as the substrate material.
- 6) The recommended curing time for both inks was at 120°C for 15 minutes.
- 7) As acetate sheets shrink at high temperatures, all the acetate sheets had to be pre- heated at a temperature of 120°C for 15 minutes. The pre-heating prevented the shrinking once the electrodes were printed.
- 8) With the use of a squeegee, first the Ag/AgCl ink was deposited through the holes in the masks onto the substrate. Figure 5.7 shows a schematic side view of a screen-printing unit.

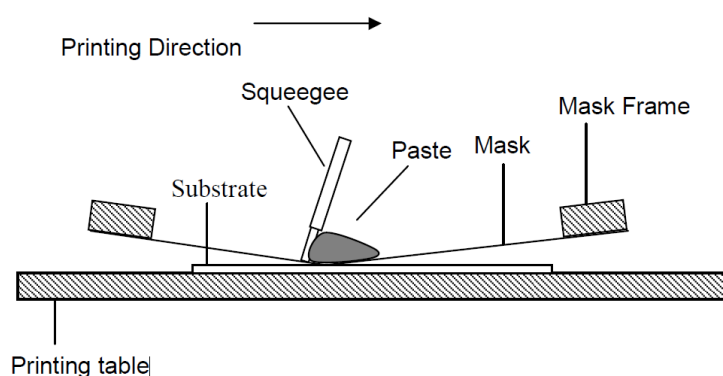


Figure 5.7 Screen printing unit (adapted from Cooper & Cass 2004)

- 9) The sheets were then cured at 120°C for 15 minutes. The curing process was required to get rid of the solvents, which were present in the Ag/AgCl ink.
- 10) The carbon printing was done once the Ag/AgCl ink was cured. Therefore, the carbon mask was used and the carbon design was printed on the previously produced Ag/AgCl printed sheets. The carbon layer was carefully aligned with the Ag/AgCl layer. It was made sure that the Ag/AgCl tracks were within the carbon layer.

The masks with the electrode design were made by a member of the Medical Devices group in the Biomedical Engineering Department at the University of Strathclyde. The printing of the electrodes was conducted by the team member and the author of this thesis.

## 5.6 *In vitro* transdermal extraction via RI

RI is a process which enables transdermal extraction of molecules by applying low current to the skin. With the help of A) a diffusion cell, B) a portable electrochemical analyser and C) the electrodes fabricated as explained in Section 5.5, *in vitro* experiments were performed to study the flux of glucose molecules during RI. The diffusion cell as well as the portable electrochemical analyser were both designed and constructed in the Biomedical Engineering Department at the University of Strathclyde.

### A) Diffusion cell

With the help of Franz cells, *in vitro* skin permeation assays can be performed. Franz cells comprise of two chambers which are separated by a membrane. The product to

be tested is placed in the top chamber and the bottom chamber consists of a fluid from where samples are taken in a fixed interval and tested if the test product has gone through the membrane (Franz, 1975). A modified Franz diffusion cell was built for RI experiments. The diffusion cell used in the laboratory was based on the Franz cells concept but was a design created at Strathclyde to allow practical connection of side by side electrode to form an iontophoresis model skin system (Connolly et al., 2002). This model system allows the characteristics of electrodes and sensors to be studied and optimised prior to human volunteer experiments. The diffusion cell (Figure 5.8) consisted of a chamber, two silicone gaskets and a top frame. The chamber and the top frame were made of Polymethylmethacrylate (PMMA). The artificial membrane, which mimicked the stratum corneum, was placed between the two gaskets. This whole cell was held together by the two aluminium side clamps, which was tightened by four stainless steel screws on each clamps. The buffer in the chamber, which simulated the interstitial fluid in the human body, was filled through the holes on both sides of the chamber using a syringe. The holes were capped with PTFE screw caps once the chamber was fully filled.

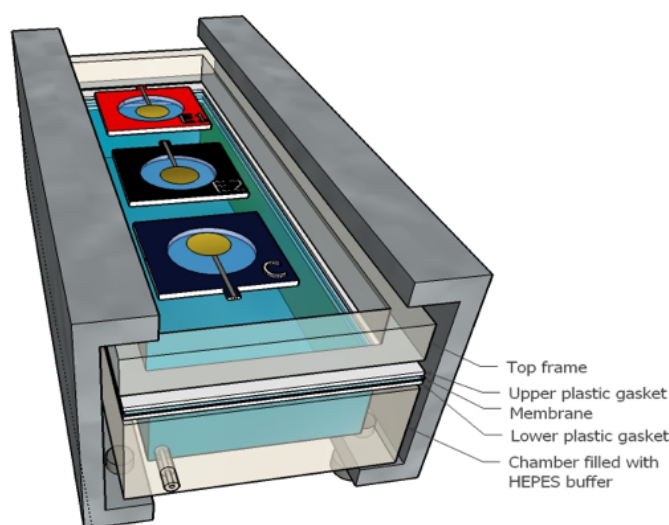


*Figure 5.8 Filled diffusion cell with electrodes attached*

### B) Electrochemical analyser

The portable electrochemical analyser, developed and programmed in “C” at Strathclyde (Ching et al., 2004), was used as a constant current source to perform

iontophoresis experiments (Figure 5.9a). It can provide an iontophoretic current up to 600  $\mu\text{M}$  in various signal waveforms. Furthermore, it has the ability to perform electroanalytic techniques such as amperometric and potentiometric measurements and it can also take cyclic voltammetry measurements in the voltage range from -1000 mV to 1000 mV and scan rate range from 1 mV/s to 100 mV/s. The desired tasks for the analyser were written in the “program sequence file” and saved on an external sd-card, which was then inserted into the device. A sample programme is given in Appendix A. The device was connected to the electrodes with a 12 pin ribbon cable, which had an Insulation- Displacement Contact (IDC) ribbon cable connector on one side and a 12 pin Flexible Flat Cable (FFC) connector on the other end (Figure 5.9b). The FFC connector was connected to the electrode and the IDC ribbon cable connector was connected to the portable electrochemical analyser. The pin configuration of the male IDC ribbon cable connector of the portable electrochemical analyser can be seen in Table 5.6. When connecting the electrode to the cable, it had to be made sure that the electrode is connected to the correct pin.

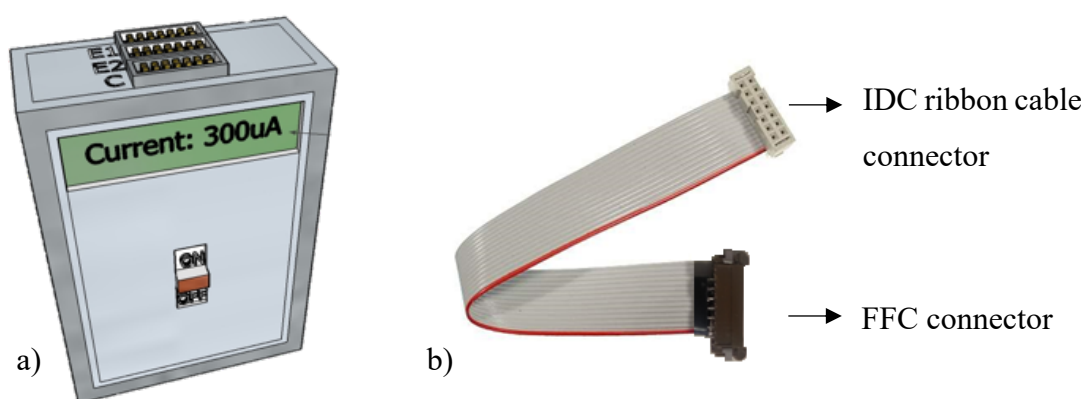


Figure 5.9 a) Portable electrochemical analyser and b) Cable which was used to connect the portable electrochemical analyser with electrodes (adapted from (Marco Specialities, 2017))

Table 5.6 Pin configuration of the male IDC ribbon cable connector of the portable electrochemical analyser

Pin	Side A of the electrode with the three-electrode arrangement	Pin		Pin	Side B of the electrode with the three-electrode arrangement
2	Working electrode	7	Iontophoresis electrode	8	Working electrode
4	Reference electrode			10	Reference electrode
6	Counter electrode			12	Counter electrode

Procedure to perform *in vitro* RI experiments using the diffusion cell:

1. The artificial membrane, which mimicked the human skin was prepared according to its protocol (see Section 5.7) and placed in-between the two gaskets of the diffusion cell.
2. The diffusion cell was then filled with HEPES buffer, which simulates the interstitial fluid, using a syringe (Figure 5.10a). Once the chamber was fully filled, the holes were capped with PTFE screw caps (Figure 5.10b).



Figure 5.10 a) Diffusion cell with syringe to fill the buffer solution b) diffusion cell with closed holes using PTFE caps

3. In the next step, the electrodes were prepared to be placed onto the diffusion cell. As discussed in Section 4.4, three electrodes were used for each RI experiment (two iontophoresis electrodes and one control electrode). Two iontophoresis electrodes (E1 and E2) were required to apply the iontophoretic current across the skin and to complete a circuit. The control electrode was needed to measure passive diffusion.

- a. First, the electrodes were connected via the cable shown in Figure 5.9b to the portable electrochemical device. Pin 7 was wired to the iontophoresis electrode; when connecting the cable to the electrode, the connection was ensured using a multimeter before starting the experiment.
  - b. 300  $\mu\text{L}$  of gel was applied onto each of the electrodes for electrical conductance using a gel pipette.
  - c. First the control electrode was mounted onto the artificial skin, then the E2 electrode and finally the E1 electrode (Figure 5.11).
4. The applied iontophoretic current of  $100 \mu\text{A}/\text{cm}^2$  was regulated and applied by the portable electrochemical analyser onto the iontophoresis electrodes. A current flow is created between the iontophoresis electrodes by the application of current.
5. The positive molecules, such as sodium and potassium, moved to the cathode and the negatively charged molecules, such as chloride, to the anode. This method also produces a solvent flow in the negatively charged pores of the membrane (similar to human skin). The approximate solvent flow rate has been estimated as  $8.5 \pm 3.2 \mu\text{L}/\text{h}$  (Sieg et al., 2004b). Glucose and other uncharged particles were carried along according to the solvent flow to the gel chamber.



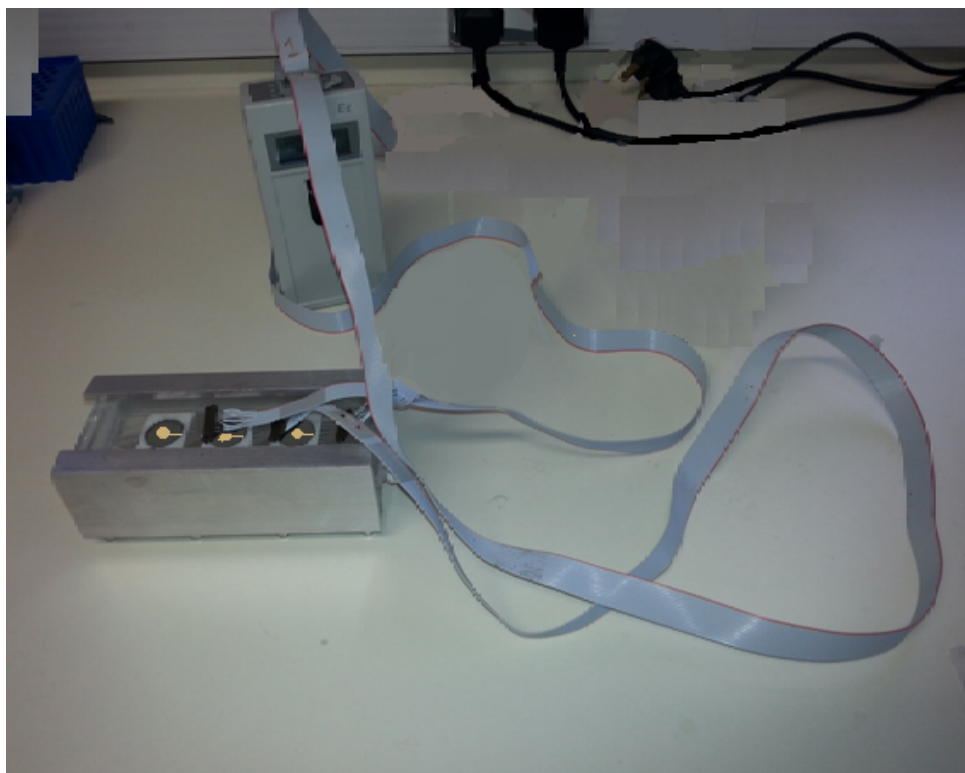


Figure 5.11 Experimental setup to perform *in vitro* transdermal extraction via RI using a diffusion cell and the portable electrochemical analyser

6. After the measurement cycle, the applied gel was collected from the gel chambers into an Eppendorf tube and weighted out using a scale. The sample was then diluted one in ten with 0.1 M phosphate buffered solution (pH 7.4) and was ready for analysis. The amount of glucose was quantified with a colorimetric assay using the Randox assay kit as it was shown that it more suitable for the required glucose concentration range (see Section 6.1.).
7. The extracted glucose concentration from the application of RI was calculated using the equation of the standard calibration curve. The calculated glucose concentration was then multiplied by the factor of 10 as the sample was first diluted by that factor.

Following *in vitro* RI experiments were conducted to study the glucose flux across an artificial membrane:

1) Variation of the glucose concentration in the buffer solution:

RI experiments were performed with the standard artificial membrane, the Spectrapore membrane and the potassium electrodes. Glucose flux was studied with two glucose

concentration (5 mM and 20 mM) in the buffer solution and with the application of RI for 60 minutes with switching polarities every 15 minutes. A glucose concentration of 5 mM was chosen as it mimics concentrations obtained from the healthy individuals in the fasted state (Arias, 2011). In addition, the glucose flux of a 20 mM glucose buffer solution was tested as it mimics the concentration obtained after a high-glucose drink from healthy individuals. Table 5.7 shows an overview of the testing conditions used in this experiment.

*Table 5.7 Overview of testing conditions of 1) Variation of the glucose concentration in the buffer solution*

<b>Glucose concentration in buffer solution</b>	<b>Duration of RI</b>	<b>Type of membrane used</b>
5 mM	60 minutes with switching polarities every 15 minutes	Spectrapore membrane
20 mM	60 minutes with switching polarities every 15 minutes	Spectrapore membrane

## 2) Changing the duration of RI

RI experiments were also carried out with varying the duration of RI and with keeping the glucose concentration in the diffusion cell constant at 5 mM. The Spectrapore membrane and the potassium electrodes were used in this experiment. As discussed in Section 2.9.2, when applying RI for 60 minutes with switching polarities, acceptable levels of glucose can be extracted. For research and comparison purposes, RI was also applied for 15 minutes with direct current and 30 minutes with direct current. Table 5.8 shows an overview of the testing conditions used in this experiment.

*Table 5.8 Overview of testing conditions of 2) Changing the duration of RI*

<b>Glucose concentration in buffer solution</b>	<b>Duration of RI</b>	<b>Type of membrane used</b>
5 mM	15 minutes of direct current	Spectrapore membrane
5 mM	30 minutes of direct current	Spectrapore membrane
5 mM	60 minutes with switching polarities every 15 minutes	Spectrapore membrane

## 5.7 Comparison of two artificial membranes in terms of glucose flux

The flux of glucose molecules within iontophoresis devices across two artificial membranes with respect to time, selected to mimic human skin in the RI model system, was studied and compared in order to improve the current *in vitro* RI measurement setup. Following two commercially available membranes were investigated in: The standard artificial membrane, Spectrapore membrane from Spectrum Laboratories with the Vitro-Skin from IMS Inc.

### Spectrapore membrane:

The Spectrapore membrane from Spectrum Laboratories Inc. is a cellulose ester membrane and has a molecular weight cut-off of 100-500 Da. It is mainly used in dialysis tubings. It is hydrophilic and has a symmetric porosity. Symmetric porous membranes have a highly voided structure and are rigid. The highly voided structure further has randomly interconnected and distributed pores (Abdullah et al., 2018).

### Preparation of Spectrapore membrane:

The Spectrapore membrane had to be preserved in a 0.05 % sodium azide solution at 4 °C. Therefore, 0.150 g of sodium azide was dissolved in 300 ml of distilled water. Before use in RI experiments, the dialysis membrane was cut out into the right size for the diffusion cell and placed in a beaker of dH<sub>2</sub>O for 15 minutes to get rid of any sodium azide residues. After the 15 minutes both sides were thoroughly rinsed in running dH<sub>2</sub>O before using it for the diffusion cell.

### Vitro-Skin®:

The Vitro-Skin® from IMS Inc. is a synthetic membrane; and it contains optimized protein and lipid components (Carnali et al., 2012). It has been used in a wide range of *in vitro* experiments, leading from measuring the SPF and UVA protection factors to evaluating the performances of adhesive bandages. It mimics the surface properties of the human skin effectively with regards to the topography, pH, critical surface tension and ionic strength.

### Preparation of Vitro-Skin:

Prior to use, the Vitro-Skin had to be hydrated using a hydration chamber. The solution for the hydration chamber was made up by 298 g of dH<sub>2</sub>O and 52 g of glycerin. The 15% glycerin/ 85% water mix provided an ideal humid environment for the Vitro Skin. An airtight container with racks inside was used as a hydration chamber. The solution was poured at the bottom of the chamber. The Vitro skin was cut out to the appropriate size for the diffusion cell before carefully placing them onto the racks in the hydration chamber. The Vitro skin had to be kept in the hydration chamber for at least 16 but up to 24 hours at the maximum. After the hydration process, the Vitro skin had to be carefully removed from the rack without getting in contact with the solution itself. Afterwards they were ready to be used for the iontophoresis experiments.

RI experiments were performed with each of the membrane as explained in section 5.6. The potassium electrodes were used for this experiment and HEPES buffer with a glucose concentration of 20 mM was prepared. A 60-minute measurement cycle was carried out with switching polarities every 15 minutes. The extracted glucose was then diluted and quantified using the Randox assay kit. Results from the Spectropore membrane were then compared with the results from the Vitro-Skin. Table 5.9 shows an overview of the testing conditions used in this experiment.

*Table 5.9 Overview of testing conditions of 5.7 Comparison of two artificial membranes in terms of glucose flux*

<b>Glucose concentration in buffer solution</b>	<b>Duration of RI</b>	<b>Type of membrane used</b>
20 mM	60 minutes with switching polarities every 15 minutes	Spectrapore membrane
20 mM	60 minutes with switching polarities every 15 minutes	Vitro-Skin

## 5.8 Activated carbon experiments

Activated carbon (AC) has the ability to adsorb organic compounds (Marsh & Rodriguez-Reinoso, 2006). In this study the use of AC to control flux of glucose in wearable devices was to be explored in accordance with the IP owned by Strathclyde for such a device (Connolly, 2014). The ways of controlling glucose in previous RI

devices were explained in Section 2.8.2. The new method to be studied here is reagentless and does not generate secondary chemicals. The theory of diffusion and glucose flux was explored in Section 4.4.3.

To explore the AC adsorption concept, preliminary experiments were performed to test glucose adsorption onto AC pellets. AC pellets were used due to its fast availability. Later on, glucose adsorption was tested using AC foam and in a sensor format.

#### Types of AC used:

Two forms of AC were used in this study, AC pellets and AC foam (Figure 5.12). Both types of AC, which were used in this project, are publicly available for every-day use purposes. The AC pellets, which were used in this project, are intended for the removal of any contaminants in aquariums. And the AC foam is intended for odour removal in compost caddies. Therefore, more detailed information such as the exact composition, any coatings, the base material of the AC, the surface charge, the polarity of the adsorbent, the pore size, the surface area or the pore structure was not given by the manufacturer.

The AC pellets had the same diameter of 0.2 cm but different lengths ranging from 0.3 cm to 0.7 cm. The AC foam came in form of sheets with a dimension of 8.9 x 0.1 x 8.9 cm. In order to suit the planned adsorption experiments, the AC foam was cut out using a paper hole punch providing us with disc-shaped AC foams with a diameter of 0.6 cm and a thickness of 0.1 cm (Figure 5.12c).

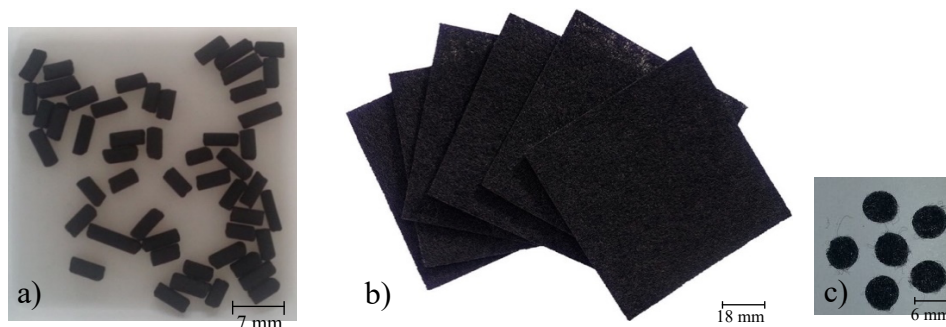


Figure 5.12 a) AC pellets b) Sheets of AC foam c) Disc-shaped AC foams

### 5.8.1 Preparation of AC for glucose adsorption experiments

AC needed to be washed with distilled water prior to use. It was observable that loose, blackened residues in powder form were coming off from AC pellets as well as the

AC foam. Therefore, the washing ensured no impurities in the test solutions due to the AC itself.

The AC was placed in a beaker filled with distilled water and placed on a magnetic stirrer for 4 hours with exchanging water for three times (Sun, 2013). The pellets of AC were dried overnight at room temperature on a blue roll paper towel in a clean container before they were used for the experiment. The same procedure was followed for the disc-shaped AC foam.

### 5.8.2 Preliminary glucose adsorption experiments to AC Pellets

In order to test glucose adsorption onto AC pellets, the experimental procedure shown in Figure 5.13 was followed:

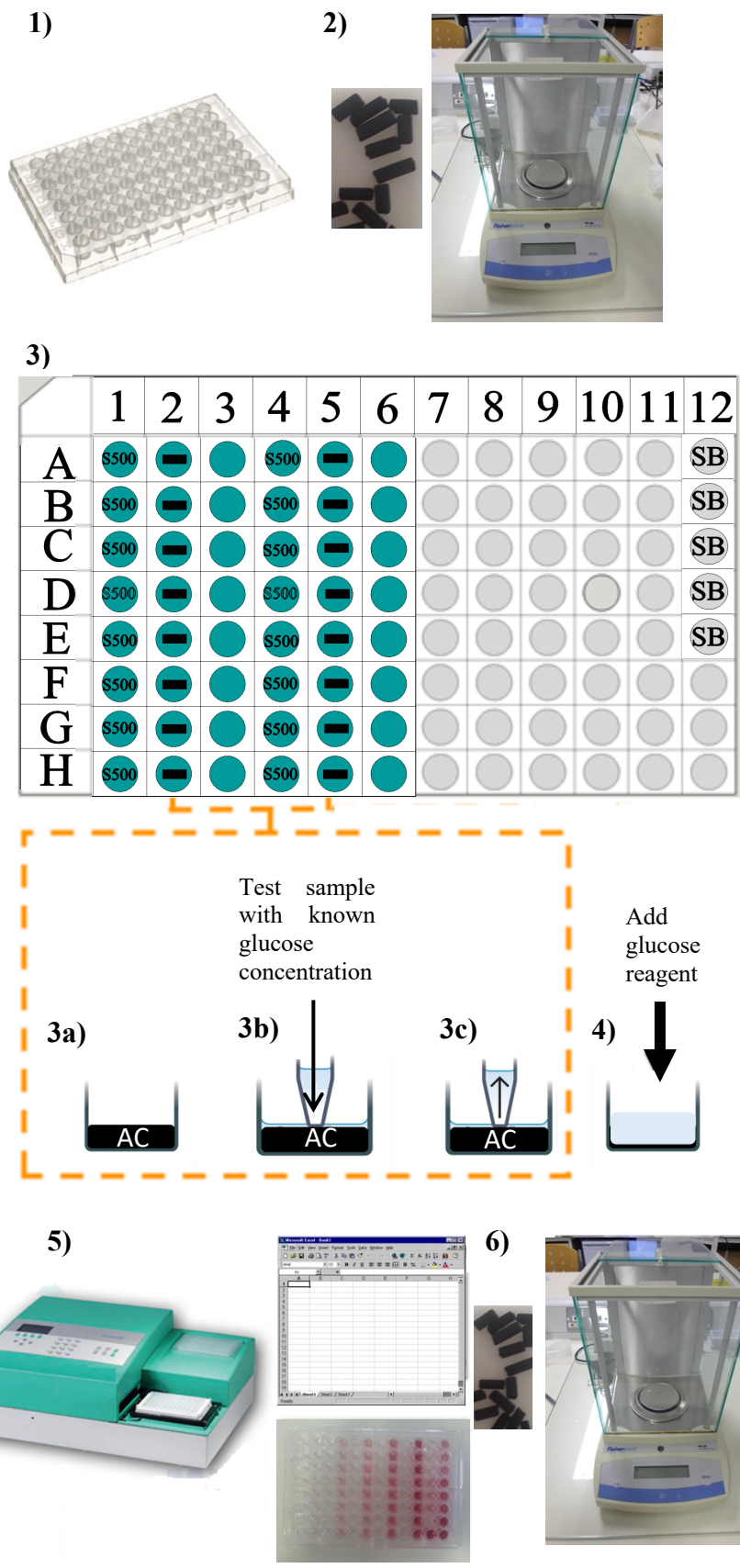


Figure 5.13 Experimental setup for preliminary glucose adsorption experiments to AC pellets

1. Ninety-six well plates were used to test glucose adsorption to AC.
2. As each pellet was different in form, each one was weighed out to get an understanding of how much AC one was dealing with.
3. In the next step, an example of the well plate arrangement can be seen.
  - 3a. First, one piece of an AC pellet was placed in the wells of Columns 2 and 5 of the ninety-six well plate (black rectangular shaped objects). 100  $\mu\text{L}$  of a 500  $\mu\text{M}$  glucose solution was added to the wells with AC pellets (Columns 2 and 5).
  - 3b. Next, 100  $\mu\text{L}$  of a standard test solution with known glucose concentrations (S500 – a 500  $\mu\text{M}$  glucose solution) were added to the wells without AC pellets (Columns 1 and 4).
  - 3c. After an incubation time of one hour, the remaining solution in the wells (which were incubated with AC pellets) was removed from the initial well and dispensed into the adjacent well (Columns 3 and 6). The incubation time of one hour was selected from existing literature (Sun, 2013). The sample volume had decreased to approximately 75  $\mu\text{L}$ . The volume left was estimated using gradual pipetting. First the pipette was set to a volume well below the expected volume. The volume was then gradually increased until all the liquid was drawn up.
4. The glucose in the test samples was quantified using a colorimetric assay with a glucose enzyme assay kit (GLUC-PAP, Randox). Therefore, the glucose reagent was added in a 1 to 1 ratio to the sample volume of the test solutions.
5. Then, the 96- well plate was put into Multiskan Ascent 96 Plate reader and after 90 minutes of incubation time at a temperature of 36.9  $^{\circ}\text{C}$  the absorbance was measured at a wavelength of 492 nm. The remaining glucose was quantified by inserting the obtained absorbance value of the unknown glucose concentration into the equation of the established calibration curve.
6. The weight of the AC pellet was also measured after the incubation with the test solution.

The results from the preliminary AC experiments showed that glucose adsorption had taken place (see Section 6.4.1). But the pellets, which were used in the experiments,



were manufactured for removal of contaminants in aquariums and they lacked in uniformity. Hence, the quality of the pellet was not suitable for actual research purpose, Therefore, AC foam was suggested as an alternative to be used for this research purpose.

### 5.8.3 Glucose adsorption experiments to AC foam

Ninety-six well plates were also used to test glucose adsorption with AC foam. The size of the cut-out disc-shaped AC foam was ideal to be used with the well plate. The cut-out AC foam were washed as explained in Section 5.8.1 and then used for glucose adsorption testing.

The same procedure as explained in 5.8.2 was applied for AC foam. But instead of one piece of AC pellet, one disc-shaped AC foam was placed in the well. One disc-shaped AC foam is referred to as one unit of AC foam.

More experiments were conducted using AC foam to better understand the glucose adsorption behaviour to AC:

#### A) Testing glucose adsorption from glucose solution samples to one unit of AC foam

In order to test glucose adsorption from glucose solution sample to one unit of AC foam, each foam was weight out and placed into a well before dispensing the glucose solution into the well. Following initial glucose concentrations were tested with AC foam: 1000  $\mu\text{M}$ , 500  $\mu\text{M}$ , 250  $\mu\text{M}$ , 125  $\mu\text{M}$ , 62.5  $\mu\text{M}$ , 31.25  $\mu\text{M}$ , 15.625  $\mu\text{M}$ , 7.8125  $\mu\text{M}$ , 3.906  $\mu\text{M}$  and 0  $\mu\text{M}$ . After an incubation time of one hour with the AC foam, the remaining glucose was quantified by adding the glucose reagent in a ratio of 1 to 1 to the sample volume and running a colorimetric assay using the GLUC-PAP from Randox.

#### B) Testing glucose adsorption from glucose solution samples to two units of AC foam

Glucose adsorption from glucose solution samples to two units of AC foam was performed by first putting one piece of AC foam at the bottom of each well, then adding the solution, and then placing another piece of AC foam on the top of the

solution. Following initial glucose concentrations were tested with AC foam: 1000  $\mu\text{M}$ , 500  $\mu\text{M}$ , 250  $\mu\text{M}$ , 125  $\mu\text{M}$ , 62.5  $\mu\text{M}$ , 31.25  $\mu\text{M}$ , 15.625  $\mu\text{M}$ , 7.8125  $\mu\text{M}$ , 3.906  $\mu\text{M}$  and 0  $\mu\text{M}$ . The total incubation time was chosen as one hour. After an incubation time of 30 minutes, the top AC foam was pushed down, so that the top side of the AC foam also got in contact with the glucose solution.

C) Testing glucose adsorption from glucose gel samples to one unit of AC foam

As the samples from experiments involving- *in vivo* glucose extraction via RI were in gel format, glucose adsorption to AC foam was also tested from gel samples. Therefore, the same procedure as for the glucose adsorption experiments with the glucose solutions was performed but with standard glucose gel samples prepared as explained in Section 5.2.5 . Following initial glucose concentrations were tested with AC foam: 900  $\mu\text{M}$ , 450  $\mu\text{M}$ , 225  $\mu\text{M}$ , 125  $\mu\text{M}$ , 112.5  $\mu\text{M}$ , 56.25  $\mu\text{M}$ , 28.125  $\mu\text{M}$ , 14.063  $\mu\text{M}$ , 7.031  $\mu\text{M}$ , 3.516  $\mu\text{M}$  and 0  $\mu\text{M}$ . After an incubation time of one hour with the AC foam, the remaining glucose was quantified by adding the glucose reagent in a ratio of 1 to 1 to the sample volume and running a colorimetric assay using the GLUC-PAP from Randox.

D) Diffusion rate of glucose in solution and gel into AC foam

In order to explore and compare the glucose diffusion time profile in solution and in the gel environment into the AC foam, experiments were carried out using a well plate. The 1000  $\mu\text{M}$  glucose solution sample and the 900  $\mu\text{M}$  glucose gel sample were chosen to study the adsorption profile over time. Therefore, the test sample was incubated with AC foam and measurements were taken every 10 minutes up to 80 minutes of incubation time.

	1	2	3	4	5	6	7	8	9	10	11	12
A	10	10	30	30	50	50	70	70				SB
B	10	10	30	30	50	50	70	70				SB
C	10	10	30	30	50	50	70	70				SB
D	10	10	30	30	50	50	70	70				S1000
E	20	20	40	40	60	60	80	80				S1000
F	20	20	40	40	60	60	80	80				S1000
G	20	20	40	40	60	60	80	80				
H	20	20	40	40	60	60	80	80				

Figure 5.14 Well- plate arrangement to measure the glucose diffusion time profile

Following procedure was followed to study the glucose adsorption profile of the 1000  $\mu$ M glucose solution sample:

1. Columns 1, 3, 5, and 7 were filled with one unit of AC foam.
2. 100  $\mu$ L of a 1000  $\mu$ M glucose concentration solution was added to the wells which were filled with AC foam. The numbers in the wells in Columns 1, 2, 3, 4, 5, 6, 7 and 8 indicate the incubation time in minutes.
3. After the incubation time, the solutions were removed into the adjacent well (Columns 2, 4, 6 and 8). For example, well 1A and 2A have the number “10” written on them. This means that the solution in 1A was incubated with AC foam for 10 minutes before removing the solution to 2A.
4. It was observable that the longer the incubation time, the less sample volume was left to dispense into the adjacent well. The volume left was estimated using gradual pipetting. First the pipette was set to a volume well below the expected volume. The volume was then gradually increased until all the liquid was drawn up. The decrease of sample volume had to be considered when adding the enzyme from the glucose assay kit as 1 to 1 ratio from enzyme to sample volume was needed.
5. The wells in Column 12 were filled with a standard solution as a control. “SB” indicates the blank solution and “S1000” indicates the 1000  $\mu$ M glucose solution. The standard solutions provided a reference to calculate how much glucose were adsorbed.

6. The same procedure was applied to study the adsorption profile of the 900  $\mu\text{M}$  glucose gel sample.

The glucose diffusion time profile experiment was conducted for glucose solutions as well as glucose gel samples. The results can be compared and a diffusion rate for glucose can be estimated in solution and in gel (see section 6.4.4)

#### 5.8.4 Developing and testing AC foam integrated electrodes

As glucose adsorption to AC was successfully shown, the next step was to integrate AC foam in the electrodes which were used for the *in vitro* RI experiments.

The idea was to place AC behind the electrode so that once glucose is extracted across the skin into the gel reservoir, it will be further drawn across the device to the glucose binding agent. This would prevent glucose build-up in the gel and help to control the diffusion of glucose through the gel layer.

##### Preparation of the AC- integrated electrode:

The hand punch press, which was used to cut the wells out for the electrodes, was also used to cut the sheets of AC foam. This provides disc-shaped AC foams with a diameter of 2 cm and a thickness of 0.1 cm. No tolerances with regards to the dimensions of the foams were given by the manufacturer as the AC foam purchased was intended for odour removal from compost caddies. The AC foam was secured at the back of the electrode design by placing another PTFE well on the back of the electrode. Both sides of the newly attached PTFE well were covered with double sided tape. On the one side it aided to adhere to the back of the electrode and on the other side it was needed to secure the AC foam, which was placed in the well, with an acetate sheet (Figure 5.15 a). 16 holes with a diameter of 0.1 cm were drilled through the electrode in order to ensure AC adsorption Figure 5.15 b. This means that at least 0.127 cm<sup>2</sup> of the AC foam (without considering the porous structure of the AC foam) was exposed to the gel. For this experiment potassium electrodes were used.

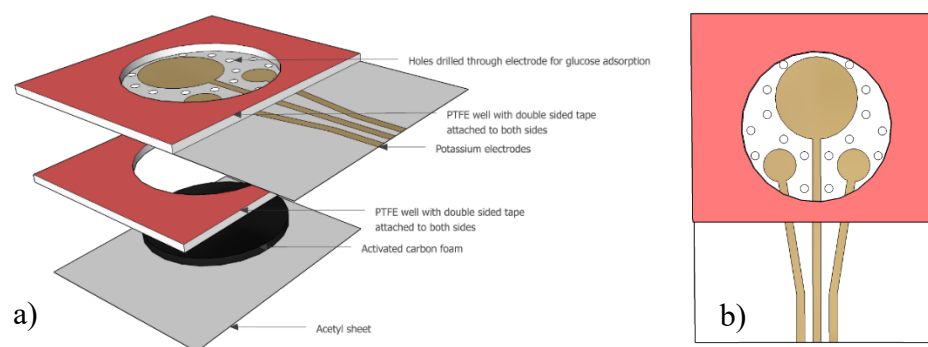


Figure 5.15 Potassium electrodes with the drilled 16 holes a) 3D view of electrode b) Front view of electrode

Once the electrodes were ready, they were tested in the *in vitro* RI environment using the diffusion cell. The procedure explained in Section 5.6 was followed using the newly designed AC- integrated electrodes. The chamber was filled with a 20 mM glucose solution and after the 60 minutes of RI cycle, the gel was carefully removed and diluted with phosphate buffer in a ratio of 1 to 10. With the help of the calibration curve the extracted glucose was quantified. These results were then compared with the experiments using the electrodes for RI without the AC present.

## 5.9 Preparation of glucose sensor

Standard laboratory techniques using laboratory kits (explained in section 5.3) were applied in the previous experiments to quantify glucose. The next aim was to integrate a glucose sensor for rapid and *in situ* glucose measurements so it can be potentially part of a wearable sensor in the RI environment.

Screen-printed electrodes in a three electrode (CE, WE, REF) arrangement with an iontophoresis electrode were fabricated as described in Section 5.5 and used for electrochemical glucose quantification.

Glucose was quantified using mediated enzymatic electrodes. The enzyme electrode was prepared by coating three different layers to the working electrode. The detailed glucose sensor fabrication can be seen below in Section 5.9.3. Glucose oxidase was used as the enzyme and 1,1 dimethylferrocene (DMFc) was used as a mediator for the glucose sensors.

The main responsibility of the mediator is to transfer electron(s) between the enzyme and the working electrode. The current produced due to the reduction – oxidation

(redox) reaction of the mediator, is proportional to the analyte concentration. Cyclic voltammetry (CV) is an electroanalytical technique where the current produced via the redox reaction of a compound on an electrode surface can be monitored as a function of potential. The means of CV was used to analyse and evaluate the performance of the biosensor. Theory of cyclic voltammetry was described in 4.3.4.

### 5.9.1 Preliminary CV experiments

Preliminary experiments were conducted to understand the fundamentals of CV, which helped to comprehend the results of the glucose sensor eventually. In particular the electrochemical characteristics of a mediator and also the interaction between mediator and enzyme was investigated in free solution.

The preliminary experiments were conducted with a different ferrocene derivative, the ferrocenemonocyclic acid (FMCA) as a mediator as it was already available for use in the laboratory. CV was applied to study the electrochemical behaviour of the FMCA.

- Experiment to study the electrochemical behaviour of a mediator

The experiments with the FMCA were conducted in free solution. A 0.5 mM FMCA solution was prepared by dissolving 0.0058 g of FMCA in approximately 300  $\mu\text{L}$  of ethanol and then making it up to a 50 mL solution by adding PBS. In addition, 0.612 g of sodium perchlorate was added to the solution as a supporting electrolyte.

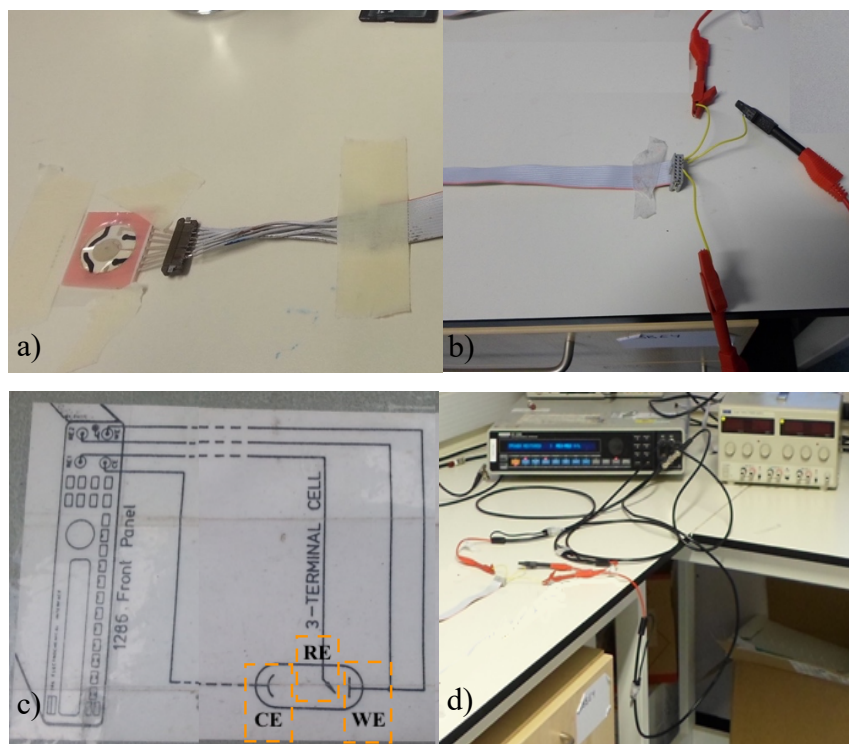


*Figure 5.16 Experimental setup for performing cyclic voltammetry experiments. a) Final electrode setup with a three-electrode system with a solution filled connected to the ribbon cable b) The other end of the ribbon cable connected to an alligator cable via wires c) the applied 3-terminal cell setup was used for the experiments and d) full experimental setup*

Once the solution was ready, the following experimental procedure was applied to perform CV:

1. First the electrode with the three-electrode system and an electrode well was connected to the FFC connector of the ribbon cable (Figure 5.16a). The other end of the ribbon cable was connected to the electrochemical interface SI1268 from Solatron using a BNC to alligator cable; whereby the alligator end of the cable was connected to the IDC ribbon cable connector via wires (Figure 5.16b).
2. The three-terminal cell configuration, which was applied to perform CV using the electrochemical interface is shown in Figure 5.16c.
3. To perform the experiment at static condition, the electrode was secured to the bench top using adhesive tape.
4. 600  $\mu\text{L}$  of the FMCA solution was applied to the well. Scans were taken at three different rates 10 mV/s, 50 mV/s and 100 mV/s and in the voltage range between 0.1 V and 0.5 V.

5. To identify the current increase solely caused by the redox reaction of the mediator, it is important to identify the capacitive current. which is caused by the double layer charging of the electrode. As explained in section 4.3.4, the capacitive current was identified using Kissinger's method (Kissinger & Heineman, 1983). Therefore, first the baseline current was extrapolated. Subsequently, the extrapolated line was described by a linear function equation (Equation 5.3) by the method of least square fitting using Microsoft Office Excel 2017.

$$y = kx + d \quad \text{Equation 5.6}$$

*x*...Anodic peak potential [V]

*y*...Current [A]

*k*...Gradient of the linear equation obtained from the extrapolated baseline current

*d*...slope of the linear equation obtained the extrapolated baseline current

To calculate the capacitive current, the anodic peak potential was inserted into the linear function equation. Ultimately, the capacitive current was deducted from the total peak current found at the anodic peak potential to identify the current solely caused by the redox reaction of the mediator.

- Experiment to study the interaction between mediator and enzyme

A second experiment was conducted to observe the electrochemical interaction between mediator and enzyme. Therefore, the experiment conducted by Allen et al. (2011) was followed. First, a 0.5 mM FMCA solution with a glucose concentration of 50 mM was prepared. Therefore, 0.0058 g of FMCA was dissolved in approximately 300  $\mu$ L of ethanol and then made up to a 50 mL solution by adding PBS. 0.45 g of glucose was added to the FMCA solution to obtain a glucose concentration of 50 mM. The same experimental setup as shown in Figure 5.16 was applied. 580  $\mu$ L of the solution with FMCA and glucose was added to the well and a scan was taken at a scan rate of 1 mV/s. Then the same solution was spiked with 20  $\mu$ L of a 10.9  $\mu$ M GOD solution and another scan with a scan rate of 1 mV/s was taken. For analysis of the voltammogram, the capacitive current was identified and then deducted from the peak current.



## 5.9.2 Testing the potential of the screen-printed reference electrodes

It was important to determine the potential of the screen-printed reference electrodes and to evaluate its performance in the liquid and in the gel environment. Therefore, it was tested with respect to a standard glass Ag/AgCl (3M KCl) reference electrode in phosphate buffer and in methylcellulose hydrogel. The screen printed RE was connected to the WE output of the potentiostat and the standard reference electrode was connected to the RE output. Both electrodes were immersed in the same beaker filled with phosphate buffer and gel respectively. The open cell potential, which is defined as the potential at the WE relative to the RE when no potential or current is applied to the electrochemical cell, was then measured with the potentiostat.

## 5.9.3 Glucose sensor fabrication

The Medical Devices group in the Biomedical Engineering Department at the University of Strathclyde developed a glucose sensor, which was similar to the methods described by Allen et al. (Hill & Sanghera, 2011). Further improvements and adaptations were done on the glucose sensors. Before preparing the glucose sensors, the electrodes were conditioned first.

Conditioning of the electrodes:

Conditioning of the working electrode had shown to improve the binding between the carbodiimide solution and the electrode surface. The conditioning was adapted from the methods used by Allen et al. (2011). In this project, for the conditioning process, a 0.1 M potassium chloride solution was made by dissolving 0.373 g of potassium chloride in 50 mL of dH<sub>2</sub>O. For the conditioning of the electrodes, a silicone well was prepared using the hand press punch and placed on the electrode to fill the electrode with the solution. 800  $\mu$ L of the potassium chloride solution was dispensed onto the electrode and a direct voltage of -2.5 V was applied on Side A and Side B of the electrode for 1 minute each using the electrochemical interface. The electrode was then rinsed with dH<sub>2</sub>O and dried overnight.

The glucose sensors were prepared by coating the working electrode of the sensor with the following solutions similarly to methods described by Allen et al. (Hill & Sanghera, 2011)

- a) 0.15 mM Carbodiimide solution (CDI): This solution was prepared by dissolving 0.0635 g of carbodiimide in 1 ml of a 1 M acetate buffer, which had a pH of 4.5. The acetate buffer was made up by dissolving 0.135g of acetate buffer.
- b) 0.25 mM 1,1'-Dimethylferrocene solution: This solution was prepared by dissolving 0.2141 g of DMFc in 4 ml of ethanol.
- c) Glucose oxidase: Glucose oxidase was prepared by dissolving 0.340 g of potassium phosphate in approximately 40 ml of dH<sub>2</sub>O and then adjusted to a pH of 4.5. The buffer was added to make up a solution of 50 ml. Then 0.08 g of GOD was dissolved in 4 mL of the potassium phosphate buffer. 55  $\mu$ L of the solution was dispensed into each of the 1 mL eppendorfer tube and defrosted when required.

The first coating on the working electrode consisted of 5  $\mu$ L of CDI on Side A and Side B of the electrode. After a drying period of 3 hours at room temperature, the electrodes were washed by placing the electrodes in a distilled water bath on a lab shaker. The container with the water bath was put on the shaker for 5 minutes at the lowest speed setting. The distilled water was changed and the washing procedure was repeated another two times. The electrodes were dried before applying the next coating. Two coatings of 0.4  $\mu$ L DMFc were applied onto Side A and Side B of the working electrode. Subsequently, 5  $\mu$ L of glucose oxidase was applied only on Side A of the working electrode and dried for 90 minutes at room temperature. Side A of the sensor is responsible to detect any glucose related current changes. Side B of the glucose sensor is intended to identify any background current or any current caused by any interfering species.

After the 90 minutes, the glucose sensors were stored in the fridge with a pack of silica gel sachets desiccant pouches to absorb any moisture. The prepared glucose sensors were used within three days after preparation.

## 5.10 Experiments with the glucose sensor

To test the sensor performance and to evaluate its suitability to be used for direct glucose measurements in the RI environment, a series of experiments were carried out using gel samples as the samples from experiments involving- *in vivo* glucose extraction via RI were in gel format.

CV was applied to understand the electrochemical behaviour of the glucose sensors. It was employed using the electrochemical interface SI1268 from Solatron with the three terminal cell configuration as shown in Figure 5.16c. The pins from the glucose sensor were carefully connected to the working, reference and counter electrode connections from the electrochemical interface.

### 5.10.1 Scan rate (SR)

As discussed in the section 4.3.4, the peak current in a voltammogram changes with respect to the applied scan rate: With increasing scan rate, the diffusion layer decreases, which in turn leads to higher peak currents (Compton et al., 2012a).

Experiments were carried out to investigate in the relationship between different scan rates and current output for the developed glucose sensor. Once the experimental setup as explained in Section 5.9.1 was prepared, 300  $\mu\text{L}$  of gel with a specific glucose concentration was dispensed onto the glucose sensor. After a wetting time of 10 minutes, CV was performed on Side A and Side B of the electrode at a scan rate of 10 mV/s. The voltage range was chosen between -0.2 V and 0.4 V. The same procedure was repeated on the same electrode at a scan rate of 20 mV/s, 30 mV/s, 40 mV/s, 50 mV/s, 60 mV/s, 70 mV/s, 80 mV/s, 90 mV/s and 100 mV/s.

### 5.10.2 Standard calibration curve for glucose sensors

It is important to know the lower limit of detection of the glucose sensor in order to determine if the sensors are sufficiently sensitive to quantify glucose extracted via RI experiments. Therefore, experiments were conducted to establish a calibration curve using the glucose biosensors. Standard glucose gel samples in the following concentrations were prepared as explained in Section 5.2.5: 500  $\mu\text{M}$ , 250  $\mu\text{M}$ , 125  $\mu\text{M}$ , 62.5  $\mu\text{M}$ , 31.25  $\mu\text{M}$ , 15.625  $\mu\text{M}$  and 0  $\mu\text{M}$ . Once the experimental setup as

explained in Section 5.9.1 was prepared, 300  $\mu\text{l}$  of gel was dispensed onto the glucose sensor. And after a settling time 10 minutes, CV was performed on Side A and Side B of the electrode at a scan rate of 60 mV/s and the voltage range between -0.2 V and 0.4 V with 5 measurement cycles. After use, electrode was discarded and a new electrode was used for the next glucose concentration. The same procedure was repeated for all the glucose concentrations. Experiments were repeated 3 times for each concentration.

#### Analysis of the voltammograms:

In the experiments carried out Section 5.10.1 and Section 5.10.2, gel samples were tested, which already had glucose in it. When analysing the obtained voltammograms, a particular peak and shape for side A and for side B of the sensor was observable (see Figure 5.17). For Side A an anodic peak potential at approximately 0.14 V was seen and for Side B a peak was observable at a voltage of 0.1249 V. If the results did not match the empirically determined shape and peak, the result was not included in the analysis.

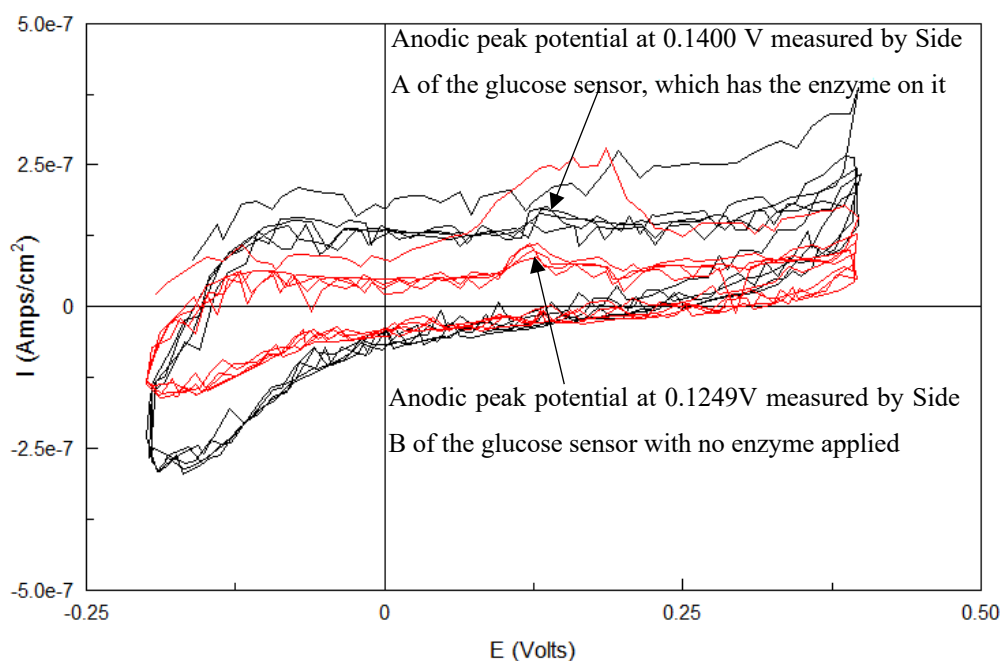


Figure 5.17 Example voltammogram of the standard calibration curve experiments from a standard gel sample with a glucose concentration of  $62 \mu\text{M}$ . The graph in the black colour shows the result of the Side A of the electrode and the red coloured graph is the result of Side B of the electrode.

Once the obtained voltammogram corresponded the expected shape and peak, it was important to identify the peak current solely caused by the redox reaction. Kissinger's method was applied to identify the capacitive current, which was explained in section 4.3.4 (Kissinger & Heineman, 1983). The baseline current in the potential region from -0.1 V to +0.1 V was extrapolated and the capacitive current was then deducted from the peak current.

#### Establishment of the calibration curve:

For the establishment of the calibration curve using the glucose sensor the ratio of the current reading of side A to the current reading at side B of the sensor at a voltage of 0.14 V. Side A of the sensor was coated with the DMFc and the carbodiimide solution and with glucose oxidase and is responsible to detect any glucose related current changes. Side B of the glucose sensor is only coated with DMFc and the carbodiimide and without glucose oxidase. It is intended to identify any background current or any current caused by any interfering species.

Taking the ratio will help to identify the current changes only caused by the glucose and eliminate any background current or current caused by any interfering species. Hence, specificity of the glucose sensor can be validated.

A linear response was seen between a limited range of the standard glucose concentrations and the respective current ratios. Microsoft Office Excel 2017 was used to apply a straight-line fit on the dataset and to express the linear relationship in the form of the linear function equation by the method of least square fitting.

### 5.10.3 RI experiments using glucose sensors with AC and glucose sensors without AC

In the next step, the glucose biosensors were tested along with the *in vitro* RI diffusion cell. Figure 5.18 shows the measurement setup used to perform *in vitro* RI experiments along with two types of glucose sensors (one with AC foam and one without AC).

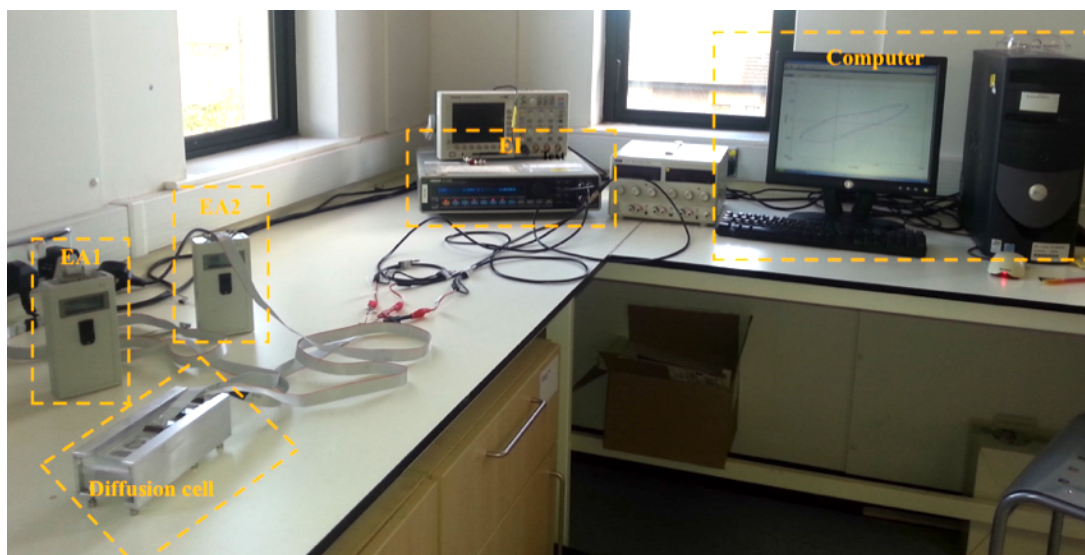


Figure 5.18 Measurement setup for RI experiments using glucose sensors with and without AC foam. EI 1 is connected to the computer and was used to perform CV to ensure sensor performance. EA 1 was responsible to apply the iontophoretic current between E1 and E2 electrodes and also to take “Pre RI” and “After RI” cyclic voltammograms of the E1 electrode. EA 2 was responsible to take “Pre-RI” and “After-RI” cyclic voltammograms of the E2 and C electrodes.

The procedure as explained in Section 5.6 was followed to perform the RI experiments with the diffusion cell:

1. The Spectrapore membrane was prepared as described in Section 5.7.
2. The buffer for the chamber was prepared with five different glucose concentrations: 0 mM, 5 mM, 10 mM, 15 mM and 20 mM. Once the diffusion cell was filled, it was rinsed in dH<sub>2</sub>O to ensure that there was no buffer on the top of the diffusion cell. Then the top of the diffusion cell was covered in dH<sub>2</sub>O (to avoid dehydration of the membrane) until the glucose sensors were prepared and ready to be applied onto the diffusion cell.
3. Two sets of electrodes were prepared for the experiments:
  - Glucose sensors without AC: The electrodes for the RI experiments without AC were prepared by only placing the PTFE wells onto the fabricated glucose sensors.
  - AC- integrated glucose sensors: A similar design to previously designed electrode using the potassium electrodes was chosen. Therefore, 11 holes with a diameter of 0.125 cm were made with the Europlier (Figure 5.19) onto the glucose sensors. This means that at least 0.135 cm<sup>2</sup> of the AC foam was exposed to the gel (without

considering the porous structure of the AC foam). PTFE wells were applied on both sides of the electrode, the front well serves as a gel reservoir and the AC foam was placed at the back of the sensor and secured with an acetate sheet.

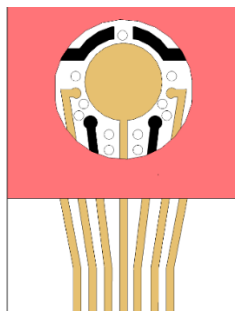


Figure 5.19 Electrode with well attached and holes drilled

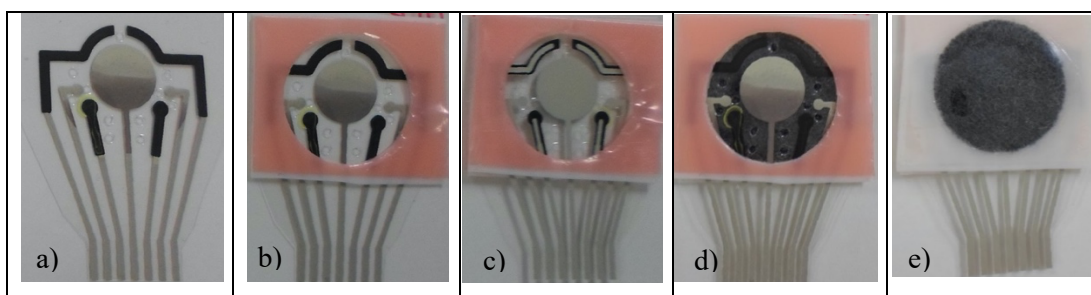


Figure 5.20 Photographed AC integrated glucose sensor preparation for RI experiment: a) Electrode with 11 holes punched; b) Electrode with well attached (front); c) Electrode with well attached (back); d) Electrode with AC foam attached (front); e) Electrode with AC foam attached and secured with an acetate sheet (back)

4. 300  $\mu\text{L}$  of gel was applied into the electrode well and set for 5 minutes.
5. Before putting sensors on diffusion cell, CV was performed on both sides of each sensor using the using the electrochemical interface SI1268 to ensure sensor performance. An empirically observed particular peak and shape for each side had to be confirmed before putting sensor on the diffusion cell (Figure 5.21). At a scan rate of 60 mV/s, CV was performed with a potential range between -0.2 V to 0.4 V versus the reference electrode.

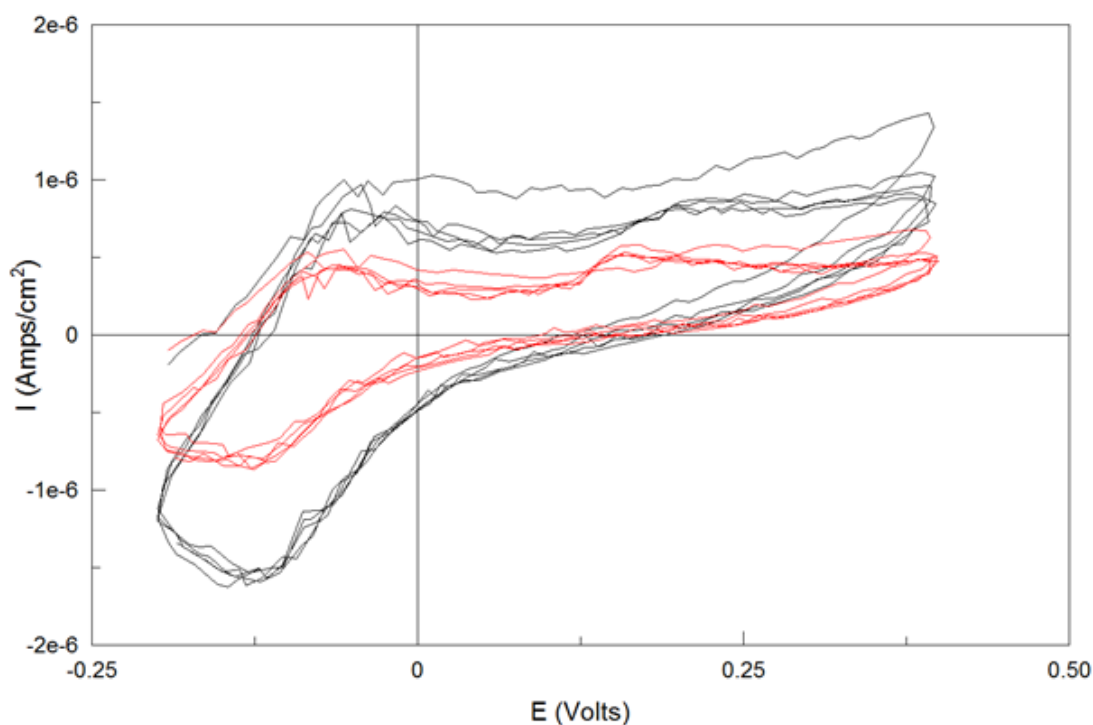


Figure 5.21 Pre-testing of sensors before using them for the RI experiment. The graph in the black colour shows the result of the Side A of the electrode and the red coloured graph is the result of Side B of the electrode.

6. If the peak and the shape did not match with the expected result, the sensor was discarded.
7. Once three electrodes were selected, first the control was placed onto the diffusion cell, then the E2 electrode and finally the E1 electrode. When placing the electrode, it was made sure that there was no bubble formed between the gel and membrane and that the double-sided tape was sticking properly on the membrane to avoid any gel leakage.
8. The cables were then connected to the portable electrochemical analyser and after a settling time of 5 minutes, CV was performed on each electrode on each side. Then iontophoresis was applied for 60 minutes between E1 and E2 with switching polarities every 15 minutes using the portable electrochemical analyser. After the iontophoresis cycle, CV was again performed on each electrode and both sides. It was important that CV was applied at the same time for the E1 and the E2 electrode for analysis purposes. Therefore, two portable electrochemical analysers were used. The EA1 took CV from the E1 electrode and was also responsible to perform RI. In contrast, the EA2 took CV



measurements from the E2 electrode (simultaneously to the E1 electrode) and then it took CV measurements from the control electrode.

9. For each measurement cycle 18 voltammograms were acquired (6 voltammograms for each electrode):

.) DC pre: Before placing the sensor onto the diffusion cell, CV was applied to confirm the empirically observed particular peak and shape (Figure 5.21) to ensure sensor performance (A - pre DC and B - pre DC).

.) Pre RI: Once three sensors were selected, a voltammogram was taken as soon as the sensors were applied onto the diffusion cell (A - pre RI and B – pre RI).

.) After RI: After the 60 minutes of RI, another voltammogram was recorded (A - after RI and B – after RI).

The voltammogram of interest to investigate in electrochemical glucose detection was the CV taken after the 60 minutes of RI, hence the “After RI” voltammograms.

Based on the results obtained in the establishment of a calibration curve using the glucose sensor, an oxidation peak at the voltage of 0.14 V was expected. However, the voltammograms taken after the application of RI had a different shape compared to the CV obtained for the establishment of the calibration curve. And no oxidation peak could be identified at a voltage of 0.14 V. Instead, two peaks were identified on the voltammogram for side A of the electrode after the application of RI for 60 minutes. One peak at a voltage of 0.082 V and the second peak at a higher potential of approximately 0.306 V. And for side B of the sensor, two peaks were also on the voltammogram after the application of RI for 60 minutes at a similar oxidation potentials as side A. One peak at a voltage of approximately 0.092 V and the second peak at a potential of approximately 0.292 V. There is the possibility that there was a shift in the glucose peak. Therefore, it was decided to investigate in the relationship between the peak currents obtained at 0.082 V and 0.306 V respectively for a possible relationship with the extracted glucose. For the identification of the capacitive current from the after RI voltammograms, Kissinger’s method was applied by extrapolating the baseline current in the potential region from -0.1V to 0.024 V and 0.199 V to 0.233 V respectively

(Kissinger & Heineman, 1983). The capacitive current was then deducted from the peak current. The ratio of current at side A to current at side B at the oxidation potential at 0.082 V and 0.306 V respectively was evaluated to identify a relationship with the extracted glucose.

10. For comparison purposes to the electrochemical glucose detection method, the extracted glucose via RI with and without the AC- integrated glucose sensors was quantified using standard laboratory techniques. Therefore, after each measurement cycle, the gel was scraped off and diluted with a phosphate buffer solution. Glucose was then quantified using the Randox glucose assay kit.

RI experiments for each glucose concentration (0 mM, 5 mM, 10 mM, 15 mM and 20 mM) in the buffer were repeated three times with AC- integrated glucose sensors and three times without AC- integrated glucose sensors.

## 6 Results

This result chapter can be divided into the following sections:

- Section 6.1 shows the results of the comparison of two commercially available glucose assay kits (the Randox laboratories assay kit and the Sigma Aldrich assay kit).
- The Randox assay kit, which showed better suitability for the required concentration range, was used to evaluate the use of the Genova Nano spectrophotometer for glucose quantification (Section 6.2).
- Basic reverse iontophoresis (RI) experiments were performed to see the impact of changing the glucose concentrations in the buffer solution in the diffusion cell on the amount of glucose extracted (Section 6.3.1) from the *in vitro* cell. In addition, experiments were also conducted to see the relation between glucose extraction and the duration of RI (Section 6.3.2). The glucose flux through the two artificial membranes (the Spectrapore membrane and the Vitro-Skin®) were compared and can be seen in Section 6.3.3.
- Section 6.4 provides proof of concept of glucose adsorption to activated carbon (AC). It details the outcomes of the preliminary glucose adsorption experiments on AC pellets (Section 6.4.1) and AC foams (Section 6.4.2) from glucose solutions. Section 6.4.3 illustrates the outcomes of the glucose adsorption to AC foam with glucose gel samples and Section 6.4.4 shows the results of the experiments of glucose adsorption to AC foam over time. The effect of glucose adsorption to the sample volume over time is shown in Section 6.4.5. Subsequently, an initial design of an AC foam integrated glucose sensor was made and tested in the *in vitro* RI setup (Section 6.4.6). The extracted glucose was then quantified using a colorimetric assay.
- In section 6.5 the results of the preliminary cyclic voltammetry experiments are demonstrated, which were carried out to understand the fundamentals of CV, the electrochemical characteristics of the mediator and also the interaction between mediator and enzyme in the liquid environment.
- Section 6.6 shows the results of the cyclic voltammetry experiments with the fabricated dimethylferrocene-mediated enzymatic glucose sensor for

electrochemical glucose detection. It includes the electrochemical characterisation of the glucose sensor in the gel environment and the establishment of a calibration curve for glucose gel samples at different concentrations using the glucose sensor. The established calibration curve should ultimately help to quantify unknown glucose concentrations from samples extracted via RI.

- The final section (section 6.7) details the results of the electrochemical glucose detection method of the glucose extracted via *in vitro* RI experiments using the glucose sensors with AC foam and glucose sensors without AC foam. In addition, for comparison purposes to the electrochemical glucose detection method, glucose was also quantified using standard laboratory techniques using colorimetric assays and an optical spectrophotometer.

## 6.1 Comparison of two commercially available glucose assay kits

This section shows the results of the comparison of two commercially available glucose assay kits in terms of glucose sensitivity, linear range, limit of detection (LOD) and limit of quantification (LOQ). The tested glucose assay kits were a glucose assay kit from Randox Laboratories and a glucose assay kit from Sigma Aldrich. In this project, the main interest was in the identification of the linearity in the lower concentration range of the assay kits because the expected glucose concentrations extracted via RI is in the micro molar range (down to 20  $\mu\text{M}$ ). The calibration curves established were eventually used to quantify glucose concentrations from unknown samples extracted via RI experiments. Therefore, the glucose assay kit used had to be suitable to quantify glucose in such low glucose concentrations. Calibration curves were established using both glucose assay kits in combination with glucose gel samples with increasing concentrations. The standard glucose gel samples were prepared as explained in section 5.2.5. Absorbance measurements were taken in a glucose gel concentration range from 0.22  $\mu\text{M}$  to 1800  $\mu\text{M}$  using the Randox assay kit. Figure 6.1 shows the calibration acquired with glucose gel samples with the Randox assay kit. The best linear fit was given when applying the linear between 0.22  $\mu\text{M}$  and 450  $\mu\text{M}$  and is shown in Figure 6.1. The linear relationship can be expressed with the following equation  $y=0.0015x+0.0485$  with an  $R^2$ -value of 0.99. The LOD and LOQ were calculated based on the Equation 4.7 and Equation 4.8 and converted to a glucose concentration of 2.39  $\mu\text{M}$  for the LOD and 7.03  $\mu\text{M}$  for the LOQ using linear equation of the calibration curve. The error bars in the figures represent the standard deviation unless otherwise stated.

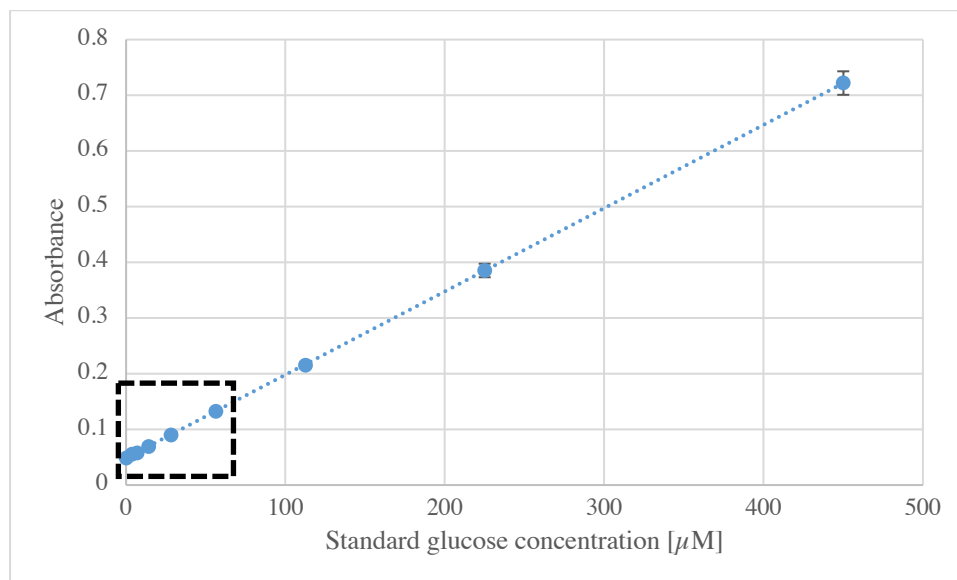


Figure 6.1a Calibration curve of glucose gel samples with increasing glucose concentrations using the Randox reagent with a colorimetric assay. The error bars represent the standard deviation ( $n=5$ )

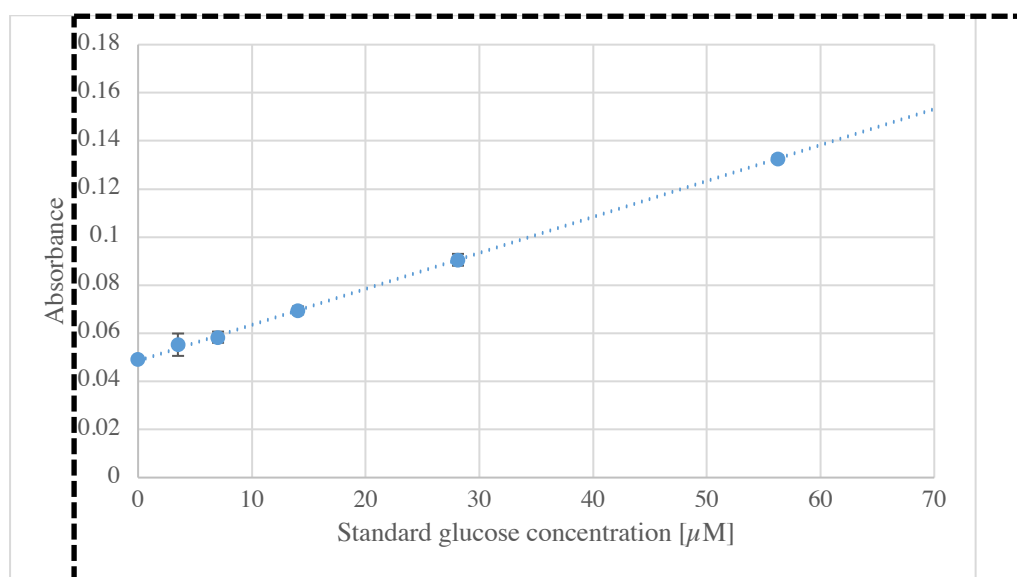


Figure 6.1b Magnification of the glucose calibration curve shown in Figure 6.1a of glucose gel samples in the concentration range of interest from  $3.51 \mu\text{M}$  to  $56.25 \mu\text{M}$

The calibration curve prepared with the glucose gel samples in combination with the Sigma Aldrich assay kit can be seen in Figure 6.1a. The same glucose concentration range ( $0.22 \mu\text{M}$  to  $1800 \mu\text{M}$ ) was tested with the Sigma Aldrich assay kit. It was observable that the background absorbance was higher than the sample absorbance value for the following standard glucose concentrations:  $0.22 \mu\text{M}$ ,  $0.44 \mu\text{M}$ ,  $0.88 \mu\text{M}$ ,  $1.76 \mu\text{M}$ ,  $3.52 \mu\text{M}$ ,  $7.03 \mu\text{M}$ ,  $14.06 \mu\text{M}$ ,  $28.13 \mu\text{M}$ ,  $56.11 \mu\text{M}$ ,  $112.5 \mu\text{M}$  and  $225 \mu\text{M}$ .

A linear relationship can be observed with  $y=0.0002x+0.176$  and an  $R^2$ -value of 0.97. An LOD of 182.44  $\mu\text{M}$  and an LOQ of 252.14  $\mu\text{M}$  were calculated.

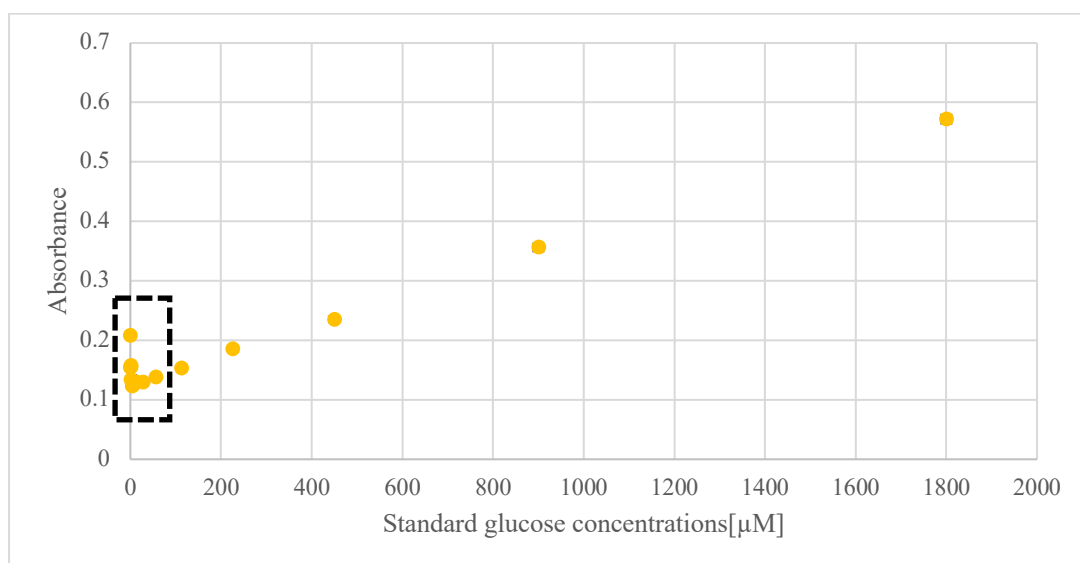


Figure 6.2a Calibration curve of glucose samples in gel with increasing glucose concentrations using the Sigma Aldrich reagent with a colorimetric assay. The error bars represent the standard deviation ( $n=5$ )

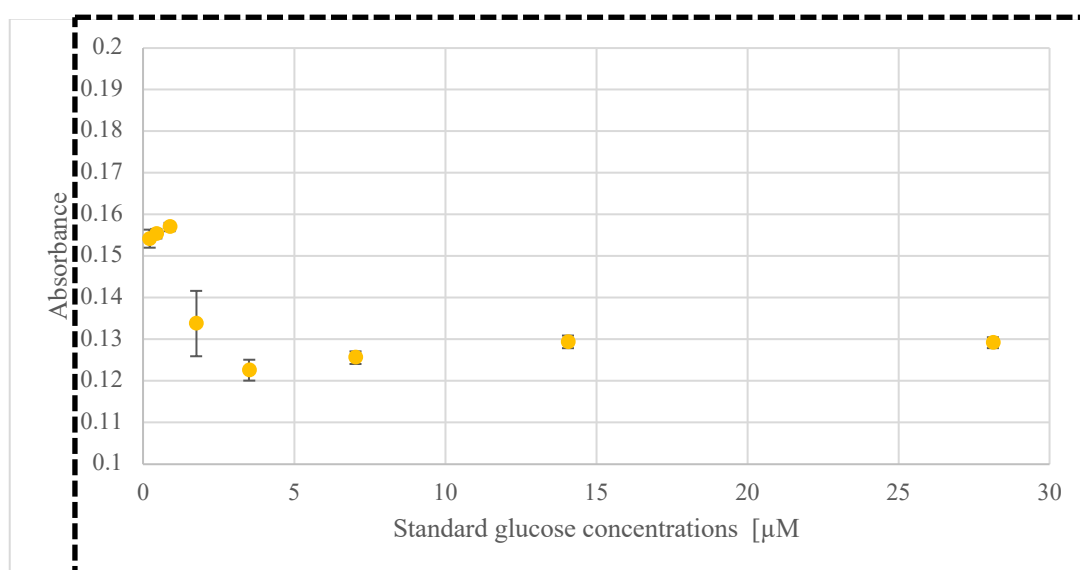


Figure 6.2b Magnification of the glucose calibration curve shown in Figure 6.2a of glucose gel samples in the concentration range of interest from 0.22  $\mu\text{M}$  to 28.13  $\mu\text{M}$

The high standard deviation of sample 4 on Figure 6.2b was probably caused by a contaminated sample.

Table 6.1 provides a comparison from the data acquired in Figure 6.1b and Figure 6.2b.

*Table 6.1 Summary of LOD, LOQ, upper limit of the linear calibration curve, equation of the linear relation using the Randox assay kit and the Sigma Aldrich Assay kit*

<b>Manufacturer of glucose assay kit</b>	<b>LOD [μM]</b>	<b>LOQ [μM]</b>	<b>Upper limit of the linear relation [μM]</b>	<b>Equation of calibration curve</b>
Randox	2.39	7.03	450	$y=0.0015x+0.0485$
Sigma Aldrich	182.44	252.14	1800	$y=0.0002x+0.1760$

It can be seen that the Randox assay kit is able to quantify glucose concentrations down to 2.39 μM for glucose gel samples. In contrast, the Sigma Aldrich assay cannot detect glucose concentrations below 182.44 μM. The differences between the assay kits could be due the use of different enzymes for the glucose measurement. Randox assay kit uses the glucose oxidase and peroxidase method and Sigma Aldrich assay kit applies the hexokinase G6PDH method. Furthermore, higher enzyme concentrations in the Randox assay kit could be the reason for its lower limit of detection.

## 6.2 Glucose quantification using Genova Nano spectrophotometer

The following section shows the results of experiments performed to evaluate the use of the Genova Nano for glucose quantification. The advantage of Genova Nano is that it can perform measurements with low sample volumes (0.5 μL to 5 μL per measurement). This is especially beneficial for research in non- invasive blood glucose monitoring by transdermal glucose extraction via RI as only a small sample size is available for the analysis.

To assess the suitability of the Genova Nano for glucose quantification, a calibration curve was established with glucose assay kit from Randox Laboratories to identify the linear range. For comparison purposes, measurements were also done with a commonly used microplate reader. Linearity was tested using the following standard glucose concentrations: 2.93 μM, 5.86 μM, 11.72 μM, 23.44 μM, 46.88 μM,



93.75  $\mu\text{M}$ , 187.5  $\mu\text{M}$ , 375  $\mu\text{M}$ , 750  $\mu\text{M}$  and 1500  $\mu\text{M}$ . Calibration curves were established using glucose solutions, which were diluted with gel samples in a ratio of 1 to 4.

Using the microplate reader, the linear relation with  $y=0.0011x + 0.0586$  with an  $R^2$ -value of 0.99 and an LOD of 1.22  $\mu\text{M}$  and an LOQ of 7.17  $\mu\text{M}$  (Figure 6.3) was established.

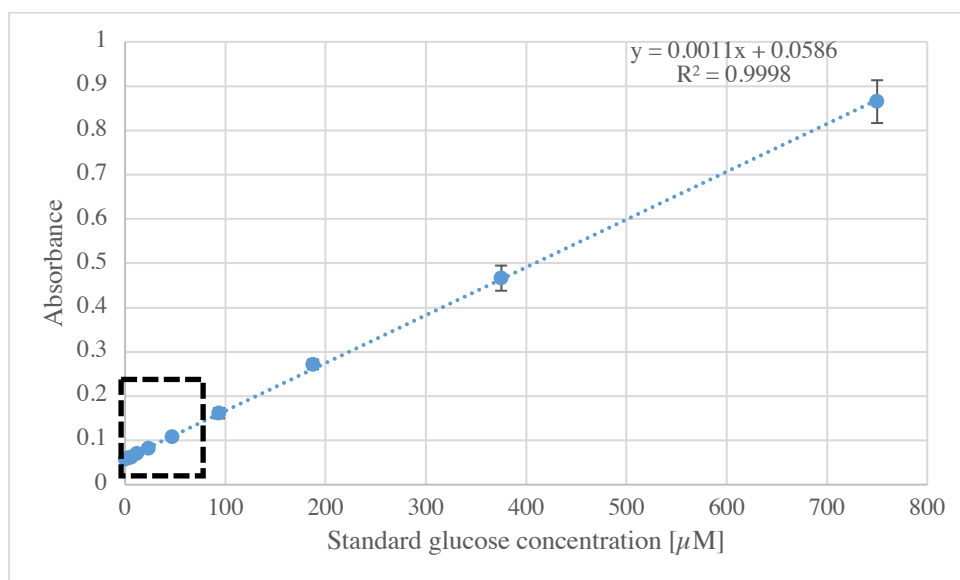


Figure 6.3a Calibration curve of glucose samples in gel format with increasing glucose concentrations using the Randox reagent with a colorimetric assay in a glucose solution to gel ratio of 1: 4.

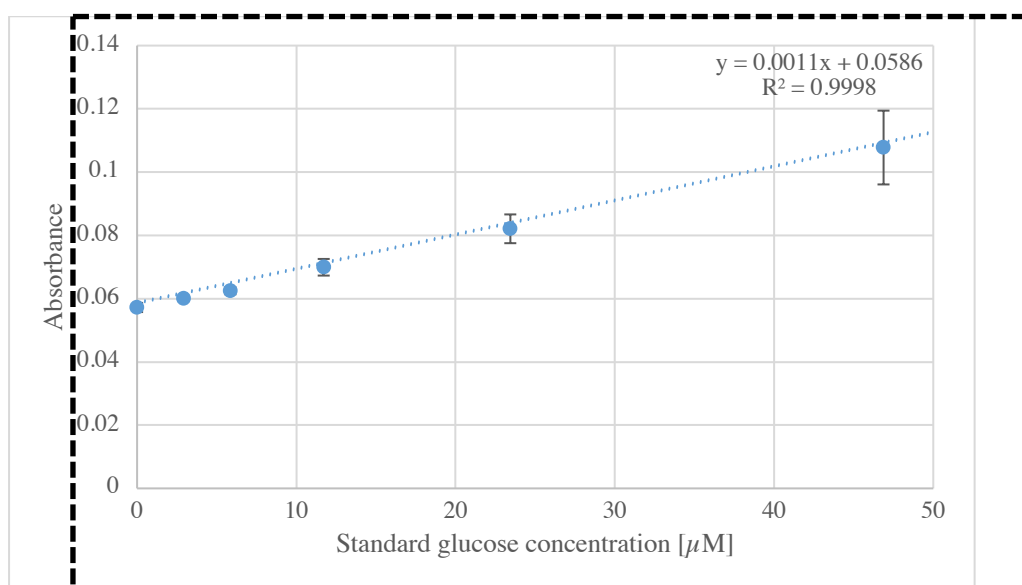


Figure 6.3b Magnification of the glucose calibration curve shown in Figure 6.3a of glucose gel samples in the concentration range of interest from 2.93  $\mu\text{M}$  to 46.88  $\mu\text{M}$

In contrast, using the same concentration range, a linear relationship was established with  $y=0.0002x + 0.002$  and an  $R^2$ -value of 0.99 with an LOD of 5.65  $\mu\text{M}$  and an LOQ of 26.14  $\mu\text{M}$  (Figure 6.4) using the Genova Nano.

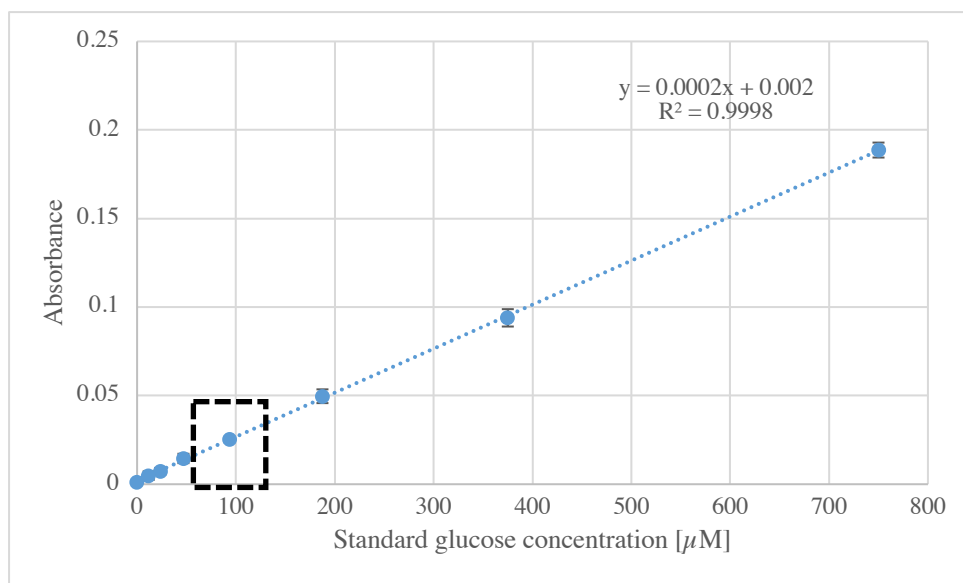


Figure 6.4a Calibration curve of glucose samples in gel format in a glucose solution to gel ratio of 1 to 4 with increasing glucose concentrations using the Radox reagent acquired using the Genova Nano.

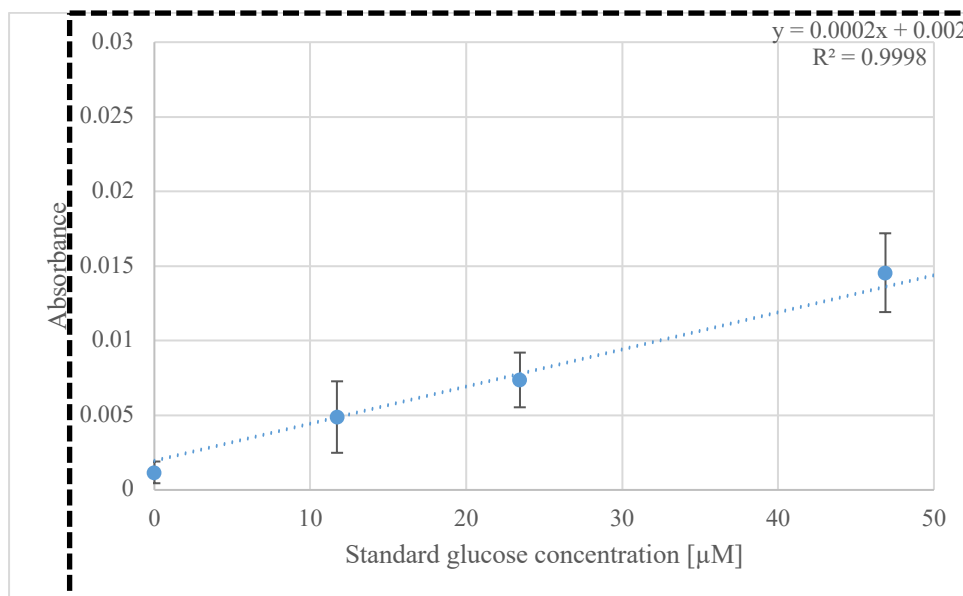


Figure 6.4b Magnification of the glucose calibration curve shown in Figure 6.4a of glucose gel samples in the concentration range of interest from 11.72  $\mu\text{M}$  to 46.88  $\mu\text{M}$

To assess the different methods and the obtained calibration curves, two glucose gel samples with known concentrations (204  $\mu\text{M}$  and 408  $\mu\text{M}$ ) were prepared. The absorbance was then measured using the microplate reader and the Genova Nano and afterwards quantified using the calibration curve established with two methods.

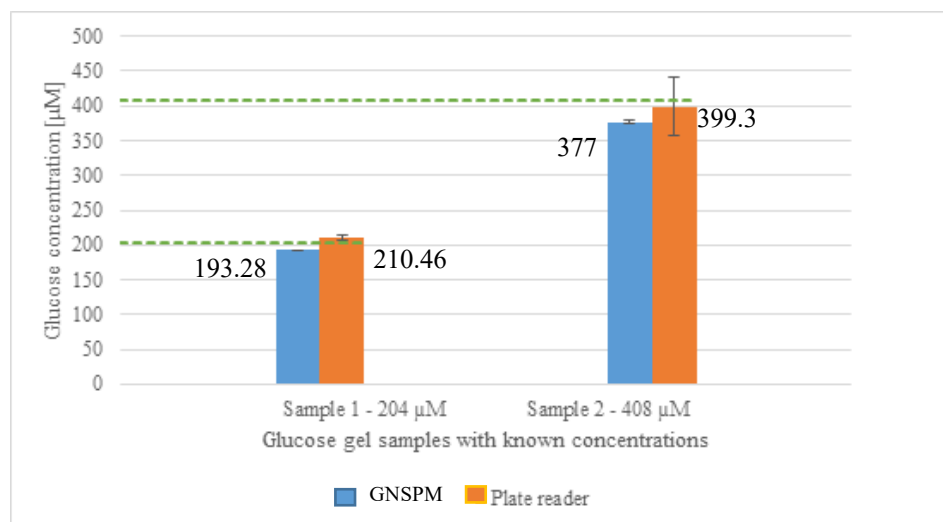


Figure 6.5 Quantification of the glucose concentration of three samples with known glucose concentrations (204  $\mu\text{M}$  and 408  $\mu\text{M}$ ) using the calibration curve acquired (1) with the microplate reader (orange bars) and (2) with the Genova Nano (blue bars). The green dashed lines indicate the actual glucose concentration in Sample 1 and Sample 2.  $n=3$

Figure 6.5 shows microplate reader measured the concentrations from the two glucose samples closer to their known concentration than the GNSPM. The microplate reader showed a difference of +6.46  $\mu\text{M}$  for Sample 1 respectively -8.7  $\mu\text{M}$  for Sample 2. And the GNSPM had a difference of -10.72  $\mu\text{M}$  and -31  $\mu\text{M}$  to the actual glucose concentrations. Lower standard deviations are seen for the measurements with the GNSPM. In the final experiments a low volume sample was not required and so the GNSPM was not deployed again. The reason why the GNSPM was underestimating the actual glucose concentration could be due to the use of sample volume of only 2  $\mu\text{l}$ .

### 6.3 Results of the RI experiments

The following section shows the results from the *in vitro* RI experiments performed using the diffusion cell. The procedure for the *in vitro* RI experiments was followed as explained in section 5.6. An iontophoretic current of 100  $\mu\text{A}/\text{cm}^2$  was applied for

all experiments. The amount of glucose extracted via RI was tested with respect to changing the glucose concentrations in the buffer solution in the diffusion cell and with respect to varying the duration of RI. For each RI experiment three electrodes were applied onto the diffusion cell, one control electrode (C) and two iontophoresis electrodes (E1 and E2).

### 6.3.1 RI experiments with changing the concentration in the buffer solution in the diffusion cell

Figure 6.6 shows the glucose extracted from samples with different glucose concentration in the diffusion cell (5 mM and 20 mM). A glucose concentration of 5 mM was chosen as it mimics concentrations obtained from the healthy individuals in the fasted state (Arias, 2011). A 20 mM glucose buffer solution was also tested as it mimics the concentration obtained after a high-glucose drink from healthy individuals.

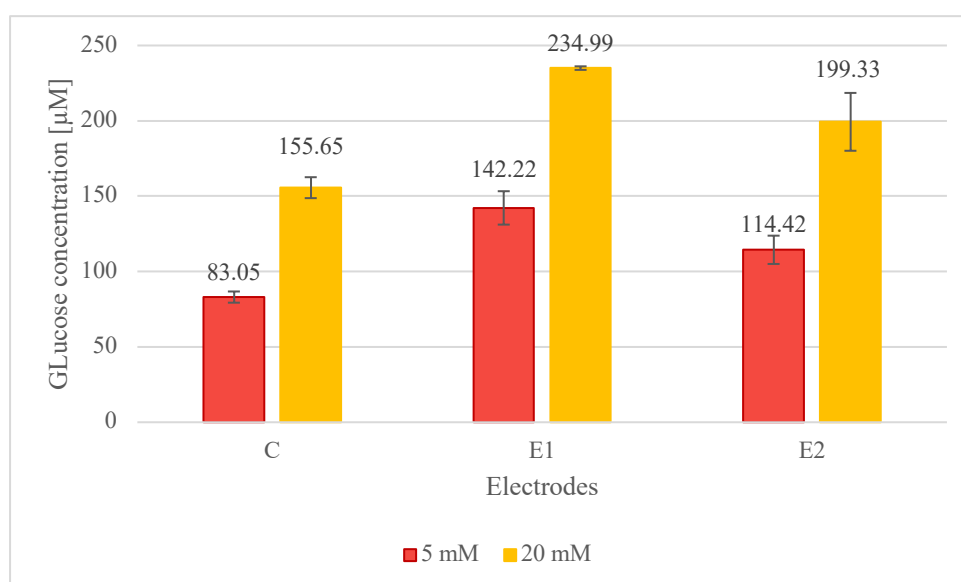


Figure 6.6 Results of glucose extraction after *in vitro* RI experiments on the diffusion cell for a duration of 60 minutes with switching polarities every 15 minutes. The diffusion cell was prepared with a concentration of 5 mM (red bars) and 20 mM (yellow bars) glucose in the buffer solution. The glucose concentrations from the extracted gel were calculated using the equation from the calibration curve. C indicates the control electrode, E1 indicates the initial anodic iontophoretic electrode and E2 indicates the initial cathodic electrode.  $n=3$

More glucose was extracted across all three electrodes in the buffer solution with the 20 mM glucose as expected. In both cases, the control electrodes extracted the least amount of glucose, followed by the E2 electrode and the E1 electrode collected the

highest amount of glucose. Higher error bars can be seen for the E2 electrodes. This could be due possibly to some leakage from the gel reservoir at the E2 electrode during RI. The iontophoresis electrodes extracted in total 247.53  $\mu\text{M}$  of glucose from the 5 mM glucose buffer solution and 426.29  $\mu\text{M}$  from the 20 mM glucose buffer solution. A significant increase of glucose across both iontophoresis electrodes was observable when applying an independent t-test ( $p \leq 0.05$ ). Table 6.2 shows the calculated glucose fluxes across each electrode from the 5mM glucose buffer solution and 20 mM glucose buffer solution. For the 5 mM glucose concentration in the diffusion cell, a transdermal flux of 24.51  $\text{nmol}/\text{cm}^2\text{h}$  was calculated across both iontophoresis electrodes and 7.93  $\text{nmol}/\text{cm}^2\text{h}$  across the control electrode. In contrast, a higher extracted rate of 41.47  $\text{nmol}/\text{cm}^2\text{h}$  was identified for the 20 mM glucose buffer solution in the diffusion cell and of 14.83  $\text{nmol}/\text{cm}^2\text{h}$  for the control electrode. The extraction rate increased on average by a factor of 1.75. It can be seen that the glucose extraction was not proportional to the amount of glucose in the diffusion cell. This might be due to the fact that the extracted glucose accumulates on the surface of the gel layer and thereby block the extraction of more glucose molecules.

Table 6.2 Transdermal flux of glucose to electrodes after RI of 60 minutes with switching polarities with a glucose concentration of a) 5 mM and b) 20 mM of glucose in the diffusion cell

Glucose concentration in diffusion cell	Transdermal flux to Control electrode [ $\frac{\text{nmol}}{\text{cm}^2\text{h}}$ ]	Transdermal flux to E1 iontophoresis electrode [ $\frac{\text{nmol}}{\text{cm}^2\text{h}}$ ]	Transdermal flux to E2 iontophoresis electrode [ $\frac{\text{nmol}}{\text{cm}^2\text{h}}$ ]
5 mM	7.93 $\pm$ 0.61	13.58 $\pm$ 1.83	10.93 $\pm$ 1.55
20 mM	14.83 $\pm$ 1.15	22.44 $\pm$ 0.20	19.03 $\pm$ 3.17

### 6.3.2 RI experiments with changing duration

Figure 6.7 shows the result of changing the duration of RI with keeping the glucose concentration in the diffusion cell constant at 5 mM. From literature, it is known that acceptable levels of glucose can be extracted when applying RI for 60 minutes with switching polarities. It was shown that switching polarities when applying the iontophoretic current reduces the effect of stinging and erythema, which is caused by a direct current. But for research and comparison purposes, RI was also applied for 15 minutes with direct current and 30 minutes with direct current.

Apart from the control electrode and the two iontophoresis electrodes, which were placed on the diffusion cell, an additional electrode was used to measure the

background glucose in the gel itself. Therefore, gel was also applied on a fourth electrode and placed on the benchtop while RI was running on the diffusion cell (n=6). The gel of the fourth electrode was also collected after the duration of RI and quantified. A background glucose of an average of  $6.5 \mu\text{M} \pm 0.35$  was identified. The background glucose can be explained by the use of the gel, which was prepared with methylcellulose powder. Methylcellulose is derived of cellulose which is polysaccharide composed of chains of glucose units (Masaoka et al., 1993).

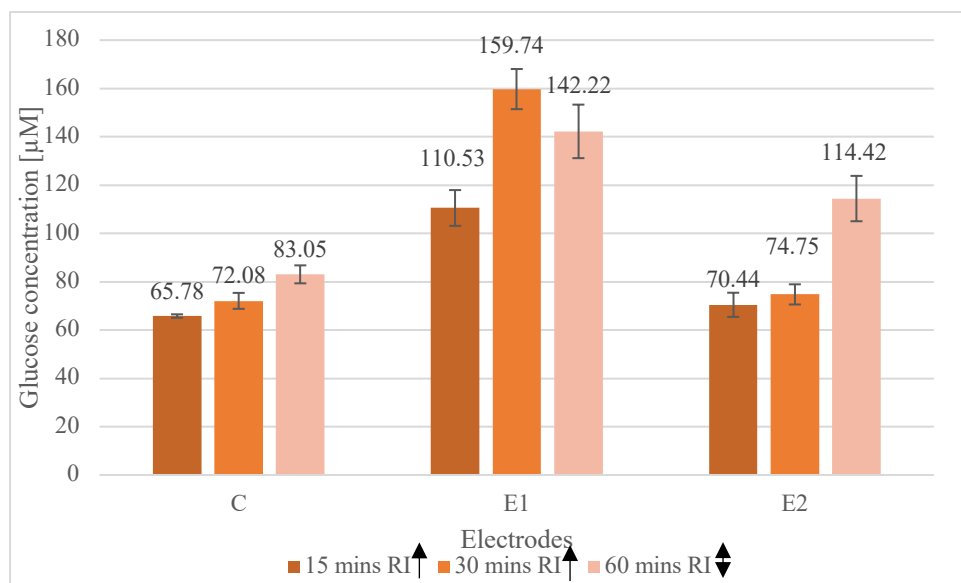


Figure 6.7 In vitro RI experiments with a glucose concentration of 5 mM in the buffer solution at three different RI durations: a) with 15 minutes of direct current (↑) b) 30 minutes of direct current (↑) and c) 60 minutes with switching polarities every 15 minutes (↕) n=3

It can be seen on Figure 6.7 that after 60 minutes of RI, more glucose ( $256.6 \mu\text{M}$ ) was extracted across both iontophoresis electrodes compared to the 15 minutes ( $180.97 \mu\text{M}$ ) and 30 minutes ( $234.49 \mu\text{M}$ ) measurement cycle. A significant increase of glucose was seen across both iontophoresis electrodes with the 60 minutes RI cycle when applying a one-way ANOVA ( $p \leq 0.05$ ). As expected the amount of glucose extracted increases with the duration of the application of the iontophoretic current. During the application of 15 minutes and 30 minutes of direct current, similar amounts of glucose was seen at the control and E2 electrode. This is due to the fact that in both cases the polarities were not switched, therefore the electroosmotic flow between the iontophoresis electrodes was only going in one direction (from the E2 to the E1 electrode). Hence, more glucose could be found at the E1 electrode. Similar amounts

were extracted at the E2 and control electrode as it was only governed by passive diffusion. However, during the application of RI for 60 minutes with switching polarities considerable more glucose was extracted at both iontophoresis electrodes compared to the control electrode. Overall, it can be seen that smaller amounts of glucose was extracted with shorter periods of RI. This is due to the fact that the movement of glucose is a time- dependent process.

On Table 6.3, the calculated glucose fluxes across each electrode with different durations of RI can be seen. The glucose flux across both iontophoresis electrodes increased from 4.32 nmol/cm<sup>2</sup>h (based on the 15 minutes of RI glucose extraction) to 11.20 nmol/cm<sup>2</sup>h (based on the 30 minutes of RI glucose extraction) to 24.51 nmol/cm<sup>2</sup>h after 60 minutes of RI. It can be seen how extraction rate does increase with time but is not proportional to duration of RI.

*Table 6.3 Calculated transdermal flux of glucose across each electrode after a) 15 minutes of RI, b) 30 minutes of RI and c) 60 minutes of RI with switching polarities with a glucose concentration of 5 mM of glucose in the diffusion cell*

<b>Duration of RI [mins]</b>	<b>Transdermal flux to Control electrode [<math>\frac{nmol}{cm^2h}</math>]</b>	<b>Transdermal flux to E1 iontophoresis electrode [<math>\frac{nmol}{cm^2h}</math>]</b>	<b>Transdermal flux to E2 iontophoresis electrode [<math>\frac{nmol}{cm^2h}</math>]</b>
15 (with direct current)	1.57 ± 0.02	2.64 ± 0.31	1.68 ± 0.05
30 (with direct current)	3.44 ± 0.27	7.63 ± 0.69	3.57 ± 0.35
60 (with switching polarities every 15 minutes)	7.93 ± 0.61	13.58 ± 1.83	10.93 ± 1.55

### 6.3.3 RI experiments comparing glucose flux through two artificial membranes

This section shows the comparison of the glucose extractions via RI using the standard membrane in the Strathclyde Laboratory (Spectrapore membrane) as reported in section 6.3.1 and 6.3.2 with an artificial skin membrane (Vitro-Skin®). The amount of glucose extracted from both membranes from a 20 mM glucose buffer solution was quantified and compared with each other. An iontophoretic current 100 µA/cm<sup>2</sup> was applied for 60 minutes of RI with switching polarities every 15 minutes. Again, three

electrodes were used for each experiment, the control electrode (C) and the RI electrodes (E1 and E2). Figure 6.8 shows glucose concentrations from the gel extractions across the two membranes, the Vitro-Skin® (blue bars) and the Spectrapore membrane (orange bars).

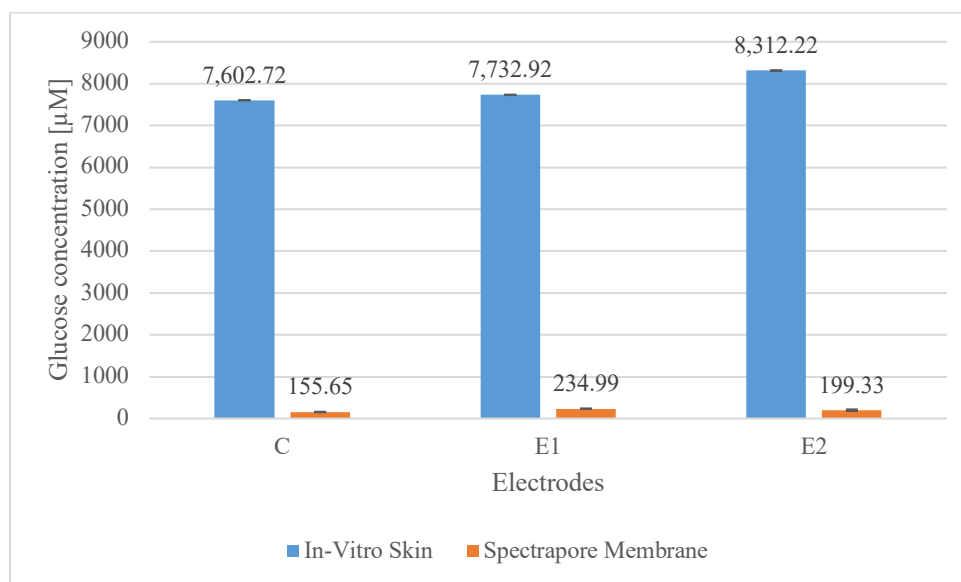


Figure 6.8 Glucose concentrations in each electrode (C, E1 and E2) from the extracted gel across the Vitro-Skin® (blue bars) with  $n=6$  and the Spectrapore membrane (orange bars) with  $n=3$ . The diffusion cell was prepared with a 20 mM glucose HEPES buffer solution and the measurement cycle was 60 minutes long with switching polarities every 15 minutes. The glucose concentrations from the extracted gel were calculated using the equation from the calibration curve.

Glucose extraction was higher at the initial cathode (E2) across the Vitro-Skin®; whereas more glucose was extracted at the initial anode (E1) when using the Spectrapore membrane. Besides, much more glucose was extracted in each of the electrodes across the Vitro-Skin® compared to the Spectrapore membrane. Extractions using the Vitro-Skin® were on average 55 times higher than with the Spectrapore membrane. More glucose extraction via the Vitro-Skin® might be due to a bigger pore size of the Vitro-Skin®. When applying an independent t-test, a significant difference was established between both iontophoresis electrodes ( $p \leq 0.05$ ).

Table 6.4 shows the summary of fluxes across each electrode using the Spectrapore membrane and the Vitro-Skin®.



Table 6.4 Transdermal flux of glucose to electrodes across Spectrapore membrane and Vitro-Skin® after 60 minutes of RI with switching polarities with a glucose concentration of 20 mM of glucose in the diffusion cell

Artificial membrane	Transdermal flux to Control electrode [ $\frac{nmol}{cm^2h}$ ]	Transdermal flux to E1 iontophoresis electrode [ $\frac{nmol}{cm^2h}$ ]	Transdermal flux to E2 iontophoresis electrode [ $\frac{nmol}{cm^2h}$ ]
Spectrapore membrane	14.83 ± 1.15	22.44 ± 0.20	19.03 ± 3.17
Vitro-Skin®	726.01 ± 40.43	738.44 ± 35.07	793.76 ± 8.97

As mentioned in Section 6.3.1 and 6.3.2, an extraction of 40.9 nmol/cm<sup>2</sup>\*h was calculated for the Spectrapore membrane across both iontophoresis electrodes with a glucose concentration of 20 mM in the diffusion cell. In contrast, for the Vitro-Skin®, a total extraction rate of 1532.2 nmol/cm<sup>2</sup>\*h was identified across both RI electrodes.

The results obtained with the Spectrapore membrane correspond well with the results obtained in other RI studies (Arias, 2011; Ching & Connolly, 2008c; Farmahan, 2008; McCormick et al., 2012) as more glucose was extracted at the initial anode and glucose was extracted in the micromolar range. As glucose was extracted in the millimolar range and more glucose was extracted in the initial cathode, which is in disagreement with other RI studies, it was concluded that the Vitro-Skin® is not suitable to mimic the human skin for RI experiments. Thus going forward, the Spectrapore remained the model skin as the Vitro-Skin® was too permeable.

## 6.4 Proof of concept of glucose adsorption to activated carbon (AC)

### 6.4.1 Adsorption of glucose to AC pellets from solutions

One of the limitations of glucose sensing in wearable sensors is the build-up of glucose in the sensor itself. Various solutions have been tried including the use of glucose oxidase in RI gel to remove the glucose (Tierney et al., 2001). In this project, a passive method to remove glucose using AC was tested. AC has adsorption characteristics to organic molecules and could therefore, act as a glucose binding agent. Thereby, it could remove excess glucose from the sensor and hence allow a more uniform transdermal glucose profile within a wearable sensor.

For the preliminary experiments, AC in pellet form was used due to fast and easy availability. The purchased AC pellets are used in aquarium filter systems for removal of contaminants such as metal ions and dyes. No product specific information such as surface area or pore size was provided. To test glucose adsorption to AC pellets, 100  $\mu\text{L}$  of a standard glucose solution sample with known glucose concentrations was incubated with one piece of an AC pellet for 60 minutes in a well of a ninety-six well microplate. The pieces of pellets lacked in uniformity and differed in size. They had the same diameter of 0.2 cm but different lengths ranging from 0.3 cm to 0.5 cm. After the incubation time, the piece of AC pellet was removed and the remaining glucose concentration in the well was measured using a colorimetric assay. Figure 6.9 shows the comparison of the standard glucose samples with a concentration of 500  $\mu\text{M}$  without incubation with AC pellets (blue bar) against the samples with the same glucose concentration with incubation of AC pellets for 60 minutes (green bar). The calibration curve acquired from the plate reader using the Randox enzyme kit was used to quantify the adsorbed glucose.

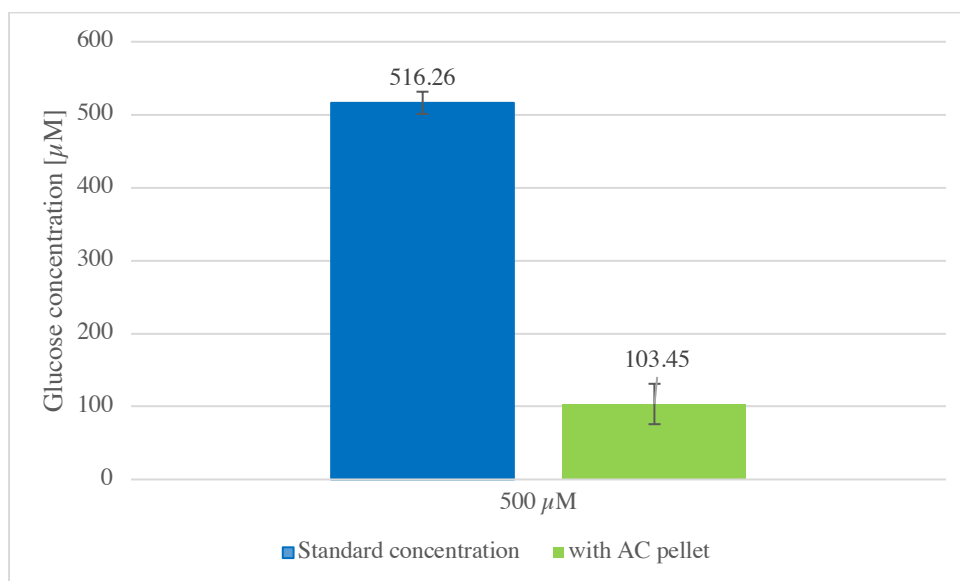


Figure 6.9 Glucose measured in the remaining solution after an incubation time of 1 hour of the standard sample with a glucose concentration of 500  $\mu\text{M}$  with AC pellets (green bar) ( $n=38$ ) in comparison to the standard concentration of 500  $\mu\text{M}$  (blue bar) ( $n=9$ ). The error bars represent the standard deviation.

The remaining concentrations from the 500  $\mu\text{M}$  glucose sample varied from 56.43  $\mu\text{M}$  up to 158.67  $\mu\text{M}$  with an average of 103.45  $\mu\text{M}$ . This corresponds to a glucose adsorption of 79.88 %  $\pm$  5.35 from the initial glucose concentration of 500  $\mu\text{M}$ . A

significant difference was established between the samples with AC and without AC ( $p > 0.05$ ) when applying the independent t-test.

Based on Figure 6.9, it can be said that glucose adsorption took place but the exact relationship between AC and glucose adsorption from the applied experimental setup cannot be determined yet as the concentrations vary too much. However, the adsorption of glucose per gram of AC pellet was calculated by dividing the amount of the quantified glucose by the initial dry weight of the AC pellet. 18.38 mM of glucose with a standard deviation of  $\pm 5.04$  mM was adsorbed per one gram of AC pellet. This has helped to get a rough idea of how much glucose had been adsorbed.

### 6.4.2 Adsorption of glucose to AC foam from solutions

The pellets used in the previous experiments, are manufactured for removal of contaminants in aquariums and lack in uniformity. Using uniformly shaped AC, gives the possibility to repeat and compare the results. Hence, the quality of the pellet was not suitable for this research purpose. In addition, the aim of this project is to ultimately integrate AC in glucose biosensors so that a better controlled and improved glucose flux within iontophoresis devices can be achieved. Therefore, another challenge with AC pellets was the practical difficulty to integrate it into the sensor to perform RI *in vitro* experiments. Consequently, AC foam, an alternative form of AC was tested to be used in this project. The AC foam purchased was intended for odour removal from compost caddies. There was no information regarding pore size or surface area.

This section shows the results of the experiments of glucose adsorption onto AC foam. The glucose adsorption experiments using AC pellets and a ninety-six well plate were repeated with the AC foam. Glucose solution samples with a concentration of 500  $\mu\text{M}$  were incubated with one piece of AC foam for 60 minutes. One piece of AC had a disc like shape with a diameter of 0.6 cm and a thickness of 0.1 cm, which is referred to as one unit of AC foam from here onwards (Figure 6.10).

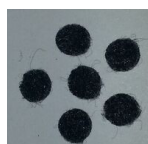


Figure 6.10 Examples of disc-shaped AC foam, which were used for the adsorption experiments

Figure 6.11 illustrates the comparison between standard concentration of 500  $\mu\text{M}$  without incubation of AC foam (blue bar) and the remaining concentrations after incubation of AC foam for 60 minutes (orange bar).

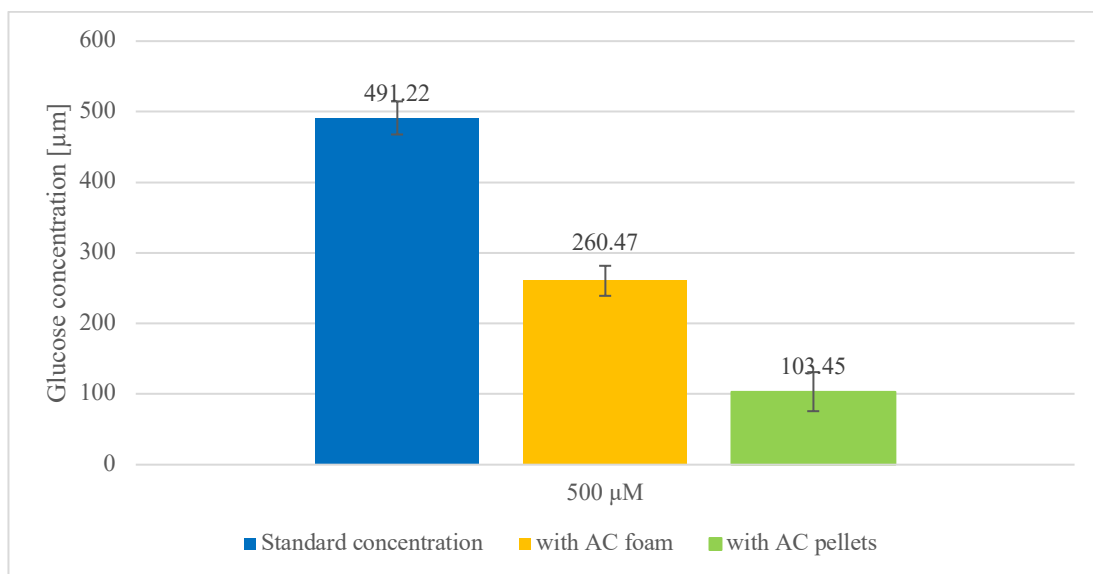


Figure 6.11 Glucose measured in the remaining solution after an incubation time of 1 hour of the standard sample with a glucose concentration of 500  $\mu\text{M}$  with one unit of AC foam (orange bar) ( $n=61$ ) in comparison with the standard solutions (blue bar) ( $n=17$ ) and the results shown in Figure 6.9, the remaining glucose concentration after an incubation time of 1 hour of the standard sample with a glucose concentration of 500  $\mu\text{M}$  with AC pellets. The error bars represent the standard deviation.

The remaining glucose concentration of the samples with the initial glucose concentration of 500  $\mu\text{M}$  vary from 223.56  $\mu\text{M}$  to 299.73  $\mu\text{M}$ , with an average of 260.47  $\mu\text{M}$ . On average 46.97 %  $\pm$  4.33 of the initial glucose concentrations was adsorbed after the incubation with one unit of AC foam. Glucose adsorption of 30.17 mM  $\pm$  5.97 by one gram of AC foam was identified. When applying the independent-sample t- test significant difference was identified for the 500  $\mu\text{M}$  glucose samples with and without AC foam ( $p<0.05$ ).

Comparison between AC pellets and AC foam:

- On Figure 6.12 the average of the initial dry weight of the used AC pellets and used AC foams are presented for comparison. It can be seen that the used AC pellets have a higher initial weight as well as a higher standard deviation compared the AC foam. A significant difference was seen between both groups ( $p < 0.05$ ) when applying the independent t-test.

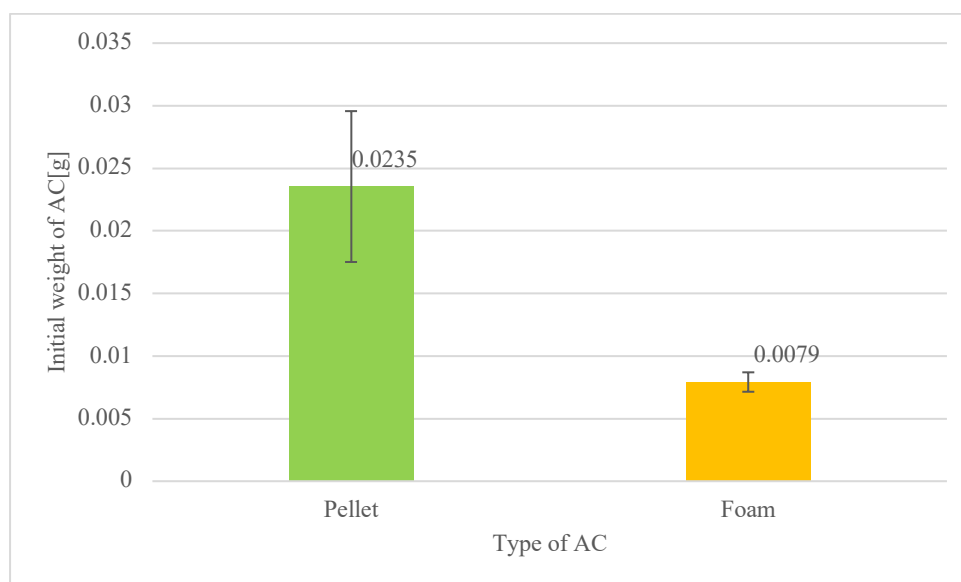


Figure 6.12 Average initial dry weight of used AC pellets (green bar) with  $n=78$  and AC foam (orange bar) with  $n=130$ . The error bars represent the standard deviation.

- The wet weight of the AC pellet and AC foam was also measured after the incubation with the glucose solution samples and is illustrated in Figure 6.13. On average a higher wet-weight of the AC foam is observable indicating that the AC foam has a higher capacity to absorb fluids compared to AC pellets.

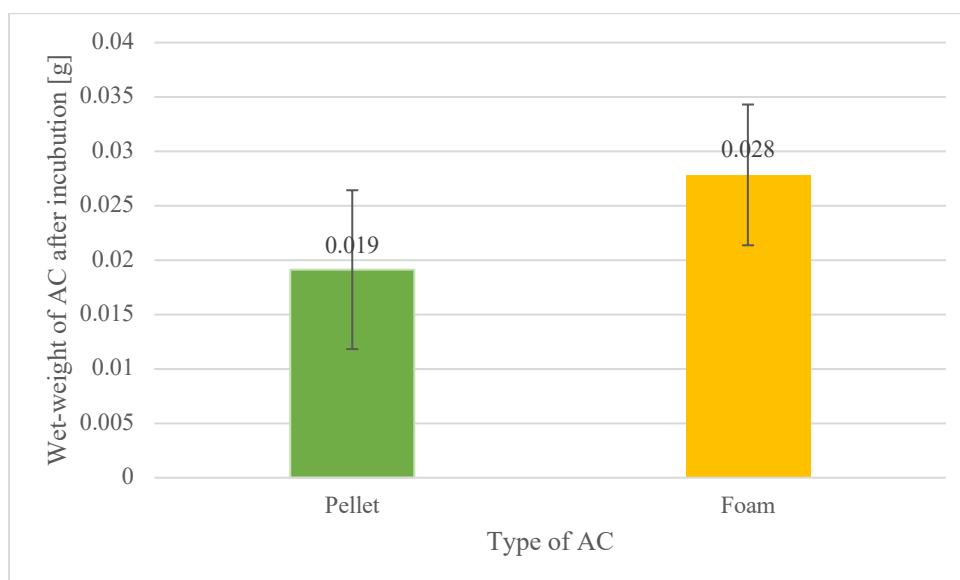


Figure 6.13 Increase of weight of the AC pellet (green bar) with  $n=38$  and AC foam (orange bar) with  $n=28$  after incubation with the glucose sample with a concentration of and  $500 \mu\text{M}$ . The error bars represent the standard deviation.

- At the same time a higher decrease of sample volume was observable after 60 minutes of incubation with the AC foam. The sample volume decreased from  $100 \mu\text{L}$  to approximately  $75 \mu\text{L}$  after the incubation with AC pellet. And after the incubation with AC foam, the sample volume decreased from  $100 \mu\text{L}$  to on average of  $60 \mu\text{L}$  after 60 minutes of incubation.
- The density of the AC pellet and the AC foam was calculated with the following equation  $\delta \left[ \frac{\text{g}}{\text{cm}^3} \right] = \frac{\text{Mass}[\text{g}]}{\text{Volume}[\text{cm}^3]}$ . Due to practical difficulties to identify the exact volume of the AC pellet and the AC foam with the porous structure, the volume was approximated by considering both as cylinders and using the following equation:  $V = \pi \cdot r^2 \cdot h$ . The AC pellet had radius of  $0.1 \text{ cm}$  and an average length of  $0.4 \text{ cm}$  and the AC foam had a radius of  $0.3 \text{ cm}$  and a thickness of  $0.1 \text{ cm}$ . Based on the before- mentioned assumptions, the AC pellet had a volume of  $0.013 \text{ cm}^3$  and a density of  $1.87 \frac{\text{g}}{\text{cm}^3}$ . In contrast, the AC foam had a volume of  $0.028 \text{ cm}^3$  and density  $0.28 \frac{\text{g}}{\text{cm}^3}$ . The AC pellets have a higher density compared to AC foam based on these calculations.
- Comparing the amount adsorbed from the initially  $500 \mu\text{M}$  glucose sample by AC pellets and AC foam, more glucose was adsorbed by the AC pellet ( $79.88 \% \pm 5.35$ ) than the AC foam ( $46.97 \% \pm 4.33$ ). Higher adsorption by the

AC pellet can be explained by higher initial weight in combination with the higher density of the AC pellet.

- Glucose adsorption by one gram of AC pellet respectively foam was established.  $18.38 \text{ mM} \pm 5.04$  of glucose can be adsorbed by one gram of AC pellets whereas  $30.17 \text{ mM} \pm 5.97$  of glucose can be adsorbed by AC foam. This indicates that one gram of AC foam adsorbed more glucose than one gram of AC pellet.
- To be able to compare the results, it is of advantage that the same amount of AC is involved in each experiment. The initial weights of the AC foam show less variability and hence, would be better suited in this aspect. When comparing the amount adsorbed by AC pellet and AC foam, a lower standard deviation for the AC foam was observable.
- For this project, the aim is to ultimately integrate the AC in glucose biosensor. Having less variation in the initial weight of the AC foam, will allow better uniformity and repeatability of the sensors, and hence enable better comparison of the results.
- Therefore, AC foam form was used for future AC experiments.

More experiments were conducted using the AC foam to investigate glucose adsorption with 1) increasing the initial glucose concentration in the sample (from  $3.9 \text{ }\mu\text{M}$  to  $1000 \text{ }\mu\text{M}$ ) and 2) increasing the amount of AC involved (using two units of AC foam in the same well of the ninety-six well plate instead of one.)

Figure 6.14 shows the remaining glucose concentration with respect to the initial glucose concentrations ranging from  $3.9 \text{ }\mu\text{M}$  to  $1000 \text{ }\mu\text{M}$  after an incubation with one (orange dots) respectively two units of AC foam (red triangles) for 60 minutes.

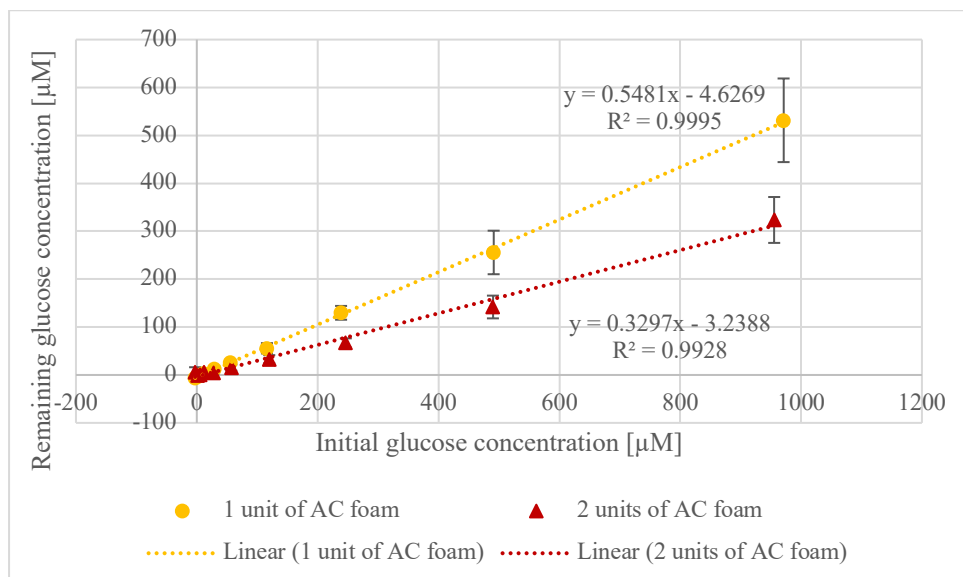


Figure 6.14 Initial glucose concentration in the glucose sample versus the remaining glucose concentration after an incubation time of 60 minutes with one unit of AC foam (orange dots) and two units of AC foam (red triangles). The error bars represent the standard deviation.

Following observations were made:

- (1) A linear relationship was observable when plotting initial glucose concentration of the sample against the remaining glucose concentration when using one respectively two units of AC foam. It can be seen that the higher the initial glucose concentration in the sample, the more glucose was adsorbed to the AC foam.
- (2) More glucose is adsorbed when increasing the amount of AC in the experiment. From the initial glucose concentration of approximately 960 µM, after an incubation of 60 minutes with one unit of AC foam, 532 µM of the glucose concentration was remaining. In contrast only 324 µM was remaining after incubating the sample with two units of AC foam.

Figure 6.15 shows the amount of glucose adsorbed per one gram of AC against the remaining glucose concentration using 1) one unit of AC (orange dots) and 2) two units of AC foam (red triangles). Figure 6.14 gives information about the type of adsorption isotherm occurring in the adsorption of glucose to AC.



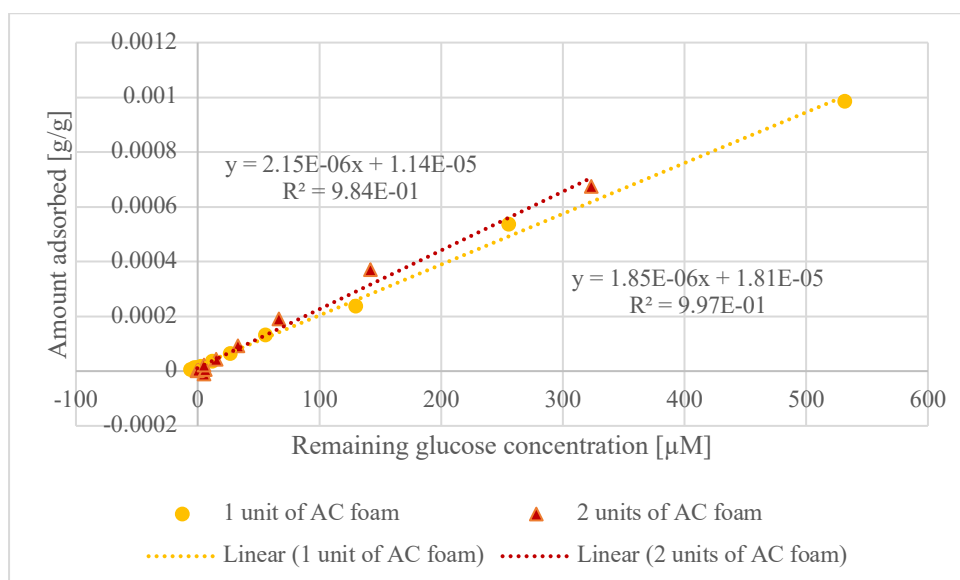


Figure 6.15 Remaining glucose concentration after the incubation of the sample with one unit of AC foam (orange dots) and two units of AC foam (red triangles) for 60 minutes in relationship with the amount of glucose adsorbed by one gram of AC foam.

A linear relationship could be established between the remaining glucose concentration and the amount of glucose adsorbed per one gram of AC foam, which indicates a linear adsorption theorem in the tested glucose concentration range. A similar gradient ( $\pm 0.29 \cdot 10^{-6}$ ) was found for the curve established with one unit of AC foam and two units of AC foam. This indicates that the adsorption by one gram of AC is in agreement using one unit of AC foam and two units of AC foam.

### 6.4.3 Glucose adsorption to AC foam from glucose gel samples

Glucose adsorption experiments were repeated using glucose concentrations in gel format as gel samples are ultimately used for RI experiments. Therefore, glucose samples in gel format with different glucose concentrations ranging from 3.5 μM to 900 μM were incubated with one unit of AC foam for a time period of 60 minutes. Figure 6.16 shows the remaining glucose concentration against the initial glucose concentration. A linear relationship was observable for glucose gel samples.

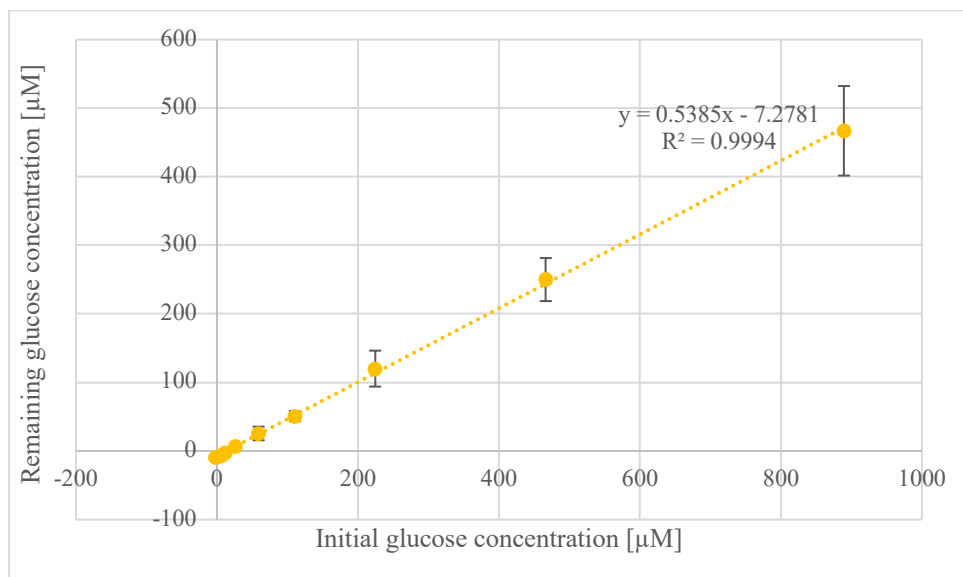


Figure 6.16 Initial glucose concentration in the glucose gel sample versus the remaining glucose concentration after an incubation time of 60 minutes with one unit of AC foam. The error bars represent the standard deviation

The gradient of 0.5385 obtained from the curve in Figure 6.16 is similar to the gradient 0.5481 obtained with the glucose solutions using one unit of AC in Figure 6.14. This indicates that the adsorption process of glucose was not majorly affecting by the changing the glucose solution samples to glucose gel samples.

Figure 6.17 shows the amount of glucose adsorbed by one gram of AC against the remaining glucose concentration. A linear relationship was also observable when one unit of AC foam and glucose samples in gel format was used, again indicating a linear adsorption isotherm.

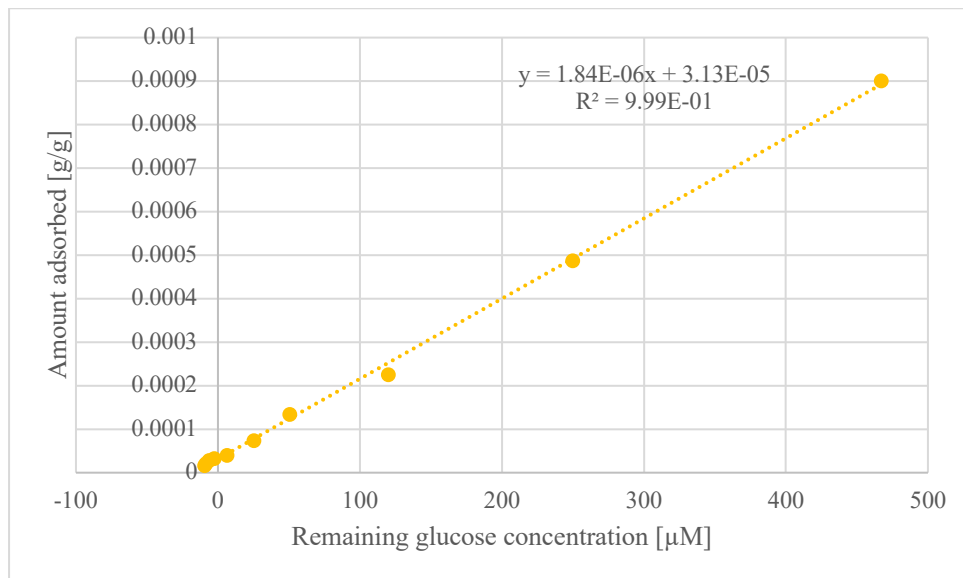


Figure 6.17 Remaining gel glucose concentration after the incubation of the sample with one unit of AC foam for 60 minutes in relationship with the amount of glucose adsorbed by one gram of AC foam.

Comparing the gradients from the experiments with glucose solution ( $1.85 \times 10^{-6}$ ) and glucose gel ( $1.84 \times 10^{-6}$ ), a similar gradient was established. This indicates that using gel only has a low impact on the adsorption process to AC.

#### 6.4.4 Glucose adsorption profile to AC foam over time

The time diffusion profile of glucose into AC foam was investigated using the highest concentration of the tested glucose concentration range. One glucose solution sample with a glucose concentration of 1000 µM and one glucose gel samples with a glucose concentration of 900 µM were used to study adsorption profiles over time.

The adsorption time profile of a glucose solution with an initial concentration of 1000 uM is observable in Figure 6.18. On the x-axis the time incubated with the AC foam is applied. And on the y-axis the amount adsorbed by one gram of AC foam is applied. Measurements were taken every 10 minutes up to 80 minutes of incubation time.

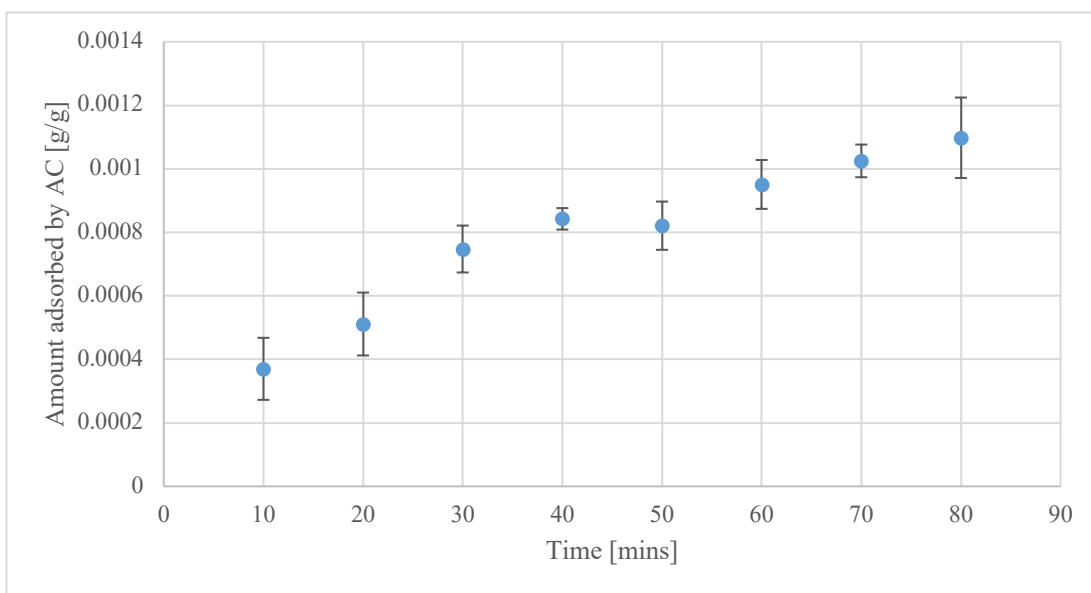


Figure 6.18 Adsorption time profile of a 1000  $\mu\text{M}$  glucose sample on AC foam.

The  $R^2$ -values of the applied straight-line fits were used to assess the best linear curve fitting range to determine the linear time period of the adsorption profile. Straight line fits were applied over the time period between 10 minutes and 60 minutes, 10 minutes and 70 minutes and 10 minutes and 80 minutes. The straight line fit applied from 10 minutes to 80 minutes was identified to have the highest  $R^2$ -value with 0.93, indicating the incubation time of 80 minutes provides the best adsorption results with glucose solutions in the given time scale. The linear relation can be expressed with:  $y = 9.82 \cdot 10^{-6} + 0.00035$ .

The adsorption time profile of a glucose gel sample with an initial concentration of 900  $\mu\text{M}$  is observable in Figure 6.19.

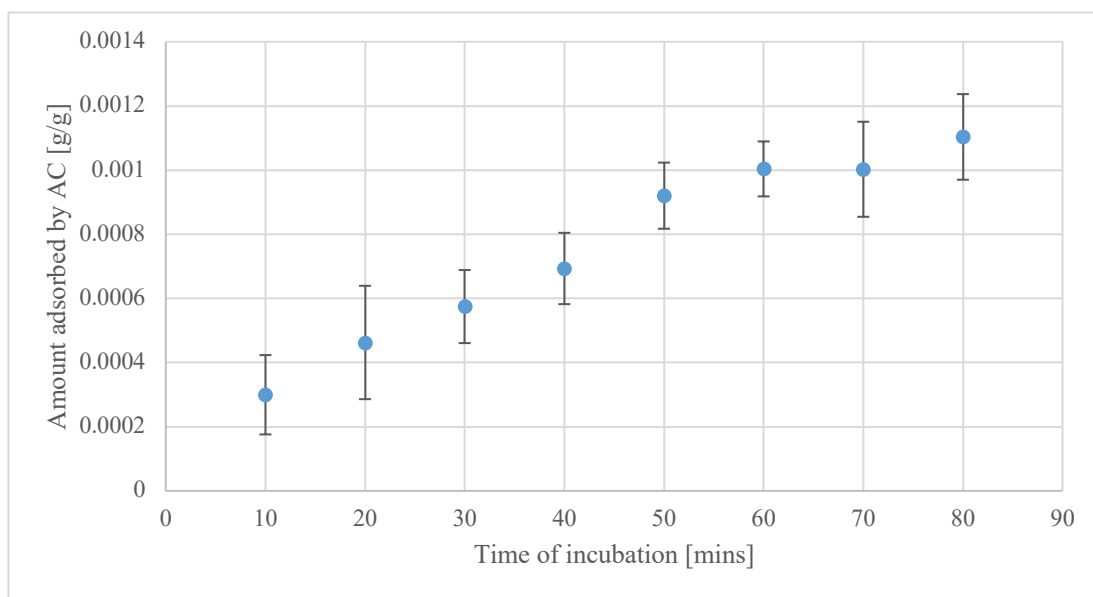


Figure 6.19 Adsorption time profile of a 900  $\mu\text{M}$  glucose sample on AC foam.

The time diffusion profile of glucose in gel format showed similar behaviour. Again, the  $R^2$ -values of the applied straight-line fits were used to assess the best linear curve fitting range to determine the linear time period of the adsorption profile before it settles down. The straight line fit applied from 10 minutes to 60 minutes was identified to have the highest  $R^2$ -value with 0.99, indicating the incubation time of 60 minutes provides the best adsorption results with glucose gel sample in the given time scale. The linear relation can be expressed with the following equation:  
 $y = 1.43 \times 10^{-6}x + 0.00016$

The diffusion rate was estimated with the following assumptions:

- As mentioned, due to practical difficulties to identify the exact volume of the AC foam with the porous structure, the volume of the AC foam was only estimated to have a cylindrical volume with a radius of 0.3 cm and a thickness of 0.1 cm.
- The adsorbed glucose was calculated by deducting the remaining concentrations after the incubation with AC foam from the initial glucose concentration in the sample with the consideration that all of it was adsorbed by the AC foam.
- The area of the diffusion profile was calculated with  $A = r^2 * \pi$  (with  $r = 0.3$  cm)

Table 6.5 shows the flux of glucose over time in solution and gel samples calculated based on the above-mentioned assumptions.

Table 6.5 Calculated glucose flux across glucose solution and glucose gel sample to AC foam

Time of diffusion [mins]	Flux across glucose solution samples to AC foam [ $\frac{nmol}{cm^2h}$ ]	Flux across glucose gel samples to AC foam [ $\frac{nmol}{cm^2h}$ ]
10	117.51	90.91
20	79.46	66.43
30	76.82	55.12
40	60.55	53.48
50	50.62	56.53
60	50.45	51.62
70	44.29	42.83
80	39.95	40.00

Initially (up to 40 minutes of incubation), a higher glucose flux is observable across solution samples. However, after 50 minutes of diffusion, gel samples speed up and after 60 minutes the diffusion rate of solution and gel samples are similar to each other ( $\pm 1.17 \frac{nmol}{cm^2h}$ ). This could be the reason why a similar gradient was found between the glucose adsorption experiments for glucose solution samples and glucose gel samples (Figure 6.15 and Figure 6.17)

#### 6.4.5 Impact of glucose adsorption to AC to sample volume

During the glucose adsorption experiments to AC, a decrease in the sample volume of 100  $\mu$ L after the incubation with AC for 60 minutes was observable. Therefore, the decrease of sample volume of the glucose solution and glucose gel samples over time was investigated (with incubating the sample with one unit of AC foam) and can be seen in Figure 6.20.

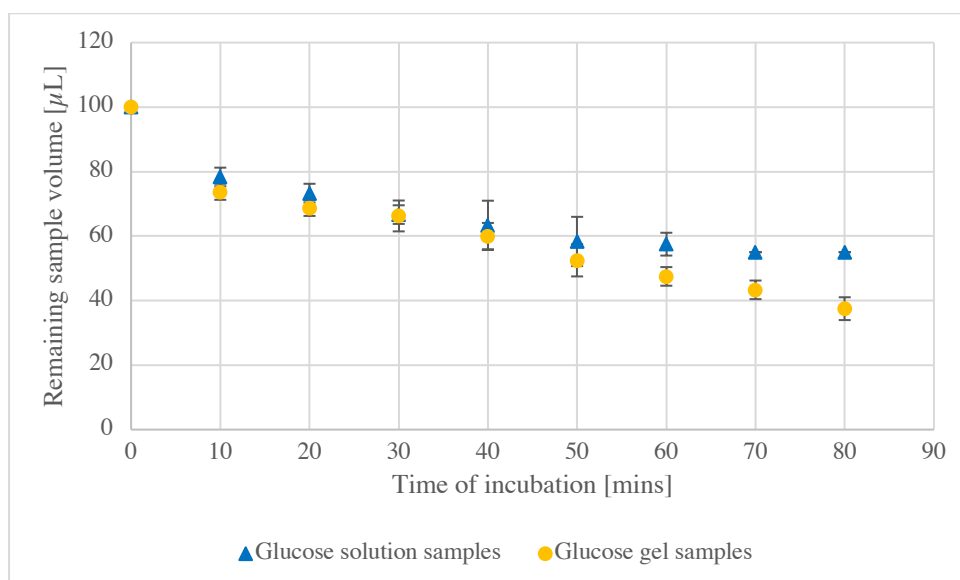


Figure 6.20 Remaining sample volume of the glucose solution samples with  $n=3$  (blue triangles) and of the glucose gel samples with  $n=3$  (orange dots) after the incubation with AC foam over a time period of 80 minutes.

It was observable that after an incubation time of 60 minutes with one unit of AC foam, only 60  $\mu\text{L}$  of the glucose solution sample was left. In contrast after an incubation time of one hour with AC foam with glucose gel samples, only 50  $\mu\text{L}$  of the initial volume was present.

#### 6.4.6 RI experiments with AC foam

The concept of glucose adsorption to AC foam was successfully proven with the previous experiments. Next, the AC foam was integrated in the electrode system used for RI experiments using the *in vitro* system. The extracted glucose was then quantified using a colorimetric assay and compared to RI experiments using electrodes without AC.

Figure 6.21 shows the amount of glucose extracted after applying RI for 60 minutes with switching polarities every 15 minutes. A buffer with 20 mM glucose concentration was used simulating the interstitial fluid. The blue bars indicate the amount of glucose extracted using sensors without AC and the yellow bars represent the results using the sensors with AC.

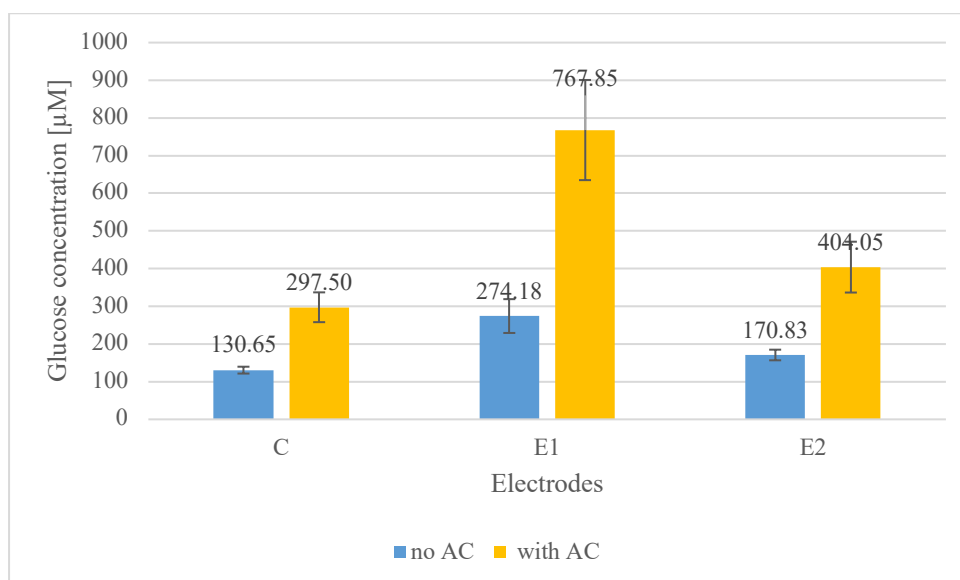


Figure 6.21 Glucose concentrations in each electrode (C, E1 and E2) from the extracted gel across the Spectrapore membrane using electrodes without AC (blue bars) and with AC (yellow bars). The diffusion cell was prepared with a 20 mM glucose HEPES buffer solution and the measurement cycle was 60 minutes long with switching polarities every 15 minutes. The glucose concentrations from the extracted gel were calculated using the equation from the calibration curve. The error bars represent the standard error.  $n=7$ .

It can be seen than more glucose was extracted with the sensors with the AC foam (Figure 6.21). As expected, glucose was extracted at the most at the E1 electrode (the initial anode) in both electrode groups, the electrodes without AC (274.18 µM) and also the electrodes with AC (767.85 µM). And the least amount of glucose was extracted in the control electrodes (130.65 µM respectively 297.50 µM), as the only transport mechanism involved for this electrode is passive diffusion. The E2 electrode extracted 170.83 µM in the electrodes without AC foam respectively 404.05 µM with AC foam. The Mann Whitney U test was applied to each type of electrode to test the differences between the sensors with AC and without AC. A significant difference was established with  $p \leq 0.05$  for all three electrodes.

Table 6.6 gives a summary of the fluxes across each electrode using the sensors with AC foam and without AC foam.



Table 6.6 Transdermal fluxes across the Spectrapore membrane using sensor without AC foam and with AC foam

Type of sensor	Transdermal flux to Control electrode $\left[\frac{\text{nmol}}{\text{cm}^2\text{h}}\right]$	Transdermal flux to E1 iontophoresis electrode $\left[\frac{\text{nmol}}{\text{cm}^2\text{h}}\right]$	Transdermal flux to E2 iontophoresis electrode $\left[\frac{\text{nmol}}{\text{cm}^2\text{h}}\right]$
Without AC foam	12.48 ± 0.87	26.18 ± 4.29	16.31 ± 1.35
With AC foam	28.41 ± 3.78	73.32 ± 12.69	38.58 ± 6.44

An increase of glucose flux between the electrodes with and without glucose is evident. The flux increased by a factor of 2.28 across the control electrodes, by a factor of 2.80 across the E1 electrodes and by a factor of 2.37 across the E2 electrodes. However, a higher standard error can also be seen with the integrated AC sensors. It was shown that AC has good potential to act as a glucose binding agent and allow an improved transdermal glucose profile within a wearable sensor.

## 6.5 Preliminary cyclic voltammetry (CV) results

This section shows the results of the experiments conducted to investigate electrochemical glucose detection using glucose sensors. In the previous experiments, glucose extracted via RI was quantified with standard laboratory means using colorimetric assays and an optical spectrophotometer. Integrating a biosensing unit in the electrode system, would allow *in situ* glucose quantification.

Experiments were conducted with a screen printed three-electrodes design shown in section 5.5.1 with an Ag/AgCl reference electrode. The means of CV was used to study the electrochemical glucose detection method. Preliminary experiments were carried out to understand the fundamentals of CV, the electrochemical characteristics of a mediator on its own and also the interaction between mediator and enzyme in the liquid environment. The procedure outlined in 5.9.1 was followed to perform the preliminary CV experiments.

As discussed, the preliminary experiments were conducted with a different ferrocene derivative than used in the glucose sensor. Ferrocenemonocarboxylic acid (FMCA) was used as a mediator as it was already available for use in the laboratory.

### 6.5.1 Study of electrochemical behaviour of FMCA

Figure 6.22 shows the CV of 0.5 mM FMCA in PBS with ethanol and sodium perchlorate as a supporting electrolyte at different scan rates (10 mV/s, 50 mV/s and 100 mV/s). The potential was swept between -0.1V and 0.5 V.

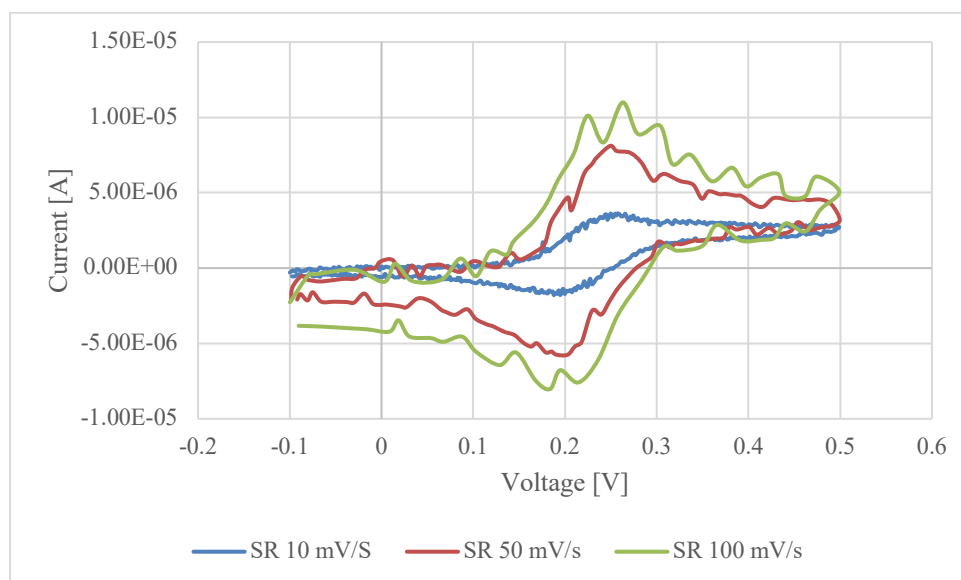


Figure 6.22 CV of 0.5 mM FMCA in PBS with ethanol and sodium perchlorate at different scan rates 10 mV/s (blue), 50 mV/s (red) and 100 mV/s (green)

From -0.1 V to approximately +0.12 V, only a non-faradaic capacitive current is observable due to the electrode double layer. At higher potential, an increase in the current can be seen as the potential is sufficiently positive to oxidise FMCA to FMCA<sup>+</sup>. The faradaic current continues to increase until FMCA gets fully depleted on the electrode surface causing a current peak ( $I_{pa}$ ) at an anodic peak potential of 0.256 V. Subsequently, a decrease in the current can be seen as the concentration of the FMCA diminishes from the surrounding of the electrode surface and as the rate of oxidation occurs faster than the mass transport of the analyte from the bulk solution to the electrode surface. At the same time an increase of FMCA<sup>+</sup> concentration at the electrode surface occurs. The reverse scan begins at the voltage of +0.5 V and gradually decreases. Once the potential is sufficiently negative to reduce FMCA<sup>+</sup> to FMCA, the cathodic current starts flowing until the concentration of the FMCA<sup>+</sup> is depleted in the vicinity of the electrode surface and a cathodic current peak ( $I_{pc}$ ) is

produced at the cathodic peak potential of 0.195 V. After that the current decays, as there is no more FMCA<sup>+</sup> in the surrounding of the electrode surface.

The noise in the voltammograms (Figure 6.22) can be explained by the initially used curing method of the screen- printed electrodes. Initially the electrodes were cured at a temperature of 70 °C for 20 minutes. This method was taken from the previous Medical Devices group at Strathclyde. However, with this method high resistance values for the screen- printed electrodes and no clean signal were measured, and improvement was needed. Therefore, the curing process was adapted and changed to 120 °C for 15 minutes as described in Section 5.5.3. This method was recommended from the manufacturer of the ink (Henkel Corporation, 2013), which has led to lower resistance values and an improvement in the noise level was observable (see Figure 6.25).

The reversibility of electron transfer of FMCA was analysed by testing its compliance with the requirements for a reversible system, which were discussed in the section 4.3.4.

An anodic peak was identified at a voltage of 0.256 V and a cathodic peak at 0.195 V. Thus, a peak separation of 0.061 V was calculated. The second characteristic states that the ratio between anodic peak current and cathodic peak current should equal to 1. To test the second requirement, first the capacitive current had to be identified and deducted from the peak current to determine the current solely caused by the electron transfer. This was done by following Kissinger's method and extrapolating the baseline current (see Figure 6.23) (Kissinger & Heineman, 1983).

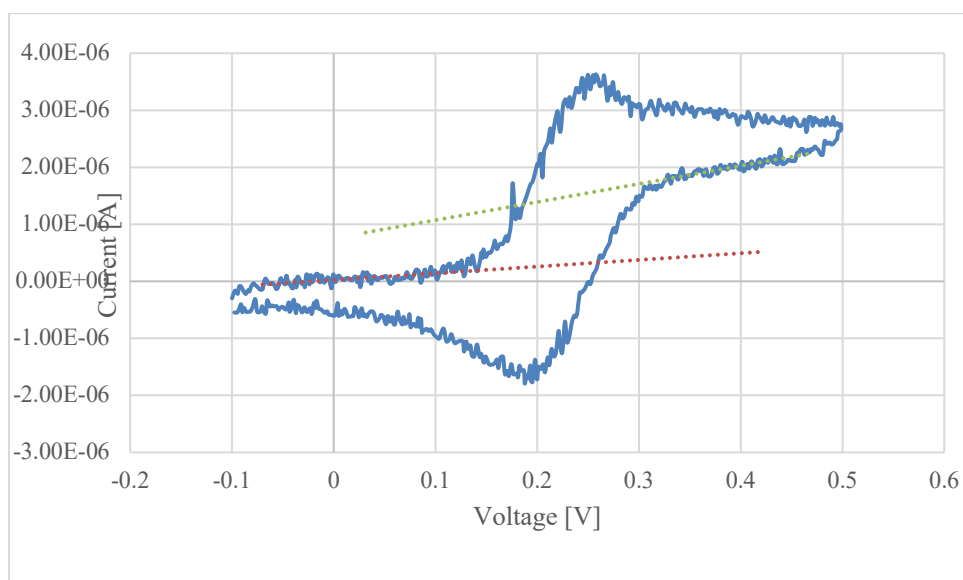


Figure 6.23 CV of 0.5 mM FMCA in PBS and sodium perchlorate with applied tangent indicating the extrapolation of the baseline current to identify capacitive current.

An anodic peak current of  $3.16 \times 10^{-6}$  A and a cathodic peak current of  $3.12 \times 10^{-6}$  A was identified at a scan rate of 10 mV/s, which provides us with a ratio of 1.01.

$$\frac{3.16 \times 10^{-6}}{3.12 \times 10^{-6}} = 1.01$$

The third rule for reversibility was tested by plotting the peak current versus the square root of the SR (Figure 6.24).

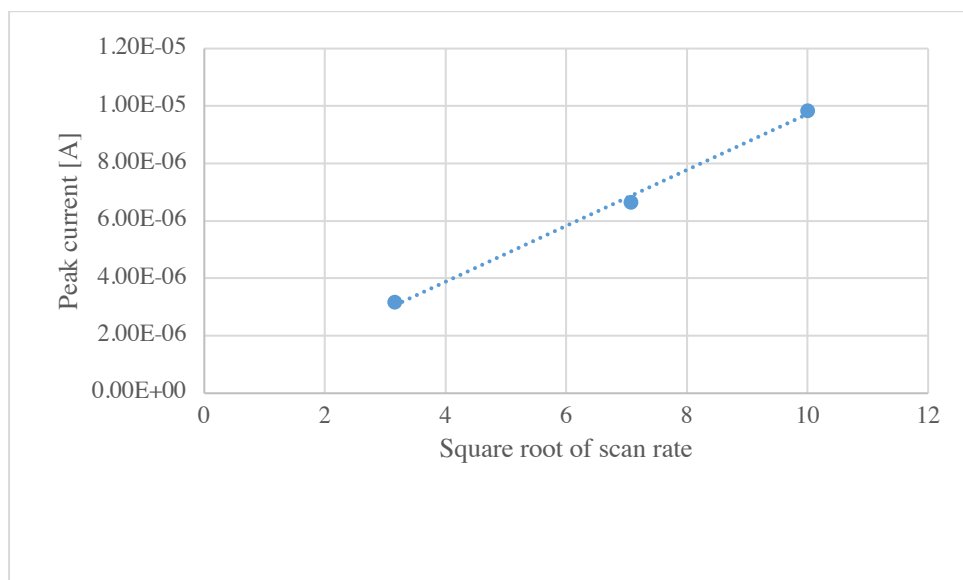


Figure 6.24 Relationship between scan rate and peak current of the 0.5 mM FMCA in PBS and sodium perchlorate

A linear relationship between the peak current and the square root of the SR can be seen. The applied straight-line fit can be described with  $y=9.73*10^{-7}x - 8.74*10^{-9}$  and an  $R^2=0.997$ .

As expected from literature, a reversible one electron transfer of FMCA could be confirmed in this experiment.

Calculation of the diffusion coefficient of FMCA:

As FMCA undergoes a one-electron transfer, Randles Sevcik equation was applied to calculate the diffusion coefficient of FMCA:

$$I_{pc} = 0.446 * n * F * A * c \left( \frac{n * F * SR * D}{R * T} \right)^{1/2}$$

Randles Sevcik equation was rearranged to express the diffusion coefficient ( $D$ ) and the parameters shown in Table 6.7 were inserted into the equation.

Table 6.7 Parameters used to calculate the glucose diffusion coefficient of FMCA

<b>I<sub>p</sub> [A]</b>	<b>n</b>	<b>F [C/mol]</b>	<b>A [cm<sup>2</sup>]</b>	<b>C [mol/cm<sup>3</sup>]</b>	<b>SR [V/s]</b>	<b>R [J/K*mol]</b>	<b>T [K]</b>	<b>D [cm<sup>2</sup>/s]</b>
3.16*10 <sup>-6</sup>	1	96500	0.12	5*10 <sup>-7</sup>	0.010	8.3145	293	3.79*10 <sup>-6</sup>

A diffusion coefficient of  $3.79 * 10^{-6} \text{ cm}^2/\text{s}$  was calculated for FMCA in PBS with ethanol and sodium perchlorate.

## 6.5.2 Mediator – enzyme interaction in free solution

In this study the aim was to ultimately integrate a ferrocene-mediated enzyme electrode in the electrode design for *in situ* glucose detection. In a mediated enzymatic reaction, the mediator is used as an electron acceptor from the enzyme. At the application of a specific potential, the mediator is re-oxidised. The current produced at heterogenous electron transfer is related to the analyte concentration.

This experiment was conducted to understand the electrochemical interaction of a mediator in the presence of glucose and upon the addition of the enzyme in the liquid environment. Figure 6.25a shows the CV obtained with 0.5 mM FMCA in the presence

of 50 mM glucose and upon the addition of the glucose oxidase (Figure 6.25b) at a scan rate of 1 mV/s. The potential was swept from 0 V to 0.5 V.

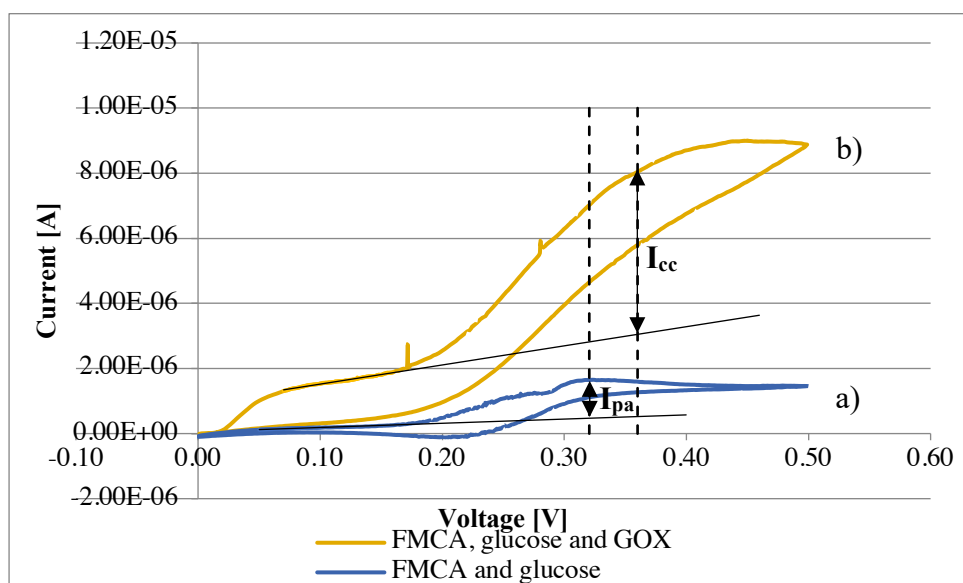


Figure 6.25 a) CV of FMCA in PBS buffer with 50 mM glucose (blue) and b) upon addition of 10.9  $\mu\text{M}$  of GOD (orange) at a scan rate of 1 mV/s with diffusion current of FMCA ( $I_{pa}$ ) and the catalytic current ( $I_{cc}$ ) upon the addition of GOD

In the absence of the glucose oxidase, the oxidation and reduction of FMCA can be seen in Figure 6.25a. An anodic peak potential of 0.32 V and a cathodic peak potential of 0.21 V was identified, which leads to a peak separation of 0.11 V. As the reversibility of FMCA was already confirmed in the previous experiment shown in section 6.5.1, it was surprising to see a high peak-to-peak separation, which is indicative of an irreversible electron transfer. The reversibility of FMCA might have been affected in this experiment by the slow scan rate. Or the higher peak current separation could be due to the fact that no supporting electrolyte was used in this experiment. A supporting electrolyte improves the solution conductivity and without it, it causes the solution to be more resistive. Therefore, a higher overpotential is needed to drive the same amount of current to facilitate the electron transfer, which can be reflected in the CV by a larger peak-to-peak separation (Compton et al., 2012a). An oxidation peak current of  $1.18 \times 10^{-6}$  A and a reduction peak current of  $1.21 \times 10^{-6}$  A was found, thus providing us with a ratio of 0.97. This ratio is in close agreement with the ratio of 1, which would be expected in a reversible system.

A diffusion coefficient of  $5.28 \times 10^{-6}$   $\text{cm}^2/\text{s}$  was calculated for FMCA using Randles-Sevcik equation.

Upon the addition of the glucose oxidase, an increase in the catalytic current ( $I_{cc}$ ) is observable starting at oxidising potential of FMCA (approximately 0.15 V). This electrocatalytic response was initiated by the oxidation of glucose, which was catalysed by GOD. This catalytic current is indicative of the regeneration of the FMCA from the reaction of  $FMCA^+$  with the reduced form of the GOD (Cass et al., 1984).

The diffusion current of FMCA ( $I_{pa}$ ) was identified as  $1.18 \times 10^{-6}$  A at the anodic peak voltage of 0.32 V in the absence of GOD. A catalytic current ( $I_{cc}$ ) of  $5.74 \times 10^{-6}$  A at a potential of 0.36 V in the presence of GOD.

This experiment shows the efficiency of the mediator to shuttle electrons between the electrode and the enzyme.

### 6.5.3 Testing screen printed Ag/AgCl reference electrode vs standard 3M Ag/AgCl electrode

The potential of the screen-printed electrode (SPE) with respect to a standard glass electrode (SE) 3M Ag/AgCl reference electrode in different buffers is illustrated in Figure 6.26. It was tested in 0.1 M phosphate buffer solution and in 3% w/v of methylcellulose gel. This experiment was conducted to see if the gel has enough chloride ions to support the screen-printed Ag/AgCl electrodes.

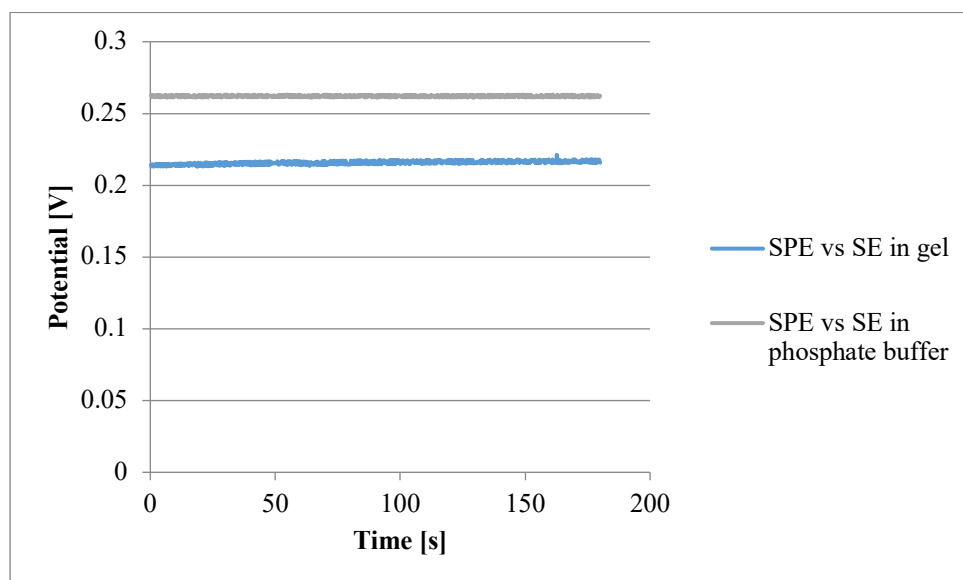


Figure 6.26 Screen printed electrodes (SPE) vs standard electrode (SE) in 0.1 M phosphate buffer solution and 3% w/v of methylcellulose gel

A stable open circuit potential can be seen in both media over the measured time period of three minutes. However, a shift in the open circuit potential can be seen with respect to the medium. The open circuit potential reduced from 0.26 V in the phosphate buffer to 0.22 V in the gel, thus providing a potential difference of 0.04V. The potential of an Ag/AgCl reference electrode depends on the concentration of the Cl<sup>-</sup> ions present (Compton et al., 2012b). Hence, it is implied that there are less Cl<sup>-</sup> ions in the gel compared to in the phosphate buffer to support the screen-printed Ag/AgCl RE.

## 6.6 Electrochemical characterisation of the DMFc - mediated enzymatic glucose sensor

In this section, the experiments conducted with the glucose sensors, which were fabricated as explained in section 5.9.3, are shown.

The glucose sensors were tested in the gel environment as the samples from experiments involving *in vivo* glucose extraction via RI were in gel format.

### 6.6.1 Testing different scan rates with glucose sensor

The relationship between different scan rates and current output of the fabricated glucose sensors can be observed in Figure 6.27. The scan rate was changed from 10 mV/s to 100 mV/s in increments of 10 mV/s. The test sample consisted of a gel sample with a glucose concentration of 62 µM.



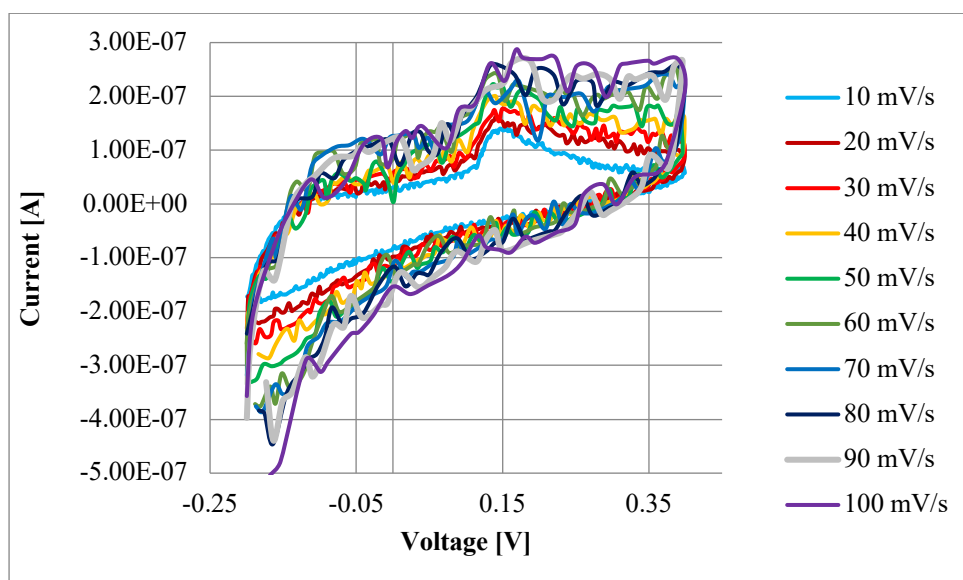


Figure 6.27 CV of Side A of the glucose sensor at a glucose concentration of 62  $\mu\text{M}$  at different scan rates

Side A of the sensor is coated with the DMFc, carbodiimide and with glucose oxidase and is responsible to detect any glucose related current changes. With increasing scan rate, an increase in the anodic peak current can be seen on side A of the glucose sensor. This is due to the fact that with increasing scan rate, the diffusion layer decreases. Consequently higher peak currents are observable (Krishnan, 2011).

A shift in the anodic peak potential from 0.136 V to 0.168 V can be detected when changing the scan rate, which is an indication for a non-reversible system. In addition, in disagreement to theory, no cathodic peak can be observable.

The peak current at the potential of 0.14 V was plotted against square root of the scan rate (Figure 6.28).

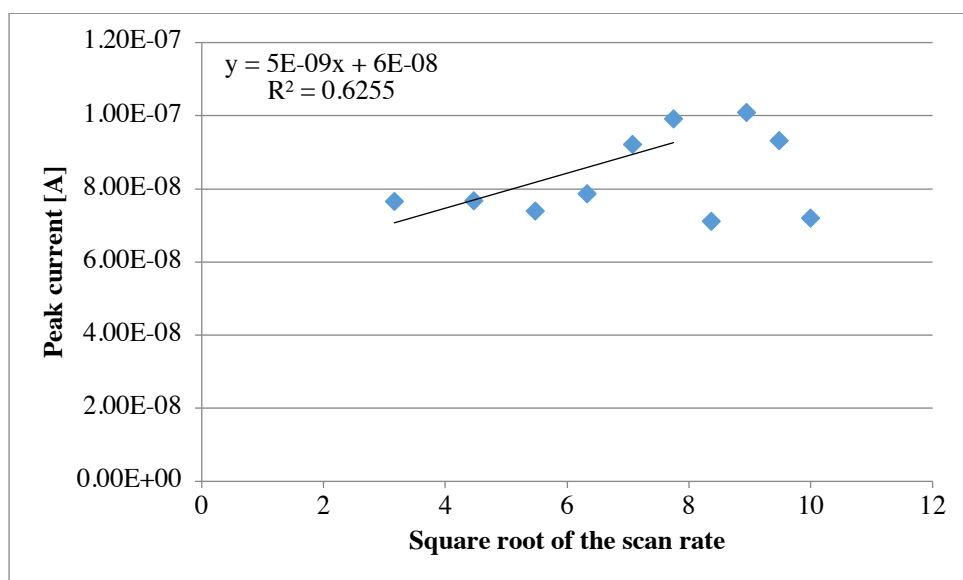


Figure 6.28 Peak current vs the square root of the scan rate. Peak current acquired using the glucose sensor tested in a glucose gel sample with a concentration of 62  $\mu\text{M}$

No clean linear relationship can be seen between the peak current and the square root of the scan rate, again indicating an irreversible system. If the electron transfer between the mediator and the working electrode is too slow, a reduction will not occur (Kissinger & Heineman, 1983).

This experiment was also conducted to identify the best scan rate to perform the experiments with the glucose sensors. The  $R^2$ -values of the applied straight-line fits were used to assess the best linear curve fitting range in Figure 6.28. The straight-line fit applied from square root from a scan rate of 10 mV/s to the square root of the scan rate of 60 mV/s was identified to have the highest  $R^2$ -value with 0.63. Therefore, the CV experiments with the glucose sensors were conducted at a scan rate of 60 mV/s.

Comparing the voltammograms obtained in the liquid environment (eg. Figure 6.25) and gel environment (Figure 6.27), a high level of noise can be seen in the latter. The noise in the gel environment suggests that the gel itself is not providing a uniform environment for the analyte to diffuse.

## 6.6.2 Establishment of a standard calibration curve with the glucose sensor

It is important to identify the detection range of the fabricated glucose sensor in order to determine if the sensors are sufficiently sensitive to quantify glucose extracted via RI experiments. Therefore, experimental procedure described in section 5.10.2 was followed to establish a calibration curve using the glucose biosensors.

The glucose standard gel samples used for the establishment of the calibration curve was prepared as explained in section 5.2.5. with the following glucose concentrations: 0  $\mu\text{M}$ , 15.63  $\mu\text{M}$ , 31.25  $\mu\text{M}$ , 62.5  $\mu\text{M}$ , 125  $\mu\text{M}$  and 250  $\mu\text{M}$ .

The capacitive current was deducted from the peak current by extrapolating the baseline current. This was required to identify the current solely caused by the faradaic processes.

The experiments were performed at static condition and the glucose was already mixed into the gel. The sensors were disposed after single use.

Figure 6.29 shows an example of the acquired voltammograms from side A of the glucose sensors at the different standard concentrations at a scan rate of 60 mV/s.

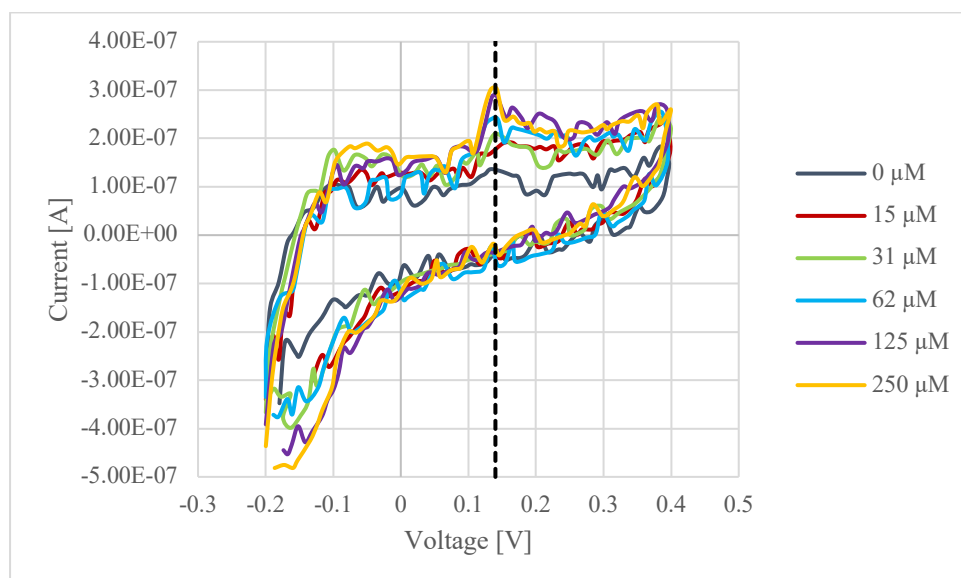


Figure 6.29 CV obtained from Side A of the glucose sensor during establishment of the calibration curve

Glucose oxidase has a high specificity towards glucose and was applied on side A of the sensor. Hence, the current reading of side A of the sensor is expected to be due to the mediator- enzyme reaction in the presence of the glucose and in relation to the

glucose in the test sample. An increase in the peak current with increasing glucose concentration in the test sample at a potential of 0.14V can be seen.

As discussed, side B of the glucose is only coated with DMFc and carbodiimide and with no glucose oxidase. It is intended to identify any background current or current caused by any interfering species. Figure 6.30 shows the voltammogram of side A in comparison to side B of a gel sample with a glucose concentration of 62  $\mu\text{M}$  at a scan rate of 60 mV/s.

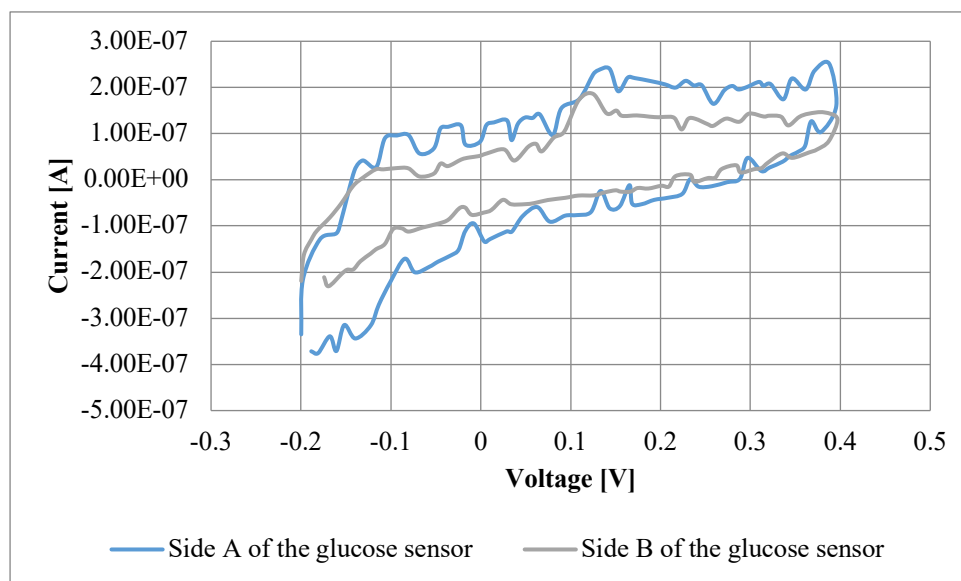


Figure 6.30 Voltammogram of a standard gel sample with a glucose concentration of 62  $\mu\text{M}$  obtained from side A of the glucose sensor, which has the immobilised enzyme on the working electrode (blue in comparison to side B of the sensor, which has no enzyme on the working electrode (grey); both voltammograms were taken at a scan rate of 60 mV/s

A peak at approximately 0.1249 V can be seen for side B of the glucose sensor, which is caused by the oxidation of the DMFc in the presence of glucose. Also for side B of the sensor, no cathodic peak is observable, indicating an irreversible electron transfer of DMFc. However, from theory it is expected that DMFc undergoes a reversible one electron transfer, therefore Randles Sevcik equation was applied to calculate the diffusion coefficient of  $2.9 \times 10^{-8}$  for DMFc.

For the establishment of the calibration curve using the glucose sensor it was decided to take the ratio of the current reading of side A to the current reading at side B of the sensor at a voltage of 0.14 V. Taking the ratio will help to identify the current changes

only caused by the glucose and eliminate any background current or current caused by any interfering species. Hence, specificity of the glucose sensor can be validated.

Figure 6.31 shows the established calibration curve with the ratio of side A to side B against the standard glucose concentrations.

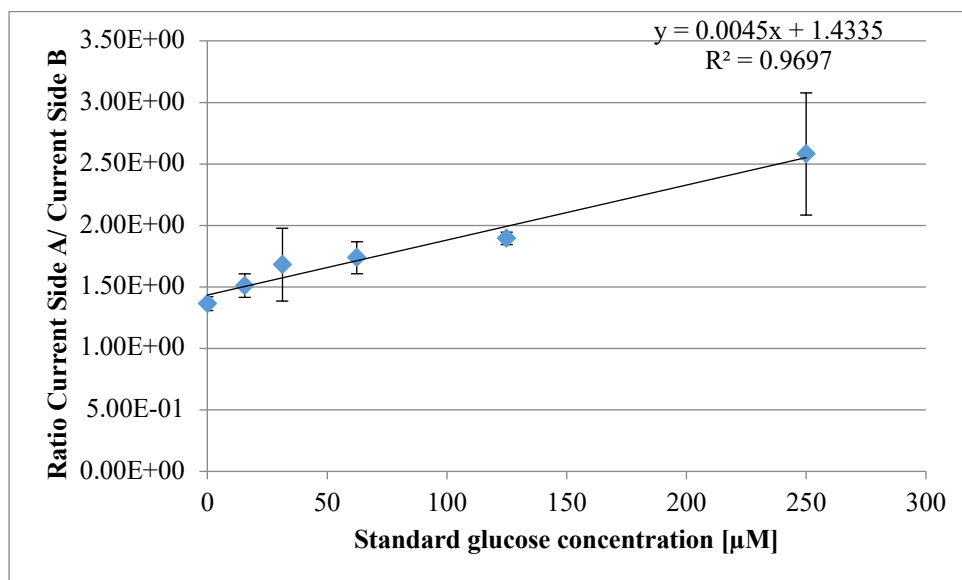


Figure 6.31 Calibration curve established using electrochemical detection of glucose using biosensors. The ratio of the current value obtained at a voltage of 0.14 V at side A of the glucose sensor to the current value obtained at a voltage of 0.14 V at side B of the glucose sensor, Side A of the sensor is immobilised with the enzyme; Side B of the sensor has no enzyme coating and is responsible to detect any background current.  $n=3$

A linear relationship between the ratio and the standard glucose concentration could be found and the linear relation can be expressed with  $y=0.0044x+1.4462$  and an  $R^2=0.97$ . An LOD of 77.09  $\mu\text{M}$  was calculated. Even though a linear relationship could be found, the standard error bars are high and overlapping, indicating the need of further improvement of the sensors.

The established calibration curve should ultimately help to quantify unknown glucose concentrations from RI samples based on the current reading from the glucose sensor.

## 6.7 *In vitro* RI experiments with the DMFc - mediated enzymatic glucose sensor with and without AC

*In vitro* RI experiments using the glucose sensors without AC and the AC- integrated glucose sensors were conducted as explained in section 5.10.3. The applied measurement setup can be seen in Figure 6.32.



Figure 6.32 Measurement setup for RI experiments using glucose sensors with and without AC foam. E1 is connected to the computer and was used to perform CV to ensure sensor performance. EA 1 was responsible to apply the iontophoretic current between E1 and E2 electrodes and also to take CV from the E1 electrode. The EA2 took CV measurements from the E2 electrode and from the control electrode.

Five different glucose concentrations were tested in the diffusion cell: 0 mM, 5 mM, 10 mM, 15 mM and 20 mM. Three electrodes were used for each experiment, one control electrode and two iontophoresis electrodes. This experiment was conducted to see 1) if the extracted glucose via RI can be electrochemically quantified using the glucose sensor and 2) if the AC-integrated glucose sensor improves glucose flux during RI.

First the results of the standard glucose detection method using glucose assay kits and an optical spectrophotometer are demonstrated before discussing the electrochemical glucose detection method using the sensors (section 6.7.2).

### 6.7.1 Standard laboratory glucose detection using colorimetric assay and an optical spectrophotometer

For comparison purposes to the electrochemical glucose detection method, the extracted glucose via RI with and without the AC- integrated glucose sensors was quantified using the Randox glucose assay kit and an optical spectrophotometer.

The amount of glucose extracted after applying RI for 60 minutes with switching polarities every 15 minutes using the glucose sensors without AC can be seen on Figure 6.33 and using the AC- integrated glucose sensors can be seen in Figure 6.34.

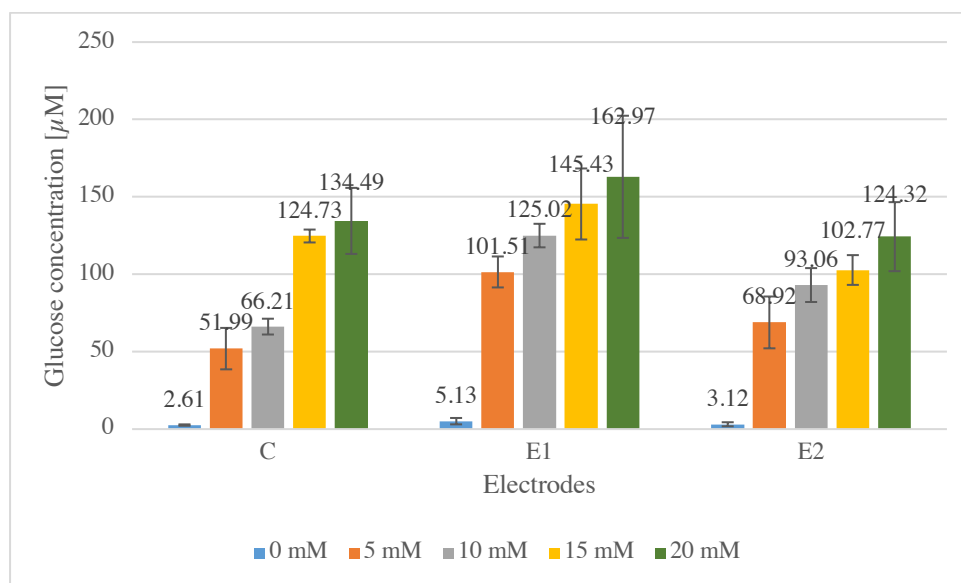


Figure 6.33 Glucose concentrations quantified using the standard method using glucose assay kit and an optical spectrophotometer. The amount of glucose extracted in each electrode (C, E1 and E2) from the extracted gel across the Spectrapore membrane using without the AC- integrated glucose sensors). The diffusion cell was prepared with a 0 mM (blue bars), 5 mM (orange bars), 10 mM (grey bars), 15 mM (yellow bars) and 20 mM (green bars) glucose HEPES buffer solution and the measurement cycle was 60 minutes long with switching polarities every 15 minutes. The glucose concentrations from the extracted gel were calculated using the equation from the gel calibration curve. The error bars represent the standard error.  $n=3$ .

The small amounts of background glucose extracted from the 0 mM glucose concentration in the buffer solution is negligible and is caused by the methylcellulose in the gel.

As it is expected from theory, glucose was extracted at the most at the E1 electrode (the initial anode) across all concentrations. It is observable that the glucose extraction increases with increasing glucose concentrations in the diffusion cell across all three electrodes. In disagreement to theory, for the 15 mM and 20 mM glucose concentration

the control electrodes exceeded the amount extracted at the E2 electrode. It was expected that the control extracts the least amount of glucose as it is only governed by passive diffusion. The higher extraction at the control electrodes could be possibly due to a damaged membrane under the control electrodes.

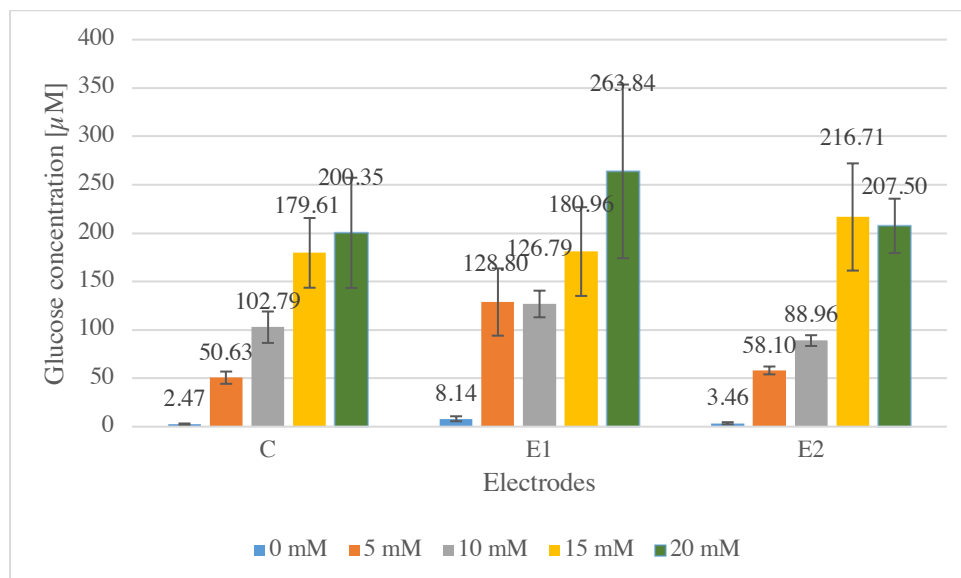


Figure 6.34 Glucose concentrations quantified using the standard method using glucose assay kit and an optical spectrophotometer. The amount of glucose in each electrode (C, E1 and E2) from the extracted gel across the Spectrapore membrane using the AC- integrated glucose sensors. The diffusion cell was prepared with a 0 mM (blue bars), 5 mM (orange bars), 10 mM (grey bars), 15 mM (yellow bars) and 20 mM (green bars) glucose HEPES buffer solution and the measurement cycle was 60 minutes long with switching polarities every 15 minutes. The glucose concentrations from the extracted gel were calculated using the equation from the gel calibration curve. The error bars represent the standard error.  $n=3$ .

Again, a negligible amount of background glucose was extracted from the 0 mM glucose concentration in the buffer solution due to the gel. E1 electrode extracted the highest amount of glucose compared to the E2 and the C electrode, except for the 15 mM glucose concentration in the diffusion cell, where the E2 electrode extracted the most. Interestingly, for the 10 mM glucose concentration in the diffusion cell more glucose was extracted at the control electrode than at the E2 electrode, which is unexpected. It is expected that the control electrode extracts the least amount of glucose as it is only governed by passive diffusion. Same as for the electrodes without AC, an increased glucose extraction can be seen with increasing glucose concentrations in the diffusion cell using with AC- integrated electrodes but with two exceptions. The 5 mM glucose concentration extracted slightly more glucose at the E1



electrode than the 10 mM glucose concentration. And more glucose was extracted from the 15 mM glucose concentration than the 20 mM glucose concentration at the E2 electrode. Even though, slight variations were observed from what was expected from theory, the differences are within acceptable limits.

Table 6.8 gives a summary of the calculated glucose fluxes across each electrode using the sensors with AC foam and without AC foam.

*Table 6.8 Transdermal fluxes across the Spectrapore membrane using sensor without AC foam and with AC foam and the 0 mM glucose diffusion cell*

Glucose concentration in diffusion cell	Type of sensor	Transdermal flux to Control electrode $[\frac{nmol}{cm^2h}]$	Transdermal flux to E1 iontophoresis electrode $[\frac{nmol}{cm^2h}]$	Transdermal flux to E2 iontophoresis electrode $[\frac{nmol}{cm^2h}]$
5 mM	Without AC foam	4.96 ± 1.27	9.69 ± 0.96	6.58 ± 1.60
	<b>With AC foam</b>	<b>4.83 ± 0.60</b>	<b>12.30 ± 3.32</b>	<b>5.55 ± 0.39</b>
10 mM	Without AC foam	6.32 ± 0.49	11.94 ± 0.73	8.89 ± 1.05
	<b>With AC foam</b>	<b>9.82 ± 1.55</b>	<b>12.11 ± 1.31</b>	<b>8.49 ± 0.53</b>
15 mM	Without AC foam	11.91 ± 0.40	13.89 ± 2.19	9.81 ± 0.92
	<b>With AC foam</b>	<b>17.15 ± 3.44</b>	<b>17.28 ± 4.38</b>	<b>20.49 ± 5.29</b>
20 mM	Without AC foam	12.84 ± 2.04	15.56 ± 3.77	11.87 ± 2.13
	<b>With AC foam</b>	<b>19.13 ± 5.44</b>	<b>25.19 ± 8.57</b>	<b>19.81 ± 2.68</b>

Overall, an increased glucose flux across the electrodes with AC can be seen compared to the fluxes across the electrodes without AC. This confirms the suitability of AC to act as a glucose binding agent. In addition, an increased flux with increasing glucose concentration in the diffusion cell can be seen as well.

Figure 6.35 shows a linear relationship between the extracted glucose at the E1 and E2 electrode and the glucose concentration in the diffusion cell using the glucose sensors with AC and without AC.

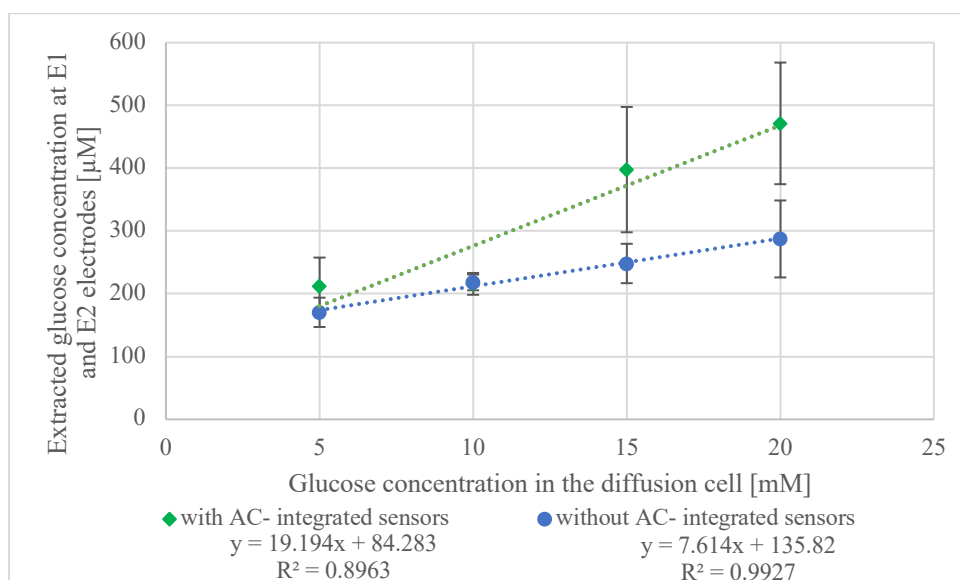


Figure 6.35 Relationship between extracted glucose at the E1 and E2 electrode and the glucose concentration in the diffusion cell.

A linear relationship was observable between the glucose concentrations in the diffusion cell and the extracted glucose across both iontophoresis electrodes using the AC- integrated glucose sensors as well as the glucose sensors without the AC. The linear curve applied across the extracted glucose with the AC- integrated sensors and the glucose concentrations in the diffusion cell can be characterised with  $y=18.80x+86.26$  with an  $R^2$  of 0.938. In contrast, with the sensor without AC a linear relation with  $y=10.24x+95.19$  with an  $R^2$  of 0.9514 was found. A steeper gradient could be established with the AC- integrated sensors, indicating a higher sensitivity of the measurement system with AC.

### 6.7.2 Electrochemical detection of glucose:

CV was applied to evaluate the electrochemical detection method of glucose extracted via RI using the fabricated biosensors. As discussed in section 5.10.3, following voltammograms were taken for each side of the sensor:

- 1) DC pre: Before placing the sensor onto the diffusion cell, CV was applied to confirm the empirically observed particular peak and shape (Figure 5.21) to ensure sensor performance (A - pre DC and B - pre DC).
- 2) Pre RI: Once three sensors were selected, a voltammogram was taken as soon as the sensors were applied onto the diffusion cell (A - pre RI and B - pre RI).

- 3) After RI: After the 60 minutes of RI, another voltammogram was recorded (A - after RI and B – after RI).

In one measurement cycle 6 voltammograms were recorded for each electrode, thus in total 18 voltammograms as three electrodes (two iontophoresis and one control electrode) were used in one experiment.

RI experiments for each glucose concentration (0 mM, 5 mM, 10 mM, 15 mM and 20 mM) in the buffer were repeated three times with AC- integrated glucose sensors and three times without AC- integrated glucose sensors. However, it has to be noted that unfortunately during one RI experiment with the AC- integrated electrodes and 5 mM glucose concentration in the buffer solution, the data from one measurement cycle was not stored properly for the E2 and C electrode. Therefore, data of only two measurements cycles was available and used for analysis.

The voltammogram of interest to investigate in electrochemical glucose detection was the CV taken after the 60 minutes of RI, hence the “after RI” voltammograms. Examples of the after RI voltammograms of side A and side B are shown in Figure 6.36.

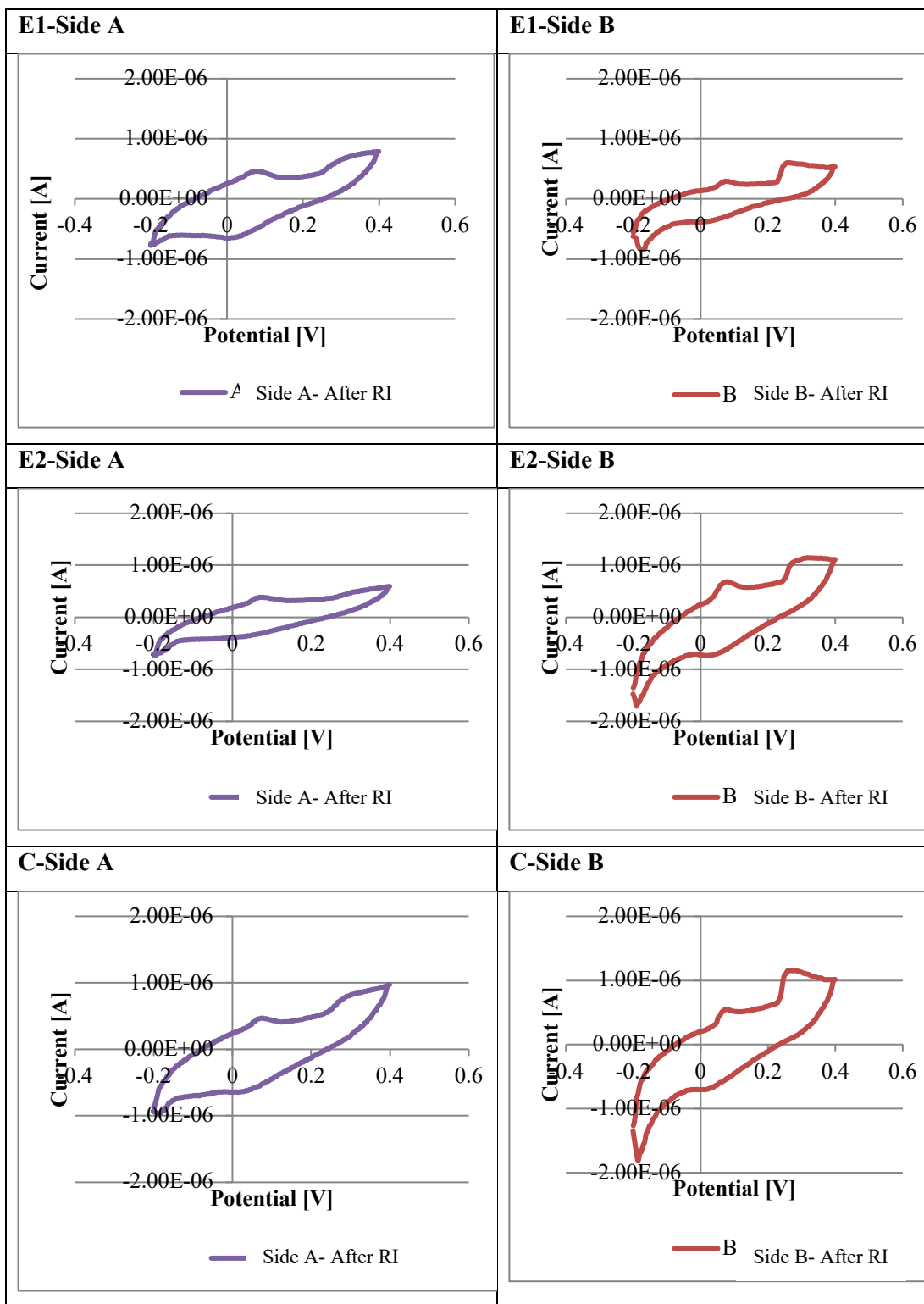


Figure 6.36 Examples of after RI voltammograms obtained from the glucose sensors without AC, which were applied on the *in vitro* cell prepared with a 5mM glucose concentration in the buffer solution a) left- E1 electrode-Side A, right - E1 electrode-Side B b) left- E2 electrode-Side A, right - E2 electrode-Side B and c) left- C electrode-Side A, right - C electrode-Side B

For side A of the glucose sensors, two peaks were identified on the voltammogram for side A of the electrode after the application of RI for 60 minutes. One peak at a voltage of 0.082 V and the second peak at a higher potential of approximately 0.306 V. And for side B of the sensor, two peaks were also on the voltammogram after the application of RI for 60 minutes at a similar oxidation potentials as side A. One peak at a voltage of approximately 0.092 V and the second peak at a potential of approximately 0.292 V.

Based on the results obtained in section 6.6.2 for the establishment of a calibration curve using the glucose sensor, an oxidation peak at the voltage of 0.14 V was expected. Hence, the initial plan was to analyse the current reading at the voltage of 0.14 V. Same as for the calibration experiments, the electrochemical glucose detection of the extracted glucose via RI was explored with considering the ratio of the current obtained at side A of the electrode to the current obtained at side B of the electrode. As discussed, Side A of the sensor is coated with the DMFc and the carbodiimide solution and with glucose oxidase and is responsible to detect any glucose related current changes. Side B of the glucose sensor is only coated with DMFc and the carbodiimide and with no glucose oxidase. It is intended to identify any current changes which were not caused by glucose. The identified ratio of the current reading of side A to the current reading of side B of the after RI voltammograms would then be inserted into the calibration curve established in 6.6.2 to identify the extracted glucose.

However, the voltammograms taken after the application of RI have a different shape compared to the CV obtained for the establishment of the calibration curve (see example Figure 6.30). And no oxidation peak could be identified at a voltage of 0.14 V. The change could be explained by the composition of sample, which was tested. The test samples used for the establishment of the calibration curve only consisted of glucose and the gel. In contrast, after the application of RI, other molecules than glucose, which were in the diffusion cell such as potassium chloride, sodium chloride or HEPES have also been extracted via RI, which might have caused the change in CV.

There is also the possibility that there was a shift in the glucose peak. Therefore, it was decided to investigate in the relationship between the peak currents obtained at 0.082 V and 0.306 V respectively for a possible relationship with the extracted glucose.

#### 6.7.2.1 Peak currents at 0.082 V

It has to be considered that the total peak current, which can be seen in the voltammogram consists of a faradaic component and a non-faradaic component. The non-faradaic current is caused by the charging and discharging of the electrode double layer at the working electrode by the application of a potential. And only the faradaic current is caused by the electron transfer processes and is in relation to the glucose concentration. Therefore, it is important to identify the capacitive current and deduct it from the peak current to identify the current solely caused by the electron transfer. In the previous CV experiments, Kissinger's method was followed and the capacitive current was determined by extrapolating the baseline current (Kissinger & Heineman, 1983).

For the identification of the capacitive current from the after RI voltammograms, Kissinger's method was also attempted by extrapolating the baseline current in the potential region from -0.1V to 0.024 V (see example Figure 6.37)

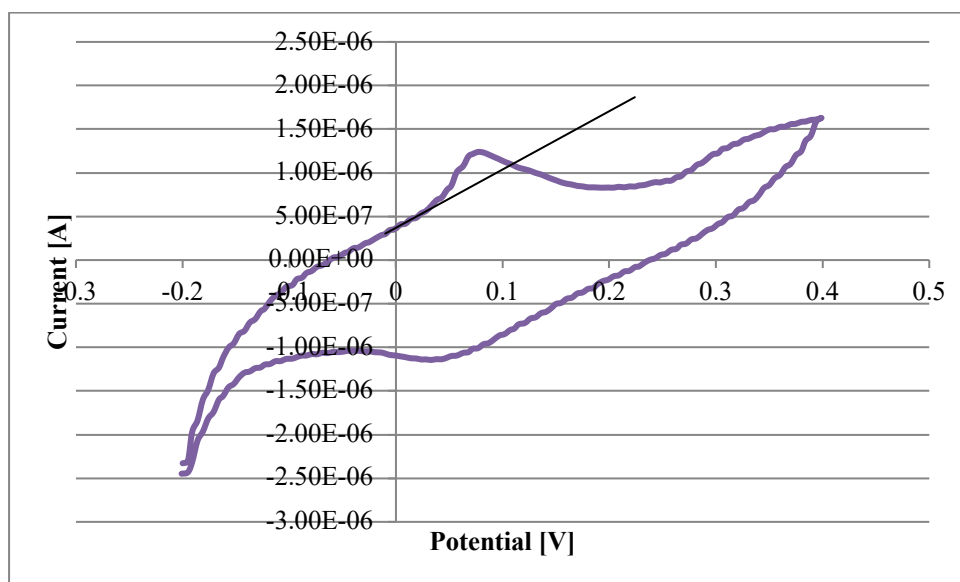


Figure 6.37 Cyclic voltammogram from side A of the E1 electrode of the AC- integrated glucose sensor after the application of RI. The sensors were applied on the *in vitro* cell prepared with a 20 mM glucose concentration in the diffusion cell. The applied tangent indicates the extrapolation of the baseline current to identify capacitive current.

However, this method could not be applied to all the voltammograms due to the shape of some voltammograms (see example Figure 6.38).

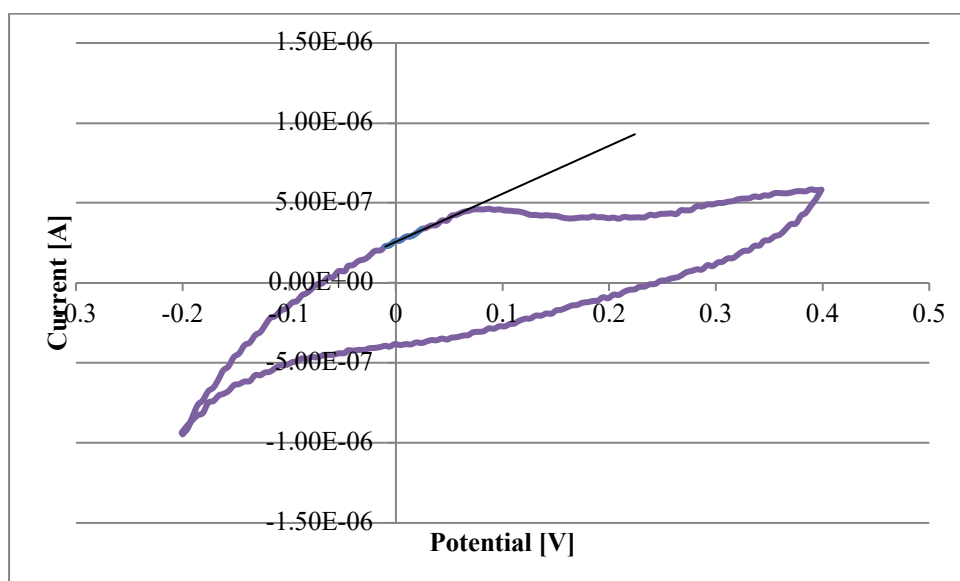


Figure 6.38 Cyclic voltammogram from side A of the E1 electrode of the AC- integrated glucose sensor after the application of RI. The sensors were applied on the *in vitro* cell prepared with a 15 mM glucose concentration in the diffusion cell. The applied tangent indicates the extrapolation of the baseline current to identify capacitive current.

For some voltammograms, the extrapolation of the baseline current would exceed the peak current at 0.082 V, thus giving a negative peak current. It was decided to still proceed with Kissinger's method, but the negative peak currents were not included in the analysis. Therefore, the number of repeats varied depending on the sensibility of the obtained value and unfortunately for one dataset (5 mM glucose concentration in the diffusion cell with AC-integrated sensors) there was not data available

Figure 6.39 shows the ratio of current side A to current of side B obtained at each electrode with no AC from the *in vitro* RI experiments with varying the glucose concentration in the diffusion cell.

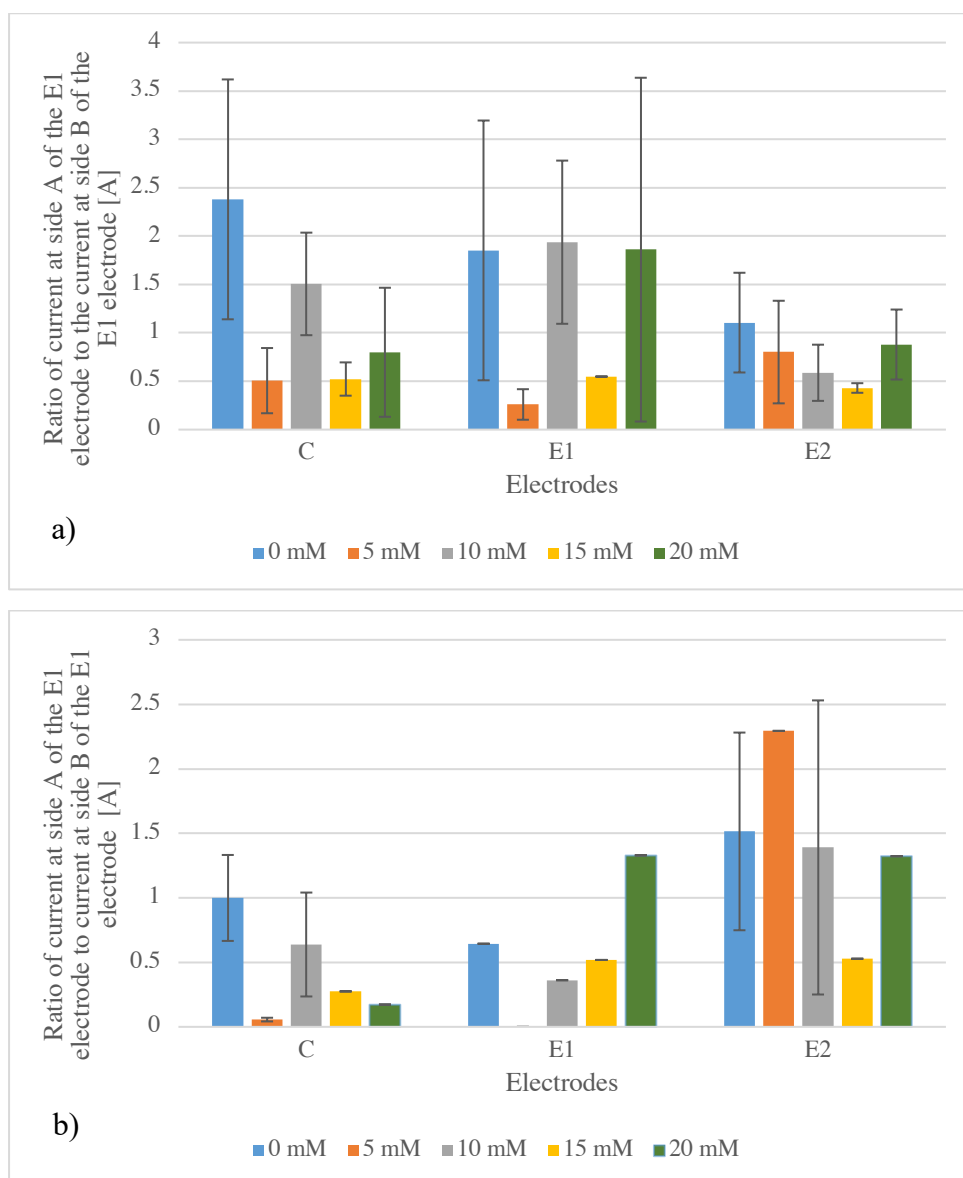


Figure 6.39 Electrochemical analysis of the extracted glucose via RI using the glucose sensors a) without AC and b) with AC. The ratio of current obtained at side A of the E1 electrode to side B of the E1 electrode of the glucose sensor without AC of each electrode (C, E1 and E2) at a potential of 0.082 V. The error bars represent the standard error. The diffusion cell was prepared with a 0 mM (blue bars), 5 mM (orange bars), 10 mM (grey bars), 15 mM (yellow bars) and 20 mM (green bars) glucose HEPES buffer solution and the measurement cycle was 60 minutes long with switching polarities every 15 minutes.

From theory it was expected, that the control electrode extracts the least amount of glucose, followed by the iontophoresis electrodes. No such behaviour can be seen here. Moreover, it is expected that the amount of glucose increases with increasing the glucose concentration in the diffusion cell. However, that pattern was also not observable. It is also surprising to see that the highest ratio was found when there was no glucose in the diffusion cell. Interestingly, a ratio below 1 was found for some



datasets, indicating that the current reading at side B was higher than the current reading of side A of the electrode.

Similar results as shown in Figure 6.33 and Figure 6.34 were expected, where the extracted glucose was quantified using the glucose assay kit. However, based on Figure 6.39 it can be said that the ratios of the current readings of side A to side B at the voltage of 0.082 V are not in relation with the extracted glucose from the diffusion cell.

### 6.7.2.2 Peak currents at 0.306 V

The current readings at the second oxidation peak of 0.306 V were also analysed to investigate in electrochemical glucose detection. For the identification of capacitive current, Kissinger's methods could be applied for all the obtained voltammograms without any problems. Therefore, the current at the region 0.199 V to 0.233 V was extrapolated from voltammograms and deducted from the peak current (see example Figure 6.40)

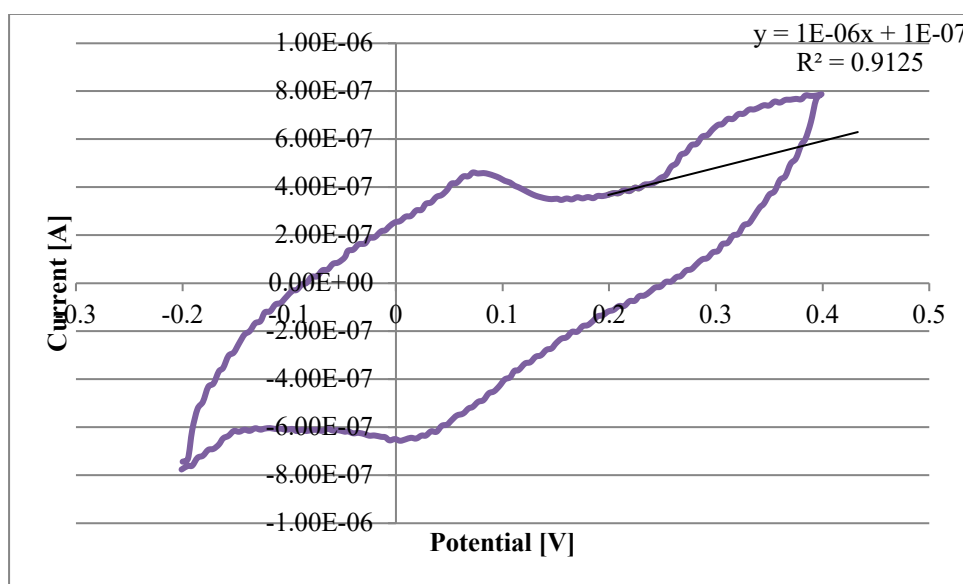


Figure 6.40 Cyclic voltammogram from side A of the E1 electrode of the glucose sensor without AC after the application of RI. The sensors were applied on the *in vitro* cell prepared with a 5 mM glucose concentration in the diffusion cell. The applied tangent indicating the extrapolation of the baseline current to identify capacitive current.

Figure 6.41 shows the ratio of current side A to current of side B obtained at each electrode with no AC from the *in vitro* RI experiments with varying the glucose concentration in the diffusion cell.

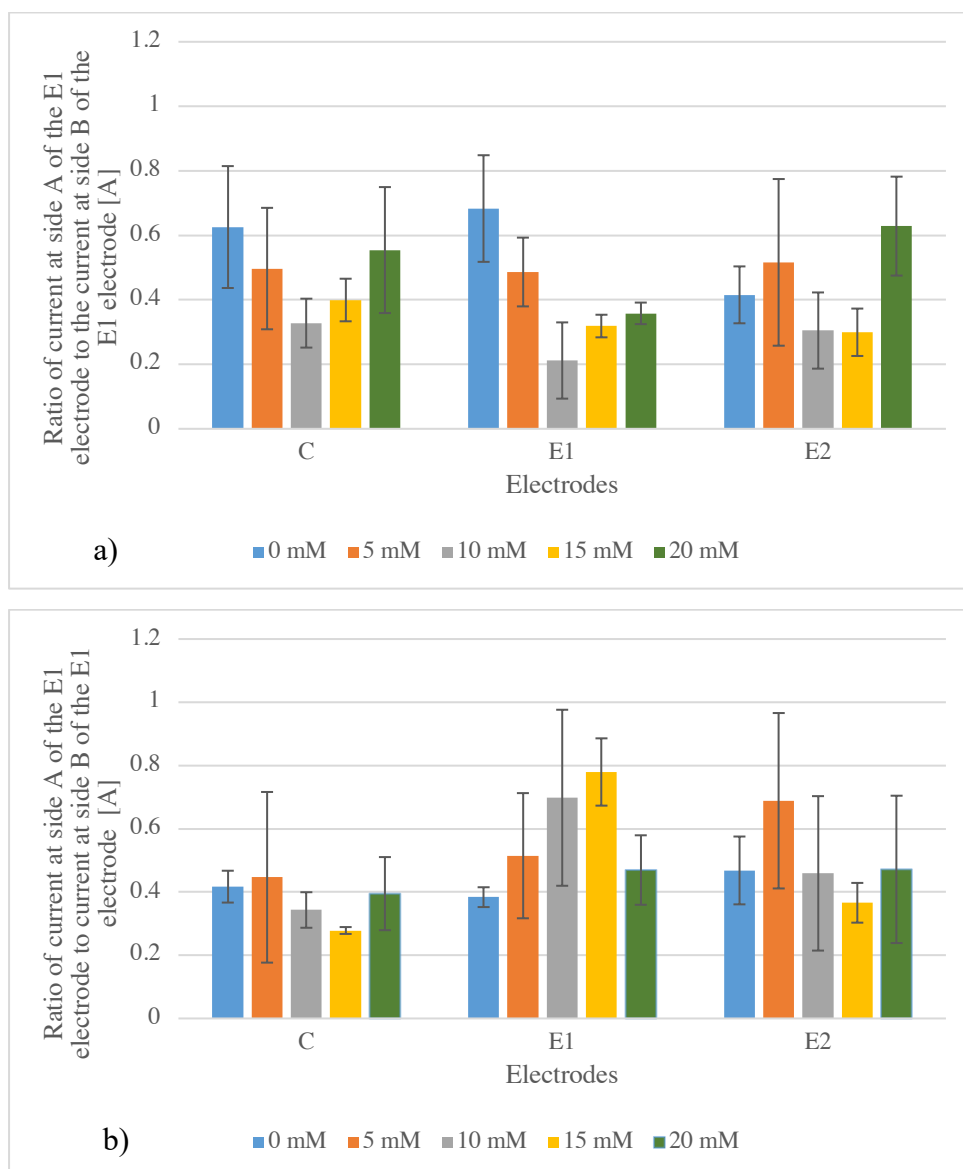


Figure 6.41 Electrochemical analysis of the extracted glucose via RI using the glucose sensors a) without AC and b) with AC. The ratio of current obtained at side A of the E1 electrode to side B of the E1 electrode of the glucose sensor without AC of each electrode (C, E1 and E2) at a potential of 0.306 V. The error bars represent the standard error. The diffusion cell was prepared with a 0 mM (blue bars), 5 mM (orange bars), 10 mM (grey bars), 15 mM (yellow bars) and 20 mM (green bars) glucose HEPES buffer solution and the measurement cycle was 60 minutes long with switching polarities every 15 minutes.

For all the results, the ratio of the current readings of side A to side B are below 1, which implies that background current was higher than the glucose current reading. From theory it was expected, that the control electrode extracts the least amount of glucose, followed by the iontophoresis electrodes. No such behaviour can be seen here as well. Moreover, it is expected that the amount of glucose increases with increasing

the glucose concentration in the diffusion cell. That pattern was also not observable. This result suggests the ratios of the current readings of side A to side B at the voltage of 0.306 V are also not in relation with the extracted glucose.

As the peak currents at both oxidation peak currents were not in relation to the glucose, it suggests that the electrochemical glucose detection using the glucose sensors of the glucose extracted via RI was not successful. It seems that due to the extraction of the other solutes of the diffusion cell, the glucose peak has been masked. Reasons for changes in the voltammograms are discussed in section 7.7.

Even though the electrochemical glucose detection method was not successful, with the help of the standard glucose detection method the extracted glucose concentrations could be identified. One of the key aims of this study was to show the suitability of AC to act as a glucose binding agent in the RI environment. And it could be shown that the integration of AC in the electrode did improve glucose flux compared to the sensors without AC. Thus, the suitability of AC to act as a glucose binding agent to allow uniform glucose diffusion across wearable sensors could be confirmed.

## 7 Discussion

The main objective of this project was to test the concept of glucose adsorption on activated carbon (AC) and ultimately develop a wearable glucose sensor with integrated AC. AC acts as a glucose binding agent and allows improved glucose flux across the skin to glucose sensor. The glucose sensor was fabricated with screen printing methods as explained in Section 5.5. An iontophoresis electrode was included in the glucose sensor design, as RI was applied for glucose extraction. Glucose was detected and quantified with the help of a mediated glucose sensor consisting of the enzyme glucose oxidase and the mediator 1,1'- dimethylferrocene. Cyclic voltammetry was applied to evaluate the sensor performance and its applicability to be part of a wearable sensor.

Basic *in vitro* RI experiments were performed to understand the principles of RI and the extraction rate of glucose in RI. Glucose flux was tested in terms of a) changing the glucose concentration in the diffusion cell, b) varying the duration of RI and c) two different artificial membranes. Furthermore, the use of the Genova Nano spectrophotometer from Jenway, was evaluated for glucose quantification. The big advantage of the spectrophotometer is that it requires a minimum sample volume of only 0.5  $\mu\text{L}$  for measurements.

## 7.1 Evaluation of two commercially available glucose assay kits

It is crucial to use a glucose assay kit which can quantify the concentrations in the expected range. Glucose is extracted transdermally in the  $\mu\text{M}$  range via the application of RI. For example McCormick et al. extracted on average  $25.9 \pm 5.4 \mu\text{M}$  of glucose across both iontophoresis electrodes after 60 minutes of RI on nine healthy patients in the fasted state (McCormick et al., 2012).

On the product information sheet of the Randox assay kit, an upper limit of the linear range of 22.2 mmol/l was given but no lower limit of the linear range. For the Sigma Aldrich assay kit no such information about linearity could be found. As discussed in Section 4.2.1, the LOD and LOQ are measures to identify the linear range of a calibration curve. In this study, a LOD of  $2.39 \mu\text{M}$  and a LOQ of  $7.03 \mu\text{M}$  were identified for the Randox assay kit. The expected glucose concentrations to be obtained via RI are above this range, which shows the suitability of the Randox assay kit for this project. In contrast, a LOD of  $182.44 \mu\text{M}$  was identified for the Sigma Aldrich assay kit, which shows that it cannot quantify glucose in the glucose concentration range expected in this project. As the linear range was identified only after a concentration of  $252.14 \mu\text{M}$ , there were only three data points to apply the linear curve on. For a reasonable calibration curve, at least five data points are needed (JoVE Science Education Database, 2018). To test the upper limit of the kit, more standard samples in the higher concentration should be prepared and tested in a future study.

The gradient in the equation of the straight-fit line, indicates the sensitivity of the system. Comparing the gradient between both assay kits, a higher gradient was observable for the calibration curves acquired using the Randox assay kit. This confirms the higher sensitivity of the Randox assay in the tested range. As explained in section 5.3, both assay kits are based on a double-enzymatic reaction using different enzymes. Both methods are commonly used for glucose measurements (Duxbury, 2004): (1) the glucose oxidase and peroxidase method (Abd-Rabboh & Meyerhoff, 2007; Barham & Trinder, 1972; Bateman & Evans, 1995; Lott & Turner, 1975) and the hexokinase and G6PDH method (Bondar & Mead, 1974; Garber et al., 1978; Neese et al., 1976; Weinzimer et al., 2005). Ambade et al. tested the following glucose

quantification method (1) glucose oxidase and peroxidase (GOD/POD) and (2) hexokinase in terms of accuracy, precision and linear range. They identified an LOD of 16.7  $\mu\text{M}$  with the GOD-POD method and an LOD of 16.1  $\mu\text{M}$  with the hexokinase method. Both methods had an upper limit of linearity at 27.75 mM. (Ambade et al., 1998). It is difficult to make direct comparison to this project as the manufacturers of the assay kits vary, and therefore the composition of the assay kits differs. But in this project, an even lower LOD of 2.39  $\mu\text{M}$  was identified with the GOD/POD kit. A major difference in the LOD can be seen for the hexokinase assay kit, where an LOD of +166.34  $\mu\text{M}$  was identified than in the study of Ambade et al. Difference between both assay kit might be due to different enzyme concentrations in both assay kits: In the Randox assay kit, the glucose oxidase and the peroxidase had an initial concentration of  $\geq 1.5$  kU/L. In contrast, the hexokinase and the G6PDH enzymes had an activity of 1U/L. An enzyme's activity is highly depended on the pH, temperature, the strength and nature of the ions, and the other compounds in assay kits (Bisswanger, 2014). In this project, the pH of the samples were same for both and the temperature was also constant at room temperature. Therefore, the differences in the assay kits are likely due to the strength and nature of the ions and the other compounds in the assay kits. These parameters need to be considered when comparing assay kits.

To summarise, the calibration curve acquired via the Randox assay kit is more suitable to be used in this project, as it covers the glucose concentration range of interest. Therefore, this calibration curve was ultimately used to calculate unknown glucose concentrations obtained in subsequent experiments conducted in this project.

## 7.2 Evaluation of the analysis method for glucose quantification with Genova Nano in comparison to the microplate reader

The Genova Nano, a micro- volume spectrophotometer, has been used for a variety of studies for absorbance readings (Couto et al., 2018; Jackson et al., 2018; Shakeel et al., 2018; Vinoth et al., 2015) but it has not been used for glucose measurements to date. The main advantage of the use of Genova Nano is that it only requires a sample volume of 0.5 to 5  $\mu\text{L}$  per measurement. This characteristic is very appealing in glucose quantifications as in case of clinical studies only limited amount of patient

samples are available. In contrast, most of the standard measurement techniques such as the microplate reader need at least 80  $\mu\text{L}$  of sample volume. Hence, more dilutions would be needed to run a colorimetric assay which lead to errors, contamination and inaccuracies in concentration calculations. The experiments conducted have helped to understand the suitability and limitations of Genova Nano for glucose quantification. Looking at the calibration curve acquired by the microplate reader (Figure 6.3) and the Genova Nano (Figure 6.4), it can be seen that both devices have a different linear range for the standard glucose concentrations and their absorbance values. The microplate reader, which was used as a standard measurement technique for comparison, had a low LOD of 1.22  $\mu\text{M}$  and a LOQ of 7.17  $\mu\text{M}$ ; whereas the GNSPM had a higher LOD of 5.65  $\mu\text{M}$  and an LOQ of 26.14  $\mu\text{M}$ .

According to the ISO 15197:2013 “*In vitro* diagnostic test systems -- Requirements for blood-glucose monitoring systems for self-testing in managing diabetes mellitus”, the accuracy level of Self-Monitoring Blood glucose devices is the following: For blood glucose concentrations  $<100$  mg/dL, which corresponds to 5.6 mmol/L, the measured concentration should be within  $\pm 15$  mg/dL ( $\pm 0.8$  mmol/L). And for blood glucose levels  $\geq 100$  mg/dL, measured blood glucose concentrations should be within  $\pm 15\%$  of the actual concentration. (Freckmann et al., 2015)

Microplate readers are commonly used for absorbance measurements as they are rapid and easy to use (Ashour et al., 1987; Durand et al., 2012). The microplate reader measured the concentrations from the two glucose samples more closely to their known concentrations compared to the GNSPM (Figure 6.5). It was able to take measurements within  $\pm 2.65\%$  from the actual glucose concentration. In contrast, the measurement taking with GNSPM showed difference of 6.57% from the actual value. However, it has to be considered that this accuracy level was achieved with a sample volume of only 2  $\mu\text{L}$ . The GNSPM provided results with lower standard deviations, which indicates good precision with the GNSPM. Higher absorbance values were observable with the calibration curves obtained from the microplate reader. This can be explained by the total amount of the glucose in the sample. When using the microplate reader, a total volume of 160  $\mu\text{L}$  (with a sample to enzyme ratio of 1:1) is used, whereas for the GNSPM measurements a sample volume of only 2  $\mu\text{L}$  (with a sample to enzyme ratio of 1:1), was applied. The absorbance values were

approximately 4.6 times higher when using the microplate reader than with the GNSPM. The gradient of the microplate reader was double the value of the gradient of GNSPM, which indicates higher sensitivity of the microplate reader.

There are a variety of advantages of using the Genova Nano, it gives the user the ability to measure absorbance at any wavelength between 200 nm and 1000 nm, whereas the plate reader used has pre-defined wavelengths (340 nm, 405 nm, 450 nm, 490 nm and 630 nm) and the user has to select the most suitable one. Furthermore, when using the Genova Nano the sample will be directly pipetted onto the read head. This means that the absorbance is solely depended on the sample itself as the light is only passing through the sample itself. On the contrary, when using the microplate reader, the light has to pass the well plate. And the clarity and quality of the well plate can have an impact on the absorbance readings. In addition, the measurements with the Genova Nano are more environmentally friendly and cost effective compared to colorimetric assays as no well plates and less volume of the reagent are required.

One of the disadvantages of the GNSPM is that it is very time consuming. After each measurement, one has to make sure that the reading head properly cleaned with a cloth in order to avoid any impurities or cross-contamination between the different samples. As all measurement are taken on the same read head, it is more prone to inaccuracies due to contamination. One measurement cycle from the lowest concentration to the highest concentration (blank sample and 10 standard glucose concentrations) took approximately 20 minutes. In this project, the measurement cycle was repeated 5 times. In contrast, the microplate reader takes only 9 seconds to perform the absorbance reading of all samples in a ninety-six well plate.

To summarise, a good level of accuracy ( $\pm 6.49\%$ ) could be established with using a sample volume of only 2  $\mu\text{L}$  with the Genova Nano based on the quantification of the two glucose concentrations (204  $\mu\text{M}$  and 408  $\mu\text{M}$ ).

An LOD of 5.65  $\mu\text{M}$  was identified was identified. Ideally, more concentrations should have been tested in the lower concentration range of the standard curve because low concentrations are expected to be extracted via RI. This would have helped to additionally confirm the suitability of GNSPM to quantify glucose samples from RI experiments.



In these experiments, a gel to glucose samples ratio of 1 to 4 ratio was used. The ratio could be further decreased to 1 to 3, which will increase the amount of glucose in the sample. This might help to bring the LOD lower.

### 7.3 *In vitro* RI experiments for glucose monitoring

The experiments conducted using the diffusion cell have helped to investigate in the glucose flux during RI, which is important to know when developing a glucose sensor. Artificial membranes were used in the *in vitro* RI setup as they prevent any sample-to-sample variation and allow the study of glucose flux without any interferences caused by the skin sample. Alternatively, excised animal skin can be used to study drug penetration across the skin. Pig skin simulates human skin better than rat skin (Schmook et al., 2001). Further alternatives are reconstructed human skin, for example the Skinethic™ HRE or epidermis equivalents such as the Graftskin™ LSE™ (Schmook et al., 2001). The Spectrapore membrane, a permselective artificial membrane, has been used in other *in vitro* RI studies and it was shown to simulate human skin well (Arias, 2011; Ching & Connolly, 2008c). It has a molecular weight cut-off of 100 to 500 Daltons and is made of cellulose ester. It is used in dialysis tubings and has symmetric porosity. A different artificial membrane, the Vitro-Skin® was tested to investigate its suitability for RI experiments. The Vitro-Skin® is a synthetic membrane and it contains optimized protein and lipid components. It mimics the surface properties of the human skin effectively with regards to the topography, pH, critical surface tension and ionic strength (Carnali et al., 2012). There was no information regarding the pore size of the membrane. It has been used in a wide range of *in vitro* experiments, such as, rapid *in vitro* SPF/ UVA testing, *in vitro* testing of make-up formulations, *in vitro* sunless tanning applications or *in vitro* testing of adhesives/ adhesive bandages to the skin (IMS Inc., 2018).

The amount of the extracted glucose depends on the duration and intensity of the applied iontophoretic current, the permeability of the artificial membrane and the initial concentration of the glucose in the diffusion cell. Comparing the glucose extraction across both commercially available membranes, it was seen that the Vitro-Skin® was able to extract glucose in the mM range (Figure 6.8). Existing literature (Bandodkar et al., 2014; Ching, 2005; McCormick et al., 2012; Potts et al., 2002; Rao

et al., 1995; Sieg et al., 2004a, 2004b; Tamada et al., 1995), which involved RI experiments on humans, demonstrated that the glucose extraction level for humans is in the  $\mu\text{M}$  range. A possible reason for more glucose extraction with the Vitro-Skin® could be due to the bigger pore size. However, this needs to be investigated in future studies. From theory it is expected that, the initial cathodal chamber (E2) receives more glucose because it is influenced by electroosmosis, electromigration and passive diffusion. 4.4.2, the main transport mechanism for glucose is the electroosmotic flow (Potts, Tamada, & Tierney, 2002), which is established from the anode to the cathode. The results obtained with the Vitro-Skin® are consistent with theory and Rao's studies (Rao et al., 1993, 1995), as more glucose was extracted at the cathode. However, they are not in agreement with other studies where more glucose was extracted at the initial anodal chamber (Arias, 2011; Ching & Connolly, 2008c; Farmahan, 2008; McCormick et al., 2012) and also with the results obtained with the Spectrapore membrane in this study. The reason for extracting more glucose at the anode could be explained by the following: Although the membrane has a net negative charge, it does not entirely have negatively charged pores, but also some neutral and positively charged ones (Pikal & Shah, 1990). Moreover, the effect of cathodal electro-osmosis might be reduced due to the occurrence of membrane polarisation (Ching & Connolly, 2008).

Even though other studies have shown that the Vitro-Skin® mimics the human skin well with regards to surface properties (Beasley & Meyer, 2010; Hanson et al., 2006; Jermann et al., 2002), it was concluded that the Vitro-Skin® is not suitable to mimic the human skin for RI experiments. In addition, another drawback of the Vitro-Skin® was that it had to be pre-hydrated before use, and it had a short life time once hydrated as it has to be used within three days (Pelizzo et al., 2012).

The results obtained with the Spectrapore membrane correspond well with the results obtained in other RI studies (Arias, 2011; Ching & Connolly, 2008c; Farmahan, 2008; McCormick et al., 2012) as more glucose was extracted at the initial anode and glucose was extracted in the micromolar range. The increase in glucose extraction when applying RI was observable when comparing the amount of extracted glucose at the control electrode to the amount extracted at the iontophoresis electrodes. It was

possible to extract on average 2.78 times more glucose after applying RI for 60 minutes compared to the control electrode. In Farmahan's study a 2.6 fold increase was identified across the iontophoresis electrodes compared to the control electrode, which is in close agreement with the value found in this study (Farmahan, 2008). In Ching & Connolly's *in vitro* study, they were able to extract 3.9 more glucose at the iontophoresis electrodes than at the control electrode. Higher extractions of glucose could be explained by the higher current they had applied. To summarise, the usability of the Spectrapore membrane for RI experiments was confirmed and therefore, also used for the other *in vitro* RI experiments in this project.

It was seen on Figure 6.6 that the glucose flux increased with higher glucose concentration in the diffusion cell. In this project, 256.64  $\mu\text{M}$  of glucose was extracted from the 5 mM glucose buffer solution and 434.32  $\mu\text{M}$  from the 20 mM glucose buffer solution. This is in agreement with other studies, where glucose extraction was increased when increasing the concentration in the cell (Jacobsen, 2001; Mackinnon, 2004; Marra et al., 2013). The glucose extraction rate of 24.51  $\text{nmol}/\text{cm}^2\text{h}$  after 60 minutes of RI found from the 5 mM glucose concentration in the diffusion cell is in close agreement with the extraction rate of approximately 21  $\text{nmol}/\text{cm}^2\text{h}$  found by Ching and Connolly (Ching & Connolly, 2008a).

On Figure 6.7 it was seen that more glucose was extracted across the iontophoresis electrodes when increasing the duration of RI, which is in agreement with Arias' study (Arias, 2011). Glucose extraction across both iontophoresis electrodes increased from 180.97  $\mu\text{M}$  after 15 minutes of direct current to 234.49  $\mu\text{M}$  after 30 minutes of direct current to 256.6  $\mu\text{M}$  after 60 minutes of RI with switching polarities. Looking at the glucose extraction rates in Table 6.3, it can be seen that the glucose extraction rate does increase with the duration of RI.

*In vivo* RI experiments:

Transdermal glucose extractions via RI have also been tested on humans subjects (Ching, 2005; McCormick et al., 2012; Potts et al., 2002; Rao et al., 1995; Sieg et al., 2004a, 2004b; Tamada et al., 1995). It is difficult to compare those studies directly

due to their methodological differences, such as the current density or the duration of RI. Rao et al were able to extract 5.8 nmol of glucose at the cathodal chamber after applying a direct current of  $250 \mu\text{A}/\text{cm}^2$  for 60 minutes. In contrast, Chang and Connolly extracted 14 nmol of glucose applying a bipolar current of  $300 \mu\text{A}/\text{cm}^2$  for 60 minutes and McCormick et al. on average 11 nmol after applying a bipolar current of  $100 \mu\text{A}/\text{cm}^2$  for the same time period. The potential of a low iontophoretic current of  $100 \mu\text{A}/\text{cm}^2$ , was successfully shown by McCormick et al as they were able to identify an average glucose flux of  $3.8 \text{ nmol}/\text{cm}^2\text{h}$  ( $2.8 \text{ nmol}/\text{cm}^2\text{h}$  in fasted state and  $4.7 \text{ nmol}/\text{cm}^2\text{h}$  after the post-glucose drink). The obtained flux is comparable with other *in vivo* experiments where even higher RI currents were applied. Tamada et al achieved a glucose flux of  $1\text{-}8 \text{ nmol}/\text{cm}^2\text{h}$  in the RI experiments they have performed. In terms of amount of glucose concentration extracted, McCormick et al. have stated that they extracted on average  $25.9 \pm 5.4 \mu\text{M}$  of glucose across both iontophoresis electrodes in the fasted state and  $47.4 \pm 7.6 \mu\text{M}$  of glucose after the high glucose drink. In the experiments in this study,  $256.64 \mu\text{M}$  of glucose was extracted across both iontophoresis electrodes from the  $5 \text{ mM}$  glucose buffer solution (which simulates the fasted state). And  $434.32 \mu\text{M}$  of glucose was extracted from the  $20 \text{ mM}$  glucose buffer solution, which is supposed to simulate concentrations after the high glucose drink. Even though higher amounts of glucose were extracted in this study compared to the *in vivo* study reported in McCormick et al's study, a similar increase (by a factor of 1.8) of glucose was identified from the fasted state to the state after the glucose drink.

## 7.4 Control of glucose flux using AC

The Medical Diagnostics and Wearables Group at Strathclyde have been working with iontophoresis devices for transdermal glucose monitoring. RI would be very beneficial for continuous, non-invasive, transdermal glucose monitoring for diabetes patients. However, it also has limitations which need to be addressed and overcome.

One of the problems with them is the poorly controlled glucose leading to glucose accumulation once it is extracted into the gel-reservoir of the sensor. This leads to 1) prevention of further glucose extraction from the interstitial fluid 2) inaccurate glucose quantification, as not all the extracted glucose reaches the sensor surface

where glucose detection takes place and 3) causes time lags in the correlation between glucose concentrations in interstitial fluid and blood.

The key aim of this study was to address this issue. Scientists have proposed different agents to overcome this problem such as different glucose binding proteins (Cummins et al., 2013; Li et al., 1998; Scognamiglio et al., 2007) or glucose specific polymers (Chen et al., 1997; Seong et al., 2002). In this study the use of AC to control glucose flux in wearable sensors was explored in accordance with the IP owned by Strathclyde for such devices. As mentioned in Section 2.10, AC has the ability to adsorb organic compounds due to its micropore structure and high surface area. The use of activated carbon (AC) as a glucose binding agent is expected to be able to control glucose molecules once it is diffused into the gel reservoir. By integrating AC in the outer layer of the device the analyte will be continuously drawn from the gel layer into the AC and create a more uniform transdermal glucose diffusion profile due to the adsorption properties of AC to organic compounds. This will prevent any accumulation of glucose in the gel reservoir and any temporal changes in the glucose can be accurately measured. The advantage of the new method using AC is that it is reagentless and does not create any secondary chemicals.

In this section the results of the experiments conducted to test glucose adsorption to AC are discussed.

A lot of research has been conducted to test adsorption of a variety of compounds to AC (e.g. textile dyes (Herrera-González et al., 2019), acetaldehyde/acetone (Wang et al., 2019), chromium and thallium (Adio et al., 2019), gold (Tauetsile et al., 2019), mercury (Hsu et al., 2019), phenols (Dąbrowski et al., 2005)). However, research on the adsorption capability of glucose to AC is limited (Al-aibi et al., 2014; Jin et al., 2017; Sun, 2013).

Both types of AC, which were used in this project, are publicly available for everyday use purposes. The AC pellets, which were used in this project, are intended for the removal of any contaminants in aquariums. And the AC foam is intended for odour removal in compost caddies. Therefore, more detailed information of the base material of the AC, the surface charge, the polarity of the adsorbent, the pore size, the surface area or the pore structure is not known. All the previously- mentioned parameters play

a role in the adsorption process (Summers & Roberts, 1988). Therefore, it was very challenging to establish the exact adsorption characteristics between the glucose and the AC. However, the focus of this project was to explore the possibility of glucose adsorption to AC so that it can be ultimately used for better controlled and improved glucose flux in wearable glucose sensors using RI.

Different experiments were conducted to explore and estimate the AC adsorption capacity to glucose in terms of (1) using two different forms of AC (pellets and foam) (2) changing the initial glucose concentration in the sample (3) changing the AC dose in the experiment and (4) changing the contact time between adsorbent and adsorbate. Also, an adsorption isotherm was established based on the outcomes of the experiments.

#### 1) AC pellets vs AC foam

Two different types of AC were tested for glucose adsorption. The pelletised form of AC is for example used in aquariums, for environmental air treatment, industrial processes and mercury removal (Calgon Carbon Corporation, 2019). It can be prepared by introducing a mixture of powdered carbon with a binder such as coal tar pitch into a pin mixer. By further introducing water to the mixture, agglomerates are built, and pellets are formed. They are then moved first to a drying carbonising furnace before being placed to an activation furnace (Voet & Lamond, 1970). A surface area of 1018 m<sup>2</sup>/g, a true density of 1.28 g/cm<sup>3</sup> and a bulk density of 0.53 g/cm<sup>3</sup> for AC pellets were established by Sarkar and Bose (Sarkar & Bose, 1997). True density is defined as the density, which excludes interparticle voids and pores. In contrast, bulk density is described as the density, which includes the interparticle voids and pores of the sample.

AC in the form of foam is a flexible and lightweight material and commonly used for air filtering (Purair Carbon Filter Company, 2019). It can be prepared using polyurethane sponge (Inagaki et al., 2004; Mercuri et al., 1968) or phenolic foam (Lei et al., 2010; Mercuri et al., 1968; Zhao et al., 2009) as the precursor material. Physical characteristics such as surface area, density, pores size of the AC foam depends on the type, heat treatment and quality of the precursor (Mercuri et al., 1968). Mercuri et al. identified a bulk density of 0.27 g/cm<sup>3</sup> with phenolic foam as a precursor (Mercuri et al., 1968). Lei et al were able to increase the bulk density of AC from 0.24 g/cm<sup>3</sup> to

0.73 g/cm<sup>3</sup> by increasing the phenolic resin concentration. A surface area of 727.62 m<sup>2</sup>/g and a pore size between 3.5 nm to 5 nm was identified with AC foam made of phenolic resins (Zhao et al., 2009).

In this project, the density of AC pellets was calculated as 1.87 g/cm<sup>3</sup> without considering the pore structure. A difference of ±0.59 g/cm<sup>3</sup> can be established compared to the true density obtained by Sarkar and Bose (Sarkar & Bose, 1997). On one side, variations could be due to the average values used for the weight of the AC pellets and for the length of the AC pellet to calculate the volume of the AC pellets. On the other side, deviations could be due the differences in base material and the manufacturing process of the AC pellets.

A true density of 0.28 g/cm<sup>3</sup> was identified for the AC foam used in this project. This indicates that the bulk density will be of lower value. In contrast, higher bulk density were identified by Mercuri et al. and Lei et al (Lei et al., 2010; Mercuri et al., 1968). Variations could be due to differences in the type, quality and heat treatment of the precursor material of the AC foam (Mercuri et al., 1968).

A decrease in the initial sample volume of 100 µL in each well was observable after the incubation with AC for 60 minutes. 75 µL of the glucose solution was left after the incubation with AC pellet and only approximately 60 µL of the sample volume was left after the incubation with AC foam. At the same time, an increase of weight of the AC pellet respectively the AC foam was observable. Water can adsorb to the O<sub>2</sub>- containing functional groups in the AC via hydrogen bonding (Bandosz, Jagiełło, and Schwarz 1996, Müller et al. 1996; Müller and Gubbins 1998; McCallum et al. 1999; Müller et al. 2000). McCallum et al. identified a surface site density of 0.675 sites/nm<sup>2</sup> when testing water adsorption to AC (McCallum et al., 1999). This could explain the decrease in the sample volume and increase of the weight of the AC pellets and foams. In addition, the decrease of sample volume could also be due to evaporation of the buffer solution.

The higher decrease in sample volume when incubating the sample with AC foam might be due to the water absorption characteristics from e.g. the polyurethane foam itself (Sabbahi & Vergnaud, 1993). This could explain the higher wet-weight for AC foam than AC pellets after the 60 minutes incubation time with the glucose solution.

For future devices, the decrease in sample volume imply that over time available binding sites of AC will be fully consumed and AC needs replacement to ensure adsorption capabilities to glucose.

A higher decrease in the sample volume (50  $\mu$ L) using gel can be explained due to practical difficulties when removing the gel out of the well into a new well. Gel is more difficult to pipette due to its higher viscosity. Furthermore, higher glucose adsorption per one gram of AC foam was calculated, which might be partially due the absorption of the glucose solution by the foam.

#### 2) Effect of increasing glucose concentration on the adsorption process

Based on the results in this project, the adsorption is improved with increasing initial glucose concentration in the sample. This phenomenon is in agreement with the experiments where adsorption was enhanced with increasing adsorbate concentration in the sample (Namasivayam & Kavitha, 2002; Suman, 2013; Sun, 2013). This can be explained by when increasing the concentration of adsorbate in the solution, there will be more solutes on the interface between adsorbate and adsorbent, which increases the adsorption. It is expected that after a certain amount of adsorbate is adsorbed saturation will be reached as all the available sites in the AC pore structure are filled.

#### 3) Effect of increasing the amount of AC to the adsorption process

In the experiments conducted here, an enhanced glucose adsorption was observable when increasing the amount of AC. This is due to the fact that increasing the amount of AC results in the rise of the surface area, which in turn leads to more adsorption sites (Hsu et al., 2019; Mohan & Singh, 2002; Namasivayam & Kavitha, 2002).

#### 4) Effect of contact time to the adsorption process

From literature it is expected that adsorption increases over time until equilibrium time is reached (Çeçen, 2014). At equilibrium maximum adsorption is reached and the amount of adsorbate in the bulk solution is equal to the amount of adsorbate adsorbed to the adsorbent. Adsorption experiments can be performed at static conditions or at an agitated state, which would decrease the contact time to reach equilibrium. However, in this project experiments were performed at static condition as the aim is to explore the potential use of AC in wearable sensors, where glucose is detected in a static state.



The main focus in this project is to observe the adsorption behaviour after 60 minutes, as the duration of RI experiments in this study is 60 minutes in total with switching polarities every 15 minutes. It was shown that during a RI duration of 60 minutes sufficient amount of glucose can be extracted for detection (Ching & Connolly, 2008c; McCormick et al., 2012).

In the experiments conducted in this project with glucose solutions, approximately 54 % was adsorbed after an incubation time of 60 minutes. Glucose adsorption was still linearly increasing after 80 minutes of contact time. The contact time should have been further increased to identify the equilibrium time from glucose solution. For gel samples, around 62 % of the initial glucose concentration was adsorbed after 60 minutes of incubation and saturation had started.

The equilibrium time depends on the adsorbate-adsorbent interaction. In Sun's project, they identified an equilibrium time of 120 minutes for glucose to adsorb to AC powder at an agitated state (Sun, 2013). Al-naibi et al. tested glucose adsorption to GAC at different speed of agitation and reported that initially adsorption occurred rapidly followed by slow down and then stagnation of the adsorption over time (Al-aibi et al., 2014). In a different study the adsorption of methylene blue was tested on AC and they identified an equilibrium time of six hours (Herrera-González et al., 2019). The equilibrium time for cadmium and zinc adsorption to AC was reached after ten to twelve hours (Mohan & Singh, 2002). An equilibrium state after ten minutes of agitation time for the dye Congo red adsorption to AC was identified by a different research group (Namasivayam & Kavitha, 2002)

According to Walter and Weber, adsorption occurs in three steps in a solid- liquid interface (Weber Jr, 1974). 1) The adsorbate needs to be transported from the bulk solution to the exterior surface of the adsorbent. 2) Some solutes will adsorb to the exterior surface of the adsorbent. Some solutes will diffuse through the pores to the interior the adsorbent. 3) Adsorption of the solutes to the interior surface of the adsorbent.

Based on the calculations of the diffusion fluxes across glucose solution and glucose gel samples, it was observable that initially (until 40 minutes of contact time) diffusion occurred faster in solution than in samples in gel format. After 60 minutes of contact,

similar fluxes were observable for glucose solution and gel samples. The rate of diffusion depends on the temperature, concentration in the sample, the diffusion distance and the medium where the diffusion occurs. As the first three mentioned parameters were held constant in both populations, the difference in rate can be explained by the different media in which diffusion occurred. Gel can interfere the diffusion of a solute (1) via binding capabilities of the solute by the gel (2) via filter action of the gel if the pores of the gel network is smaller than the solutes (3) via increasing the path length for diffusion as the solute has to detour due to gel threads or gel particles (Lauffer, 1961). Another aspect to consider is the possibility of the gel to block the AC adsorption sites and therefore limit the adsorption capabilities of AC. In addition, the higher viscosity of the gel which makes it more difficult for the glucose to diffuse into the foam.

- Adsorption isotherm of glucose adsorption to AC

Adsorption isotherms are ideal to understand the adsorption process and the adsorbent-adsorbate relationship. A linear adsorption isotherm for glucose adsorption to AC foam was found in this project in the selected low glucose concentration range for glucose sample in solution format ( $< 600\mu\text{M}$ ) and in gel format ( $< 500\mu\text{M}$ ). Sun identified a BET adsorption isotherm when testing glucose adsorption to a powdered form of AC (Sun, 2013). However, the tested glucose concentration range was above  $500\mu\text{M}$ . Al-aibi et al. identified a Freundlich adsorption isotherm model when testing glucose adsorption to granular AC (Al-aibi et al., 2014). Different adsorption isotherms were identified when looking at glucose adsorption to AC but this could be due to the difference in the glucose concentration range. As it was observable in Figure 2.31, a linear relationship is observable in most adsorption isotherms in low concentrations. Furthermore, the adsorption depends on a variety of factors, such as type of adsorbent and concentration of the adsorbate, temperature etc. which can cause differences in the established adsorption isotherms.

- AC in RI experiments

The successful glucose adsorption to AC, indicates that AC could have the potential for improved and better controlled glucose flux in wearable glucose sensors.

Therefore, a prototype of an AC- integrated electrode system was developed and tested in the *in vitro* RI experiments using the diffusion cell.

An increase of glucose extraction was observable with the with AC- integrated electrodes were seen. Glucose extraction was improved by a factor of 2.8 across the E1 electrode. The glucose fluxes in the control group agree with the results obtained in the RI experiments in Section 6.3.3. The increase of glucose using the AC- integrated sensors is due to the use of AC as this was the only difference between both groups.

The increase of glucose flux can be explained through the following mechanism: The application of RI allows glucose to enter the gel reservoir of the sensor. glucose was further attracted to diffuse through the gel because of the adsorption characteristics of AC. Approximately 12.57 mm<sup>2</sup> of the surface of the AC foam, which was positioned at the back of the sensor, was exposed to gel in the gel reservoir. This in turn allowed the diffusion of more glucose molecules into the reservoir. The problem with the sensors without AC is the glucose build-up in the gel and the resulting blockage of the diffusion of more glucose molecules. Hence, it can be concluded that AC foam did improve glucose flux and has the potential to act as a glucose binding agent in glucose sensors for RI experiments.

High standard deviations can be seen on the RI experiment with the AC- integrated sensors. This indicates the variation of the adsorption capabilities of AC foam to AC foam. When performing the experiments, only the initial weight of AC foam was considered to ensure uniformity and therefore AC foams with similar weight were involved in each sensor. But the important parameter to ensure uniformity and repeatability of the sensor is to use AC foams with similar surface areas. However, the identification of the surface area of the AC foam would exceed the scope of this project. Advanced techniques such as such as the nitrogen adsorption at 77K (Sing, 1995) or the iodine number (Mianowski et al., 2007) could be used to determine the surface area of AC.

As no other research groups have attempted improved glucose extraction via RI with the help of AC, the results obtained here, could not be compared to other relevant literature.

The extracted glucose from the RI experiments was measured via colorimetric assay. The ultimate aim is to quantify glucose via electrochemical means which allows direct glucose quantification using a glucose sensor. The next section discusses the experiments conducted to develop a mediated enzymatic glucose sensor, which can be potentially used to quantify glucose extracted via RI.

## 7.5 Electrochemical detection of glucose

The integration of a biosensor in the electrode system enables in-situ quantification of the extracted glucose via the application of RI.

Thick-film technology by screen printing methods are often applied to produce biosensors. The main advantages of this method are that it is of low cost, has high reproducibility and it permits mass production (Galán-Vidal et al., 2000). The means of cyclic voltammetry (CV) was used to analyse the embedded glucose sensor in the electrode system. The preliminary experiments conducted with the three-electrode system design helped to get familiarised with the fundamentals of CV and to comprehend the electrochemical characteristics of the mediator and mediator-enzyme interaction in the liquid environment before performing experiments in the gel environment. This was important as studies have shown different behaviour of the glucose sensor in liquid and gel environment.

### 7.5.1 Preliminary experiments

The ferrocene derivate, ferrocene monocarboxylic (FMCA) was the analyte of interest in the preliminary experiments. In this study an anodic peak potential of 0.256 V and a cathodic peak potential at 0.195 V was identified for FMCA. The three characteristics of a reversible system, which were discussed in section 4.1.3.4 (Wang, 2001), could be confirmed for the FMCA experiment with slight inaccuracies: 1) A peak to peak separation of 0.061 V was yielded between the anodic and cathodic peak potential in this study. Compared to theory, a one-electron transfer in a reversible system is characterised with a peak separation of 0.059 V indicating a difference of only 0.002 V to the voltage found in this study. 2) The second criteria of a reversible system states that the ratio of the anodic and cathodic peak current equals to 1. In this

study a ratio of 1.01 was found, which is in close agreement with the expected value of 1. 3) A linear relationship was found between the square root of the scan rate and the anodic peak potential as expected from theory. 4) And finally, the anodic peak potential did not vary with changing the scan rate, which is in agreement with the final criteria of a reversible system.

A redox potential of 0.226 V vs the screen-printed Ag/AgCl electrode was found for FMCA in this study. In McColl's study (McColl, 2001) a similar protocol was followed as in this study and a redox potential of approximately 0.25 V for FMCA was identified. The redox potential from McColl's study is similar to the redox potential identified in this study. However, it is in disagreement with the redox potential of FMCA identified by Sakura and Buck (Sakura & Buck, 1992). They identified a redox potential of 0.3 V vs Ag/AgCl. The difference might be due to methodological differences between the studies.

A diffusion coefficient of  $3.8 \times 10^{-6} \text{ cm}^2/\text{s}$  was calculated for FMCA in this study. Cass et al. identified a diffusion coefficient of approximately  $3 \times 10^{-6} \text{ cm}^2/\text{s}$  for FMCA (Cass et al., 1984) and Sakura et al identified a diffusion coefficient of  $6.97 \times 10^{-6} \text{ cm}^2/\text{s}$  in their study (Sakura & Buck, 1992), which is in the similar range to the one identified in this study.

- FMCA – Glucose oxidase (GOD) interaction in the liquid environment:

The FMCA (mediator) -GOD (enzyme) interaction in free solution was conducted to understand the effectiveness and operation of the second-generation glucose sensor where a mediator is used to transfer electrons from the GOD to the electrode. The CV obtained with the mediator in the presence of glucose and upon addition of the enzyme is similar to the experiments conducted by other researchers (Cass et al., 1984; Harper & Anderson, 2006; Iwuoha & Smyth, 1994; McColl, 2001; Sakura & Buck, 1992). Upon the addition of the enzyme, a high catalytic current was observable at oxidising potential, which is commonly seen at slower scan rates and can be explained by the regeneration of the FMCA.

In the first generation of glucose sensors, glucose is quantified based on the amount of  $\text{H}_2\text{O}_2$ , which is produced in the oxidation process of glucose to gluconolactone catalysed by GOD. The oxidation potential of  $\text{H}_2\text{O}_2$  is at 0.6 V vs Ag/AgCl, and the

current produced at the oxidation process is proportional to the glucose concentration. The disadvantage of the high oxidation potential of  $\text{H}_2\text{O}_2$  is that other electroactive species in biological fluids such as ascorbic acid, acetaminophen or uric acid might get oxidised as well, which reduces the specificity of the signal to glucose. In this experiment the catalytic current could be measured at a lower potential of 0.36 V vs Ag/AgCl.

An anodic peak potential of 0.32 V for FMCA was found in this study which is in close agreement with other research groups. Wang et al identified an anodic peak potential of 0.33 V to 0.35 V vs Ag/AgCl for FMCA and Sakura and Buck found an oxidation potential of 0.335 V vs Ag/AgCl (Sakura & Buck, 1992; Wang et al., 1990). However, big differences were found in the reduction peak potential. In this study a reduction peak was found at the potential of 0.21 V, the reduction peak found by Sakura and Buck was at 0.265 V. The high peak to peak separation in this study indicating a non-reversible system could be due to the slow scan rate or due to the absence of a supporting electrolyte (Compton et al., 2012a) Even though a high peak current separation was seen, the ratio of the anodic peak current to the cathodic peak current was 0.97, which is close to what is expected from a reversible electron transfer. A similar diffusion coefficient of  $5.28 \cdot 10^{-6} \text{ cm}^2/\text{s}$  for FMCA in solution was established for this experiment as in previous FMCA experiments ( $3.79 \cdot 10^{-6} \text{ cm}^2/\text{s}$ ) conducted in section 6.5.1.

The experiment conducted with the FMCA and GOD in the solution in the liquid environment helped to understand electrochemical characterisation of a mediated enzymatic sensor.

Obtaining sensible results in the preliminary CV experiments, which are comparable to literature shows good operation of the three-electrode design, which were produced in the Biomedical Engineering department via screen-printing methods.

## 7.6 Glucose sensors

In the RI environment the glucose sensor should ultimately measure the glucose extracted from the interstitial fluid (ISF). As discussed in section 2.6, good correlation between glucose concentration in interstitial fluid and capillary blood glucose

concentration were identified in several studies (Bantle & Thomas 1997; Thennadil et al. 2001; Cengiz & Tamborlane 2009). The challenge in developing a glucose sensor in the RI environment is that the glucose extracted from ISF via RI is about two orders of magnitude less of the corresponding actual glucose concentration in the ISF (Bandodkar et al., 2014; Kim et al., 2018; McCormick et al., 2012). Therefore, the glucose sensors in the RI environment need to be more sensitive and have a lower detection limit.

The golden standard for glucose measurement by biosensors is based on an enzymatic reaction.

Until now, only one product based on RI combined with biosensing technology has been commercialised, the GlucoWatch Biographer by Cygnus Inc. However, it was withdrawn from the market in 2008 due to several limitation of the devices itself such as, inaccuracy and skin irritation (Oliver et al., 2009). More research in the field of RI is underway and other research groups were able to develop working examples of iontophoresis devices for transdermal monitoring of glucose (Bandodkar et al., 2014; Kim et al., 2018).

Table 7.1 shows a list of selected glucose sensors, which were used for the quantification of glucose sampled from interstitial fluid via RI.

*Table 7.1 Details of selected glucose sensors used for glucose quantification sampled by RI*

<b>Enzyme</b>	<b>Based on</b>	<b>Applied potential</b>	<b>Working electrode</b>	<b>Reference electrode</b>	<b>Reference</b>	<b>LOD</b>	<b>Upper linear range</b>
GOD	H <sub>2</sub> O <sub>2</sub> detection	-0.1 V	Prussian Blue modified carbon	Ag/AgCl	(Bandodkar et al., 2014)	3 μM	100 μM
GOD	H <sub>2</sub> O <sub>2</sub> detection	0.42	Platinum-graphite	Ag/AgCl	(Tierney et al., 1999)	5 μM	-
GOD	H <sub>2</sub> O <sub>2</sub> detection	-0.2 V	Prussian Blue modified carbon	Ag/AgCl	(Kim et al., 2018)	-	160 μM

It can be seen that all of the glucose sensors belong to the first generation of glucose sensors, which are based on an enzymatic reaction and the amount of hydrogen peroxide produced, which is in relation to the glucose concentration, is detected (Karyakin et al., 1995). All three sensors were tested in the low glucose concentration and a sufficiently low LOD was identified for Tierney et al's and Bandodkar et al's sensor indicating its suitability to quantify glucose concentrations expected from RI experiments. Even though the LOD of sensor developed by Kim et al was not provided, it was reported that the sensors were able to detect glucose extracted via RI (Kim et al., 2018).

In this study glucose detection was attempted by integrating a mediated enzymatic glucose sensor in the electrode system, which belong to the second generation of glucose sensors. The main responsibility of a mediator is to transfer electron(s) between the enzyme and the working electrode. The current produced due to the oxidation of the mediator, is proportional to the glucose concentration.

The sensor fabrication in this study was adapted from the glucose sensor developed by Cass et al (Cass et al., 1984). For the fabrication of the glucose sensor in this study, glucose oxidase was used as the enzyme as it is commonly used in glucose biosensors due to its high selectivity and sensitivity towards glucose (Bandodkar et al., 2014; Tamada et al., 1995; Tierney et al., 2001). 1,1 Dimethylferrocene (DMFc) was used as the mediator for the glucose sensors as it showed best characteristics within the ferrocene derivatives with regards to oxidation of glucose oxidase and immobilisation of the mediator onto the sensor (Hill & Sanghera, 1990; Wang et al., 1990). This type of ferrocene-mediated glucose sensors has also been implemented in *in vivo* studies where the sensors were subcutaneously implanted in the neck of the pigs (Claremont et al., 1986).

In the glucose sensors shown in Table 7.1, different methods for enzyme immobilisation were applied. For example, in the GlucoWatch, the GOD was dissolved in the gel itself (Tierney et al., 1999). However, one of the reported problems of the GlucoWatch was the temporary skin irritations (Eastman et al., 2002; Gandrud et al., 2004; Garg et al., 1999; Tamada et al., 1999; Tierney et al., 1999). On one side skin irritations could have been developed due to intensity of the applied iontophoretic current. On the other side, it was considered that as the gel is in contact with the skin,



the accumulation of  $\text{H}_2\text{O}_2$  in the gel reservoir could be the source itself to cause skin irritation (Agency for Toxic Substances and Disease Registry, 2014). In Bandodkar's and Kim's study the GOD solution was mixed with a chitosan solution and immobilised onto the working electrode (Bandodkar et al., 2014; Kim et al., 2018). In the mediated enzymatic glucose sensor in this project, the mediator and enzyme were directly embedded onto the working electrode surface to prevent any skin contact. DMFc was covalently bound to the carbon electrode surface and the GOD was bound to the DMFc via a carbodiimide layer.

The fabricated glucose sensor was tested in the gel environment as the samples from experiments involving- *in vivo* glucose extraction via RI were in gel format.

### 7.6.1 Electrochemical characterisation of the DMFc-GOD sensor in the gel environment

The operation of a glucose sensor in the gel environment is different to a fluid environment. Only limited number of researchers have investigated in the glucose sensor operation in gel (Bandodkar et al., 2014; Kim et al., 2018; Künzelmann & Böttcher, 1997; Kurnik et al., 1998; Tierney et al., 1999).

The means of cyclic voltammetry (CV) was used for electrochemical characterisation of the fabricated sensor.

As it was shown in section 5.5, the fabricated glucose sensor had two sensing units integrated: Side A of the sensor was coated with the DMFc and the carbodiimide solution and with glucose oxidase and is responsible to detect any glucose related current changes. Side B of the glucose sensor is only coated with DMFc and the carbodiimide and without glucose oxidase. It is intended to identify any background current or any current caused by any interfering species.

For the voltammogram taken on side B of the sensor (Figure 6.30.), an oxidation and reduction peak of DMFc was expected. As from theory it is expected that DMFc undergoes a reversible one electron transfer at a redox potential of 0.100 V vs SCE (Cass et al., 1984). The redox potential was converted to 0.132 V vs Ag/AgCl (3M KCl) with an anodic peak potential of 0.1615V and a cathodic peak potential of 0.1025 V vs an Ag/AgCl (3 M KCl) standard electrode as shown in section 4.3.5.

In this study an anodic peak potential at 0.12 V could be identified for side B of the sensor. The shift in the oxidation potential of DMFc could be explained by results of the open circuit potential experiments, which were shown in section 6.5.3. A shift in the open circuit potential was observable when testing the screen-printed RE against the commercially available standard glass Ag/AgCl (3 M KCl) electrode reference electrode in different media. The open cell potential shifted from of 0.26 V in the phosphate buffer to an open cell potential of 0.22 V in gel. Thus, a difference of 0.04 V was identified between both media. Considering the open cell potential shift in the DMFc oxidation peak given by Cass et al, the oxidation would be expected at a potential of 0.1215 V, which is in close agreement with the oxidation potential found in this study.

In disagreement to theory (Cass et al., 1984), no reduction peak was seen for DMFc. If the electron transfer between the mediator and the working electrode is too slow, a reduction will not occur (Kissinger & Heineman, 1983). The electrode reaction rate depends on several factors: 1) the mass transfer, the transport of the analyte from the bulk solution to the electrode surface 2) the electron transfer, which occurs on the electrode surface, 3) the chemical reaction causing the electron transfer and 4) any other reactions occurring on the surface (Krishnan, 2011). For the electrochemical reversibility, it is required that the electron transfer is faster than the mass transfer.

Side A of the sensor is coated with the GOD and is responsible to detect any glucose related current changes. With the help of CV, an oxidation potential at 0.14 V vs the screen-printed pseudo Ag/AgCl reference electrodes was identified for the DMFc-GOD reaction with Side A of the glucose sensor. However, in disagreement to literature (Cass et al., 1984) and same as for side B of the sensor no reduction peak was seen, which is possibly due to slow electron transfer.

- FMCA-GOD interaction in solution vs DMFc - GOD interaction in gel:

Similar results were expected for the FMCA-GOD interaction shown in Figure 6.25 and the DMFc-GOD interaction in Figure 6.30. They are both based on the same principle, where a voltammogram was recorded in the presence of the mediator and analyte and another voltammogram was taken in the presence of the mediator, analyte

and enzyme. Side B was expected to agree with Figure 6.25a, where without the presence of the enzyme, the redox reaction of the ferrocene should be shown. And side A should correspond to Figure 6.25b, where upon the presence of the enzyme, a catalytic current is expected to flow.

For DMFc, a peak current of 84.33 nA was identified at an oxidation potential of 0.1249 V and a catalytic current of 99.24 nA at a potential of 0.14 V was observable in the presence of GOD with a glucose concentration of 62  $\mu\text{M}$  in the test sample.

In contrast, for FMCA, a diffusion current of 1.18  $\mu\text{A}$  at the anodic peak voltage of 0.32 V was identified in the absence of GOD. A catalytic current of 5.74  $\mu\text{A}$  at a potential of 0.36 V in the presence of GOD with a glucose concentration of 50 mM.

The higher increase of the catalytic current could be due to the higher glucose concentrations involved. Peak currents were found in the  $\mu\text{A}$  range in the liquid environment, whereas in the gel environment currents were observed in the nA range. The lower currents in the gel environment corresponds well to the lower diffusion coefficient of  $2.9 * 10^{-8} \text{ cm}^2/\text{s}$ , which was found for DMFc in the gel environment. For FMCA, a diffusion coefficient of  $5.28 * 10^{-6} \text{ cm}^2/\text{s}$  was found in in the liquid environment, which was in close agreement with the diffusion coefficient found by Cass et al. The diffusion coefficient is expressed with the Einstein-stokes equation (Equation 4.28) and it relates to the diffusion and viscous flow in a system. Based on the equation, it can be seen how the diffusion coefficient is dependent on the viscosity of the medium. Hence, the lower diffusion coefficient for DMFc can be explained by the higher viscosity of the gel compared in solution. Also in McColl's study, a decrease in the diffusion coefficient was found when increasing the viscosity of the gel (McColl, 2001).

It was shown that the response time of the sensor is slower in hydrogel compared to in an aqueous solution because of the lower diffusion coefficient in gel (Kurnik et al., 1998). In McColl's study the developed biosensor was tested by amperometric measurements. Thereby, a drop of a highly concentrated glucose solution was dropped into the gel and the current over time was measured at a constant potential. A current response due to the glucose was only seen after 30 minutes in the 2% gel and after 60 minutes in 4% gel. In contrast in fluid environment an instantaneous response was seen in McColl's study. Wang et al identified a fast response time of 30 s in the DMFc

– GOD, where the mediator and enzymes was incorporated in the carbon paste and glucose detection was tested in the liquid environment (Wang et al., 1990).

A reduced catalytic current in the gel environment could be also caused by the immobilisation of the mediator and enzyme onto the electrode, thus slightly compromising their activity. In contrast, in the FMCA-GOD experiment, both mediator and enzyme were both in liquid form.

A high level of noise was observable in the cyclic voltammetry experiments using the sensor in the gel environment. This suggests that the gel itself is not providing a uniform environment for the analyte to diffuse.

Even though, the operation of the glucose sensors is compromised in the gel environment compared to the liquid environment, the use of gel is crucial in the RI environment. It is required for electrical conductance to apply the iontophoretic current and it also serves as a receptacle for the extracted molecules.

## 7.6.2 Sensor performance

A calibration curve was established using the developed glucose sensor. The aim was to quantify unknown glucose concentration in the  $\mu\text{M}$  range from samples obtained via RI. For the establishment of the calibration curve with the glucose sensor, the ratio of the current reading of side A to the current reading of side B was plotted against the standard glucose concentrations. A linear relationship could be seen with a straight line fit of  $y=0.0097x+1.4127$  and an  $R^2=0.87$ . An LOD of  $77.09 \mu\text{M}$  could be identified. High error bars were seen in the calibration curve on Figure 6.31. They could be due to differences from sensor to sensor. All three coatings from glucose sensors were carefully applied to maintain consistency between the sensors. However, it has to be considered that they were all done manually, hence slight inconsistencies might have arisen due to human error.

However, the LOD found in this study is higher compared to the sensors used in the RI environment shown in Table 7.1. Therefore, more research needs to be conducted to improve the sensitivity of the sensor so that the LOD can be further lowered.

In Bandodkar's study, the developed sensor was tested in the glucose concentration range from  $0 \mu\text{M}$  to  $100 \mu\text{M}$  in increments of  $10 \mu\text{M}$  (Bandodkar et al., 2014). The

chronoamperometric current responses had a linear response to the tested glucose concentrations and they identified a LOD of 3  $\mu\text{M}$ . The current increased by approximately 2  $\mu\text{A}$  from the 0  $\mu\text{M}$  to the 100  $\mu\text{M}$  concentration. Kim et al analysed their developed sensor over the 0  $\mu\text{M}$  to 160  $\mu\text{M}$  glucose concentration range in increments of 20  $\mu\text{M}$  (Kim et al., 2018). In their study the current increased by approximately 1.5  $\mu\text{A}$  from the 0  $\mu\text{M}$  glucose concentration to the 160  $\mu\text{M}$  concentration.

In comparison, the current increase found in this study was in a much lower current range. In this study, a current of 0.14  $\mu\text{A}$  was identified in a 250  $\mu\text{M}$  glucose sample in 3% methylcellulose gel and an average background current of 75.6 nA was found in the gel sample without any glucose. Thus, the current only increased by 65.4 nA.

In McColl's study, a current of 0.3  $\mu\text{A}$  was identified at a glucose concentration of 10 mM in a 4% hydrogel and a higher current of 0.9  $\mu\text{A}$  was found using a 2% hydrogel (McColl, 2001). Compared to McColl's study, a slightly lower current could be identified with 3% gel for a much lower concentration. However, it has to be kept in mind that in this study, cyclic voltammetry was applied to analyse the sensor performance. However, in the other reported studies (Bandodkar et al., 2014; Kim et al., 2018; McColl, 2001), the sensor was evaluated using amperometric measurements. Hence, direct comparison cannot be made due to methodological differences.

## 7.7 Glucose sensors used *in vitro* RI experiments using the diffusion cell

The glucose sensors were also used alongside the diffusion cell to test its ability to electrochemically detect glucose, which was extracted via RI. From the previous experiments with the fabricated glucose sensor, an oxidation peak at a voltage of 0.14 V was expected.

But instead, two oxidation peaks appeared in the voltammograms after RI for side A and side B of the electrode, one at 0.082 V and the second one at 0.306 V. The occurrence of the peak could have been due to a shift of the glucose peak. However, based on the results obtained in section 6.7.2, it can be said that both peaks are not in relation to the extracted glucose as no correlation could be established.

The total peak current, which can be seen in the voltammogram consists of a faradaic component and a non-faradaic component. Only the faradaic current is caused by the electron transfer processes and is in relation to the glucose concentration.

The non-faradaic current is caused by the charging and discharging of the electrode double layer at the working electrode in response to the variation of the applied potential. The charge of the electrode changes with the varying the applied potential. Consequently, a rearrangement of ions in the electrical double layer occurs. Depending on the charge of the electrode, the ions in the solution will either be attracted or repelled from electrode surface without necessarily having to go through a redox reaction (Compton et al., 2012a). For example, at the application of a positive current, anions will be attracted, and cations will be repelled from the electrode. This phenomenon causes a capacitive current, which needs to be accounted for to identify the current solely caused by the electron transfer.

As discussed, the identification of the capacitive current of the voltammograms after the RI experiments was not a straight-forward process due to the complexity of the CV. Kissinger's method was nevertheless applied to approximate the capacitive current. However, in some cases, the capacitive current exceeded the peak current when applying Kissinger's method. On the one hand, the high capacitive current could be an indication of the inapplicability of the method for the obtained voltammograms. There are other methods than Kissinger's method for the identification of the capacitive current of a voltammogram (Papaderakis, 2016; Silva et al., 2001) . However, they are not feasible to be applied retrospectively. For example, the electrical double layer (EDL) capacitance can be identified using electrical impedance spectroscopy. Thereby, an AC signal in a broad range of frequency is applied to an electrochemical cell to capture its impedance spectrum, which in turn enables to measure the diffusion, the capacitive and the inductive processes at the electrode-electrolyte interface.

On the other hand, the higher capacitive current could be due to the fact that the EDL capacitance having an effect on the faradaic processes on the electrode surface due to the adsorption of the co-extracted molecules during RI onto the EDL. Especially in

electrode reactions, which involve redox reactions of electroactive species at low concentrations, there is the chance that the non-faradaic current caused by the EDL is higher than the faradaic current (Bard & Faulkner, 2001b). The capacitive current depends on the scan rate, the electrode area and also involved salt concentration (Compton et al., 2012a). Therefore, it seems that the change in the CV might have been resulted from the co-extracted solutes such as NaCl and the KCl, from the diffusion cell, which have caused the masking of the glucose peak. More cyclic voltammetry experiments should be conducted to investigate the glucose sensor performance in the presence of each solutes of in the buffer solution of the diffusion cell separately in future studies.

In comparison to the electrochemical glucose detection method, the extracted glucose was also measured using the standard laboratory method using the glucose assay kit and an optical spectrophotometer. From theory, it was expected that the E1 electrode extracts the glucose the most, followed by the E2 electrode and the control electrode extracts the least amount of glucose. Overall, this pattern was followed with minor exceptions. Higher error bars were seen on the RI experiment with the AC- integrated sensors. Similar behaviour was seen in the results shown in section 6.4.6. and could be explained by the variation of the adsorption capabilities of AC foam to AC foam. Even though all the AC foams had a thickness of 0.1 cm and a diameter of 2 cm, it is important to account for the surface area of the use AC to ensure uniformity and repeatability of the sensor. However, this information was not known. Advanced techniques such as such as the nitrogen adsorption at 77K (Kenneth S.W. Sing, 1995) or the iodine number (Mianowski et al., 2007) could be used to determine the surface area of AC.

As discussed, one of the key aims in this study was to address the glucose accumulation in the sensor, which ultimately causes time lags in the correlation between the glucose in the interstitial fluid and blood. Poor correlations with  $R^2 = 0.53$  (McCormick et al., 2012) and  $R^2 = 0.44$  (Ching & Connolly, 2008c) were found in the *in vivo* studies between the blood glucose concentrations and the extracted glucose via RI which were explained by the skin variability in terms of pore size and permeability in humans. The GlucoWatch overcame this problem by using invasive means where users had to take

a fingerstick blood glucose measurement every 12 hours for calibration purposes. Studies showed a correlation factor of 0.89 with the GlucoWatch (Tamada et al., 1995, 1999).

In this study, good correlation with  $R^2 = 0.99$  could be established between the extracted glucose via RI across both iontophoresis electrodes and the glucose concentration in the diffusion cell as it can be seen in Figure 6.35. Also with the AC-integrated glucose sensor, a good correlation of  $R^2 = 0.90$  could be identified. The linear relationship, which was observable between the glucose concentrations in the diffusion cell and the extracted glucose across both iontophoresis using the AC-integrated glucose sensors, had a higher gradient compared to the sensors without AC, indicating its higher sensitivity of the system with AC.



## 7.8 Research limitations

### Limitation of adsorption studies

Glucose extraction was improved when using AC- integrated electrodes in the *in vitro* RI experiments using the diffusion cell. When performing the RI experiments with the AC foam integrated electrodes, only the initial dry weight of AC foam and the volume without considering the porous structure were taken into account to ensure consistency within the AC foams involved in each sensor. However, the porous structure of the AC and thereby increased surface area plays a major role in the adsorption capabilities of the AC. No such information was provided for the used AC. Therefore, the adsorption capabilities might vary from foam to foam.

In the initial design of the AC-integrated electrodes, the AC foam was secured at the back of the electrode design. Holes were drilled through the electrodes design so that the analyte is drawn from the gel layer to AC foam. They were evenly distributed over the whole electrode design as it can be seen in Figure 5.15 and approximately 0.126 cm<sup>2</sup> of the AC foam was exposed to gel.

It is possible that some of the extracted glucose diffused through the gel into the AC. Consequently, when analysing the gel for glucose, it is possible that not all of the extracted glucose was accounted for. Nevertheless, more glucose was extracted using AC- integrated electrodes than using the electrodes without any AC.

Although the suitability of AC as glucose binding agent in RI experiments were successfully shown in this study, it has to be noted that all experiments were conducted *in vitro* using a diffusion cell and an artificial membrane. The effectivity and suitability of the AC as a glucose binding agent might be different in the *in vivo* RI environment.

### Limitation of work conducted with glucose sensors

It is important that the fabricated glucose sensors are all prepared in the same manner to maintain consistency within the sensors and so that the results can be compared. The fabrication of the sensors involved the application of three layers of coatings including washing procedure of the electrodes after the first coating. Even though,

highest amount of care and precision was given, it has to be considered that they were all done manually, hence causing slight inconsistencies.

As discussed in section 5.10.3, before putting sensors on diffusion cell, CV was performed on both sides of all three sensor to ensure sensor performance. An empirically observed particular peak and shape for each side had to be confirmed before putting sensor on the diffusion cell. Only once three electrodes could be selected, they were applied onto the diffusion cell. This caused some time delays exposing the sensor to air, which might have affected the consistency of the gel.

In the AC-integrated glucose sensors, the AC foam was secured at the back of the electrode design. Holes were punched through the electrodes design so that the analyte is drawn from the gel layer to AC foam. They were evenly distributed over the whole electrode design as it can be seen in Figure 5.19 and approximately  $0.135 \text{ cm}^2$  of the AC foam was exposed to gel.

For electrochemical glucose detection it is important that the analyte reaches working electrode where the glucose sensing takes place. The size of the sensing unit within the sensor is smaller than the gel reservoir where glucose is collected. Consequently, due to the current electrode design it is possible that the glucose extracted outside the sensing area might have diffused directly through the gel layer to the closest AC without reaching the sensing unit. Hence, not all the glucose extracted could be quantified.

#### Limitations of Data analysis

Cyclic voltammetry is a powerful electroanalytical technique, which allows the monitoring of the current produced via a redox reaction as a function of potential. It allowed the electrochemical characterisation of the fabricated glucose sensors. However, when applying CV, it has to be kept in mind that the peak current consists of a faradaic and a non-faradaic component. And only the faradaic current is caused by the electron transfer processes and is in relation to the glucose concentration. Therefore, it is important to identify the capacitive current and deduct it from the peak current. However, the identification of the capacitive current of the CV of the glucose

sensors after RI was a challenge due to the shape of the recorded voltammograms possibly caused by the co-extracted molecules from the diffusion cell. Therefore, the analysis of glucose sensor performance in the *in vitro* RI experiments was not feasible by using cyclic voltammetry.

### Recommendations for future work:

This section aims to give suggestions to overcome the experienced limitations, which were reported in section 7.8. In addition, this section details areas of improvements which need to be explored for the device to be part of a wearable sensor.

#### Adsorption studies

The use of AC foam for glucose adsorption was successfully shown. However, more glucose adsorption experiments to AC should be carried out to better understand the adsorption kinetics and adsorption characteristics. All the experiments were only conducted at physiological pH of 7.4. However, pH imbalance can occur in the human body in case of pathologic or metabolic stress and adsorption is a pH dependent process. Therefore, glucose adsorption experiments should also be conducted at different pH levels. As the adsorption process is also dependent on temperature, glucose adsorption should be tested at different temperatures to see the effect of changing the temperature to the adsorption capabilities.

Adsorption depends on a variety of other factors such as the base material of the AC, the surface charge, the polarity of the adsorbent, the pore size, the surface area and the pore structure. None of this information was known of both types of AC used in this study. Having all technical information will help to estimate the adsorption capabilities of AC (such as the number of adsorption sites). The use of a different form of AC is also worthwhile. For example, the use of an AC cloth would be even better suited to be part of a wearable sensor due to its flexibility and its narrow width.

Based on the cyclic voltammetry results, it was observable that the used gel is not providing a uniform environment for the analyte to diffuse. It is highly important that the gel is physically and chemically uniform. A clean diffusion path is crucial for potential real time monitoring, as it leads to better correlation between glucose

concentration in blood and interstitial fluid. Therefore, improvements should be made in the gel fabrication and/or the use of a commercially available gel should be considered for this purpose.

#### Sensor improvement and sensor evaluation

More research needs to be conducted to further lower the limit of detection of the glucose sensor so it can quantify glucose in the even lower  $\mu\text{M}$  range (down to  $20 \mu\text{M}$ ).

Electrochemical impedance spectroscopy (EIS) could be used to improve consistency within the fabricated glucose. EIS is not only used for diagnostic and quantitative detection methods but can also be used for sensor evaluation. Each coating can be characterised with a particular spectra obtained via EIS (Brett, 2008) and this would ensure that the manual coatings performed on each sensor is the same and hence would improve consistency of the sensors. In addition, EIS could be also used to identify the electrical double layer capacitance which will allow the electrochemical glucose detection of glucose extracted via RI using cyclic voltammetry.

A mask should be included in the glucose sensor to direct the extracted glucose to the sensing unit (similar to the one in the GlucoWatch). Otherwise, the glucose extracted at the peripheral area of the sensor would not be detected and quantified.

#### Further areas to explore:

This study has successfully shown the capabilities of AC to act as a glucose binding agent and improve glucose flux during RI. However, ultimately it is important to test this method in the practical setting and observe how well the use of AC improves the correlation between the extracted glucose and the blood glucose concentration in a human. Therefore, a healthy volunteer study should be conducted with the AC-integrated electrodes in combination with RI and the results should be compared with electrodes without AC and RI. Blood glucose measurements should be taken simultaneously to establish a correlation between the blood glucose measurements and the glucose extracted from the interstitial fluid using the AC- integrated sensors.

The development of a glucose sensor in combination with RI is a promising field but there are more limitations and challenges to overcome for it to be part of a wearable sensor for continuous glucose monitoring. To allow the use of the device as a wearable sensor, the calibration aspects of the device need to be carefully considered. In addition, it should be operated wirelessly and powered by small electronics. A transmitter for wireless data transfer to a data processing unit should be integrated so that the acquired readings can be converted to sensible values for the user. The device could have the potential to be ultimately used in connection with a closed loop insulin delivery system where the insulin pump, would automatically administer the adequate amount of insulin based on the measured glucose concentration. This emerging development would be a big step towards pain free glucose monitoring and an immense improvement in quality of life of people with diabetes.

In addition, RI does not only have potential for glucose monitoring in diabetes care but also can be expanded and adapted for the non-invasive, continuous monitoring of other analytes in the interstitial fluid such as lactate or sodium.

## 8 Summary and Conclusion

The state of the art for self-monitoring of glucose is based on blood samples. The problem is that it causes pain and discomfort to the patients and therefore, impedes with the compliance of treatment regimens of people with diabetes. The advantage of using RI is that it enables glucose sensing without having to pierce the skin. The aim of this study was to combine RI with sensor technology to enable continuous, non-invasive glucose monitoring.

This section summarises the findings of this study in reference to the research question, which were posed in section 3.3:

- Which glucose assay kit is more suitable to quantify glucose in the required glucose concentration range?
- Is the level of sensitivity of the Genova Nano spectrophotometer sufficient to quantify glucose in samples obtained from RI experiments if only very small sample volumes are available?
- Which of the tested artificial skin membrane mimics the human skin better in RI experiments?

The first three research questions were intended for the optimisation of the *in vitro* RI experimental setup and glucose analysis method. It is crucial to use a glucose assay kit which can quantify glucose in the expected  $\mu\text{M}$  concentration range. The results in section 6.1 showed that the Randox assay kit has a lower limit of detection of  $2.39 \mu\text{M}$  and a LOQ of  $7.03 \mu\text{M}$  and hence, is more suitable to be used to quantify extracted glucose from RI experiments.

The main advantage of the use of Genova Nano spectrophotometer is that it only requires a sample volume of 0.5 to 5  $\mu\text{L}$  per measurement. This characteristic is very appealing in glucose quantifications as in case of clinical studies only limited amount of patient samples are available and standard laboratory techniques such as the colorimetric assay require at least 80  $\mu\text{L}$  per measurement. A good level of accuracy ( $\pm 6.49\%$ ) could be established with using a sample volume of only 2  $\mu\text{L}$  with the Genova Nano based on the quantification of the two glucose concentrations (204  $\mu\text{M}$  and 408  $\mu\text{M}$ ). A calibration curve could be established with the Genova Nano

spectrophotometer with an LOD of 5.65  $\mu\text{M}$ , indicating its potential to quantify glucose samples obtained from RI experiments.

In Section 5.4 it was demonstrated that the standard artificial membrane used in the Strathclyde lab, the Spectrapore membrane had better characteristics to mimic the human skin for RI experiments than the Vitro-Skin®.

- Proof of concept: Does glucose adsorb to activated carbon (AC)?

Organic molecules adsorb to activated carbon (AC). The results shown in Section 6.4.1 and Section 6.4.2 provided proof of concept that glucose adsorbs to AC. Glucose was successfully adsorbed to AC pellets as well as AC from glucose solution samples as well as glucose gel samples. It was important to test glucose adsorption from gel as gel samples are ultimately used for RI experiments.

- Can AC be used as a glucose binding agent in a wearable sensor in the RI environment and allow a more uniform transdermal glucose profile?

Successful glucose adsorption to AC as demonstrated in Section 6.4.1 and Section 6.4.2 suggests that AC can be used in RI sensors as a glucose binding agent for improved glucose flux. Further investigations were conducted to test the use of AC in RI environment. Section 6.4.6 showed the results of the *in vitro* RI experiments with the initial design of the AC- integrated electrode. Increased glucose fluxes across the diffusion cell could be observed confirming its suitability as a glucose binding agent in a wearable sensor in the RI environment.

A wearable sensor should also be able to provide *in situ* glucose quantifications. Therefore, the next research questions relate to the integrated glucose sensor in the electrode design for direct glucose measurements.

- How does the biosensor operate in the gel environment?

Studies have shown difference in the operation of a glucose sensor in the fluid and gel environment. As RI experiments involve gel samples, it is of importance to evaluate the operation of the glucose sensor in the gel environment.

Cyclic voltammetry was used to characterise the electrochemical behaviour of the glucose sensors. Slower electron transfer, lower diffusion coefficients for mediator and

reduced peak currents were identified in the gel environment compared to the liquid environment.

- Can the embedded glucose biosensor quantify glucose in the required glucose concentration range?

A calibration curve could be established using the glucose sensor and a linear current response was observable. However, an LOD of only 77.09  $\mu\text{M}$  of the glucose sensor was identified, indicating that the sensor is not sufficiently sensitive to measure the extracted glucose. Hence, more research needs to be done on the glucose sensor to increase its sensitivity so it can measure in the lower  $\mu\text{M}$  glucose range (down to 20  $\mu\text{M}$ ).

- Is it possible to electrochemically quantify the extracted glucose via RI with the glucose sensor?

It was not possible to quantify the extracted glucose via electrochemical means. The peak current expected at the potential of 0.14 V based on the calibration experiments, was not observable at the voltammograms after RI. An increase in the capacitive current was observed, which might be due to the extraction of the co-molecules from the diffusion cell. It seems the extracted molecules caused a redistribution of the charge layer at the working electrode. And as the glucose extracted via RI are at low concentration, it seems that the non-faradaic processes were masking the faradaic current.

- Is it possible to link the extracted glucose via RI to the glucose concentration of diffusion cell?

Based on the glucose quantification of the extracted glucose using the standard method using a glucose assay kit, it was possible to link the extracted glucose with the glucose concentration in the diffusion cell. Figure 6.35 shows a linear relationship between the extracted glucose via RI across both iontophoresis electrodes and the glucose concentration in the diffusion cell with and without the AC- integrated electrodes.



- How does the integration of AC impact the glucose sensor?

A linear relationship with a steeper gradient was observable between the extracted glucose via RI and the AC- integrated sensors. This indicates the AC- integrated sensor provide a more sensitive experimental measurement setup than without AC.

To conclude, this project has successfully demonstrated that the use of AC is a viable method to increase accuracy in the glucose concentration measurements extracted via RI. The increase in accuracy will ultimately lead to better correlation between the glucose concentration in the interstitial fluid and in blood, thus bringing the device one step closer to the make RI a sustainable method for glucose monitoring.

The use of AC to increase accuracy has not been applied in this field before making this finding a significant and unique contribution to this field.

This knowledge is not only relevant and promising for glucose monitoring but AC can be also used to assist the transdermal monitoring of any organic analytes in biological fluid.

## REFERENCES

- Abbott. (2013). *Evaluation of the FreeStyle Precision Neo blood glucose and ketone monitoring system*. Retrieved on 2017-10-30. <https://doi.org/10.1097/POC.000000000000128>
- Abbott Laboratories Limited. (2017a). *Freestyle Libre Reader*. Retrieved on 2017-10-25. <https://www.freestylelibre.co.uk/libre/products/reader.html>
- Abbott Laboratories Limited. (2017b). *Freestyle Libre Sensor*. Retrieved on 2017-10-25. <https://www.freestylelibre.co.uk/libre/products/sensors.html>
- Abd-Rabboh, H. S. M., & Meyerhoff, M. E. (2007). Determination of glucose using a coupled-enzymatic reaction with new fluoride selective optical sensing polymeric film coated in microtiter plate wells Hisham. *Talanta*, 72(3), 1129–1133. <https://doi.org/10.1038/jid.2014.371>
- Abdullah, N., Rahman, M. A., Othman, M. H. D., Jaafar, J., & Ismai, A. F. (2018). Membranes and Membrane Processes: Fundamentals. In A. Basile, S. Mozia, & R. Molinari (Eds.), *Current Trends and Future Developments on (Bio-) Membranes* (pp. 45–70). Elsevier.
- Adio, S. O., Asif, M., Mohammed, A. R. I., Baig, N., Al-Arfaj, A. A., & Saleh, T. A. (2019). Poly (amidoxime) modified magnetic activated carbon for chromium and thallium adsorption: Statistical analysis and regeneration. *Process Safety and Environmental Protection*, 121, 254–262. <https://doi.org/10.1016/j.psep.2018.10.008>
- Agency for Toxic Substances and Disease Registry. (2014). *Medical Management Guidelines for Hydrogen Peroxide (H2O2)*. Retrieved on 2019-02-14. <https://www.atsdr.cdc.gov/mmg/mmg.asp?id=304&tid=55>
- Ahmadpour, A., & Do, D. D. (1996). The preparation of active carbons from coal by chemical and physical activation. *Carbon*, 34(4), 471–479. [https://doi.org/10.1016/0008-6223\(95\)00204-9](https://doi.org/10.1016/0008-6223(95)00204-9)
- Al-aibi, S., Al-naja, J., Mahood, H. B., Sharif, A., & Derwish, G. (2014). Kinetic Adsorption Study of Glucose Osmotic Agent onto Granular Activated Carbon in SET Technique. *International Journal of Scientific Research in Chemical Engineering*, 1(3), 34–43.
- Allen, N. A., Fain, J. A., Braun, B., & Chipkin, S. R. (2008). Continuous glucose monitoring counseling improves physical activity behaviors of individuals with type 2 diabetes: A randomized clinical trial. *Diabetes Research and Clinical Practice*, 80(3), 371–379. <https://doi.org/10.1016/j.diabres.2008.01.006>
- Alvarez-Figueroa, M. J., & Blanco-Méndez, J. (2001). Transdermal delivery of methotrexate: Iontophoretic delivery from hydrogels and passive delivery from microemulsions. *International Journal of Pharmaceutics*, 215(1–2), 57–65. [https://doi.org/10.1016/S0378-5173\(00\)00674-8](https://doi.org/10.1016/S0378-5173(00)00674-8)
- Ambade, V. N., Sharma, C. Y., & Somani, D. B. (1998). Methods for Estimation Of Blood Glucose: A comparative Evaluation. *Medical Journal Armed Forces India*, 54, 131–133. [https://doi.org/10.1016/S0377-1237\(17\)30502-6](https://doi.org/10.1016/S0377-1237(17)30502-6)
- American Diabetes Association. (2013). Standards of medical care in diabetes - 2013. *Diabetes Care*, 36(Supplement 1), S11–S66. <https://doi.org/10.2337/dc13-S011>
- American Diabetes Association. (2014). Diagnosis and classification of diabetes mellitus. *Diabetes Care*, 37(SUPPL.1), 81–90. <https://doi.org/10.2337/dc14-S081>

- Andersson, J., Edelman, G. M., Möller, G., & Sjöberg, O. (1972). Activation of B lymphocytes by locally concentrated concanavalin A. *European Journal of Immunology*, 2(3), 233–235. <https://doi.org/10.1002/eji.1830020307>
- Arias, S. R. (2011). *Modelling of Ions and Small Molecules Through Human Skin In vivo*. Master Thesis, University of Strathclyde, Glasgow.
- Ashour, M.-B. A., Gee, S. J., & Hammock, B. D. (1987). Use of a 96-Well Microplate Reader for Measuring Routine Enzyme Activity. *Analytical Biochemistry*, 166, 353–360. <https://doi.org/10.1016/j.apmr.2018.03.015>
- Atkinson, M., & Maclaren, N. (1994). The Pathogenesis of Insulin-Dependent Diabetes Mellitus. *The New England Journal of Medicine*, 24, 1428–1436.
- Axtell, H. C., Hartley, S. M., & Sallavanti, R. A. (2008). *Multi-functional protective materials and methods for use* (Patent No. US20080161631 A1).
- Aygün, a., Yenisoy-Karakaş, S., & Duman, I. (2003). Production of granular activated carbon from fruit stones and nutshells and evaluation of their physical, chemical and adsorption properties. *Microporous and Mesoporous Materials*, 66(2–3), 189–195. <https://doi.org/10.1016/j.micromeso.2003.08.028>
- Bailey, T. S., Alva, S., Bode, B. W., Christiansen, M. P., & Klaff, L. J. (2016). The Performance and Usability of a Factory-Calibrated Flash Glucose Monitoring System. *Diabetes Technology & Therapeutics*, 18(5), 336–337. <https://doi.org/10.1089/dia.2016.0093>
- Ballerstadt, R., Evans, C., McNichols, R., & Gowda, A. (2006). Concanavalin A for in vivo glucose sensing: A biotoxicity review. *Biosensors and Bioelectronics*, 22(2), 275–284. <https://doi.org/10.1016/j.bios.2006.01.008>
- Bandodkar, A. J., Jia, W., Yardimci, C., Wang, X., Ramirez, J., & Wang, J. (2014). Tattoo-based noninvasive glucose monitoring: a proof-of-concept study. *Analytical Chemistry*, 87(1), 394–398. <https://doi.org/10.1021/ac504300n> [doi]
- Bandosz, T. J., Jagiełło, J., & Schwarz, J. A. (1996). Effect of Surface Chemistry on Sorption of Water and Methanol on Activated Carbons. *Langmuir*, 12, 6480–6486. <https://doi.org/10.1021/la960340r>
- Banga, A. K., & Chien, Y. W. (1988). Iontophoretic delivery of drugs: Fundamentals, developments and biomedical applications. *Journal of Controlled Release*, 7(1), 1–24.
- Banga, A. K., & Chien, Y. W. (1993). Hydrogel-Based Iontotherapeutic Delivery Devices for Transdermal Delivery of Peptide/Protein Drugs. *Pharmaceutical Research*, 10(5), 697–702.
- Bantle, J. P., & Thomas, W. (1997). Glucose measurement in patients with diabetes mellitus with dermal interstitial fluid. *The Journal of Laboratory and Clinical Medicine*, 130(4), 436–441. [https://doi.org/10.1016/S0022-2143\(97\)90044-5](https://doi.org/10.1016/S0022-2143(97)90044-5)
- Bard, A. J., & Faulkner, L. R. (2001a). Electrochemical Instrumentation. In *Electrochemical Methods - Fundamentals and Applications* (Edition 2, pp. 632–658). John Wiley&Sons, Inc.
- Bard, A. J., & Faulkner, L. R. (2001b). Introduction and Overview of Electrode Processes. In *Electrochemical Methods - Fundamentals and Applications* (Edition 2, pp. 1–43). John Wiley&Sons, Inc.
- Bard, A. J., & Faulkner, L. R. (2001c). Mass Transfer by Migration and Diffusion. In *Electrochemical Methods - Fundamentals and Applications* (Edition 2, pp. 137–155). John Wiley&Sons, Inc.
- Bard, A. J., & Faulkner, L. R. (2001d). Methods Involving Forced Convection -

- Hydrodynamic Methods. In *Electrochemical Methods - Fundamentals and Applications* (Edition 2, pp. 331–367). John Wiley&Sons, Inc.
- Barham, D., & Trinder, P. (1972). An improved colour reagent for the determination of blood glucose by the oxidase system. *The Analyst*, 97(1151), 142–145. <https://doi.org/10.1039/an9729700142>
- Barry, B. W. (2002). Drug delivery routes in skin: A novel approach. *Advanced Drug Delivery Reviews*, 54(SUPPL.), 31–40. [https://doi.org/10.1016/S0169-409X\(02\)00113-8](https://doi.org/10.1016/S0169-409X(02)00113-8)
- Basu, A., Dube, S., Veetil, S., Slama, M., Kudva, Y. C., Peyser, T., Carter, R. E., Cobelli, C., & Basu, R. (2015). Time lag of glucose from intravascular to interstitial compartment in type 1 Diabetes. *Journal of Diabetes Science and Technology*, 9(1), 63–68. <https://doi.org/10.1177/1932296814554797>
- Bateman, R. C., & Evans, J. A. (1995). Using the Glucose Oxidase/Peroxidase System in Enzyme Kinetics. *Journal of Chemical Education*, 72(12), A240. <https://doi.org/10.1021/ed072pA240>
- Beasley, D. G., & Meyer, T. A. (2010). Characterization of the UVA Protection Provided by Avobenzone, Zinc Oxide, and Titanium Dioxide in Broad-Spectrum Sunscreen Products. *American Journal of Clinical Dermatology*, 11(6), 431–421.
- Beck, R. W., Riddlesworth, T., Ruedy, K. J., Ahmann, A., Bergenstal, R. M., Haller, S., Kollman, C., Kruger, D., McGill, J. B., Polonsky, W., Toschi, E., Wolpert, H., & Price, D. (2017). Effect of Continuous Glucose Monitoring on Glycemic Control in Adults With Type 1 Diabetes Using Insulin Injections. *Jama*, 317(4), 371. <https://doi.org/10.1001/jama.2016.19975>
- Belhamdi, B., Merzougui, Z., Trari, M., & Addoun, A. (2016). A kinetic, equilibrium and thermodynamic study of l -phenylalanine adsorption using activated carbon based on agricultural waste ( date stones ). *Journal of Applied Research and Technology*, 14(5), 354–366. <https://doi.org/10.1016/j.jart.2016.08.004>
- Benedict, S. R. (1909). A reagent for the detection of reducing sugars. *The Journal of Biological Chemistry*, 5, 485–487.
- Berk, Z. (2009). Reaction kinetics. In *Food Process Engineering and Technology* (Edition 1, pp. 115–124). Elsevier.
- Best, C. H., & Scott, D. A. (1923). The preparation of Insulin. *The Journal of Biological Chemistry*, 57, 709–723.
- Betts, J., Desaix, P., Johnson, E., Johnson, J., Korol, O., Kruse, D., Poe, B., Wise, J., Womble, M., & Young, K. (2017a). The Endocrine System. In *Anatomy Physiology* (pp. 731–782). openstax.
- Betts, J., Desaix, P., Johnson, E., Johnson, J., Korol, O., Kruse, D., Poe, B., Wise, J., Womble, M., & Young, K. (2017b). The Integumentary System. In *Anatomy Physiology* (pp. 179–212). openstax.
- Bibby Scientific. (2012). Genova Plus Spectrophotometer - Operating Manual Jenway. In *Bibby Scientific*.
- Biniak, S., Świątkowski, A., Pakuła, M., & Radovic, L. R. (2001). Electrochemical Studies of Phenomena at Active Carbon- Electrolyte Solution Interfaces. In *Chemistry and Physics of Carbon -A Series of Advances - Volume 27* (pp. 125–225). MARCEL DEKKER, INC.
- Bisswanger, H. (2008). Enzyme Kinetics. In *Enzyme Kinetics - Principles and Methods* (Edition 2, pp. 59–193). Wiley-Vch.
- Bisswanger, H. (2014). Enzyme assays. *Perspectives in Science*, 1(1–6), 41–55.

<https://doi.org/10.1016/j.pisc.2014.02.005>

- Blevins, T., Bode, B. W., Garg, S. K., Grunberger, G., Hirsch, I. B., Jovanovic, L., Nardacci, E., Orzech, E., Roberts, V., & Tamborlane, W. V. (2010). Statement by the American Association of Clinical Endocrinologists Consensus Panel on Continuous Glucose Monitoring. *Endocrine Practice*, *16*, 731–745.
- Bockris, J. O., & Reddy, A. K. N. (1998). Ion Transport in Solutions. In *Modern Electrochemistry - Volume 1* (Edition 2, pp. 361–586). Plenum Press.
- Bode, B. W., Gross, T. M., Thornton, K. R., & Mastrototaro, J. J. (1999). Continuous glucose monitoring used to adjust diabetes therapy improves glycosylated hemoglobin: A pilot study. *Diabetes Research and Clinical Practice*, *46*(3), 183–190. [https://doi.org/10.1016/S0168-8227\(99\)00113-8](https://doi.org/10.1016/S0168-8227(99)00113-8)
- Bode, B. W., & Hirsch, I. B. (2000). Using the continuous glucose monitoring system to improve the management of type 1 diabetes. *Diabetes Technology Therapeutics*, *2*(1), 43–48.
- Bolis, V. (2013). Fundamentals in Adsorption at the Solid-Gas Interface. Concepts and Thermodynamics. In A. Auroux (Ed.), *Calorimetry and Thermal Methods in Catalysis* (Vol. 154, pp. 3–50). Springer-Verlag Berlin Heidelberg 2013. <https://doi.org/10.1007/978-3-642-11954-5>
- Bondar, R. J. L., & Mead, D. C. (1974). Evaluation of Glucose-6-Phosphate Dehydrogenase from *Leuconostoc mesenteroides* in the Hexokinase Method for Determining Glucose in Serum. *Clinical Chemistry*, *20*(5), 586–590.
- Boyne, M. S., Silver, D. M., Kaplan, J., & Saudek, C. D. (2003). Timing of Changes in Interstitial and Venous Blood Glucose Sensor. *Diabetes*, *52*(November), 2790–2794.
- Brett, C. M. A. (2008). Electrochemical Impedance Spectroscopy for Characterization of Electrochemical Sensors and Biosensors. *The Electrochemical Society Transactions*, *13*(13), 67–80.
- Brindisi, M.-C., Hahn, J., Chiasson, J.-L., & Rabasa-Lhoret, R. (2007). Underutilization of capillary glucose monitoring by type 2 diabetic patients. *Diabetes Research and Clinical Practice*, *75*(1), 123–125. <https://doi.org/10.1016/j.diabres.2006.05.005>
- Britton, T. S. (1955). *Hydrogen Ions*. Chapman & Hall.
- Buchwald, H., Estok, R., Fahrbach, K., Banel, D., Jensen, M. D., Pories, W. J., Bantle, J. P., & Sledge, I. (2009). Weight and Type 2 Diabetes after Bariatric Surgery: Systematic Review and Meta-analysis. *American Journal of Medicine*, *122*(3), 248–256.e5. <https://doi.org/10.1016/j.amjmed.2008.09.041>
- Burnette, R. R., & Marrero, D. (1986). Comparison between the iontophoretic and passive transport of thyrotropin releasing hormone across excised nude mouse skin. *Journal of Pharmaceutical Science*, *75*(8), 738–743.
- Burnette, R. R., & Ongpipattanakul, B. (1987). Characterization of the permselective properties of excised human skin during iontophoresis. *Journal of Pharmaceutical Sciences*, *76*(10), 765–773. <https://doi.org/10.1002/jps.2600761003>
- Burnette, R. R., & Ongpipattanakul, B. (1988). Characterization of the pore transport properties and tissue alteration of excised human skin during iontophoresis. *Journal of Pharmaceutical Sciences*, *77*(2), 132–137.
- Caduff, A., Mueller, M., Megej, A., Dewarrat, F., Suri, R. E., Klisic, J., Donath, M., Zakharov, P., Schaub, D., Stahel, W. a., & Talary, M. S. (2011). Characteristics

- of a multisensor system for non invasive glucose monitoring with external validation and prospective evaluation. *Biosensors & Bioelectronics*, 26(9), 3794–3800. <https://doi.org/10.1016/j.bios.2011.02.034>
- Calgon Carbon Corporation. (2019). *Pelletized Activated Carbon*. Retrieved on 2019-02-05. <https://www.calgoncarbon.com/pelletized-activated-carbon/>
- Calkin, A. C., Sudhir, K., Honisett, S., Williams, M. R. I., Dawood, T., & Komesaroff, P. A. (2002). Rapid potentiation of endothelium-dependent vasodilation by estradiol in postmenopausal women is mediated via cyclooxygenase 2. *Journal of Clinical Endocrinology and Metabolism*, 87(11), 5072–5075. <https://doi.org/10.1210/jc.2002-020057>
- Cárdenas-López, C., Camargo, G., Giraldo, L., & Moreno-Piraján, J. C. (2007). Design of an adsorbent employing activated carbon fiber to remove lead. *Eclética Química*, 32(3), 61–72. <https://doi.org/10.1590/S0100-46702007000300009>
- Carnali, J. O., Madison, S. A., Shah, P., & Qiu, Q. (2012). Structure / Property Relationship for Ethylenediamine Derivatives as Aids in sunless Tanning. *Industrial & Engineering Chemistry Research*, 51, 15573–15581.
- Cass, A. E. G., Davis, G., Francis, G., Hill, H. A. O., Aston, W., Higgins, I. J., Plotkin, E., Scott, L., & Turner, A. P. F. (1984). Ferrocene-Mediated Enzyme Electrode for Amperometric Determination of Glucose. *Anal. Chem*, 56(2), 667–671. <https://doi.org/10.1021/ac00268a018>
- Castle, J. R., & Jacobs, P. G. (2016). Nonadjunctive Use of Continuous Glucose Monitoring for Diabetes Treatment Decisions. *Journal of Diabetes Science and Technology*, 10(5), 1169–1173. <https://doi.org/10.1177/1932296816631569>
- Cavell, B., Svenningsen, N., Thulin, T., & Schersten, B. (1973). Rapid detection of neonatal hypoglycaemia. Evaluation of Dextrostix Reflectance Meter system. *Archives of Disease in Childhood*, 48, 398–400.
- Çeçen, F. (2014). Activated carbon. In *Kirk-Othmer Encyclopedia of Chemical Technology* (John Wiley, Vol. 1914, Issue 1, pp. 1–34).
- Cengiz, E., & Tamborlane, W. V. (2009). A Tale of Two Compartments : Interstitial Versus Blood Glucose Monitoring. *Diabetes Technology & Therapeutics*, 11(1), S11–S16.
- Chan, J., & Cheng-Lai, A. (2017). Inhaled Insulin: A Clinical and Historical Review. *Cardiology in Review*, 25(3), 140–146.
- Chaplin, S. (2016). Non-invasive blood glucose testing: the horizon. *Practical Diabetes*, 33(9), 313–316.
- Chase, H. P., Roberts, M. D., Wightman, C., Klingensmith, G., Garg, S. K., Wyhe, M. Van, Desai, S., Harper, W., Lopatin, M., Bartkowiak, M., Tamada, J. A., & Eastman, R. C. (2003). Use of the GlucoWatch Biographer in Children With Type 1 Diabetes. *Pediatrics*, 111(4).
- Chaubey, A., & Malhotra, B. D. (2002). Mediated biosensors. *Biosensors and Bioelectronics*, 17(6–7), 441–456. [https://doi.org/10.1016/S0956-5663\(01\)00313-X](https://doi.org/10.1016/S0956-5663(01)00313-X)
- Cheah, J., & Wong, A. (1974). A rapid and simple blood sugar determination using the Ames reflectance meter and Dextrostix system: a preliminary report. *Singapore Medical Journal*, 15(1), 51–52.
- Chen, G., Guan, Z., Chen, C. T., Fu, L., Sundaresan, V., & Arnold, F. H. (1997). A glucose-sensing polymer. *Nature Biotechnology*, 15(4), 354–357. <https://doi.org/10.1038/nbt0497-354>

- Chen, J. P., Wu, S., & Chong, K. (2003). Surface modification of a granular activated carbon by citric acid for enhancement of copper adsorption. *Carbon*, *41*, 1979–1986.
- Chien, Y. W., Lelawongs, P., Siddiqui, O., Sun, Y., & Shi, W. M. (1990). Facilitated transdermal delivery of therapeutic peptides and proteins by iontophoretic delivery devices. *Journal of Controlled Release*, *13*(2–3), 263–278.
- Chien, Y. W., Siddiqui, O., Sun, Y., Shi, W. M., & Liu, J. C. (1987). Transdermal Iontophoretic Delivery of Therapeutic Peptides/Proteins I: Insulin. *Annals of the New York Academy of Sciences*, *507*, 32–51.
- Children With Type 1 Diabetes. (2016). *Freestyle Libre Review 2016*. Retrieved on 2017-10-19. <http://childrenwithtype1diabetes.org/freestyle-libre-for-children-review-2016>
- Ching, C. (2005). *Non-invasive monitoring of glucose and lactate in humans via reverse iontophoresis*. PhD Thesis, University of Strathclyde.
- Ching, C., Camilleri, I., & Connolly, P. (2004). Low- Cost Iontophoresis Devices for Transdermal Drug Delivery. *The Institution of Electrical Engineers*, *3*, 1–4.
- Ching, C., & Connolly, P. (2008a). A novel diffusion cell ideal for the study of membrane extraction/permeation processes and for device/sensor development. *Sensors and Actuators, B: Chemical*, *129*(1), 30–34. <https://doi.org/10.1016/j.snb.2007.07.070>
- Ching, C., & Connolly, P. (2008b). Reverse iontophoresis: A non-invasive technique for measuring blood lactate level. *Sensors and Actuators, B: Chemical*, *129*(1), 352–358. <https://doi.org/10.1016/j.snb.2007.08.031>
- Ching, C., & Connolly, P. (2008c). Simultaneous transdermal Extraction of Glucose and Lactate from human Subjects by reverse Iontophoresis. *International Journal of Nanomedicine*, *3*(2), 211–223.
- Christiansen, M. P., Garg, S. K., Brazg, R. L., Bode, B. W., Bailey, T. S., Slover, R. H., Sullivan, A., Shin, J., Lee, S. W., & Kaufman, F. R. (2017). Accuracy of a Fourth-Generation Subcutaneous Continuous Glucose Sensor. *Diabetes Technology & Therapeutics*, *19*(9), 1–11. <https://doi.org/10.1089/dia.2017.0087>
- Christiansen, M. P., Klaff, L. J., Bailey, T. S., Brazg, R., Carlson, G., & Tweden, K. S. (2019). A Prospective Multicenter Evaluation of the Accuracy and Safety of an Implanted Continuous Glucose Sensor: The PRECISION Study. *Diabetes Technology & Therapeutics*, *21*(5), 1–7. <https://doi.org/10.1089/dia.2019.0020>
- Claremont, D. J., Sambrook, I. E., Penton, C., & Pickup, J. C. (1986). Subcutaneous implantation of a ferrocene-mediated glucose sensor in pigs. *Diabetologia*, *29*, 817–821.
- Clarke, L. C. (1956). Monitor and control of blood and tissue oxygen tension. *Transactions- American Society for Artificial Internal Organs*, *2*, 41–48.
- Clarke, L. C., & Lyons, C. (1962). Electrode systems for continuous monitoring in cardiovascular surgery. *Ann. NY Acad. Sci.*, *102*, 29.
- Clarke, S., & Foster, J. (2012). A history of blood glucose meters and their role in self-monitoring of diabetes mellitus. *British Journal of Biomedical Science*, *69*, 83–93.
- Clarke, W. L., Cox, D. J., Gonder-Frederick, L. A., Carter, W. R., & Pohl, S. L. (1987). Evaluating clinical accuracy of systems for self-monitoring of blood glucose. *Diabetes Care*, *10*(5), 622–628. <https://doi.org/10.2337/diacare.10.5.622>
- Compton, R. G., Batchelor-Mcauley, C., & Dickinson, E. J. F. (2012a). Cyclic

- Voltammetry at Macroelectrodes. In *Understanding Voltammetry: Problems and Solutions* (pp. 67–86). Imperial College Press.
- Compton, R. G., Batchelor-Mcauley, C., & Dickinson, E. J. F. (2012b). Equilibrium Electrochemistry and the Nerst Equation. In *Understanding Voltammetry: Problems and Solutions* (pp. 1–34). Imperial College Press.
- Connolly, P. (2014). *Transdermal devices* (Patent No. US2014/0155703A1).
- Connolly, P., Cotton, C., & Morin, F. (2002). Opportunities at the Skin Interface for continuous Patient monitoring : A reverse Iontophoresis Model tested on Lactate and Glucose. *IEEE Transactions on Nanobioscience*, *1*(1), 37–41.
- Considine, R., Denoyel, R., Pendleton, P., Schumann, R., & Wong, S. H. (2001). The influence of surface chemistry on activated carbon adsorption of 2-methylisoborneol from aqueous solution. *Colloids and Surfaces A: Physicochemical and Engineering Aspects*, *179*(2–3), 271–280. [https://doi.org/10.1016/S0927-7757\(00\)00647-6](https://doi.org/10.1016/S0927-7757(00)00647-6)
- Cooper, J., & Cass, T. (2004). Screen printing methods for biosensor production. In *Biosensors A Practical Approach* (Edition 2, p. 47). Oxford University Press.
- Coston, A. F., & Li, J. K. (2002). Iontophoresis: Modeling, Methodology, and Evaluation. *Cardiovascular Engineering: An International Journal*, *1*(3), 127–136.
- Couto, C. C., Santos, T. F., Mamede, A. M. G. N., Oliveira, T. C., Souza, A. M., Freitas-Silva, O., & Oliveira, E. M. M. (2018). Coffea arabica and C. canephora discrimination in roasted and ground coffee from reference material candidates by real-time PCR. *Food Research International*, *May*, 0–1. <https://doi.org/10.1016/j.foodres.2018.08.086>
- Cox, D. J., Clarke, W. L., Gonder-Frederick, L. A., Pohl, S. L., Hoover, C., Snyder, A., Zimelman, L., Carter, W. R., Bobbtt, S., & Pennebaker, J. (1985). Accuracy of Perceiving Blood Glucose. *Diabetes Care*, *8*(6), 529–536.
- Cullander, C. (1992). What are the pathways of iontophoretic current flow through mammalian skin? *Advanced Drug Delivery Reviews*, *9*, 119–135.
- Cummins, B. M., Garza, J. T., & Coté, G. L. (2013). Optimization of a Concanavalin A-Based Glucose Sensor Using Fluorescence Anisotropy. *Analytical Chemistry*, *85*(11), 5397–5404. <https://doi.org/10.1021/ac303689j>
- D’Costa, E. J., Higgins, I. J., & Turner, A. P. F. (1986). Quinoprotein glucose dehydrogenase and its application in an amperometric glucose sensor. *Biosensors*, *2*(2), 71–87. [https://doi.org/10.1016/0265-928X\(86\)80011-6](https://doi.org/10.1016/0265-928X(86)80011-6)
- Dąbrowski, A., Podkościelny, P., Hubicki, Z., & Barczak, M. (2005). Adsorption of phenolic compounds by activated carbon - A critical review. *Chemosphere*, *58*(8), 1049–1070. <https://doi.org/10.1016/j.chemosphere.2004.09.067>
- Daley, M. A., Tandon, D., Economy, J., & Hippo, E. J. (1996). Elucidating the porous structure of activated carbon fibers using direct and indirect methods. *Carbon*, *34*(10), 1191–1200. [https://doi.org/10.1016/0008-6223\(96\)00065-6](https://doi.org/10.1016/0008-6223(96)00065-6)
- Daly, M. E., Vale, C., Walker, M., Littlefield, A., George, K., Alberti, K. G. M. M., & Mathers, J. C. (1998). Acute effects on insulin sensitivity and diurnal metabolic profiles of a high-sucrose compared with a high-starch diet. *American Journal of Clinical Nutrition*, *67*(6), 1186–1196.
- Damiano, E. R., McKeon, K., El-Khatib, F. H., Zheng, H., Nathan, D. M., & Russell, S. J. (2014). A Comparative Effectiveness Analysis of Three Continuous Glucose Monitors. *Journal of Diabetes Science and Technology*, *8*(4), 699–708.



- <https://doi.org/10.1177/1932296814532203>
- Danowski, T. S., & Sunder, J. H. (1978). Jet injection of insulin during self-monitoring of blood glucose. *Diabetes Care*, *1*(1), 27–33.
- DeFronzo, R. A. (2017). Combination therapy with GLP-1 receptor agonist and SGLT2 inhibitor. *Diabetes, Obesity and Metabolism*, *19*(10), 1353–1362. <https://doi.org/10.1111/dom.12982>
- Deiss, D., Bolinder, J., Rivelino, J. P., Battelino, T., Bosi, E., Tubiana-Rufi, N., Kerr, D., & Phillip, M. (2006). Improved glycemic control in poorly controlled patients with type 1 diabetes using real-time continuous glucose monitoring. *Diabetes Care*, *29*(12), 2730–2732. <https://doi.org/10.2337/dc06-1134>
- Del Terzo, S., Bhel, C., & Nash, R. (1989). Iontophoretic transport of a homologous series of ionized and nonionized model compounds: Influence of Hydrophobicity and mechanistic interpretation. *Pharmaceutical Research*, *6*, 85–90.
- Delamater, A. M. (2006). Improving Patient Adherence. *Clinical Diabetes*, *24*(2), 71–77. <https://doi.org/10.2337/diaclin.24.2.71>
- Delgado-Charro, M. B., & Guy, R. H. (1994). Characterization of Convective Solvent Flow During Iontophoresis. *Pharmaceutical Research*, *11*(7), 929–935.
- Dexcom Inc. (2019). *Dexcom G6 - Continuous Glucose Monitoring System - User Guide*.
- Dhote, V., Bhatnagar, P., Mishra, P. K., Mahajan, S. C., & Mishra, D. K. (2012). Iontophoresis: A potential emergence of a transdermal drug delivery system. *Scientia Pharmaceutica*, *80*(1), 1–28. <https://doi.org/10.3797/scipharm.1108-20>
- Diabetes.co.uk. (2017a). *Blood Sugar Converter*. Retrieved on 2017-10-02. <http://www.diabetes.co.uk/blood-sugar-converter.html>
- Diabetes.co.uk. (2017b). *Insulin Types and Information*. Retrieved on 2017-10-06. <https://www.diabetes.co.uk/insulin/insulin-types.html>
- Diabetes UK. (2016). *Facts and Stats*. Retrieved on 2017-10-06. <https://doi.org/10.1007/s11245-009-9073-4>
- Dimotakis, E. D., Cal, M. P., Economy, J., Rood, M. J., & Larson, S. M. (1995). Chemically Treated Activated Carbon Cloths for Removal of Volatile Organic Carbons from Gas Streams: Evidence for Enhanced Physical Adsorption. *Environmental Science and Technology*, *29*(7), 1876–1880. <https://doi.org/10.1021/es00007a027>
- Diridollou, S., Black, D., Lagarde, J., Gall, Y., Berson, M., Vabre, V., & Patat, F. (2000). Sex- and site-dependent variations in the thickness and mechanical properties of human skin in vivo. *Int J Cosmet Sci.*, *22*(6), 421–435.
- DOW. (2013). *Chemistry of METHOCEL™ Cellulose Ethers -A Technical Review Pharma & Food Solutions*.
- Dubinin, M. M. (1960). The Potential Theory of Adsorption of Gases and Vapors for Adsorbents with Energetically Nonuniform Surfaces. *Chemical Reviews*, *60*(2), 235–241. <https://doi.org/10.1021/cr60204a006>
- Durand, A., Chase, Z., Remenyi, T., & Quéroué, F. (2012). Microplate-reader method for the rapid analysis of copper in natural waters with chemiluminescence detection. *Frontiers in Microbiology*, *3*(JAN), 1–9. <https://doi.org/10.3389/fmicb.2012.00437>
- Duxbury, M. (2004). An enzymatic clinical chemistry laboratory experiment incorporating an introduction to mathematical method comparison techniques. *Biochemistry and Molecular Biology Education*, *32*(4), 246–249.

- <https://doi.org/10.1002/bmb.2004.494032040366>
- Eastman, R. C., Chase, H. P., Buckingham, B. A., Hathout, E. H., Fuller-Byk, L., Leptien, A. D., Van Wyhe, M. M., Davis, T. L., Fermi, S. J., Pechler, H., Sahyun, G., Lopatin, M., Wang, B. Y., Wei, C., Bartkowiak, M., Ginsberg, B. H., Tamada, J. A., & Pitzer, K. R. (2002). Use of the GlucoWatch biographer in children and adolescents with diabetes. *Pediatric Diabetes*, 3(3), 127–134. <https://doi.org/10.1034/j.1399-5448.2002.30302.x>
- Edelman, S. V. (2017). Regulation Catches Up to Reality. *Journal of Diabetes Science and Technology*, 11(1), 160–164. <https://doi.org/10.1177/1932296816667749>
- Elias, P. (1983). Epidermal lipids, barrier function, and desquamation. *J Invest Dermatol.*, 80, 44–49.
- Ellis, C., Ramzy, A., & Kieffer, T. (2017). Regenerative medicine and cell-based approaches to restore pancreatic function. *Nature Reviews Gastroenterology & Hepatology*.
- Eriksson, J., Lindström, J., Valle, T., Aunola, S., Hämäläinen, H., Ilanne-Parikka, P., Keinänen-Kiukaanniemi, S., Laakso, M., Lauhkonen, M., Lehto, P., Lehtonen, A., Louheranta, A., Mannelin, M., Martikkala, V., Rastas, M., Sundvall, J., Turpeinen, A., Viljanen, T., Uusitupa, M., & Tuomilehto, J. (1999). Prevention of Type II diabetes in subjects with impaired glucose tolerance: The Diabetes Prevention Study (DPS) in Finland. Study design and 1-year interim report on the feasibility of the lifestyle intervention programme. *Diabetologia*, 42(7), 793–801. <https://doi.org/10.1007/s001250051229>
- Eurachem. (2014). Method Performance Characteristics. In B. Magnusson & U. Örnemark (Eds.), *Eurachem Guide: The Fitness for Purpose of Analytical Methods – A Laboratory Guide to Method Validation and Related Topics*. (2nd ed., pp. 19–40). <https://doi.org/978-91-87461-59-0>
- Farmahan, M. (2008). *Transdermal Extraction of Glucose and Lactate through Reverse Iontophoresis*. EngD Thesis, University of Strathclyde, Glasgow.
- Fetita, L., Sobngwi, E., Serradas, P., Calvo, F., & Gautier, J. (2006). Consequences of Fetal Exposure to Maternal Diabetes in Offspring. *The Journal of Clinical Endocrinology & Metabolism*, 91, 3718–3724.
- Fokkert, M. J., van Dijk, P. R., Edens, M. A., Abbes, S., de Jong, D., Slingerland, R. J., & Bilo, H. J. G. (2017). Performance of the FreeStyle Libre Flash glucose monitoring system in patients with type 1 and 2 diabetes mellitus. *BMJ Open Diabetes Research & Care*, 5(1), e000320. <https://doi.org/10.1136/bmjdr-2016-000320>
- Food and Drug Administration. (2018). *PMA P160007: FDA Summary of Safety and Effectiveness Data*. Retrieved on 2019-10-18. [https://www.accessdata.fda.gov/cdrh\\_docs/pdf16/P160007B.pdf](https://www.accessdata.fda.gov/cdrh_docs/pdf16/P160007B.pdf)
- Franke, W., & Deffner, M. (1939). Zur Kenntnis der sog. Glucose-oxydase. II. *Liebigs Annalen*, 541, 117–150.
- Franke, W., & Lorenz, F. (1937). Zur Kenntnis der sog. Glucose-oxydase. I. *Liebigs Annalen*, 532(1), 1–28.
- Franz, M., Arafat, H. A., & Pinto, N. G. (2000). Effect of chemical surface heterogeneity on the adsorption mechanism of dissolved aromatics on activated carbon. *Carbon*, 38(13), 1807–1819. [https://doi.org/10.1016/S0008-6223\(00\)00012-9](https://doi.org/10.1016/S0008-6223(00)00012-9)
- Franz, T. J. (1975). Percutaneous Absorption on the Relevance of in vitro Data. *The*

- Journal of Investigative Dermatology*, 64(3), 190–195.
- Freckmann, G., Schmid, C., Baumstark, A., Rutschmann, M., Haug, C., & Heinemann, L. (2015). Analytical performance requirements for systems for self-monitoring of blood glucose with focus on system accuracy: Relevant differences among ISO 15197:2003, ISO 15197:2013, and current FDA recommendations. *Journal of Diabetes Science and Technology*, 9(4), 885–894. <https://doi.org/10.1177/1932296815580160>
- Free, A. H., & Free, H. M. (1984). Self testing, an emerging component of clinical chemistry. *Clinical Chemistry*, 30(6), 829–838.
- Freger, D., Gal, A., & Raykhman, A. M. (2005). *Method of monitoring glucose level* (Patent No. US 6954662 B2).
- Freundlich, H. (1906). Adsorption in solution. *Phys Chem Soc*, 40, 1361–1368.
- Frew, J. E., & Hill, H. A. O. (1987). Electrochemical Biosensors. *Analytical Chemistry*, 59(15), 933–944. <https://doi.org/10.1021/ac00142a001>
- Friis, E. P., Andersen, J. E. T., Madsen, L. L., Bonander, N., Moller, P., & Ulstrup, J. (1998). Dynamics of pseudomonas aeruginosa azurin and its Cys3Ser mutant at single-crystal gold surfaces investigated by cyclic voltammetry and atomic force microscopy. *Electrochimica Acta*, 43(9), 1114–1122. [https://doi.org/10.1016/S0013-4686\(98\)99006-5](https://doi.org/10.1016/S0013-4686(98)99006-5)
- Gaines, P. (2018). *Linearity and detection limits*. Inorganic Ventures, ICP Operations Guide: Part 7; Retrieved on 2018-10-27. <https://www.inorganicventures.com/linearity-and-detection-limits>
- Galán-Vidal, C. A., Muñoz, J., Domínguez, C., & Alegret, S. (2000). Thick-Film Biosensors. In V. C. Yang & T. T. Ngo (Eds.), *Biosensors and Their Applications* (pp. 299–309). Springer.
- Gandrud, L. M., Paguntalan, H. U., Van Wyhe, M. M., Kunselman, B. L., Leptien, A. D., Wilson, D. M., Eastman, R. C., & Buckingham, B. A. (2004). Use of the Cygnus GlucoWatch biographer at a diabetes camp. *Pediatrics*, 113(1 Pt 1), 108–111. <https://doi.org/10.1542/peds.113.1.108>
- Garber, C. C., Feldbruegge, D., Miller, R. C., & Carey, R. N. (1978). Evaluation of the co-immobilized hexokinase/glucose-6-phosphate dehydrogenase method for glucose, as adapted to the Technicon SMAC. *Clinical Chemistry*, 24(7), 1186–1190.
- Garg, S. K., Potts, R. O., Ackerman, N., Fermi, S. J., Tamada, J. A., & Chase, H. P. (1999). Correlation of fingerstick blood glucose measurements with GlucoWatch biographer glucose results in young subjects with type 1 diabetes. *Diabetes Care*, 22, 1708–1714.
- Ghindilis, A. L., Atanasov, P., & Wilkins, E. (1997). Enzyme-catalyzed direct electron transfer: Fundamentals and analytical applications. *Electroanalysis*, 9(9), 661–674. <https://doi.org/10.1002/elan.1140090902>
- Ghosh, P. (2014). *Adsorption at Fluid – Solid Interfaces*. NPTEL - Chemical Engineering - Interfacial Engineering. <https://nptel.ac.in/courses/103103033/module4/lecture4.pdf>
- Giacomoni, P. U., Mammone, T., & Teri, M. (2009). Gender-linked differences in human skin. *Journal of Dermatological Science*, 55(3), 144–149. <https://doi.org/10.1016/j.jdermsci.2009.06.001>
- Goldstein, D. E., Little, R. R., Lorenz, R. A., Malone, J. I., Nathan, D. M., Peterson, C. M., & Sacks, D. B. (2004). Tests of glycemia in diabetes. *Diabetes Care*,

27(7), 1761–1773.

- Gough, S., & Narendran, P. (2010). Insulin and Insulin Treatment. In *Textbook of Diabetes* (Forth edit, pp. 427–439). Blackwell Publishing.
- Gray, L. E. (2008). *A Novel Electrochemical Lateral Flow Immunoassay*. PhD Thesis, University of Strathclyde, Glasgow.
- Gross, T. M., Bode, B. W., Einhorn, D., Kayne, D. M., Reed, J. H., White, N. H., & Mastrototaro, J. J. (2000). Performance evaluation of the MiniMed continuous glucose monitoring system during patient home use. *Diabetes Technol Ther*, 2(1), 49–56. <https://doi.org/10.1089/152091500316737>
- Grundy, S. M., Brewer, H. B., Cleeman, J. I., Smith, S. C., & Lenfant, C. (2004). Definition of metabolic syndrome: Report of the National Heart, Lung, and Blood Institute/American Heart Association conference on scientific issues related to definition. *Circulation*, 109(3), 433–438. <https://doi.org/10.1161/01.CIR.0000111245.75752.C6>
- Guilbault, G., & Lubrano, G. (1973). An enzyme electrode for the amperometric determination of glucose. *Anal Chim Acta*, 64, 439–455.
- Gunther, G. R., Wang, J. L., Yahara, I., Cunningham, B. a., & Edelman, G. M. (1973). Concanavalin A derivatives with altered biological activities. *Proceedings of the National Academy of Sciences of the United States of America*, 70(4), 1012–1016. <https://doi.org/10.1073/pnas.70.4.1012>
- Guy, R. H., Kalia, Y. N., Delgado-Charro, M. B., Merino, V., López, A., & Marro, D. (2000). Iontophoresis: Electrorepulsion and electroosmosis. *Journal of Controlled Release*, 64(1–3), 129–132. [https://doi.org/10.1016/S0168-3659\(99\)00132-7](https://doi.org/10.1016/S0168-3659(99)00132-7)
- Haak, T., Hanaire, H., Ajjan, R., Hermanns, N., Riveline, J. P., & Rayman, G. (2017). Flash Glucose-Sensing Technology as a Replacement for Blood Glucose Monitoring for the Management of Insulin-Treated Type 2 Diabetes: a Multicenter, Open-Label Randomized Controlled Trial. *Diabetes Therapy*, 8(1), 55–73. <https://doi.org/10.1007/s13300-016-0223-6>
- Haghseresht, F., Nouri, S., Finnerty, J. J., & Lu, G. Q. (2002). Effects of Surface Chemistry on Aromatic Compound Adsorption from Dilute Aqueous Solutions by Activated Carbon. *J. Phys. Chem.*, 106, 10935–10943. <https://doi.org/10.1021/jp025522a>
- Hanson, K. M., Gratton, E., & Bardeen, C. J. (2006). Sunscreen enhancement of UV-induced reactive oxygen species in the skin. *Free Radical Biology and Medicine*, 41(8), 1205–1212. <https://doi.org/10.1016/j.freeradbiomed.2006.06.011>
- Harland, J., White, M., Drinkwater, C., Chinn, D., Farr, L., & Howel, D. (1999). The Newcastle exercise project: a randomised controlled trial of methods to promote physical activity in primary care. *BMJ (Clinical Research Ed.)*, 319(7213), 828–832. <https://doi.org/10.1136/bmj.319.7213.828>
- Harman-Boehm, I., Gal, A., Raykhman, A. M., Naidis, E., & Mayzel, Y. (2010). Noninvasive glucose monitoring: increasing accuracy by combination of multi-technology and multi-sensors. *Journal of Diabetes Science and Technology*, 4(3), 583–595.
- Harman-Boehm, I., Gal, A., Raykhman, A. M., Zahn, J. D., Naidis, E., & Mayzel, Y. (2009). Noninvasive glucose monitoring: a novel approach. *Journal of Diabetes Science and Technology*, 3(2), 253–260. <https://doi.org/10.1177/193229680900300205>

- Harper, A. C., & Anderson, M. R. (2006). Electrostatic Assembly of a Redox Catalysis System for Detection of Glutamate. *Electroanalysis*, 18(24), 2397–2404. <https://doi.org/10.1002/elan.200603704>
- Harper, N. J., Gray, S., De Groot, J., Parker, J. M., Sadrzadeh, N., Schuler, C., Schumacher, J. D., Seshadri, S., Smith, A. E., Steeno, G. S., Stevenson, C. L., Taniere, R., Wang, M., & Bennett, D. B. (2007). The design and performance of the exubera pulmonary insulin delivery system. *Diabetes Technology & Therapeutics*, 9 Suppl 1, S16–S27. <https://doi.org/10.1089/dia.2007.0222>
- Harris, P. J. F., Liu, Z., & Suenaga, K. (2008). Imaging the atomic structure of activated carbon. *Journal of Physics Condensed Matter*, 20(36). <https://doi.org/10.1088/0953-8984/20/36/362201>
- Harvey, D., Cooper, L., Fancourt, R., Levene, M., & Schoberg, T. (1976). The use of dextrostix and dextrostix reflectance meters in the diagnosis of neonatal hypoglycemia. *Journal of Perinatal Medicine*, 4, 106–110.
- Hasslacher, C., Auffarth, G., Platten, I., Rabsilber, T., Smith, B., Kulozik, F., Knuth, M., Nikolaus, K., & Müller, A. J. (2012). Safety and accuracy of a new long-term subconjunctival glucose sensor. *Journal of Diabetes*, 4(3), 291–296. <https://doi.org/10.1111/j.1753-0407.2012.00192.x>
- Hayford, J. T., Weydert, J. A., & Thompson, R. G. (1983). Validity of urine glucose measurements for estimating plasma glucose concentration. *Diabetes Care*, 6(1), 40–44.
- Health and Social Care Information Centre. (2016). *Statistics on Obesity, Physical Activity and Diet*. NHS Digital; Retrieved on 2017-02-12. <https://files.digital.nhs.uk/publicationimport/pub20xxx/pub20562/obes-phys-acti-diet-eng-2016-rep.pdf>
- Healthcare4All. (2014). *Accu-Chek Aviva Glucose Meter*. Retrieved on 2014-07-02. <http://www.healthcare4all.co.uk/accu-chek+aviva+glucose+meter>
- Heinemann, L. (2011). New ways of insulin delivery. *Int J Clin Pract Suppl.*, 170, 31–46.
- Heinemann, L., Baughman, R., Boss, A., & Hompesch, M. (2017). Pharmacokinetic and Pharmacodynamic Properties of a Novel Inhaled Insulin. *Journal of Diabetes Science and Technology*, 11(1), 148–156. <https://doi.org/10.1177/1932296816658055>
- Heinemann, L., Pfützner, A., & Heise, T. (2001). Alternative routes of administration as an approach to improve insulin therapy: update on dermal, oral, nasal and pulmonary insulin delivery. *Current Pharmaceutical Design*, 7(14), 1327–1351. <https://doi.org/10.2174/1381612013397384>
- Henkel Corporation. (2013). *Henkel Solutions - Medical Electronics*. [https://doi.org/10.1016/S0140-6736\(61\)92524-7](https://doi.org/10.1016/S0140-6736(61)92524-7)
- Herrera-González, A. M., Caldera-Villalobos, M., & Peláez-Cid, A.-A. (2019). Adsorption of textile dyes using an activated carbon and crosslinked polyvinyl phosphonic acid composite. *Journal of Environmental Management*, 234(December 2018), 237–244. <https://doi.org/10.1016/j.jenvman.2019.01.012>
- Hilditch, P., & Green, M. (1991). Disposable Electrochemical Biosensors. *Analyst*, 116, 1217–1220.
- Hill, H. A. O., & Sanghera, G. S. (1990). Mediated amperometric enzyme electrodes. In *Biosensor A Practical Approach* (pp. 19–45). Oxford University Press.
- Hill, H. A. O., & Sanghera, G. S. (2011). Mediated amperometric enzyme electrodes.

- In A. E. G. Cass (Ed.), *Biosensors A Practical Approach*s (pp. 19–46). Oxford University Press.
- Hirvonen, J., Hueber, F., & Guy, R. H. (1995). Current profile regulates iontophoretic delivery of amino acids across the skin. *Journal of Controlled Release*, 37(3), 239–249. [https://doi.org/10.1016/0168-3659\(95\)00081-X](https://doi.org/10.1016/0168-3659(95)00081-X)
- Holman, N., Young, B., & Gadsby, R. (2015). Current prevalence of Type 1 and Type 2 diabetes in adults and children in the UK. *Diabetic Medicine*, 32(9), 1119–1120. <https://doi.org/10.1111/dme.12791>
- Holt, T., & Kumar, S. (2010a). Diagnosing Diabetes. In *ABC of Diabetes* (Edition 6, pp. 1–4). Wiley-Blackwell.
- Holt, T., & Kumar, S. (2010b). Insulin Therapy. In *ABC of Diabetes* (Edition 6, pp. 34–36). Wiley-Blackwell.
- Hönes, J., Müller, P., & Surridge, N. (2008). The Technology Behind Glucose Meters : Test Strips. *Diabetes Technology & Therapeutics*, 10, 10–26. <https://doi.org/10.1089/dia.2008.0005>
- Horman, K., Mayzel, Y., Gal, A., Bahartan, K., Drexler, A., & Lin, T. (2016). *Performance and User Experience Evaluation of a Non-Invasive Glucose Monitoring Device*. 1(2), 1–7.
- Howard, J. P., Drake, T. R., & Kellogg, D. L. (1995). Effects of alternating Current Iontophoresis on Drug Delivery. *Arch Phys Med Rehabil*, 76(May), 463–466.
- Howell, C. A., Sandeman, S. R., Zheng, Y., Mikhalovsky, S. V., Nikolaev, V. G., Sakhno, L. A., & Snezhkova, E. A. (2016). New dextran coated activated carbons for medical use. *Carbon*, 97, 134–146. <https://doi.org/10.1016/j.carbon.2015.09.042>
- Hsu, C. J., Chiou, H. J., Chen, Y. H., Lin, K. S., Rood, M. J., & Hsi, H. C. (2019). Mercury adsorption and re-emission inhibition from actual WFGD wastewater using sulfur-containing activated carbon. *Environmental Research*, 168(October 2018), 319–328. <https://doi.org/10.1016/j.envres.2018.10.017>
- Hsueh, C.-J., Janyasupab, M., Lee, Y.-H., & Liu, C.-C. (2014). Electrochemical Glucose Sensors. In G. Kreysa, K. Ota, & R. F. Savinell (eds) (Eds.), *Encyclopedia of Applied Electrochemistry* (pp. 479–485). Springer. <https://doi.org/10.1007/978-1-4419-6996-5>
- Ikeda, Y., Tajima, N., Minami, N., Ide, Y., & Yokoyama, J. (1978). Pilot study of self measurement of blood glucose using the Dextrostix-Eyetone System for juvenile onset diabetes. *Diabetologia*, 15, 91–93.
- IMS Inc. (2018). *VITRO-SKIN The Global Standard for Rapid, Predictive In Vitro Testing*. Retrieved 2018-10-20. <https://www.ims-usa.com/vitro-skin-substrates/vitro-skin/>
- Inagaki, M., Morishita, T., Kuno, A., Kito, T., Hirano, M., Suwa, T., & Kusakawa, K. (2004). Carbon foams prepared from polyimide using urethane foam template. *Carbon*, 42(3), 497–502. <https://doi.org/10.1016/j.carbon.2003.12.080>
- Integrity Applications. (2017). *GlucoTrack Non-invasively measure glucose levels in the body*. Retrieved on 2017-09-18. <http://www.integrity-app.com/the-glucotrack/>
- International Diabetes Federation. (2017). Executive Summary. In *IDF Diabetes Atlas - 8th edition* (pp. 8–11).
- International Diabetes Federation. (2019a). Action on Diabetes. In *IDF Diabetes Atlas - 9th edition* (pp. 106–133).

- International Diabetes Federation. (2019b). Global Picture. In B. Malanda, S. Karuranga, P. Saeedi, & P. Salpea (Eds.), *IDF Diabetes Atlas - 9th edition* (pp. 32–61).
- International Diabetes Federation. (2019c). What is Diabetes? In *IDF Diabetes Atlas - 9th edition* (pp. 10–21).
- International Organization for Standardization. (2017). *ISO 15197:2013 - In vitro diagnostic test systems -- Requirements for blood-glucose monitoring systems for self-testing in managing diabetes mellitus*. Retrieved on 2017-10-16. <https://www.iso.org/standard/54976.html>
- Iwuoha, E. I., & Smyth, M. R. (1994). Organic-phase Application of an Amperometric Glucose Sensor. *Analyst*, *119*, 265–267.
- Jackson, T. C., Kotermanski, S. E., Jackson, E. K., & Kochanek, P. M. (2018). BrainPhys® increases neurofilament levels in CNS cultures, and facilitates investigation of axonal damage after a mechanical stretch-injury in vitro. *Experimental Neurology*, *300*(October 2017), 232–246. <https://doi.org/10.1016/j.expneurol.2017.11.013>
- Jacobi The Carbon Company. (2015). *Activated Carbon for Medicinal and Pharmaceutical Processes*. Retrieved on 2019-01-19. <https://jacobi.net/wp-content/uploads/2015/05/Medical-Pharma.pdf>
- Jacobsen, J. (2001). Buccal iontophoretic delivery of atenolol·HCl employing a new in vitro three-chamber permeation cell. *Journal of Controlled Release*, *70*(1–2), 83–95. [https://doi.org/10.1016/S0168-3659\(00\)00328-X](https://doi.org/10.1016/S0168-3659(00)00328-X)
- Jafar-Mohammadi, B., & McCarthy, M. I. (2008). Genetics of type 2 diabetes mellitus and obesity-a review. *Annals of Medicine*, *40*, 2–10.
- Jahn, H. (1900). Über den Dissociationsgrad und das Dissociationsgleichgewicht stark dissociierter Elektrolyte. *Zeitschrift Für Physikalische Chemie*, *33U*(1), 545–576.
- Jarrett, R. J., Keen, H., & Hardwick, C. (1970). “Instant” blood sugar measurement using Dextrostix and a reflectance meter. *Diabetes*, *19*(10), 724–726.
- Jermann, R., Toumiat, M., & Imfeld, D. (2002). Development of an in vitro efficacy test for self-tanning formulations. *Internation Journal of Cosmetic Science*, *24*(1), 35–42.
- Jin, F., Zhang, X., Xu, H., Si, H., Hua, D., Zuo, B., Zhang, Y., Bori, S., & Energy, B. (2017). Study on Adsorption Behavior of Glucose , Sucrose and Soluble Starch in Activated Carbon. *International Conference on Energy, Power and Environmental Engineering (ICEPEE 2017)*, 495–499.
- Joslin, E. (1918). *A diabetic manual*. Lea & Febiger.
- JoVE Science Education Database. (2018). *Calibration Curves*. Retrieved on 2018-10-13. <https://www.jove.com/science-education/10188/calibration-curves>
- Junker, K., & Ditzel, J. (1972). Inaccuracy of test strips with reflectance meter in determination of high blood sugars. *The Lancet*, *299*(7755), 815–817.
- Juurlink, D. N. (2016). Activated charcoal for acute overdose: A reappraisal. *British Journal of Clinical Pharmacology*, *81*(3), 482–487. <https://doi.org/10.1111/bcp.12793>
- Kaneko, Y., Abe, M., & Ogino, K. (1989). Adsorption Characteristics of Organic Compounds Dissolved in Water on Surface-Improved Activated Carbon Fibres. *Colloids and Surfaces*, *37*, 211–222.
- Karanfil, T., & Kilduff, J. E. (1999). Role of granular activated carbon surface chemistry on the adsorption of organic compounds. 1. Priority pollutants.

- Environmental Science and Technology*, 33(18), 3217–3224.  
<https://doi.org/10.1021/es981016g>
- Karyakin, A. A., Gitelmacher, O. V., & Karyakina, E. E. (1995). Prussian Blue-Based First-Generation Biosensor. A Sensitive Amperometric Electrode for Glucose. *Anal. Chem.*, 67(14), 2419–2423.
- Kasaoka, S., Sakata, Y., Tanaka, E., & Naitoh, R. (1987). Preparation of activated fibrous carbon from phenolic fabric and its molecular sieving properties. *Nippon Kagaku Kaishi*, 60(6), 990–1000. <https://doi.org/10.1246/nikkashi.1987.990>
- Kasting, G. B., Smith, R. L., & Cooper, E. G. (1987). Effect of lipid solubility and molecular size on percutaneous absorption. In B. Shrooff and H. Schaefer (Ed.), *Skin Pharmacokinetics* (pp. 138–153). Karger AG.
- Kaufman, F. R., Gibson, L. C., Halvorson, M., Carpenter, S., Fisher, L. K., & Pitukcheewanont, P. (2001). A Pilot Study of the Continuous Glucose Monitoring System. *Diabetes Care*, 24(12).
- Keenan, D. B., Mastrototaro, J. J., Zisser, H., Cooper, K. A., Raghavendhar, G., Lee, S. W., Yusi, J., Bailey, T. S., Brazg, R. L., & Shah, R. V. (2012). Accuracy of the Enlite 6-Day Glucose Sensor with Guardian and Veo Calibration Algorithms. *Diabetes Technology & Therapeutics*, 14(3), 225–231. <https://doi.org/10.1089/dia.2011.0199>
- Keilin, D., & Hartree, E. F. (1948). Properties of glucose oxidase (Notatin). *Biochemical Journal*, 42, 221–229.
- Kern, F., Niaux, T., & Baccarini, M. (2011). Ras and Raf pathways in epidermis development and carcinogenesis. *British Journal of Cancer*, 104(2), 229–234. <https://doi.org/10.1038/sj.bjc.6606009>
- Kim, J., Campbell, A. S., & Wang, J. (2018). Wearable non-invasive epidermal glucose sensors: A review. *Talanta*, 177(August 2017), 163–170. <https://doi.org/10.1016/j.talanta.2017.08.077>
- Kim, J., Sempionatto, J. R., Imani, S., Hartel, M. C., Barfidokht, A., Tang, G., Campbell, A. S., Mercier, P. P., & Wang, J. (2018). Simultaneous Monitoring of Sweat and Interstitial Fluid Using a Single Wearable Biosensor Platform. *Advanced Science*. <https://doi.org/10.1002/advs.201800880>
- Kissinger, P. T., & Heineman, W. R. (1983). Cyclic Voltammetry. *Journal of Chemical Education*, 60(9), 702–706. <https://doi.org/10.1021/ed060p702>
- Kleinman, N. J., Shah, A., Shah, S., Phatak, S., & Viswanathan, V. (2017). Improved Medication Adherence and Frequency of Blood Glucose Self-Testing using an m-Health Platform Versus Usual Care in a Multisite Randomized Clinical Trial Among People with Type 2 Diabetes in India. *Telemedicine and E-Health*, 23(9), tmj.2016.0265. <https://doi.org/10.1089/tmj.2016.0265>
- Kovatchev, B. P., Patek, S. D., Ortiz, E. A., & Breton, M. D. (2015). Assessing Sensor Accuracy for Non-Adjunct Use of Continuous Glucose Monitoring. *Diabetes Technology & Therapeutics*, 17(3), 177–186. <https://doi.org/10.1089/dia.2014.0272>
- Krishnan, G. (2011). *Cyclic voltammetry*. Russ College of Engineering and Technology; Retrieved on 2019-08-09. <https://www.ohio.edu/engineering/ceer/research/upload/CYCLICVOLTAMMETRY-GEETHA1.pdf>
- Kuenzi, S., Meurville, E., & Ryser, P. (2010). Automated characterization of dextran/concanavalin A mixtures-A study of sensitivity and temperature



- dependence at low viscosity as basis for an implantable glucose sensor. *Sensors and Actuators, B: Chemical*, 146(1), 1–7. <https://doi.org/10.1016/j.snb.2009.12.029>
- Kulcu, E., Tamada, J. A., Reach, G., Potts, R. O., & Lesho, M. J. (2003). Physiological differences between interstitial glucose and blood glucose measured in human subjects. *Diabetes Care*, 26(8), 2405–2409. <https://doi.org/10.2337/diacare.26.8.2405>
- Künzelmann, U., & Böttcher, H. (1997). Biosensor Properties of Glucose Oxidase Immobilized within SiO<sub>2</sub> Gels. *Sensors and Actuators B*, 38–39, 222–228. [https://doi.org/10.1016/S0925-4005\(97\)80208-0](https://doi.org/10.1016/S0925-4005(97)80208-0)
- Kurnik, R. T., Berner, B., Tamada, J. A., & Potts, R. O. (1998). Design and Simulation of a Reverse Iontophoretic Glucose Monitoring Device. *J Electrochem. Soc.*, 145(12), 4119–4125.
- Kurnik, R. T., Oliver, J. J., Waterhouse, S. R., Dunn, T., Jayalakshmi, Y., Lesho, M. J., Lopatin, M., Tamada, J. A., Wei, C., & Potts, R. O. (1999). Application of the mixtures of expert algorithms for signal processing in a noninvasive glucose monitoring system. *Sensors and Actuators, B*, B60(1), 19–26. [https://doi.org/10.1016/S0925-4005\(99\)00239-7](https://doi.org/10.1016/S0925-4005(99)00239-7)
- Langmuir, I. (1918). The adsorption of gases on plane surfaces of glass, mica and platinum. *J Am Chem Soc*, 40, 1361–1403. <https://doi.org/10.1021/ja02242a004>
- Lauffer, M. A. (1961). Theory of Diffusion in Gels. *Biophysical Journal*, 1, 205–213.
- Lean, M. E. J., Leslie, W. S., Barnes, A. C., Brosnahan, N., Thom, G., McCombie, L., Peters, C., Zhyzhneuskaya, S., Ross, H. M., Mcilvenna, Y., Stefanetti, R., Trenell, M., Welsh, P., Kean, S., Ford, I., Mcconnachie, A., Sattar, N., & Taylor, R. (2018). Primary care-led weight management for remission of type 2 diabetes (DiRECT): an open-label , cluster-randomised trial. *The Lancet*, 391(10120), 541–551. [https://doi.org/10.1016/S0140-6736\(17\)33102-1](https://doi.org/10.1016/S0140-6736(17)33102-1)
- Lean, M. E. J., Leslie, W. S., Barnes, A. C., Brosnahan, N., Thom, G., McCombie, L., Peters, C., Zhyzhneuskaya, S., Ross, H. M., Mcilvenna, Y., Welsh, P., Kean, S., Ford, I., Mcconnachie, A., Messow, C., Sattar, N., & Taylor, R. (2019). Durability of a primary care-led weight-management intervention for remission of type 2 diabetes : 2-year results of the DiRECT open-label , cluster-randomised trial. *THE LANCET Diabetes & Endocrinology*, 8587(19), 1–12. [https://doi.org/10.1016/S2213-8587\(19\)30068-3](https://doi.org/10.1016/S2213-8587(19)30068-3)
- Leboulanger, B., Guy, R. H., & Delgado-Charro, M. B. (2004). Reverse iontophoresis for non-invasive transdermal monitoring. *Physiological Measurement*, 25(3), R35–R50. <https://doi.org/10.1088/0967-3334/25/3/R01>
- Ledger, P. W. (1992). Skin biological issues in electrically enhanced transdermal delivery. *Advanced Drug Delivery Reviews*, 9(2–3), 289–307. [https://doi.org/10.1016/0169-409X\(92\)90027-N](https://doi.org/10.1016/0169-409X(92)90027-N)
- Lefrou, C., Fabry, P., & Poignet, J.-C. (2012). Current flow: a non-equilibrium process. In *Electrochemistry - The Basics, With Examples* (pp. 169–260). Springer.
- Lei, S., Guo, Q., Shi, J., & Liu, L. (2010). Preparation of phenolic-based carbon foam with controllable pore structure and high compressive strength. *Carbon*, 48(9), 2644–2646. <https://doi.org/10.1016/j.carbon.2010.03.017>
- Leist, M., & Wendel, A. (1996). A novel mechanism of murine hepatocyte death inducible by Concanavalin A. *Journal of Hepatology*, 25(6), 948–959.

- [https://doi.org/10.1016/S0168-8278\(96\)80301-1](https://doi.org/10.1016/S0168-8278(96)80301-1)
- León, C. A. L., & Radovic, L. R. (2001). Interfacial chemistry and electrochemistry of carbon surfaces. *Chemistry and Physics of Carbon*, 24, 225–310.
- Li, D., Pu, Z., Liang, W., Liu, T., Wang, R., Yu, H., & Xu, K. (2015). Non-invasive measurement of normal skin impedance for determining the volume of the transdermally extracted interstitial fluid. *Measurement: Journal of the International Measurement Confederation*, 62, 215–221. <https://doi.org/10.1016/j.measurement.2014.11.015>
- Li, L., Quinlivan, Patricia, A., & Knappe, Detlef, R. U. (2002). Effects of activated carbon surface chemistry and pore structure on the adsorption of organic contaminants from aqueous solutions. *Carbon*, 40, 2085–2100. [https://doi.org/10.1016/S0008-6223\(02\)00069-6](https://doi.org/10.1016/S0008-6223(02)00069-6)
- Li, T., Lee, H.-B., & Park, K. (1998). Comparative stereochemical analysis of glucose-binding proteins for rational design of glucose-specific agents. *Journal of Biomaterials Science. Polymer Edition*, 9(4), 327–344. <https://doi.org/10.1080/09205063.1998.9753059>
- Lin, Y.-H., Lin, J.-H., Wang, S.-H., Ko, T.-H., & Tseng, G.-C. (2012). Evaluation of silver-containing activated carbon fiber for wound healing study: *In vitro* and *in vivo*. *Journal of Biomedical Materials Research Part B: Applied Biomaterials*, 100B(8), 2288–2296. <https://doi.org/10.1002/jbm.b.32800>
- Lindström, J., Louheranta, A., Mannelin, M., Rastas, M., Salminen, V., Eriksson, J., Uusitupa, M., & Tuomilehto, J. (2003). The Finnish Diabetes Prevention Study (DPS). *Diabetes Care*, 26(12), 3230–3236. <https://doi.org/10.2337/diacare.26.12.3230>
- Lott, J. A., & Turner, K. (1975). Evaluation of Trinder's glucose oxidase method for measuring glucose in serum and urine. *Clinical Chemistry*, 21(12), 1754–1760.
- Lourvanji, K. (1995). *Partial Dehydration of Glucose to Oxygenated Hydrocarbons in Molecular-Sieving Catalysts*. <https://doi.org/10.1016/j.biortech.2008.02.014>
- MacDougall, D., & Crummett, W. B. (1980). Guidelines for data acquisition and data quality evaluation in environmental chemistry. *Analytical Chemistry*, 52(14), 2242–2249. <https://doi.org/10.1021/ac50064a004>
- Mackinnon, J. (2004). *Minimally invasive monitoring of diabetic patients*. EngD Mini Project Report, University of Strathclyde, Glasgow.
- Madec, A. M., Mallone, R., Afonso, G., Abou Mrad, E., Mesnier, A., Eljaafari, A., & Thivolet, C. (2009). Mesenchymal stem cells protect NOD mice from diabetes by inducing regulatory T cells. *Diabetologia*, 52(7), 1391–1399. <https://doi.org/10.1007/s00125-009-1374-z>
- Magliano, D., Zimmet, P., & Shaw, J. E. (2015). Classification of diabetes mellitus and other categories of glucose intolerance. In *International Textbook of Diabetes Mellitus* (pp. 3–16). Wiley-Blackwell.
- Mangun, C. L., Benak, K. R., Daley, M. A., & Economy, J. (1999). Oxidation of activated carbon fibers: Effect on pore size, surface chemistry, and adsorption properties. *Chemistry of Materials*, 11(12), 3476–3483. <https://doi.org/10.1021/cm990123m>
- Marco Specialties. (2017). *RIBBON CABLE - 14 PIN 6 INCH DMD TO CONTROL*. Retrieved on 2017-07-25. <http://www.marcospecialties.com/pinball-parts/036-5260-00>
- Marra, F., Nicoli, S., Padula, C., & Santi, P. (2013). Amikacin reverse iontophoresis:

- Optimization of in vitro extraction. *International Journal of Pharmaceutics*, 440(2), 216–220. <https://doi.org/10.1016/j.ijpharm.2012.07.023>
- Marsh, H., & Rodriguez-Reinoso, F. (2006). Introduction to the Scope of the Text. In *Activated Carbon* (pp. 1–12). Elsevier Ltd.
- Martini, F. H., Nath, J. L., & Bartholomew, E. F. (2014a). The Endocrine System. In *Fundamentals of Anatomy & Physiology* (pp. 634–677). Pearson Education.
- Martini, F. H., Nath, J. L., & Bartholomew, E. F. (2014b). The Integumentary System. In *Fundamentals of Anatomy & Physiology* (Edition 10, pp. 176–205). Pearson Education.
- Masaoka, S., Ohe, T., & Sakota, N. (1993). Production of Cellulose from Glucose by *Acetobacter xylinum*. *Journal of Fermentation and Bioengineering*, 75, 18–22.
- Mastrototaro, J. J. (2000). The MiniMed Continuous Glucose Monitoring System. *Diabetes Technology & Therapeutics*, 2(1), 13–18.
- Matthews, D. R., Bown, E., Watson, A., Holman, R. R., Steemson, J., Hughes, S., & Scott, D. (1987). Pen-Sized Digital 30-Second Blood Glucose Meter. *The Lancet*, 329(8536), 778–779. [https://doi.org/10.1016/S0140-6736\(87\)92802-9](https://doi.org/10.1016/S0140-6736(87)92802-9)
- Mazzaferri, E. L., Lanese, R. R., Skillman, T. G., & Keller, M. P. (1970). Use of Test Strips with Colour Meter to measure Blood-Glucose. *The Lancet*, 295(7642), 331–333.
- Mazzucchelli, S., & Corsi, F. (2017). Diabetes management strategies: can nanoparticles be used to therapeutically deliver insulin? *Therapeutic Delivery*, 8(2).
- McCallum, C. L., Bandosz, T. J., McGrother, S. C., Müller, E. A., & Gubbins, K. E. (1999). A Molecular Model for Adsorption of Water on Activated Carbon: Comparison of Simulation and Experiment. *Langmuir*, 15(6), 533–544. <https://doi.org/10.1021/la9805950>
- McCull, D. (2001). *A Glucose Biosensor for a Hydrogel Environment*. Master Thesis, University of Strathclyde, Glasgow.
- McCormick, C., Heath, D., & Connolly, P. (2012). Towards blood free measurement of glucose and potassium in humans using reverse iontophoresis. *Sensors and Actuators, B: Chemical*, 166–167, 593–600. <https://doi.org/10.1016/j.snb.2012.03.016>
- MediWise. (2017). *Imagine living a healthier life with GlucoWise™*. Retrieved on 2017-09-18. <http://www.gluco-wise.com>
- Medtronic. (2019a). *GUARDIAN™ SENSOR 3 WITH GUARDIAN™ LINK 3 TRANSMITTER*. Retrieved on 2019-10-18. <https://www.medtronicdiabetes.com/download-library/guardian-link-transmitter>
- Medtronic. (2019b). *MiniMed™ 670G Insulin Pump System*. Retrieved on 2019-10-18. <https://www.medtronicdiabetes.com/products/minimed-670g-insulin-pump-system>
- Mendosa, D. (2006). *History of blood glucose meters- Transcripts of the interviews*. Retrieved on 2017-07-25. <http://www.mendosa.com/history.htm>
- Mercuri, R. A., Wessendorf, T. R., & Criscione, J. M. (1968). Carbon Foam - Its Preparation and Properties. *Div Fuel Chem*, 12(4), 103–108.
- Merino, V., Kalia, Y. N., & Guy, R. H. (1997). Transdermal therapy and diagnosis by iontophoresis. *Trends Biotechnol.*, 15(8), 288–290.
- Merino, V., López, A., Hochstrasser, D., & Guy, R. H. (1999). Noninvasive sampling of phenylalanine by reverse iontophoresis. *Journal of Controlled Release*, 61(1–

- 2), 65–69. [https://doi.org/10.1016/S0168-3659\(99\)00102-9](https://doi.org/10.1016/S0168-3659(99)00102-9)
- META. (2021). *Imagine living a healthier life with GlucoWise™*. <https://gluco-wise.com/>
- Mianowski, A., Owczarek, M., & Marecka, A. (2007). Surface area of activated carbon determined by the iodine adsorption number. *Energy Sources, Part A: Recovery, Utilization and Environmental Effects*, 29(9), 839–850. <https://doi.org/10.1080/00908310500430901>
- Mohan, D., & Singh, K. P. (2002). *Single- and multi-component adsorption of cadmium.pdf*. 36, 2304–2318. [https://doi.org/10.1016/S0043-1354\(01\)00447-X](https://doi.org/10.1016/S0043-1354(01)00447-X)
- Moreno-Castilla, C. (2004). Adsorption of organic molecules from aqueous solutions on carbon materials. *Carbon*, 42(1), 83–94. <https://doi.org/10.1016/j.carbon.2003.09.022>
- Moussy, F., Jakeway, S., Harrison, D. J., & Rajotte, R. V. (1994). In Vitro and in Vivo Performance and Lifetime of Perfluorinated Ionomer-Coated Glucose Sensors after High-Temperature Curing. *Analytical Chemistry*, 66(22), 3882–3888. <https://doi.org/10.1021/ac00094a007>
- Müller, A. J., Knuth, M., Nikolaus, K. S., Krivánek, R., Küster, F., & Hasslacher, C. (2013). First clinical evaluation of a new percutaneous optical fiber glucose sensor for continuous glucose monitoring in diabetes. *Journal of Diabetes Science and Technology*, 7(1), 13–23. <https://doi.org/10.1177/193229681300700103>
- Muller, D. (1928). Detection of glucose oxidase from *Aspergillus niger*. *Biochemical Journal*, 199, 136–170.
- Müller, E. A., & Gubbins, K. E. (1998). Molecular Simulation Study of Hydrophilic and Hydrophobic Behavior of Activated Carbon Surfaces. *Carbon*, 36(10), 1433–1438.
- Müller, E. A., Hung, F. R., & Gubbins, K. E. (2000). Adsorption of Water Vapor - Methane Mixtures on Activated Carbons. *Langmuir*, 16(13), 5418–5424. <https://doi.org/10.1021/la991312m>
- Müller, E. A., Rull, L. F., Vega, L. F., & Gubbins, K. E. (1996). Adsorption of Water on Activated Carbons: A Molecular Simulation Study. *J. Phys. Chem.*, 100, 1189–1196. <https://doi.org/10.1021/jp952233w>
- Nakamura, K., & Balo, A. (2015). The Accuracy and Efficacy of the Dexcom G4 Platinum Continuous Glucose Monitoring System. *Journal of Diabetes Science and Technology*, 9(5), 1021–1026. <https://doi.org/10.1177/1932296815577812>
- Namasivayam, C., & Kavitha, D. (2002). Removal of Congo Red from water by adsorption onto activated carbon prepared from coir pith, an agricultural solid waste. *Dyes and Pigments*, 54, 47–58.
- Neese, J., Duncan, P., Bayse, D., M, M. R., Cooper, T., & Stewart, C. (1976). *Development and evaluation of a hexokinase/glucose-6-phosphate dehydrogenase procedure for use as a national glucose reference method*. HEW Publication No. (CDC) 77–8330.
- Neisser, A., Ogston, A., Koch, R., & Pfeiffer, R. (2005). From Matula to Mass Spectrometry discovered isolated discovered identified. In *IBMS Biomedical Sciences Congress* (Issue September).
- Nemaaura. (2016). *SugarBEAT®*. Retrieved on 2017-10-27. <http://www.nemaauramedical.com/sugarbeat/>
- Newcombe, G., Drikas, M., & Hayer, R. (1997). Influence of characterised natural

- organic material on activated carbon adsorption: II. Effect on pore volume distribution and adsorption of 2-methylisoborneol. *Water Research*, 31(5), 1065–1073. [https://doi.org/10.1016/S0043-1354\(96\)00325-9](https://doi.org/10.1016/S0043-1354(96)00325-9)
- Newman, J. D., & Turner, A. P. F. (2005). Home blood glucose biosensors: a commercial perspective. *Biosensors & Bioelectronics*, 20(12), 2435–2453. <https://doi.org/10.1016/j.bios.2004.11.012>
- NHS Cambridgeshire and Peterborough Clinical Commissioning Group. (2016). *Guideline on Self-Monitoring of Blood Glucose in People with Diabetes*. Retrieved on 2017-08-23. <https://www.cambridgeshireandpeterboroughccg.nhs.uk/easysiteweb/getresource.axd?assetid=12353&type=0&servicetype=1>
- Nishida, A., Kobayashi, T., & Ariyuki, F. (1997). In vitro developmental toxicity of concanavalin A in rat embryos: analysis of neural crest cell migration using monoclonal antibody HNK-1. *Teratog Carcinog Mutagen*, 17(3), 103–114.
- Noon, J. P., Walker, B. R., Hand, M. F., & Webb, D. J. (1998). Studies with iontophoretic administration of drugs to human dermal vessels in vivo: Cholinergic vasodilatation is mediated by dilator prostanoids rather than nitric oxide. *British Journal of Clinical Pharmacology*, 45(6), 545–550. <https://doi.org/10.1046/j.1365-2125.1998.00718.x>
- Nunnhold, T., Colberg, S. R., Herriott, M. T., & Somma, C. T. (2004). Use of the noninvasive GlucoWatch(registered trademark) Biographer(registered trademark) during exercise of varying intensity. *Diabetes Technology and Therapeutics*, 6(4), 454–462.
- Ogden, C. L., Carroll, M. D., Fryar, C. D., & Flegal, K. M. (2015). Prevalence of Obesity Among Adults and Youth: United States, 2011–2014. *NCHS Data Brief*, 219, 1–8. <https://doi.org/10.1017/S1368980017000088>
- Oggu, G., Sasikumar, S., Reddy, N., Ella, K., Rao, C., & Bokara, K. (2017). Gene Delivery Approaches for Mesenchymal Stem Cell Therapy: Strategies to Increase Efficiency and Specificity. *Stem Cell Reviews and Reports*, 1–16.
- Oldroyd, J. C., Unwin, N. C., White, M., Imrie, K., Mathers, J. C., & Alberti, K. G. M. M. (2001). Randomised controlled trial evaluating the effectiveness of behavioural interventions to modify cardiovascular risk factors in men and women with impaired glucose tolerance: outcomes at 6 months. *Diabetes Research and Clinical Practice*, 52(1), 29–43. [https://doi.org/10.1016/S0168-8227\(00\)00244-8](https://doi.org/10.1016/S0168-8227(00)00244-8)
- Oldroyd, J. C., Unwin, N. C., White, M., Mathers, J. C., & Alberti, K. G. M. M. (2006). Randomised controlled trial evaluating lifestyle interventions in people with impaired glucose tolerance. *Diabetes Research and Clinical Practice*, 72(2), 117–127. <https://doi.org/10.1016/j.diabres.2005.09.018>
- Oliver, N. S., Toumazou, C., Cass, A. E. G., & Johnston, D. G. (2009). Glucose sensors: A review of current and emerging technology. *Diabetic Medicine*, 26(3), 197–210. <https://doi.org/10.1111/j.1464-5491.2008.02642.x>
- Oppel, E., Kamann, S., Reichl, F., & Högg, C. (2019). The Dexcom glucose monitoring system — An isobornyl acrylate-free alternative for diabetic patients. *Contact Dermatitis*, 81, 32–36. <https://doi.org/10.1111/cod.13248>
- Palmisano, F., Zambonin, P. G., Chimica, D., Orabona, V., Centonze, D., Quinto, M., & Alimentari, P. (2002). Glucose Biosensor Based on Overoxidized Poly ( pyrrole )/ Tetrathiafulvalene- Tetracyanoquinodimethane Composite. *Anal.*

- Chem.*, 74(23), 5913–5918.
- Pan, X.-R., Li, G.-W., Hu, Y.-H., Wang, J.-X., Yang, W.-Y., An, Z.-X., Hu, Z.-X., Lin, J., Xiao, J.-Z., Cao, H.-B., Liu, P.-A., Jiang, X.-G., Jiang, Y.-Y., Wang, J.-P., Zheng, H., Zhang, H., Bennett, P. H., & Howard, B. V. (1997). Effects of Diet and Exercise in Preventing. *Diabetes Care*, 20(4), 537–544.
- Papaderakis, A. (2016). *How to calculate capacitance from cyclic voltammetry?* Researchgate; Retrieved on 2019-10-04. [https://www.researchgate.net/post/How\\_to\\_calculate\\_capacitance\\_from\\_cyclic\\_voltammetry](https://www.researchgate.net/post/How_to_calculate_capacitance_from_cyclic_voltammetry)
- Paulev, P.-E., & Zubieta-Calleja, G. (2004). Blood Glucose and Diabetes. In *Textbook in Medical Physiology and Pathophysiology: Essential and Clinical Problems* (Edition 2).
- Pelizzo, M., Zattra, E., Nicolosi, P., Peserico, A., Garoli, D., & Alaibac, M. (2012). *In Vitro* Evaluation of Sunscreens: An Update for the Clinicians. *ISRN Dermatology*, 2012(August 2007), 1–4. <https://doi.org/10.5402/2012/352135>
- Pendleton, P., Wong, S. H., Schumann, R., Levay, G., Denoyel, R., & Rouquerol, J. (1997). Properties of activated carbon controlling 2-methylisoborneol adsorption. *Carbon*, 35(8), 1141–1149. [https://doi.org/10.1016/S0008-6223\(97\)00086-9](https://doi.org/10.1016/S0008-6223(97)00086-9)
- Penn, L., White, M., Oldroyd, J. C., Walker, M., Alberti, K. G. M. M., & Mathers, J. C. (2009). Prevention of type 2 diabetes in adults with impaired glucose tolerance: the European Diabetes Prevention RCT in Newcastle upon Tyne, UK. *BMC Public Health*, 9, 342. <https://doi.org/10.1186/1471-2458-9-342>
- Peterson, D., Jones, D., Dupuis, A., Bernstein, R., & O'Shea, M. (1978). Feasibility of tight control of juvenile diabetes mellitus through patient-monitored glucose. *Diabetes*, 27(437).
- Petrovski, G., Dimitrovski, C., & Milenkovic, T. (2005). Clinical performance of continuous glucose monitoring system in type 1 diabetics. *Diabetologia Croatica*, 33(4), 125–129.
- Phillips, J. H., & Lanier, L. L. (1986). Lectin-dependent and anti-CD3 induced cytotoxicity are preferentially mediated by peripheral blood cytotoxic T lymphocytes expressing Leu-7 antigen. *Journal of Immunology (Baltimore, Md. : 1950)*, 136(5), 1579–1585.
- Phipps, J. B., Padmanabhan, R. V., & Lattin, G. A. (1989). Iontophoretic delivery model inorganic and drug ions. *Journal of Pharmaceutical Sciences*, 78(5), 365–369. <https://doi.org/10.1002/jps.2600780505>
- Pickup, J. C., Hussain, F., Evans, N. D., & Sachedina, N. (2005). In vivo glucose monitoring: the clinical reality and the promise. *Biosensors & Bioelectronics*, 20(10), 1897–1902. <https://doi.org/10.1016/j.bios.2004.08.016>
- Pikal, M. J. (1990). Transport Mechanisms in Iontophoresis. I. A Theoretical Model for the Effect of Electroosmotic Flow on Flux Enhancement in Transdermal Iontophoresis. *Pharmaceutical Research*, 7(2), 118–126.
- Pikal, M. J. (1992). The role of electroosmotic flow in transdermal iontophoresis. *Advanced Drug Delivery Reviews*, 9(1–3), 201–237. [https://doi.org/10.1016/S0169-409X\(00\)00138-1](https://doi.org/10.1016/S0169-409X(00)00138-1)
- Pikal, M. J., & Shah, S. (1990). Transport Mechanisms in Iontophoresis. III. An experimental Study of the Contributions of electroosmotic Flow and Permeability Change in Transport of low and high molecular Weight Solutes. *Pharmaceutical Research*, 7(3), 222–229.

- Pitzer, K. R., Desai, S., Dunn, T., Edelman, S., Jayalakshmi, Y., Kennedy, J., Tamada, J. A., & Potts, R. O. (2001). Detection of Hypoglycemia with the GlucoWatch Biographer. *Diabetes Care*, 24(5), 881–885. <https://doi.org/10.2337/diacare.24.5.881>
- Pleus, S., Schoemaker, M., Morgenstern, K., Schmelzeisen-Redeker, G., Haug, C., Link, M., Zschornack, E., & Freckmann, G. (2015). Rate-of-Change Dependence of the Performance of Two CGM Systems During Induced Glucose Swings. *Journal of Diabetes Science and Technology*, 9(4), 801–807. <https://doi.org/10.1177/1932296815578716>
- Polonsky, W. H., Fisher, L., Hessler, D., & Edelman, S. V. (2014). What is so tough about self-monitoring of blood glucose? Perceived obstacles among patients with Type 2 diabetes. *Diabetic Medicine*, 31(1), 40–46. <https://doi.org/10.1111/dme.12275>
- Poole, R. K., & Kalnenieks, U. (2000). Introduction to light absorption: visible and ultraviolet spectra. In M. G. Gore (Ed.), *Spectrophotometry & Spectrofluorimetry - A Practical Approach* (pp. 1–32). Oxford University Press.
- Porstmann, T., & Kiessig, S. T. (1992). Enzyme immunoassay techniques An overview. *Journal of Immunological Methods*, 150, 5–21.
- Potts, R. O., Tamada, J. A., & Tierney, M. J. (2002). Glucose monitoring by reverse Iontophoresis. *Diabetes/Metabolism Research and Reviews*, 18 Suppl 1(Suppl 1), S49-53.
- Purair Carbon Filter Company. (2019). *Activated Carbon Foam - Different Pore Sizes for Air Filtering*. Retrieved on 2019-02-05. <https://www.carbon-filter.com/filterelements/activated-carbon-foam.html>
- Quianzon, C. C., & Cheikh, I. (2012). History of insulin. *Journal of Community Hospital Internal Medicine Perspectives*, 1–3. <https://doi.org/http://dx.doi.org/10.3402/jchimp.v2i2.18701>
- Raccah, D., Sulmont, V., Reznik, Y., Guerci, B., Renard, E., Hanaire, H., Jeandidier, N., & Nicolino, M. (2009). Incremental Value of Continuous Glucose Monitoring When Starting Pump Therapy in Patients With Poorly Controlled Type 1 Diabetes. *Diabetes Care*, 32(12), 2245–2250. <https://doi.org/10.2337/dc09-0750>.
- Randox Laboratories Limited. (2008). *Glucose (Gluc-Pap) Manual*.
- Rao, G., Glikfeld, P., & Guy, R. H. (1993). Reverse Iontophoresis: Development of a Noninvasive Approach for Glucose monitoring. *Pharmaceutical Research*, 10(12).
- Rao, G., Guy, R. H., Glikfeld, P., LaCourse, W. R., Leung, L., Tamada, J. A., Potts, R. O., & Azimi, N. (1995). Reverse Iontophoresis: Noninvasive Glucose Monitoring in Vivo in Human. *Pharmaceutical Research*, 12(12).
- Rees, G. O. (1838). On diabetic blood. *Guy's Hosp Rep*, 398–400.
- Research Solutions & Resources LLC. (2014). *Converting Potentials to Another Reference Electrode*. Retrieved on 2019-02-11. <http://www.consultrsr.net/resources/ref/refpotls2.htm>
- Rodbard, D. (2017). Continuous Glucose Monitoring: A Review of Recent Studies Demonstrating Improved Glycemic Outcomes. *Diabetes Technology & Therapeutics*, 19(S3), S-25-S-37. <https://doi.org/10.1089/dia.2017.0035>
- Rodriguez-Reinoso, F. (1997). Activated carbon: Structure characterization preparation and applications. In H. Marsh, E. A. Heintz, & F. Rodriguez-Reinoso (Eds.), *Introduction to Carbon Technologies* (p. 35). Universidad de Alicante.

- Ross, D., Heinemann, L., & Chantelau, E. A. (1990). Short-term evaluation of an electro-chemical system (ExacTech) for blood glucose monitoring. *Diabetes Research and Clinical Practice*, *10*(3), 281–285. [https://doi.org/10.1016/0168-8227\(90\)90071-Z](https://doi.org/10.1016/0168-8227(90)90071-Z)
- Rouquerol, J., Avnir, D., Fairbridge, C. W., Everett, D. H., Haynes, J. H., Pernicone, N., Ramsay, J. D. F., Sing, K. S. W., & Unger, K. K. (1994). Recommendations for the Characterization of Porous Solids (Technical Report). *Pure & Applied Chemistry*, *66*(8), 1739–1758. <https://doi.org/10.1001/jama.1902.02480490036009>
- Russell, R. J., Pishko, M. V., Gefrides, C. C., McShane, M. J., & Cote, G. L. (1999). A fluorescence-based glucose biosensor using concanavalin A and dextran encapsulated in a poly(ethylene glycol) hydrogel. *Analytical Chemistry*, *71*(15), 3126–3132. <https://doi.org/10.1021/ac990060r>
- Ruthven, D. M. (2008). Sorption Equilibrium in Microporous Solids. In H. G. Karge & J. Weitkamp (Eds.), *Molecular Sieves: Science and Technology- - Vol.7 - Adsorption and Diffusion* (pp. 4–19). Springer. <https://doi.org/10.1007/978-3-540-73966-1>
- Sabbahi, A., & Vergnaud, J. M. (1993). Absorption of water by polyurethane foam. Modelling and Experiments. *Eur. Polym. J*, *29*(9), 1243–1246.
- Sage, B. H. (2000). FDA Panel Approves Cygnus's Noninvasive GlucoWatch™. *Diabetes Technology & Therapeutics*, *2*(1), 115–117. <https://doi.org/10.1089/152091599316829>
- Sage, B. H., & Riviere, J. E. (1992). Model systems in iontophoresis — transport efficacy. *Advanced Drug Delivery Reviews*, *9*(2–3), 265–287.
- Sakura, S., & Buck, R. P. (1992). Amperometric processes in the electrode with glucose oxidase embedded. *Bioelectrochemistry and Bioenergetics*, *28*, 387–400.
- Salins, L. L., Ware, R. A., Ensor, C. M., & Daunert, S. (2001). A novel reagentless sensing system for measuring glucose based on the galactose/glucose-binding protein. *Analytical Biochemistry*, *294*(1), 19–26. <https://doi.org/10.1006/abio.2001.5131>
- Santi, P., & Guy, R. H. (1996a). Reverse iontophoresis: Parameters determining electro-osmotic flow. II. Electrode chamber formulation. *Journal of Controlled Release*, *42*(1), 29–36. [https://doi.org/10.1016/0168-3659\(96\)01345-4](https://doi.org/10.1016/0168-3659(96)01345-4)
- Santi, P., & Guy, R. H. (1996b). Reverse iontophoresis - Parameters determining electroosmotic flow: I. pH and ionic strength. *Journal of Controlled Release*, *38*, 159–165.
- Sarkar, S. ., & Bose, a. (1997). Role of activated carbon pellets in carbon dioxide removal. *Energy Conversion and Management*, *38*, S105–S110. [https://doi.org/10.1016/S0196-8904\(96\)00254-3](https://doi.org/10.1016/S0196-8904(96)00254-3)
- Schauer, P. R., Bhatt, D. L., Kirwan, J. P., Wolski, K., Aminian, A., Brethauer, S. A., Navaneethan, S. D., Singh, R. P., Pothier, C. E., Nissen, S. E., & Kashyap, S. R. (2017). Bariatric Surgery versus Intensive Medical Therapy for Diabetes — 5-Year Outcomes. *New England Journal of Medicine*, *376*(7), 641–651. <https://doi.org/10.1056/NEJMoal600869>
- Schauer, P. R., Hanipah, Z. N., & Rubino, F. (2017). Metabolic surgery for treating type 2 diabetes mellitus: Now supported by the world's leading diabetes organizations. *Cleveland Clinic Journal of Medicine*, *84*(7 suppl 1), S47–S56. <https://doi.org/10.3949/ccjm.84.s1.06>



- Schersten, B., Kuhl, C., Hollender, A., & Ekman, R. (1974). Blood Glucose Measurement with Dextrostix and New Reflectance Meter. *British Medical Journal*, 3, 384–387.
- Schmelz, M., Schmidt, R., Bickel, A., Handwerker, H. O., & Torebjörk, H. E. (1997). Specific C-Receptors for Itch in Human Skin. *The Journal of Neuroscience*, 17(20), 8003–8008. <https://doi.org/10.1523/JNEUROSCI.17-20-08003.1997>
- Schmook, F. P., Meingassner, J. G., & Billich, A. (2001). Comparison of human skin or epidermis models with human and animal skin in in-vitro percutaneous absorption. *International Journal of Pharmaceutics*, 215(1–2), 51–56. [https://doi.org/10.1016/S0378-5173\(00\)00665-7](https://doi.org/10.1016/S0378-5173(00)00665-7)
- Scognamiglio, V., Aurilia, V., Cennamo, N., Ringhieri, P., Iozzino, L., Tartaglia, M., Staiano, M., Ruggiero, G., Orlando, P., Labella, T., Zeni, L., Vitale, A., & D’Auria, S. (2007). D-galactose/D-glucose-binding Protein from Escherichia coli as Probe for a Non-consuming Glucose Implantable Fluorescence Biosensor. *Sensors*, 7(10), 2484–2491. <https://doi.org/10.3390/s7102484>
- Senseonics. (2019a). *eversense Continuous Glucose Monitoring System*. Retrieved on 2019-11-11. <https://www.eversenseddiabetes.com>
- Senseonics. (2019b). *Senseonics Announces FDA Approval for a Non-Adjunctive Indication (Dosing Claim) for the Eversense® 90-day CGM System*. Retrieved on 2019-10-18. <https://www.senseonics.com/investor-relations/news-releases/2019/06-06-2019-213456270>
- Seong, H., Lee, H.-B., & Park, K. (2002). Glucose binding to molecularly imprinted polymers. *Journal of Biomaterials Science. Polymer Edition*, 13(6), 637–649. <https://doi.org/10.1163/156856202320269139>
- Setford, S., Grady, M., Phillips, S., Miller, L., Mackintosh, S., Cameron, H., & Corrigan, K. (2017). Seven-Year Surveillance of the Clinical Performance of a Blood Glucose Test Strip Product. *Journal of Diabetes Science and Technology*, 0, 1–8. <https://doi.org/10.1177/1932296817703133>
- Shah, V. N., Laffel, L. M., Wadwa, R. P., & Garg, S. K. (2018). Performance of a Factory-Calibrated Real-Time Continuous Glucose Monitoring System Utilizing an Automated Sensor Applicator. *Diabetes Technology & Therapeutics*, 20(6), 428–433. <https://doi.org/10.1089/dia.2018.0143>
- Shakeel, M., Irfan, M., & Khan, I. A. (2018). Rare genetic mutations in Pakistani patients with dilated cardiomyopathy. *Gene*, 673(May), 134–139. <https://doi.org/10.1016/j.gene.2018.06.019>
- Sharpe, A. G., & Housecroft, C. E. (2005). Organometallic compounds of d-block elements. In *Inorganic Chemistry* (Edition 2, pp. 700–740). Pearson Education Limited.
- Shrivastava, A., & Gupta, V. (2011). Methods for the determination of limit of detection and limit of quantitation of the analytical methods. *Chronicles of Young Scientists*, 2(1), 21. <https://doi.org/10.4103/2229-5186.79345>
- Sieg, A., Guy, R. H., & Delgado-Charro, M. B. (2004a). Noninvasive glucose monitoring by reverse iontophoresis in vivo: Application of the internal standard concept. *Clinical Chemistry*, 50(8), 1383–1390. <https://doi.org/10.1373/clinchem.2004.032862>
- Sieg, A., Guy, R. H., & Delgado-Charro, M. B. (2004b). Simultaneous extraction of urea and glucose by reverse iontophoresis in vivo. *Pharmaceutical Research*, 21(10), 1805–1810. <https://doi.org/10.1023/B:PHAM.0000045233.54878.f6>

- Siegmund, T., Heinemann, L., Kolassa, R., & Thomas, A. (2017). Discrepancies between Blood Glucose and Interstitial Glucose - Technological Artifacts or Physiology: Implications for Selection of the Appropriate Therapeutic Target. *Journal of Diabetes Science and Technology*, 11(4), 766–772. <https://doi.org/10.1177/1932296817699637>
- Sigma-Aldrich Inc. (2004). *Technical Bulletin of Glucose (HK) Assay Kit*.
- Silva, L. M. Da, Faria, L. A. De, & Boodts, J. F. C. (2001). Determination of the morphology factor of oxide layers. *Electrochimica Acta*, 47, 395–403.
- Simoni, R., Hill, R., & Vaughan, M. (2002). Benedict's Solution a Reagent for Measuring Reducing Sugars the Clinical Chemistry of Stanley R Benedict. *Journal of Biological Chemistry*, 277(16), 10–11. <https://doi.org/10.1074/jbc.X400012200>
- Sing, K. S. W., Everett, D. H., Haul, R. A. W., Moscou, L., Pierotti, R. A., Rouquerol, J., & Siemieniewska, T. (1985). Reporting Physisorption Data for Gas/Solid Systems with Special Reference to the Determination of Surface Area and Porosity (Recommendations 1984). *Pure & Applied Chemistry*, 57(4), 603–619. <https://doi.org/10.1351/pac198557040603>
- Sing, Kenneth S.W. (1995). Physisorption of Nitrogen by Porous Materials. *Journal of Porous Materials*, 2, 5–8. <https://doi.org/10.1007/s10623-011-9592-z>
- Singh, K., & Mohan, S. (2004). Adsorption behavior of selected monosaccharides onto an alumina interface. *Journal of Colloid and Interface Science*, 270(1), 21–28. <https://doi.org/10.1016/j.jcis.2003.05.002>
- Singh, P., & Maibach, H. I. (1994). Iontophoresis in drug delivery: basic principles and applications. *Crit Rev Ther Drug Carrier Syst.*, 11(2-3), 161-213.
- Skyler, J., Lasky, I. A., Skyler, D. L., Robertson, E. G., & Mintz, D. H. (1978). Home Blood Glucose Monitoring As an Aid in Diabetes Management. *Diabetes Care*, 1(3), 150–157.
- Sönksen, P., Judd, S., & Lowy, C. (1978). Home monitoring of blood glucose. *Lancet*, 311(8067), 729–732.
- Šoupal, J., Petruželková, L., Flekač, M., Pelcl, T., Matoulek, M., Daňková, M., Škrha, J., Svačina, Š., & Prázný, M. (2016). Comparison of Different Treatment Modalities for Type 1 Diabetes, Including Sensor-Augmented Insulin Regimens, in 52 Weeks of Follow-Up: A COMISAIR Study. *Diabetes Technology & Therapeutics*, 18(9), 532–538. <https://doi.org/10.1089/dia.2016.0171>
- Srinivasan, K. R., Mansouri, S., & Schultz, J. S. (1986). Coupling of concanavalin A to cellulose hollow fibers for use in glucose affinity sensor. *Biotechnology and Bioengineering*, 28(2), 233–239. <https://doi.org/10.1002/bit.260280213>
- Srinivasan, V., Higuchi, W. I., Sims, S. M., Ghanem, A. H., & Behl, C. R. (1988). Transdermal Iontophoretic Drug Delivery: Mechanistic Analysis and Application to Polypeptide Delivery. *Journal of Pharmaceutical Sciences*, 78(5), 370–375.
- Srinivasan, V., Higuchi, W. I., & Su, M. (1989). Baseline Studies with the Four-Electrode System: The Effect of Skin Permeability Increase and Water Transport on the Flux of a Model Uncharged Solute during Iontophoresis. *Journal of Controlled Release*, 10, 157–165.
- Stein, W. D., & Litman, T. (2015). Simple Diffusion of Nonelectrolytes and Ions. In *Channels, Carriers and Pumps - An Introduction to Membrane Transport* (Edition 2, pp. 37–80). Academic press inc.
- Sternberg, R., Bindra, D. S., Wilson, G. S., & Thévenot, D. R. (1988). Covalent

- Enzyme Coupling on Cellulose Acetate Membranes for Glucose Sensor Development. *Analytical Chemistry*, 60(24), 2781–2786.
- Stewart, T. (1976). Evaluation of a reagent-strip method for glucose in whole blood, as compared with a hexokinase method. *Clin Chem*, 22, 74–78.
- SugarBEAT™. (2017). *sugarBEAT®*. Retrieved on 2019-11-11. <https://sugarbeat.com/faq/>
- Sugihara, T., Ohura, T., Homma, K., & Igawa, H. H. (1991). The extensibility in human skin: variation according to age and site. *British Journal of Plastic Surgery*, 44(6), 418–422. [https://doi.org/10.1016/0007-1226\(91\)90199-T](https://doi.org/10.1016/0007-1226(91)90199-T)
- Suman, A. (2013). *Adsorption Studies of Sugars Onto Various Surfaces*. PhD Thesis, University of Lucknow.
- Summers, R. S., & Roberts, P. V. (1988). Activated Carbon Adsorption of Humic Substances II. Size Exclusion and Electrostatic Interactions. *Adsorption Journal Of The International Adsorption Society*, 122(2), 382–397. [https://doi.org/10.1016/0021-9797\(88\)90373-6](https://doi.org/10.1016/0021-9797(88)90373-6)
- Sun, Y. (2013). *Glucose and Cellobiose Adsorption onto Activated Carbon*. Master Thesis, Indiana University of Pennsylvania, Indiana.
- Swinehart, D. F. (1962). The Beer-Lambert Law. *Journal of Chemical Education*, 39(7), 333–335. <https://doi.org/10.1021/ed039p333>
- Tamada, J. A., Bohannon, N., & Potts, R. O. (1995). Measurement of glucose in diabetic subjects using noninvasive transdermal extraction. *Nature Medicine*, 1(11), 1198–1201.
- Tamada, J. A., Garg, S. K., Jovanovic, L., Pitzer, K. R., Fermi, S., Potts, R. O., & Cyngus Research Team. (1999). Noninvasive Glucose Monitoring-Comprehensive Clinical Results. *American Medical Association*, 282(19), 1839–1844.
- Tamborlane, W. V., Beck, R. W., Bode, B. W., Buckingham, B. A., Chase, H. P., Clemons, R., Fiallo-Scharer, R., Fox, L. A., Gilliam, L. K., Hirsch, I. B., Huang, E. S., Kollman, C., Kowalski, A. J., Laffel, L., Lawrence, J. M., Lee, J., Mauras, N., O’Grady, M., Ruedy, K. J., ... Xing, D. (2008). Continuous glucose monitoring and intensive treatment of type 1 diabetes. *N Engl J Med*, 359(14), 1464–1476. <https://doi.org/10.1056/NEJMoa0805017>
- Tateno, H., Nakamura-Tsuruta, S., & Hirabayashi, J. (2009). Comparative analysis of core-fucose-binding lectins from *Lens culinaris* and *Pisum sativum* using frontal affinity chromatography. *Glycobiology*, 19(5), 527–536. <https://doi.org/10.1093/glycob/cwp016>
- Tauetsile, P. J., Oraby, E. A., & Eksteen, J. J. (2019). Activated carbon adsorption of gold from cyanide-starved glycine solutions containing copper. Part 1: Isotherms. *Separation and Purification Technology*, 211(September 2018), 594–601. <https://doi.org/10.1016/j.seppur.2018.09.024>
- Terry, J. (1994). The major electrolytes: sodium, potassium, and chloride. *Journal of Infusion Nursing*, 17(5), 240–247.
- The Diabetes Control and Complications Trial Research Group. (1993). The Effect of intensive Treatment of Diabetes on the Development and Progression of long-term Complications in insulin-dependent Diabetes Mellitus. *The New England Journal of Medicine*, 329(14).
- Thennadil, S., Rennert, J., Wenzel, B., Hazen, K., Ruchti, T., & Block, M. (2001). Comparison of Glucose Concentration in Interstitial Fluid, and Capillary and

- Venous Blood During Rapid Changes in Blood Glucose Levels. *Diabetes Technology & Therapeutics*, 3(3), 357–365.
- Thome-Duret, V., Reach, G., Gangnerau, M. N., Lemonnier, F., Klein, J. C., Zhang, Y., Hu, Y., & Wilson, G. S. (1996). *Use of a Subcutaneous Glucose Sensor To Detect Decreases in Glucose Concentration Prior to Observation in Blood*. 68(21), 3822–3826.
- Thwala, L. N., Pr at, V., & Csaba, N. S. (2017). Emerging delivery platforms for mucosal administration of biopharmaceuticals: a critical update on nasal, pulmonary and oral routes. *Expert Opinion on Drug Delivery*, 14(1).
- Tierney, M. J., Garg, S. K., Ackerman, N., Fermi, S. J., Kennedy, J., Lopatin, M., Potts, R. O., & Tamada, J. A. (2000). Effect of acetaminophen on the accuracy of glucose measurements obtained with the GlucoWatch biographer. *Diabetes Technology & Therapeutics*, 2(2), 199–207. <https://doi.org/10.1089/15209150050025140>
- Tierney, M. J., Jayalakshmi, Y., Parris, N. a., Reidy, M. P., Uhegbu, C., & Vijayakumar, P. (1999). Design of a Biosensor for Continual, Transdermal Glucose Monitoring. *Clin. Chem.*, 45(9), 1681–1683.
- Tierney, M. J., Tamada, J. A., Potts, R. O., Jovanovic, L., & Garg, S. K. (2001). Clinical evaluation of the GlucoWatch biographer: a continual, non-invasive glucose monitor for patients with diabetes. *Biosensors & Bioelectronics*, 16(9–12), 621–629.
- Toghill, K. E., & Compton, R. G. (2010). Electrochemical Non-enzymatic Glucose Sensors: A Perspective and an Evaluation.pdf. *International Journal of Electrochemical Sciences*, 5, 1246–1301.
- Tolosa, L., & Rao, G. (2006). The Glucose Binding Protein as Glucose Sensor: Protein engineering for low-cost optical sensing of glucose. *Topics in Fluorescence Spectroscopy Volume 11 Glucose Sensing, 11*, 323–331.
- Tomohira, Y., Machida, Y., Onishi, H., & Nagai, T. (1997). Iontophoretic transdermal Absorption of Insulin and Calcitonin in Rats with newly-devised switching Technique and addition of Urea. *International Journal of Pharmaceutics*, 155, 231–239.
- Tuomilehto, J., Indstrom, J., Eriksson, J., Valle, T., Hamalainen, E., & Uusitupa, M. (2001). Prevention of Type 2 Diabetes Mellitus By Changes in Lifestyle Among Subjects With Impaired Glucose Tolerance. *The New England Journal of Medicine*, 344(18), 1343–1350. <https://doi.org/10.1056/NEJM200105033441801>
- U.S. Food and Drug Administration. (2016). *Dexcom G5 Mobile Continuous Glucose Monitoring System - P120005/S041*. Retrieved on 2017-09-21. <https://www.fda.gov/MedicalDevices/ProductsandMedicalProcedures/DeviceApprovalsandClearances/Recently-ApprovedDevices/ucm533969.htm>
- U.S. Food and Drug Administration. (2018). *FDA authorizes first fully interoperable continuous glucose monitoring system , streamlines review pathway for similar devices*. Retrieved on 2019-10-17. <https://www.fda.gov/news-events/press-announcements/fda-authorizes-first-fully-interoperable-continuous-glucose-monitoring-system-streamlines-review>
- UK Prospective Diabetes Study (UKPDS) Group. (1998). Effect of intensive blood-glucose control with metformin on complications in overweight patients with type 2 diabetes (UKPDS 34). *The Lancet*, 352(9131), 854–865.

[https://doi.org/10.1016/S0140-6736\(98\)07037-8](https://doi.org/10.1016/S0140-6736(98)07037-8)

- Updikes, S., & Hicks, G. (1967). The Enzyme Electrode. *Nature*, *214*, 986–988.
- Vincze, G., Barner, J., & Lopez, D. (2004). Factors Associated With Adherence to Self-Monitoring of Blood Glucose Among Persons With Diabetes. *Diabetes Educ*, *30*(1), 112–125.
- Vinoth, A., Thirunalasundari, T., Tharian, J. A., Shanmugam, M., & Rajkumar, U. (2015). Effect of thermal manipulation during embryogenesis on liver heat shock protein expression in chronic heat stressed colored broiler chickens. *Journal of Thermal Biology*, *53*, 162–171. <https://doi.org/10.1016/j.jtherbio.2015.10.010>
- Vitha, M. F. (2019). UV-Visible Spectrophotometry. In *Spectroscopy - Principles and Instrumentation* (Edition 1, pp. 39–134). John Wiley&Sons, Inc.
- Voet, A., & Lamond, T. G. (1970). *Method of producing spherical pellets of activated carbon* (Patent No. US3533961A).
- Wagner, J., Malchoff, C. D., & Abbott, G. (2005). Invasiveness as a barrier to self-monitoring of blood glucose in diabetes. *Diabetes Technology & Therapeutics*, *7*(4), 612–619. <https://doi.org/10.1089/dia.2005.7.612>
- Walford, S., Gale, E. A. M., Allison, S. P., & Tattersall, R. B. (1978). Self-monitoring of blood glucose. *The Lancet*, *311*(8067), 732–735.
- Walter J. Weber Jr. (1974). Adsorption processes. *Pure and Applied Chemistry*, *37*(3), 375–392.
- Wang, H., Wang, B., Li, J., & Zhu, T. (2019). Adsorption equilibrium and thermodynamics of acetaldehyde/acetone on activated carbon. *Separation and Purification Technology*, *209*(May 2018), 535–541. <https://doi.org/10.1016/j.seppur.2018.07.076>
- Wang, J. (2001). Study of Electrode Reactions. In *Analytical Electrochemistry* (Edition 2, pp. 28–59). John Wiley&Sons, Inc.
- Wang, J. (2008). Electrochemical glucose biosensors. *Electrochemical Sensors, Biosensors and Their Biomedical Applications*, 57–69. <https://doi.org/10.1016/B978-012373738-0.50005-2>
- Wang, J., & Lu, F. (1998). Oxygen-rich oxidase enzyme electrodes for operation in oxygen-free solutions. *Journal of the American Chemical Society*, *120*(5), 1048–1050. <https://doi.org/10.1021/ja972759p>
- Wang, J., Wu, L.-H., Lu, Z., Li, R., & Sanchez, J. (1990). Mixed ferrocene-glucose oxidase-carbon-paste electrode for amperometric determination of glucose. *Analytica Chimica Acta*, *228*, 251–257.
- Wang, X. S., Chen, L. F., Li, F. Y., Chen, K. L., Wan, W. Y., & Tang, Y. J. (2010). Removal of Cr (VI) with wheat-residue derived black carbon: Reaction mechanism and adsorption performance. *Journal of Hazardous Materials*, *175*(1–3), 816–822. <https://doi.org/10.1016/j.jhazmat.2009.10.082>
- Watkins, P., Amiel, S., Howell, S., & Turner, E. (2003). Clinical Presentation and Treatment. In *Diabetes and its Management* (pp. 49–94).
- Weinzimer, S. A., Beck, R. W., Chase, H. P., Fox, L. A., Buckingham, B. A., Tamborlane, W. V., Kollman, C., Coffey, J., Xing, D., & Ruedy, K. J. (2005). Accuracy of Newer Generation Home Blood Glucose Meters in a Diabetes Research in Children Network (DirecNet) Inpatient Exercise Study The. *Diabetes Technol Ther*, *7*(5), 675–683. <https://doi.org/10.1038/jid.2014.371>
- Weng, Y., Qiu, S., Ma, L., Liu, Q., Ding, M., Zhang, Q., Zhang, Q., & Wang, T. (2015). Jet-Fuel Range Hydrocarbons from Biomass-Derived Sorbitol over Ni-

- HZSM-5/SBA-15 Catalyst. *Catalysts*, 5(4), 2147–2160.  
<https://doi.org/10.3390/catal5042147>
- Wesley, N., & Maibach, H. I. (2003). Racial (Ethnic) Differences in Skin Properties. *American Journal of Clinical Dermatology*, 4(12), 843–860.  
<https://doi.org/10.2165/00128071-200304120-00004>
- Wilmington, Delaware, & Ashdod. (2017). A truly non-invasive glucose monitoring device that may improve diabetes management in patients with type 2 diabetes or prediabetes Wilmington,. *53rd EASD Annual Meeting*.
- Wilson, R., & Turner, A. P. F. (1992). Glucose oxidase : An ideal enzyme Review article Glucose oxidase : an ideal enzyme. *Biosensors & Bioelectronics*, 7, 165–185. [https://doi.org/10.1016/0956-5663\(92\)87013-F](https://doi.org/10.1016/0956-5663(92)87013-F)
- Wood, E. J., & Bladon, P. T. (1985). *The human skin*. Edward Arnold.
- World Health Organization. (2006). *Definition and Diagnosis of Diabetes Mellitus and Intermediate Hyperglycemia*. [https://doi.org/ISBN 92 4 159493 4](https://doi.org/ISBN%2092%204%20159493%204)
- World Health Organization. (2011). *Use of glycated haemoglobin (HbA1c) in the diagnosis of diabetes mellitus*. <https://doi.org/WHO/NMH/CHP/CPM/11.1>
- Zhao, X., Lai, S., Liu, H., & Gao, L. (2009). Preparation and characterization of activated carbon foam from phenolic resin. *Journal of Environmental Sciences*, 21(SUPPL. 1), 121–123. [https://doi.org/10.1016/S1001-0742\(09\)60053-X](https://doi.org/10.1016/S1001-0742(09)60053-X)
- Zhou, X., Yi, H., Tang, X., Deng, H., & Liu, H. (2012). Thermodynamics for the adsorption of SO<sub>2</sub>, NO and CO<sub>2</sub> from flue gas on activated carbon fiber. *Chemical Engineering Journal*, 200–202(2), 399–404.  
<https://doi.org/10.1016/j.cej.2012.06.013>

## APPENDIX

Example code for the electrochemical analyser to perform iontophoresis experiments for 60 minutes with switching polarities every 15 minutes, followed by cyclic voltammetry measurements on side B and side A of the sensor

```
# calibrate
CALIBRATE {
}
# Iontophoresis
IONTOPHORESIS {
CURRENT(300) #Current applied [ $\mu A$ ]
LENGTH(15) #Duration of current application [mins]
}
IONTOPHORESIS {
CURRENT(-300) #Current applied [ $\mu A$ ]
LENGTH(15) #Duration of current application [mins]
}
IONTOPHORESIS {
CURRENT(300) #Current applied [ $\mu A$ ]
LENGTH(15) #Duration of current application [mins]
}
IONTOPHORESIS {
CURRENT(-300) #Current applied [ $\mu A$ ]
LENGTH(15) #Duration of current application [mins]
}

#Cyclic Measurement of E1 Electrode-Side B
CYCLIC {
ELECTRODE(1B) #Electrode
MIN(-200) #Starting potential [mV]
MAX(400) #Switching potential [mV]
RAMPRATE(60) #Scan rate [mV/s]
MEASURE(5) #Increment of voltage for next current reading [mV]
CYCLES(3) #Number of cycles to repeat
}
#Cyclic Measurement of E1 Electrode-Side A
CYCLIC {
ELECTRODE(1A) #Electrode
MIN(-200) #Starting potential [mV]
MAX(400) #Switching potential [mV]
RAMPRATE(60) #Scan rate [mV/s]
MEASURE(5) #Increment of voltage for next current reading [mV]
CYCLES(3) #Number of cycles to repeat
}
```